THE HYBRID MULTI-EFFECT DESALINATION (MED) AND THE ADSORPTION (AD) CYCLE FOR DESALINATION

MUHAMMAD WAKIL SHAHZAD

(BSc Eng., UET, Lahore, Pakistan)

A THESIS SUBMITTED

FOR THE DEGREE OF DOCTOR OF PHILOSOPHY

DEPARTMENT OF MECHANICAL ENGINEERING

NATIONAL UNIVERSITY OF SINGAPORE

2013

DECLARATION

I hereby declare that the thesis is my original work and it has been written by me in its entirety. I have duly acknowledged all the sources of information which have been used in this thesis.

This thesis has almost not been submitted for any degree in any university previously.

Muhammad Wakil Shahzad

23 December 2013

ACKNOWLEDGEMENTS

"In The Name of Allah, The Most Beneficent, The Most Merciful"

First of all I praise and express my heartiest gratitude to the most merciful ALLAH who has given me the power and ability to write this thesis. Without his help it would have been impossible to finish this project and compile this doctoral thesis.

I would like to express my deepest sense of gratitude and heartfelt thanks to my supervisor, ***Professor Kim Choon Ng*** for giving me opportunity to work on this project, his guidance, encouragement and motivation throughout this project. I am truly thankful to my supervisor for his efforts for funding of my project.

I would like to extend my special thanks to Dr. Kyaw Thu for his kind help and motivation throughout my candidature without which it was impossible for me to finish this project.

I would also like to express my thanks and gratitude to my seniors, Dr. Loh Wai Soong (JTC, Singapore), Dr. Aung Myat (A-Star, Singapore), Dr. Jayaprakash Saththasivam (KAUST, Saudi Arabia) and Dr. Kazi Afzalurrahman (Chittagog University of Engineering and Technology) for their support and suggestions, which have been greatly helpful for me in advances of my research. I am also truly thankful to Dr. Youngdeuk Kim (KAUST, Saudi Arabia) for his kind help during my project.

I wish to extend my appreciation to all the technical staff of EBTS group particularly Mr. Scadevan Raghvan for his technical and moral helps during my project.

I have to specially thank to my closest lab buddies, Azhar Bin Ismail, Li Ang and Muhammad Burhan who always helped me during hard time in my candidature.

I also have to specially thank to my best buddy Mr. Qasim Saeed (Lindy Gas) and my roommate Mr. Muhammad Shehzad Khalid (AECOM, Singapore) and for their great support and motivation throughout my PhD journey.

Last but not least, I am truly grateful to all my respected family members for their prayers, support and motivation. I would like to specially thank to my father, Muhammad Ramzan for his prayers and moral support. I dedicate my thesis to him.

List of Publications

I am truly grateful to my supervisor ***Professor Kim Choon Ng*** to be co-author for the following publications.

Award

Best Paper Award

Muhammad Wakil Shahzad, Aung Myat, Chun Won Gee and Kim Choon Ng, *Solar Thermal Rating: A methodology for evaluating the long term performance of renewable energy systems*, 6th International Meetings of Advances in Thermofluids, November 18-19, 2013, NUS, Singapore

Patent

Kim Choon Ng, Kian Jon Ernest Chua, Kyaw Thu, **Muhammad Wakil Shahzad**, *Adsorption (AD) and M-Cycle (ADM) for all Weather Cooling* (ILO Ref: 13370N)

Journal Publications

1. **Muhammad Wakil Shahzad,** Kyaw Thu, Won Gee Chun and Kim Choon Ng, *An Experimental Investigation on MEDAD Hybrid Desalination Cycle*, Applied Energy (under reviewer review)

2. **Muhammad Wakil Shahzad**, Kim Choon Ng, Kyaw Thu , Bidyut Baran Saha and Won Gee Chun, *Multi Effect Desalination and Adsorption Desalination (MEDAD): A Hybrid Desalination Method*, Applied Thermal Engineering (under reviewer review)

3. Kim Choon NG, Kyaw Thu, **Muhammad Wakil Shahzad** and WonGee Chun, *Progress of adsorption cycle and its hybrid with conventional MSF/MED processes in the field of desalination*, International Desalination Association (IDA) Journal of Water Desalination and Reuse (DOI:10.1177/2051645214Y.0000000020)

4. **Muhammad Wakil Shahzad**, Kyaw Thu , Won Gee Chun, Kim Choon Ng, *Multi-Effect desalination for low temperature applications*, Journal of Science and Technology (under reviewer review)

5. **Muhammad Wakil Shahzad**, Aung Myat, Chun Won Gee and Kim Choon Ng, *Bubble-assisted film evaporation correlation for saline water at sub-atmospheric pressures in horizontal-tube evaporator*, Applied Thermal Engineering 50 (2013) 670-676.

6. **Muhammad Wakil Shahzad**, Kim Choon Ng, Kyaw Thu, Aung Myat and Chun Won Gee, *An Improved Film Evaporation Correlation for Saline Water at Sub-atmospheric Pressures*, AIP Conf. Proc. 1440, 1085-1091 (2012).

Conference Publications

1. **Muhammad Wakil Shahzad,** Kyaw Thu, Youn Cheol Park, Wongee Chun and Kim Choon Ng, *Solar Thermal Rating: A methodology for evaluating the long term performance of renewable energy systems*, 6th International Meetings of Advances in Thermofluids, November 18-19, 2013, NUS, Singapore

2. Kyaw Thu, Young-deuk Kim, **Muhammad Wakil Shahzad**, Kim Choon Ng, *Advanced Multi-effect Adsorption Desalination Cycle: Numerical Simulation and Performance Investigation*, 6th International Meetings of Advances in Thermofluids, November 18-19, 2013, NUS, Singapore

3. Ang Li, Azhar Bin Ismail, Kyaw Thu, **Muhammad Wakil Shahzad** and Kim Choon Ng *Dynamic Modeling of a Low Grade Heat Driven Zeolite –*

Water Adsorption Chiller, 6th International Meetings of Advances in Thermofluids, November 18-19, 2013, NUS, Singapore

4. Kim Choon NG, Kyaw Thu, **Muhammad Wakil Shahzad** and WonGee Chun*, Progress of Adsorption Cycle and its Hybrid with Conventional MSF/MED processes in the field of Desalination,* International Desalination Association World Congress, October 20-25, 2013, Tianjin, China.

5. **Muhammad Wakil Shahzad**, Kim Choon Ng, Kyaw Thu , Bidyut Baran Saha and Won Gee Chun , *Multi Effect Desalination and Adsorption Desalination (MEDAD) Cycle*, International Symposium on Innovative Materials for Processes in energy Systems (IMPRES), September 4-6, 2013, Fukuoka, Japan.

6. Ang LI, **Muhammad Wakil SHAHZAD**, Kim Choon NG, *Experimental investigation of design parameters for a cogeneration system with a micro-turbine generator and adsorption chiller*, International Symposium on Innovative Materials for Processes in Energy Systems (IMPRES), September 4–6, 2013.

7. **Muhammad Wakil Shahzad**, Kyaw Thu , Won Gee Chun ,Azhar Bin Ismail and Kim Choon Ng, *An Experimental Test on a 3-Stage Multi-Effect Distillation System*, International Conference on Applied Energy (ICAE), July 1-4, 2013, Pretoria, South Africa.

8. Kim Choon Ng, Kyaw Thu and **Muhammad Wakil Shahzad**, *An Emerging Low Cost Adsorption Desalination and Cooling Using Exhaust and Radiator Heat Sources of Ships' Engines*, BIT's 2nd Annual World Congress of Ocean (WCO) , September 23-25, 2013, Hangzhou, China

9. **Muhammad Wakil Shahzad**, Kyaw Thu, Won Gee Chun and Kim Choon Ng, *3-Stages Multi Effect Distillation System: Design and Experiments*, The Fifth International Symposium on Physics of Fluids (ISPF5), June10-13, 2013, Changbaishan, China.

10. **Muhammad Wakil Shahzad**, Kyaw Thu , Won Gee Chun and Kim Choon Ng, *Multi Effect Desalination for Low Temperature Application*, International Conference on Mechanical, Automotive and Aerospace Engineering (ICMAAE '13), July 2-4, 2013, Kuala Lumpur, Malaysia

11. **Muhammad Wakil Shahzad**, Kim Choon Ng, K. Thu, and Chun Won Gee, *An investigation of film evaporation correlation of saline solution at low*

pressures & high concentration, The 7th International Green Energy Conference & The 1st DNL Conference on Clean Energy IGEC-DCCE, May 28-30, 2012, Dalian, China.

12. **Muhammad Wakil Shahzad**, Kim Choon Ng and Won Gee Chun, *MED+AD Desalination Cycle*, 5th International Meetings of Advances in Thermofluids (IMAT), November 11-12, 2012, Bintan, Indonesia

13. **Muhammad Wakil Shahzad**, Won Gee Chun and Kim Choon Ng , *Development of Film Evaporation Correlation at Sub-atmospheric Pressures for Saline Water*, 9th International Symposium on New Carbon Resource Sciences, November-2012 , Kyushu University, Japan.

14. **Muhammad Wakil Shahzad**, Aung Myat, Chun Won Gee and Kim Choon Ng, *An Improved Film Evaporation Correlation for Saline Water at Sub-atmospheric Pressure*, 4th International Meetings of Advances in Thermofluids, October 03-04, 2011, Melaka Malaysia.

Table of Contents

Chapter 7 Experimental Investigation of Hybrid MEDAD Desalination System

Chapter 8 Economic Analysis of Desalination Systems

Chapter 9 Conclusion

Summary

This thesis presents a theoretical and an experimental study of hybrid cycles of multi-staged distillation (MED) and adsorption desalination (AD) or simply called the MEDAD cycle. It is an innovative cycle because the hybridization yielded thermodynamic synergy between two thermally-driven desalination processes, resulting in two to three folds in water production rates and yet at the same top-brine temperatures (TBT).

For a theoretical simulation of the MED cycle, an accurate falling film correlation is needed for the low saturation pressures and saline concentrations that are representative of the actual desalting processes. A literature review indicates that there is a dearth of correlation that could be used: The Hans and Fletcher correlation is found to be inadequate for the mentioned desalination conditions. An experiment was conducted in a purposed-built evaporator that can reproduced the evaporative processes at conditions of saturation pressures of 0.93 to 3.60 kPa (corresponding to saturation temperatures 279 to 300 K) and solution concentration ranges from 15,000 to 90,000 ppm, and a new correlation is proposed which is described in Chapter 3.

Theoretical models are developed for MED, AD and for hybrid MEDAD systems using mass, energy and material balances. The heat transfer coefficient is calculated based on above developed falling film heat transfer coefficient. The governing equations are developed using thermodynamic properties such as the enthalpy, the

density, the internal energy, the viscosity and the heat capacity. These properties are calculated as a function of pressure (P), temperature (T) and salt concentration (X). For AD operating as a batch manner with water-silica gel adsorbate-absorbent pair, the governing equations also include the adsorbent uptake (q) calculation. For the hybrid MEDAD system, the governing equations include both MED and AD and some additional linking equations. These distributed models are transformed into user defined library and solved in FORTRAN by using International Math and Statistics Libraries (IMSL). Simulation results are presented for 8-stage MED and hybrid MEDAD systems. A remarkable improvement is observed in terms of water production and system performance by hybridization.

To validate the simulation results, a 3-stage MED facility is designed, fabricated and installed in air-conditioning laboratory NUS. MED system investigated here consists of horizontal tubes evaporators with parallel feed supply. An extensive experimental testing of the system is conducted in two stages.

Firstly, the 3-stage MED plant is tested as a conventional system where last stage vapors are condensed in water cooled condenser. Extensive experiments are conducted for a wide range of heat source temperatures. Experimental temperatures and pressures profiles of MED components are presented. Their time average values are tabulated for all heat source temperatures. The performance results of MED system are also presented in terms of key parameters such as (i) water production (LPM), (ii) total primary energy consumption (kWh) and (iii) performance ratio. It is

found that maximum production is 0.79 LPM at highest heat source temperature 70^{o}C and PR is 2.5. However at lowest heat source temperature 38^{o}C, the water production observed is 0.15 LPM and PR is 2.90. It is also observed that inter-stage temperature difference varies from 0.8^{o}C to 1^{o}C for all heat source temperature ranges.

In the second stage, the conventional MED system is combined with existing AD cycle and tested as a hybrid MEDAD system. In hybridization, the condenser of the conventional MED system is by-passed and last stage of MED connected to adsorbent bed for direct vapor communication. Experiments are repeated for a wide range of heat source temperatures (15^{o}C to 70^{o}C) to MED steam generator (SG) also called the 1st stage. Similarly, experimental temperatures and pressures profiles of MEDAD components are presented and their time average values are tabulated for all heat source temperatures. Based on experimental results, performance parameters of MEDAD system such as (i) water production (LPM), (ii) total primary energy consumption (kWh) and (iii) performance ratio are calculated and presented. It is found that the water production of the hybrid system is more than two fold as compared to the conventional MED system with the same operational parameters at all heat source temperatures. At highest SG temperature 70^{o}C, the water production observed is 1.89 LPM that is more than twice that of a conventional MED system at the same temperature while the PR is 2.89. It is also observed that at a given top-brine-temperature (TBT), the combined MEDAD cycle yields a larger temperature difference (3^{o}C to 4^{o}C) for each MED stage: It increases the distillate production by

as much as two fold. In the case of the hybrid the MEDAD cycle, the last stage of MED connected to AD beds is operating below ambient temperature (<10^{o}C) that extends the overall operational gap (70^{o}C – 5^{o}C) as compared to conventional MED operation (70^{o}C – 40^{o}C) with the same heat input temperature. This large operation range helps to insert more number of stages that can increase the system production and hence system performance. This increase in water production with the same operating parameters reduces the unit water production cost.

Unit water production cost mainly depends on primary fuel cost. Primary fuel cost apportioning for desalination plants integrated with power plant is very critical. A new exergy model is proposed for the first time for cost apportioning on the basis of quality of energy utilized by processes (power generation and water production). This exergy model provides the fair cost distribution unlike the energy based model in which desalination processes are charged equally. It is found that with 25% steam extraction plant, the portion of energy used by desalination is 25% and 75% is utilized by power plant. It is also found that MEDAD system primary fuel cost is lower as compared to RO processes for 10 or more stages plant. The total unit water production cost for different desalination processes are calculated in terms of \$/m^3 and it is found that MEDAD production cost is the lowest (\$0.58 /m3) among all desalination methods.

Finally, the major findings of this research work are outlined followed by recommendations for future work.

List of Figures

List of Tables

List of Appendices

Nomenclature

v	Specific volume (m^3/kg)
k	Thermal conductivity (W/m. K)
S	Feed water salinity (ppm)
S_{ref}	Reference sea water salinity (30000ppm)
h_{fg}	Latent heat of vaporization or condensation (kJ/kg)
h_f	Sensible heat (kJ/kg)
q	Heat flux (W/m^2)
Q	Heat input (W)
T	Temperature (K)
ΔT	Temperature difference
$\dot{m}$	Mass flow rate (kg/sec)
C_P	Specific heat (kJ/kg-K)
Nu	Nusselt number
U	Overall heat transfer coefficient (W/m^2)
h	Local heat transfer coefficient (W/m^2)
A	Area of heat transfer (m^2)
M	Mass (kg)
X	Salt concentration (ppm)
d	Inside diameter of tube (mm)
D	Outside diameter of tube (mm)
L	Length of tube (mm)
C	Velocity (m/sec)
P	Pressure (kPa)
P_o	Reference pressure (kPa)
H_{ads}	Heat of adsorption (kJ/kg)
R	Gas constant (kJ/kg-K)
K_o	Pre-exponential constant (k/Pa)
t	Heterogeneity parameter
D_{so}	Kinetic constant for silica gel water system (m^2/sec)
K_o	Pre-exponential constant (k/Pa)

E_a	Activation energy (kJ/kg)
q(t)	Instantaneous uptake (kg/kg of silica gel)
q_∞	Maximum adsorbed amount (kg/kg of silica gel)
q^*	Equilibrium uptake (kg/kg of silica gel)
R_P	Particle radius (mm)
Q_{st}	Maximum adsorbed amount (kg/kg of silica gel)
q^o	Maximum adsorbed amount (kg/kg of silica gel)
Q_{ads}	Heat rejected during adsorption process (kW)
Q_{des}	Heat added during desorption process (kW)
Q_{cond}	Heat rejected during condensation process (kW)
Q_{SG}	Heat input to steam generator (kW)

Subscripts description

evap	evaporator / evaporation
in	input / inlet / inside
out	outlet / outside
ch, w	chilled water
cw	cooling water
sat	saturation
l	liquid
g	vapor / gas
ref	reference
HX	heat exchanger
Thw	temperature of hot water
v	vapor
f	feed
b	brine
Tf	temperature of feed
Tb	temperature of brine
Tv	temperature of vapors

cond	condenser
Tcond	condenser side temperature
d	distillate
sg	silica gel
ads	adsorption
SG	steam generator

Greek symbols description

μ	Dynamic viscosity (kg/m-sec)
ρ	Density (kg/m3)

Abbreviations description

UN	United Nation
TDS	Total dissolves solids
MSF	Multi-stage flash
MED	Multi-effect desalination
TVC	Thermal vapor compression
MVC	Mechanical vapor compression
AD	Adsorption desalination
RO	Reverse osmosis
ED	Electro dialysis
GCC	Gulf Cooperation Council
MEDAD	Multi-effect desalination adsorption desalination
HABs	Hazardous algae blooms
TBT	Top brine temperature
BBT	Bottom brine temperature
P&ID	Pressure and instrument diagrams
P&FD	Pressure and flow diagrams
SG	Steam generator
WHO	World health organization
UN-MG	United Nation millennium goal
Mm^3	Million cubic meters
Bm^3	Billion cubic meters
IDA	International desalination association
MENA	Middle East and North Africa

SDWP	Specific daily water production
FFHTC	Falling film heat transfer coefficient
OD	Outer diameter
LMTD	Log mean temperature difference
KPa	Kilo Pascal
ppm	Part per million
ppt	Part per thousands
RMS	Root mean square
Re	Reynolds number
Pr	Prandtl number
FF	Forward feed
BF	Backward feed
PF	Parallel feed
CF	Cross feed
MIGD	Million gallons per day
NF	Nano filtration
BPE	Boiling point elevation
AHT	Area of heat transfer
IMSL	International math and state library
PR	Performance ratio
GOR	Gain output ratio
PLC	Programmable logic control
TPE	Total primary energy consumption

Chapter 1 Introduction

1.1 Background

Clean drinking water is a basic need for everyone but unfortunately more than one in six people in the world is deprived of it. Of the total estimated volume of water of 1.4 billion km^3 (10^{18} m^3) in the world, more than 1.36 billion km^3 (97.5%) is seawater and only 35 million km^3 (2.5%) is fresh water. A substantial amount of the mentioned fresh water, about 24 million km^3 or 70%, is locked in the form of ice and permanent snow on the mountains, the Antarctic, and the Arctic regions [1]. UN document pegged the water "poverty level" at 1000 m^3 per capita per year where nominally water is consumed by three major sectors of an economy, namely, i) irrigation 70%, ii) industry 22% and iii) domestic 8% [2]. Many countries in the semi desert and desert regions suffer from acute water shortage (500 m^3 per capita per year), caused by high population growth, diminishing underground water and increase rate of economic development [3]. Increase in fresh water demand exceeded 2% annually has been reported in many economies of the world, and such projections almost double the population growth rates of these countries [4]. With such trends, it is predicted that some regions of the world will be plagued by water scarcity, affecting more than 1.8 billion people by 2025, as compared to 0.25 billion presently in 2010 [5].

The shortage of fresh water for some regions or countries can be overcome by seawater desalination processes but they require substantial amount of energy

irrespective of the methodology employed. However, the thermodynamic limit for desalination is dependent of the salinity and the temperature of seawater and the accepted specific energy consumption of seawater, with total dissolved solids (tds) of 28,000 to 45,000 ppm, ranges from 0.78 to about 1 kWh/m^3 [6], and major desalination methods found in the industry have specific energy consumption from 3 to 8 kWh/m^3 [7]. Presently, the total desalination capacity in the world is 70 billion m^3 per year, of which about 50 % is by membrane using the concept of reverse osmosis, and the remaining shares are by thermal processes such as the multi-stage flashing (MSF), the multi effect desalination (MED), vapor compression (VC) and adsorption desalination (AD) [8]. Although the non-membrane methods are lower in the world's shares of desalination capacity, yet they are dominantly (70% share) used in the Gulf Cooperation Council (GCC) countries [9]. The percentages of thermal methods can be as high as 94% in some countries such as the Saudi Arabia, UAE, Qatar, Kuwait, etc [10, 11]. The major reasons for adopting the thermal methods in the GCC countries are; Firstly, the high feed salinity in the Gulf and the fouling susceptibility of membranes at high brine concentration limits the water recovery ratio of RO process. Secondly, the frequent occurrences of harmful algae blooms (HABs) in the water of Gulf tend to contain high concentration of toxins in seawater feed that may pass through the membrane pores, causing human illnesses and death if the toxins are ingested [12].

Thermal desalination methods are deemed more robust over the membrane or RO method. Both the MSF and MED processes hitherto are energy intensive because of the limitation in the top-brine and the ambient temperature levels. Recent

hybridization trends of proven thermal methods to the adsorption processes and the effective anti-scallant dosing for seawater feed have enabled better process design that leads to better cost competitiveness compared to ROs. The hybridization of thermal desalination systems is a novel concept because it latches on the proven thermally-driven processes by extracting low temperature waste or renewable heat sources for the AD cycles whist maintaining the same operational parameters for the conventional thermal processes. Hybrid desalination methods are new and no experimental results are available in the literature. There is a need of research to investigate the performance of hybrid desalination systems experimentally.

To meet these objectives a hybrid desalination method, comprising the Multi-Effect Desalination and Adsorption Desalination or simply called "MEDAD", is proposed and forms the main objectives and direction for the research investigation of the thesis. This hybrid desalination method has the potential to be highly energy efficient because the synergetic effect of vapor extraction from the last-stage of the MED reduces the bottom brine temperature and thereby increases the number of stages for latent re-use and hence, increase the utilization of process heat input. In addition to producing freshwater, it can also produce cooling as an additional effect from last MED stages operating below ambient temperature. Thus, the prime objective of this research is to investigate the potential of MEDAD cycle for desalination and to evaluate system performance for future desalination industry reference. The overview of hybrid MEDAD system is given in the following section.

1.2 MEDAD Hybrid Desalination System

The prime objective of thermal system hybridization is to reduce the specific energy consumption and its dependence on the frequency of repeatedly re-utilization of vapor energy. MED system is a vapor cascade system in which the latent heat of vapors is re-utilized multiple times for the evaporation of saline water to reduce the specific energy consumption in term of kWh/m^3.

In conventional MED systems the overall temperature difference is limited by the top brine temperature (TBT) and the last stage temperature also called the bottom brine temperature (BBT) and that limits the number of stages (the frequency of energy re-utilization). In case of MEDAD, this operational temperature rage is extended by adsorption beds connected to last stage of MED. The adsorption system, also called the thermal compressor, helps last stages of MED to operate well below ambient temperature and thus increase the overall operational temperature range toward BBT (as low as 5^oC) with same TBT.

As low-grade process waste-heat or solar energy driven, MEDAD system has the lowest specific energy consumption and great potential in the future desalination market. It is an emerging technique and we believe that MEDAD will soon be the dominant technology especially in Gulf and GCC countries.

This thesis will describe the theoretical modeling and experimental investigation of the conventional MED system and hybrid MEDAD system for portable water production from brackish or seawater at assorted heat source temperatures. In addition, since the MEDAD system works at a low pressure, a new heat transfer

correlation is developed for the evaporator design and discussed in this thesis in detail. Moreover, economic analysis on exergy basis and commercialization of MEDAD system is also presented.

1.3 Objectives of Research

The objectives of the thesis are:

1- To develop a heat transfer coefficient correlation for low pressure applications and for different salt concentrations. This correlation has crucial importance in designing of desalination plant evaporators.

2- To develop a detailed mathematical modelling of a MED system. A detailed FORTRAN code is developed to estimate the system performance at assorted heat source temperatures. These codes are also very important as they are used to find the optimum parameters (area of heat transfer, heat source flow rate etc.) in MED evaporator design.

3- To develop detailed design drawing, P & IDs and P & FDs of a 3-stages MED system as a reference for desalination plant designs.

4- To design, fabricate, install and commission a 3-stage MED system for experimental investigation.

5- To investigate the performance of 3-stage MED system experimentally at waste-heat source temperature ranges from 70^{o}C to 38^{o}C. For experiments, an electric heater was used to simulate the heat source temperature. The system performance is then compared with simulation results.

6- To develop a detailed mathematical modelling of a hybrid MEDAD system. Simulation code is developed for this novel system in FORTRAN using IMSL. The system performance is mapped for assorted MED-SG heat source

temperatures. Performance ratio (PR) is used as a performance indicator to map the system performance.

7- To link the MED system with existing AD system and conduct the experiments as a hybrid MEDAD system to investigate the performance of the hybrid system. MEDAD experiments are conducted at assorted heat source temperature ranges from 70^{o}C to 15^{o}C. Experimental results are also compared with simulation results at same heat source temperature.

8- To develop a detailed operational strategy of hybrid MEDAD system for future reference of the desalination community. Conventional MED is linked to AD reactor through pneumatic vacuum valve operating at batch operation mode.

9- To compare the hybrid MEDAD system performance with conventional MED system performance at same operation conditions to prove the superiority of hybrid desalination system. The superior performance of hybrid desalination system was first observed in simulation investigation using mathematical modelling.

10- To develop an exergy model for cost apportioning in dual purpose (power plant and desalination) plant on the basis of quality of energy utilized and to conduct the economic analysis and CO_2 savings of the hybrid MEDAD desalination system.

11- To highlight the future market and potential applications of hybrid desalination system.

1.4 Research Scope

For better understanding, the thesis is divided into sections in the form of Chapters. The brief introduction of sections or of Chapters is as follows:

- ***Chapter 1*** describes the general introduction, objective, and scope of the research or thesis.
- ***Chapter 2*** explores more on the literature review on fresh water need, supply-demand gap, desalination and desalination methods.
- ***Chapter 3*** give the information on falling film heat transfer coefficient (FFHTC). Advantages of horizontal tube falling film evaporators are highlighted followed by literature review. A novel FFHTC for low temperature (below ambient) conditions and for different salt concentration is proposed. In the last section, experimental results are compared with proposed correlation and with conventional Han & Fletcher's correlation.
- ***Chapter 4*** provides the detailed study of conventional Multi-Effect Desalination (MED) systems. MED plant operation is discussed followed by limitations of traditional plants. A comprehensive description of a conventional MED system is provided. In the last portion, mathematical modeling of MED system is provided followed by simulation results.
- ***Chapter 5*** describes the 3-stage MED experimental facility installed in NUS. Design of each component is discussed in detail followed by P & ID and P & FD development. Experimentation procedure and detailed results are presented. In the last section, numerical results are compared with experiments.

- ***Chapter 6*** explores the development of the hybrid MEDAD system. Detailed analysis of Adsorption Desalination (AD) system is provided. Operational strategy of MEDAD system is discussed followed by mathematical modeling of the system components. In the last section, simulation results are presented.

- ***Chapter 7*** provides the detailed information on MEDAD experimental facility installed in NUS. Experimentation at assorted heat source temperature is discussed in second part in detail. In the last part of the chapter, comparison of simulation and experimental results is provided.

- ***Chapter 8*** provides the exergy model for cost portioning in dual purpose (power plant and desalination) plant. Primary energy consumption (kW/m^3) is compared for different desalination sources followed by unit water production cost calculation and CO_2 emission calculation. Potential market and applications of MEDAD are discussed in the last section.

- ***Chapter 9*** summarizes the major findings of the research along with the recommendations.

Chapter 2 Literature Review

2.1 Background

Fresh water is necessary not only for continuation of human life but also for economic development in the sectors such as agriculture, manufacturing and industries. The world population is increasing at a very high pace that indirectly increasing the straws into available fresh water sources. Fresh water available resources are being depleted due to pressure of increasing trend of population. Although more than half (70%) of earth is covered by water but there is still inadequate fresh water supply and this not only affects human life but is also the main bottleneck in economic development [13-15]. Most of the available water is in the form of sea and high salt concentration is the main hindrance of its direct utilization [16, 17].

Researchers are thus pressurized from both the community and the industry to develop new techniques to produce fresh water form seawater or brackish water. This would fulfill the water demand especially for economic development. Many methods have been introduced in the past few years namely: 1) conservation, 2) management and 3) re-use of fresh water but there is a prediction that all these solution still cannot meet the world water demand. To utilize the seawater, desalination is the only solution to fuel the population and to supply water to industry for economic growth in future. The sections below will highlight the water secrecy, desalination methods and a novel desalination cycle.

2.2 World Water Distribution

More than 70% of earth surfaces are covered with water but the maximum portion (>97%) is in the form of ocean and deep ground water. According to World Health Organization (WHO), water having TDS less than 500ppm is drinkable and in some cases it can be up to 1000 ppm [18]. Standard seawater salt concentration varies from 35,000~45,000ppm and cannot be used as a portable or process water due to high TDS. Out of 3% of fresh water, more than 2% is locked in icecaps and glaciers and is very difficult to recover for use. Figure 2.1 shows the distribution of earth surface water and it can be seen that only less than 1% of fresh water is available in the form of lake and rivers [19].

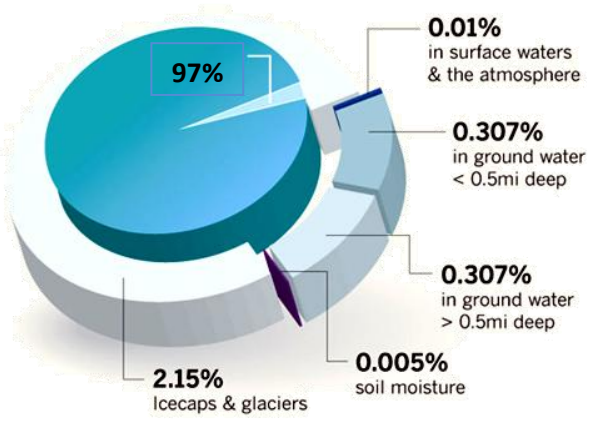

Figure 2.1 Global water distributions on earth surface [19]

This small amount of fresh water is not sufficient to fulfill the demand in different sectors of life cycle such as to quench the thrust of large World population, industrial

development and agricultural purposes. Table 2.1 shows the amount of water in volume as fresh and salt water available in different form on earth surface [20]. A large quantity of water is not useable because of high TDS and millions of people will be sacrificed in near the future due to poor water quality.

Table 2.1 Distribution of fresh water and salt water by volume in different forms of earth surface water [20]

Source	Volume, in cubic kilometer	
	Fresh water	**Salt water**
Oceans	0	1,338,000,000
Ice sheets, Glaciers	24,364,000	0
Ground water	10,530,000	12,870,000
Surface water	122,210	85,400
Atmosphere	12,900	0
Total	**35,029,110**	**1,350,955,400**
Grand Total	**1,386,000,000 (rounded)**	

2.3 Global Population and Water Demand

Population dynamics is an important factor that affects the fresh water demand. World population growth is very fast as shown in Figure 2.2 and it is expected that it will grow up to 9 billion in 2050 compared to 7 billion in 2013 [21]. The spread of population growth is not even in the world and most of population is concentrated in the developing countries.

Only a small percentage of global population (about 20%) have access to running water because of over pumping their non-replenish aquifers while over 1 billion people do not have access to clean water and this inadequate water supply results more than 15 million death annually. In the developing countries, almost 80% diseases are due to water quality and leading to more than 3 million deaths annually [22].

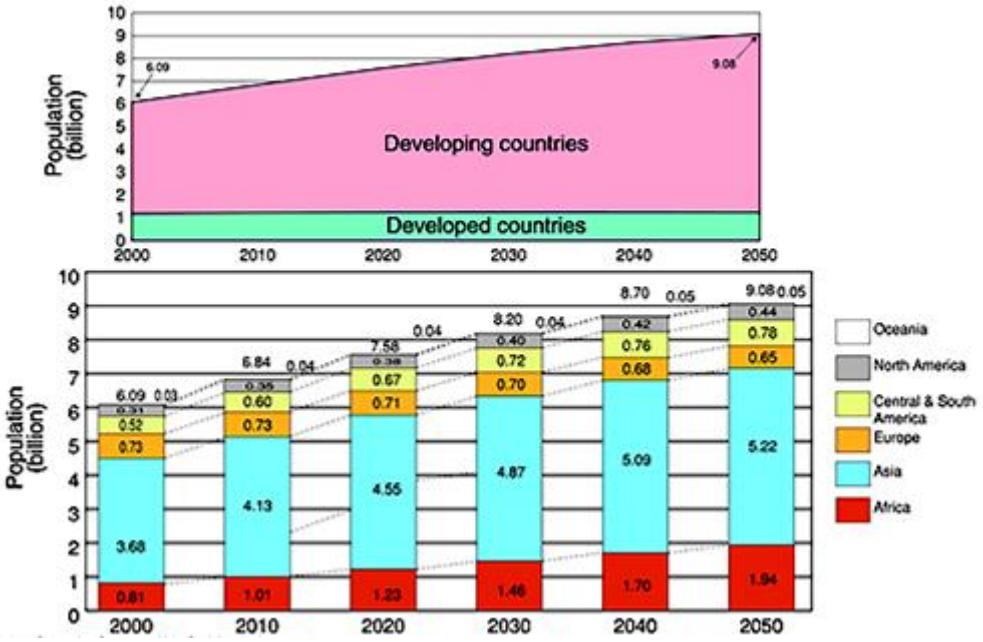

Figure 2.2 **World total population growth per year and trend in different parts of the World** (UN World population projection 2004 revision) [21]

Figure 2.3 shows total water related deaths with and without United Nation Millennium Goals (UN-MG) that is "to halve, by the year 2015, the proportion of people who are unable to reach or to afford safe drinking water. It can be seen that water related death rate may be increase from 5 million in 2000 to 120 million in 2050 without UN-MG. This trend can be reduced to 80 million by 2025 by achieving UN-MG [23].

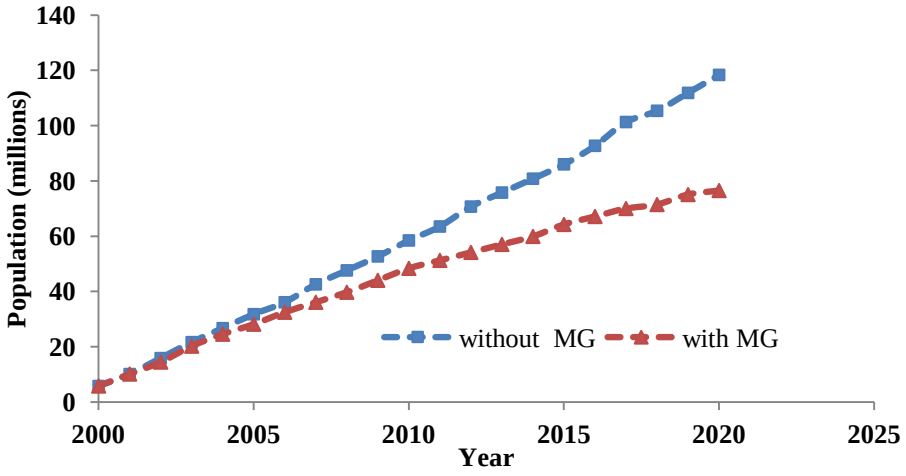

Figure 2.3 **Total water related deaths per years with/without United Nation Millennium Goals (UN-MG) [23]**

These developing countries have greater demand for life commodities even with poor technologies. With increase in global population, pressure on water demand is also increasing and it almost doubles in every twenty years, a rate that is twice than the pace of growth of population. In the developing regions, the water consumption is very high as compared to the developed part of the world and it is due to three main factors such as 1) high population growth, 2) industrialization thrust and 3) agricultural need. Fresh water consumption in these sectors is different in different part of the World. Figure 2.4 shows the water consumption in each sector in developed and developing countries. Developing countries are using most of the fresh water for agricultural purposes to feed their huge population while developed countries utilized them for industrial processes to enhance their economic growth [24].

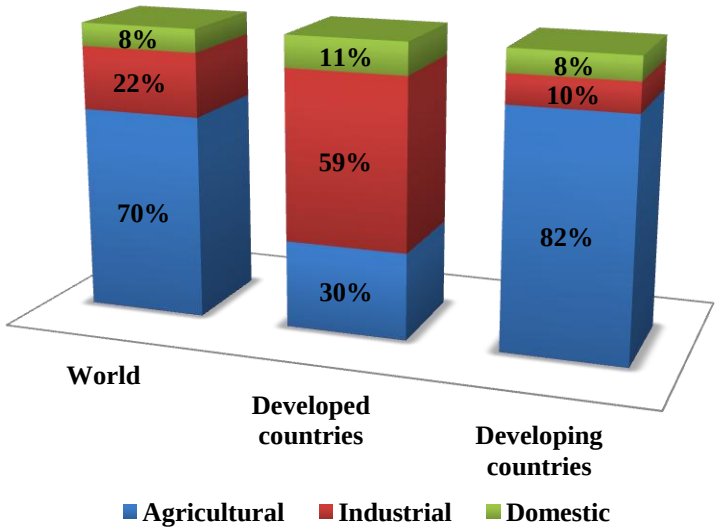

Figure 2.4 **Share of different sectors (by percentage) in water consumption in different part of the world and total Global water consumption [24]**

Figure 2.5 shows fresh water requirement in billion cubic meters (Bm^3) per year in different parts of the world. It can be seen that major contribution is by Asian developing countries that is more than 50% of the world requirement followed by America and Europe [29-31].

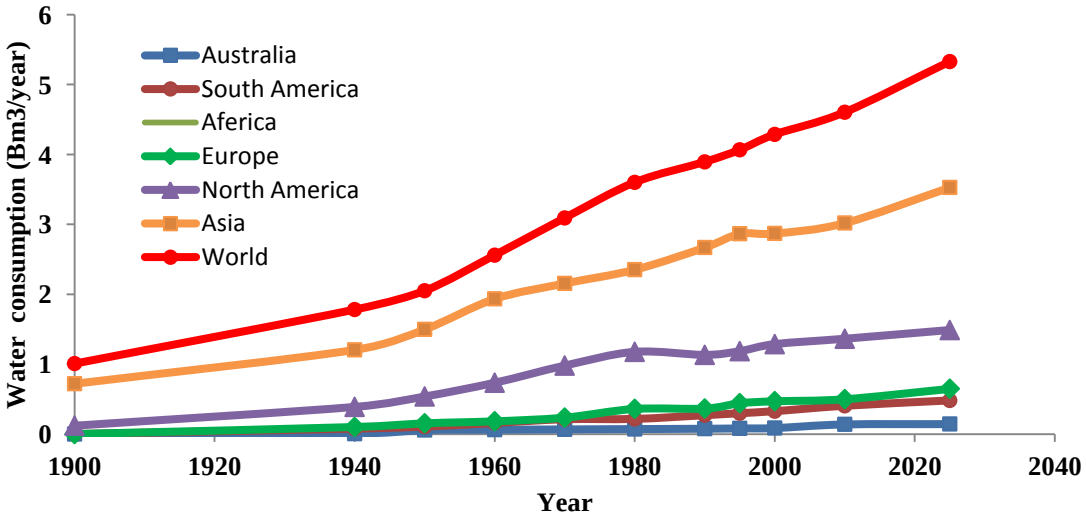

Figure 2.5 **Fresh water consumption in different parts of the world and total global water consumption [31]**

The gluttony of high GDP of highly dense populated regions i.e. developing countries is exerting more pressure on water demand and because of maximum intake the world water demand is increasing exponentially. Even though many measures are taken to handle the water problem like: implementing the technologies and policies for water re-use and conservation, improved water usage and population control, but as fresh water is very limited and not renewable so it cannot fulfill the world water demand. The unlimited source of water "the ocean" can only fulfill the world water demand in all sectors of life. Excess salt needs to be removed before using by desalination methods to convert high TDS saline water to low TDS portable water. Although desalination is not new, but the available technologies such as thermal and membrane are need to develop for most energy efficient and environment friendly processes. Fresh water shortfall and desalination methods are discussed in the following sections.

2.4 Water Deficit & Desalination: An Overview

In 2010, the sustainable supply of fresh water from the Earth's natural water cycle was 4500 billion cubic meters (Bm^3) and it is predicted to increase up to 6,900 Bm^3 by 2030 with 2% annual increment due to population growth and industrialization thrust [32-34]. Presently, the total water demand is already higher (about 40%) than current accessible reliable supply as shown in Figure 2.6 [33-35]. The drivers of this resource challenge are fundamentally tied to economic growth and development.

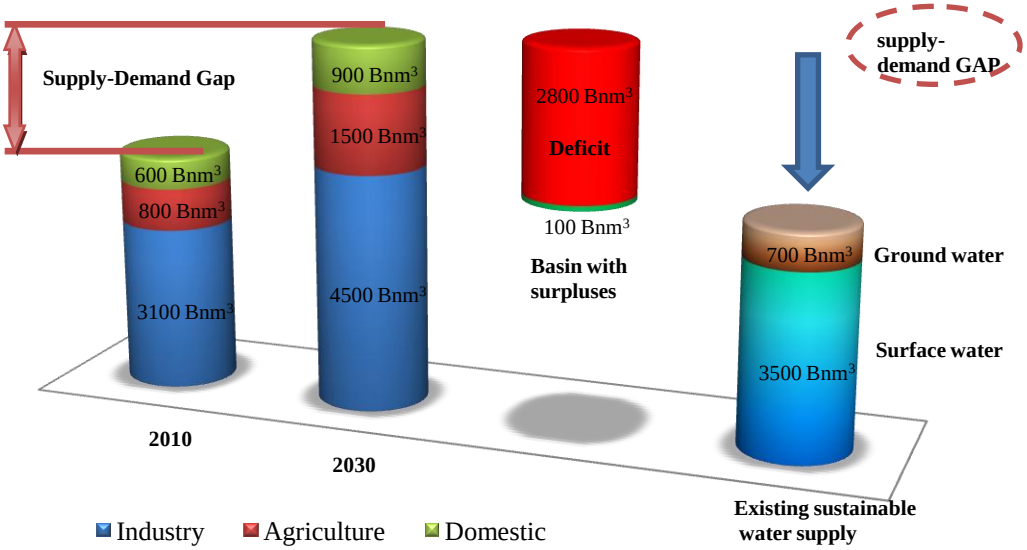

Figure 2.6 **Available global total freshwater, consumption in past and expected increase in future and supply-demands GAP [32-35]**

For agriculture and industry to sustain its rate to 2030 for economic development, improvements in water efficiency can only address 20 percent of the supply-demand gap, leaving a large deficit to be filled. Similarly, a business-as-usual supply build-out as shown in Figure 2.7, assuming constraints in infrastructure rather than raw resources, will address only a further 20 percent of the gap. Even after considering these two measures, there is still a large gap between water supply and demand [35].

Most developing and developed countries focus on addressing the water challenge by considering alternative sources in many cases through energy-extensive measures such as desalination.

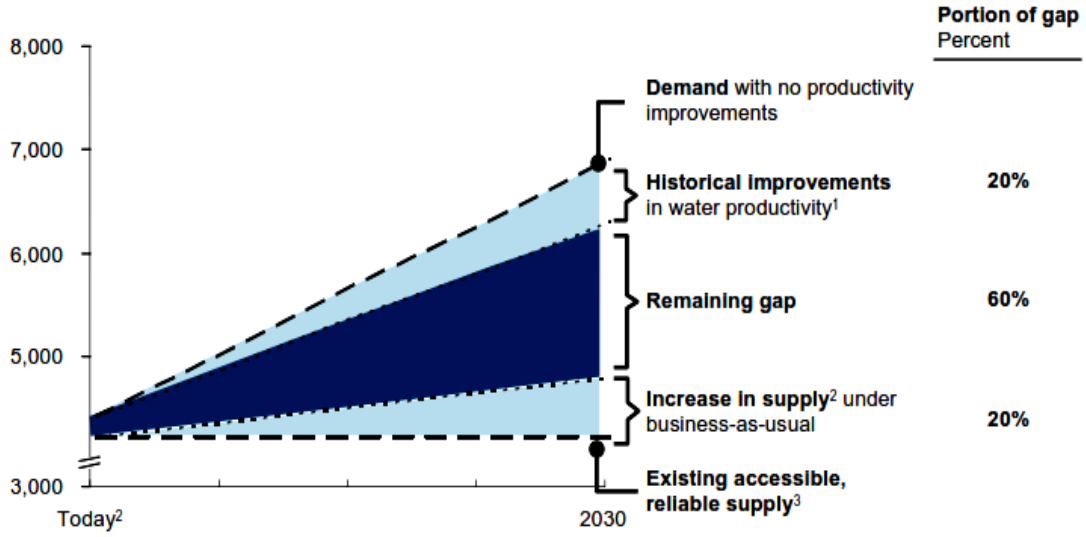

Figure 2.7 **Water supply-demand gap with business as usual and with water productivity improvement.**

1 Based on historical agricultural yield growth rates from 1990-2004 from FAOSTAT, agricultural and industrial efficiency improvements from IFPRI

2Total increased capture of raw water through infrastructure build out, excluding unsustainable extraction

3Supply shown at 90% reliability and includes infrastructure investments scheduled and funded through 2010. Current 90%-reliable supply does not meet average demand

Source: 2030 Water Resources Group – Global Water Supply and Demand model; IFPRI; FAOSTAT

In the water stressed countries, potable water is supplied by the desalting of seawater, brackish and recycled water. "*Desalination is a process that removes the excess amount of salt and minerals from sea water and brackish water to make it portable/drinkable*". Desalination processes actually separate the input water into two streams one with permissible limit of dissolved salts (the portable water stream) and the other containing the remaining high percentage dissolved salts (the rejected brine stream). Figure 2.8 shows the basic concept of a desalination process.

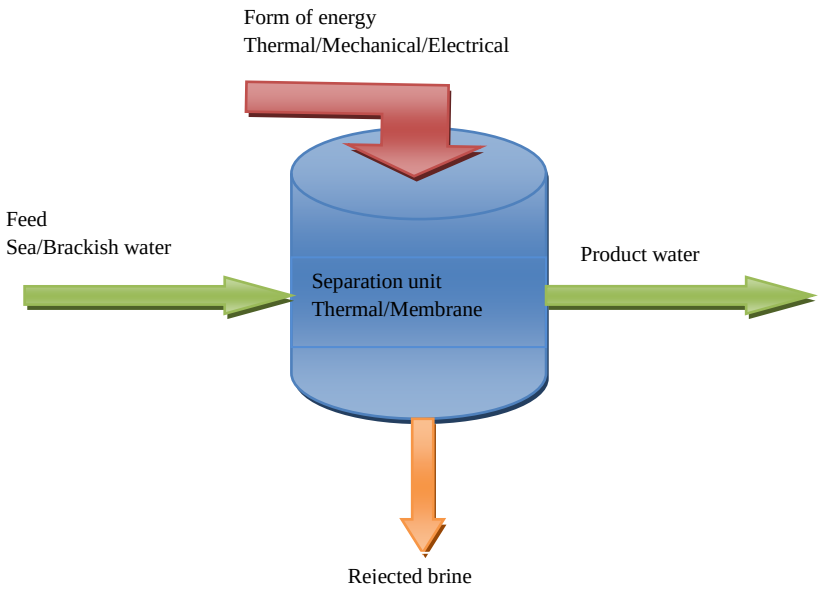

Figure 2.8 **Basic operational concept of a desalter to remove the salt from seawater and brackish water.**

Since "the ocean" is the un-limited source of water, seawater desalination is being applied at 58% of installed capacity worldwide, followed by brackish water desalination accounting for 23% of installed capacity. Fig.2.9 outlines the global desalting capacities by feed water sources [36-40]. The global desalination capacities are increasing at a rapid pace and according to International Desalination Association (IDA) 20th inventory the total global installed desalination capacities were increased from 44 million cubic meters per day (Mm^3/day) in 2006 [41] to 69 Mm^3/day in 2010 and is expected to double by 2015 [42]. Figure 2.10 shows the projected growth of the desalination market including all sources of feed water [43]. It can be seen that the growth rate is higher in gulf and GCC countries as compared to rest part of the world.

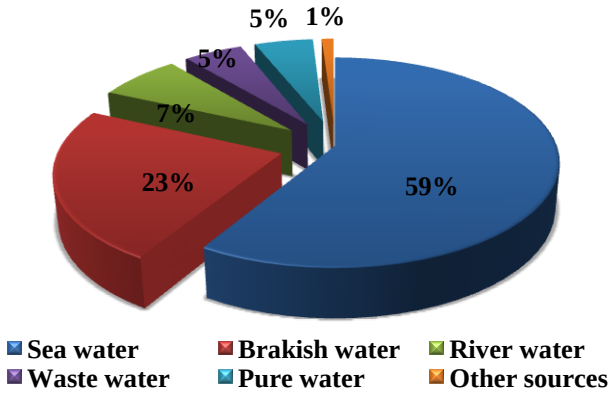

Figure 2.9 **Share (by percent) of different feed sources in global desalination capacities [36-40]**

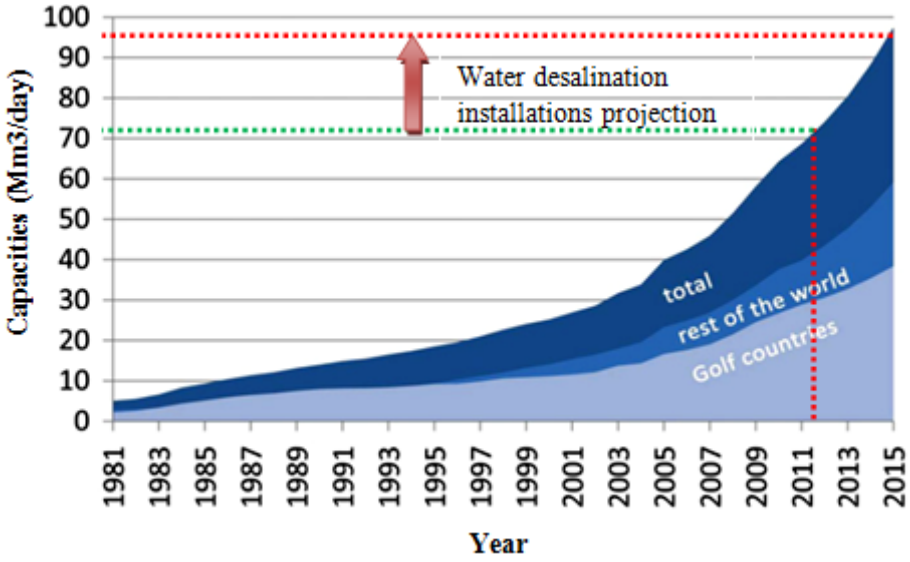

Figure 2.10 **Desalination capacities in past and estimated trend increase in future in different parts of the world and in total [43]**

More than half (65%) of desalination capacities in the world are installed in the Middle East and Gulf Cooperation Council (GCC) countries [42]. Despite a higher desalination market share in GCC, the fresh water availability is dropping rapidly to below the acute water poverty level of 500 m^3 per capital per [44] year for all consumption, caused by an exponential growth in population boom. Figure 2.11

shows the annual fresh water available per capita in desalination production and water demand requirements of GCC countries, spanning from the early decades in 1950 to the future years up to 2025 [45-48].

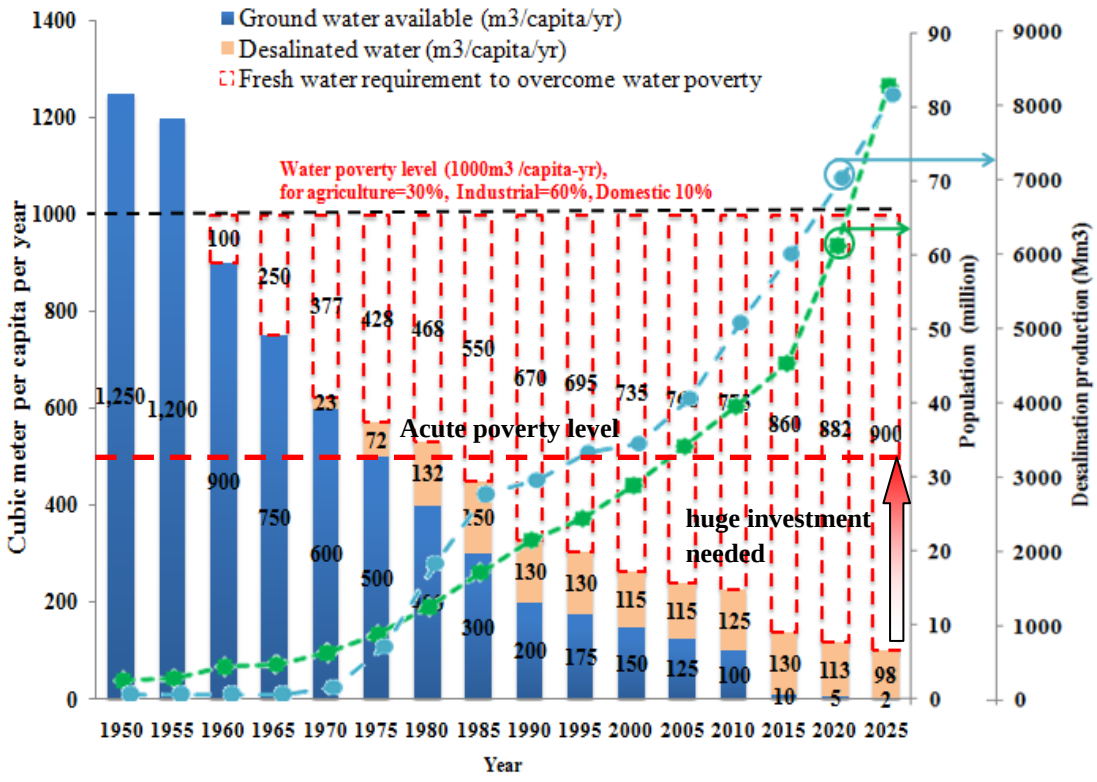

Figure 2.11 **Fresh water availability per capita, desalination capacities trend and population increase in GCC countries [45-48]**

It can be seen that the available fresh water sources and present desalination capacities are not sufficient even to supply the water to meet acute water poverty level. Water production by desalination processes can have a significant effect on the energy requirement and environment. The intricate nexus between water, energy and environment has encouraged scientists and engineers to innovate desalination methods with better energy efficiency and environment friendly processes. The

overview of presently available desalination technologies is provided in the following sections.

2.5 Desalination Technologies

Conventional desalination methods are divided into three major categories, namely: 1) thermal desalination systems (MED, MSF, AD and MED-TVC) which utilize thermal and electric energy, 2) membrane desalination systems (RO) which utilize the pressure energy and 3) chemical desalination systems (ion-exchange, liquid-liquid extraction and gas hydrates) which utilize the chemical potential [49-52]. Fig.2.12 provides an overview of the main desalination process categories [53].

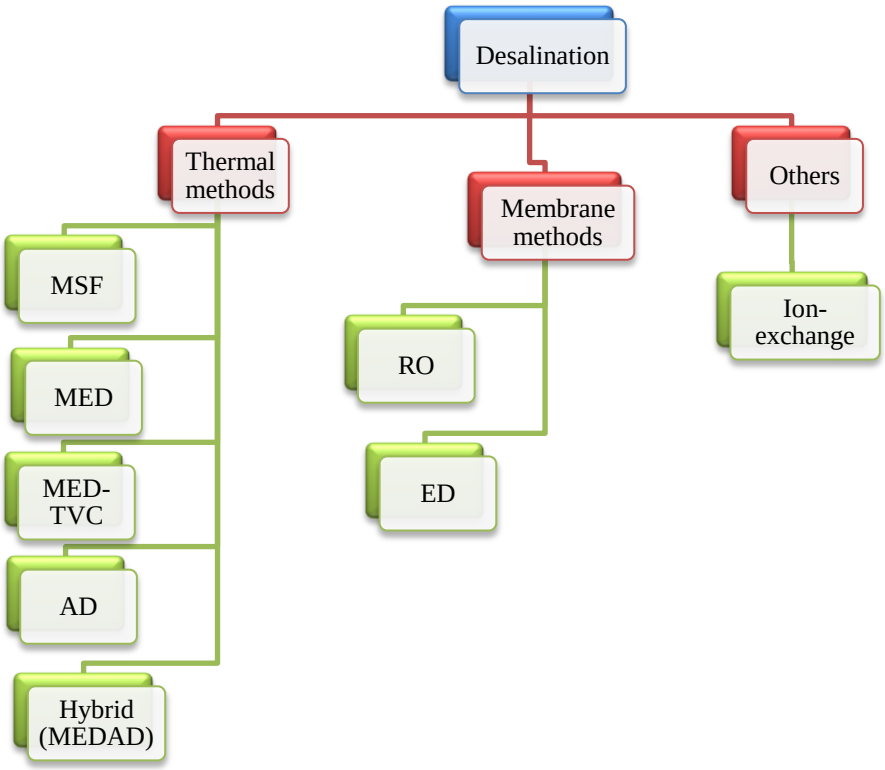

Figure 2.12 Categories of main desalination processes [53]

1-Thermal desalination systems: In thermal desalination, seawater or brackish water is evaporated and then fresh water is produced by condensing these vapors. This is actually an energy re-use or energy recovery process and number of recoveries depends on number of stages. Thermal desalination includes multi-effect desalination (MED), multi stage flash desalination (MSF), mechanical vapor compression (MVC) and adsorption desalination (AD).

The MED process is an old method and has been used since the late 1950s and early 1960s [54]. Multi-effect distillation uses the principles of evaporation and condensation at progressively reduced pressure and it occurs in a series of vessels (effects). In the MED, the vapour produced at the first effect/stage is used as evaporating medium for the next stage because water evaporates at the lower temperature as the pressure is reduced. This process continues and the last stage vapours are condensed in the separate water cooled condenser. The performance ratio of the MED system is directly related to number of effects. MED stages vary from eight to sixteen [55]. The process schematic of conventional MED system is shown in Figure 2.13.

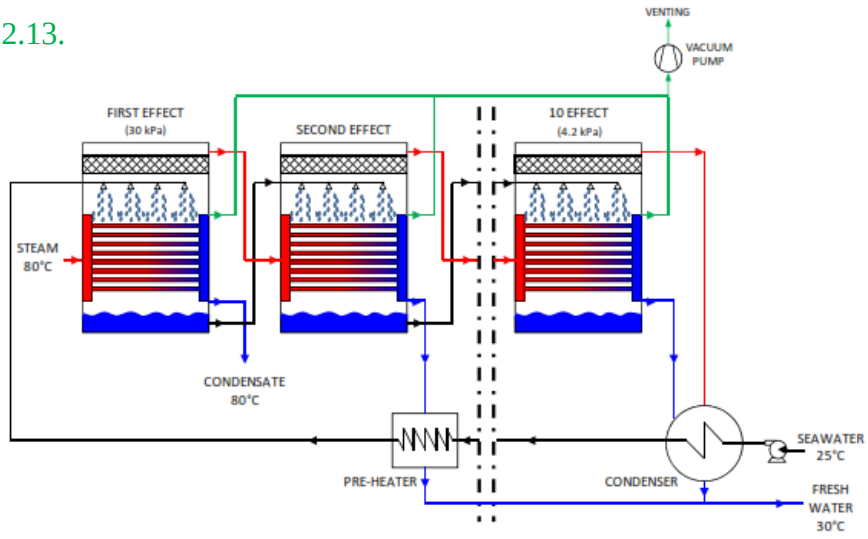

Figure 2.13 Typical process flow schematic of conventional MED system

MED units can be classified as horizontal tube, vertical tube or vertically stacked tube bundles on the basis of heat exchanger tubes arrangement in the effect/stage**.** It can also be classified as forward feed, backward feed and parallel feed on the basis feed supply.

Extensive literature is available on MED systems. El-Desouky et. al. [56] and Hisham et. al. [57] analyzed the thermal performance of MED system with different configurations. Their model includes all the parameters effect as in real plant namely: 1) temperature, 2) salt concentration, 3) temperature depression due to pressure losses, 4) non-condensable gases and 4) flash boxes effects. They found that the specific power consumption decreases with higher heat input temperature. Many researchers [58, 59] have provided the theoretical modeling and simulation codes for MED different parameter calculations at steady state conditions. E1-Nashar et al [58] used the real plant data at Abu Dhabi, UAE and he found good agreement with simulated results. However, dynamic operation modeling in provided by Aly et. al. [60].

MSF was first patented by R.S. Silver after his major improvement over the 1st Westinghouse design. Westinghouse designed a four stage MSF in 1957 and was installed in Kuwait [61], but later R.S. Silver improved the design by providing the partitions to reduce the capital cost of the system [62]. The MSF invention gave the new direction to desalination industry in which evaporation can occur by flashing from large amount of feed water. MSF has higher performance because the heat of

condensation is utilized to pre-heat the feed before flashing in the chamber [63]. The MSF plant can also be coupled with steam power plants to operate the system and to enhance the power plant energy utilization [64, 65]. In the Gulf and MENA region this process was very attractive because of its low corrosion and fouling benefits.

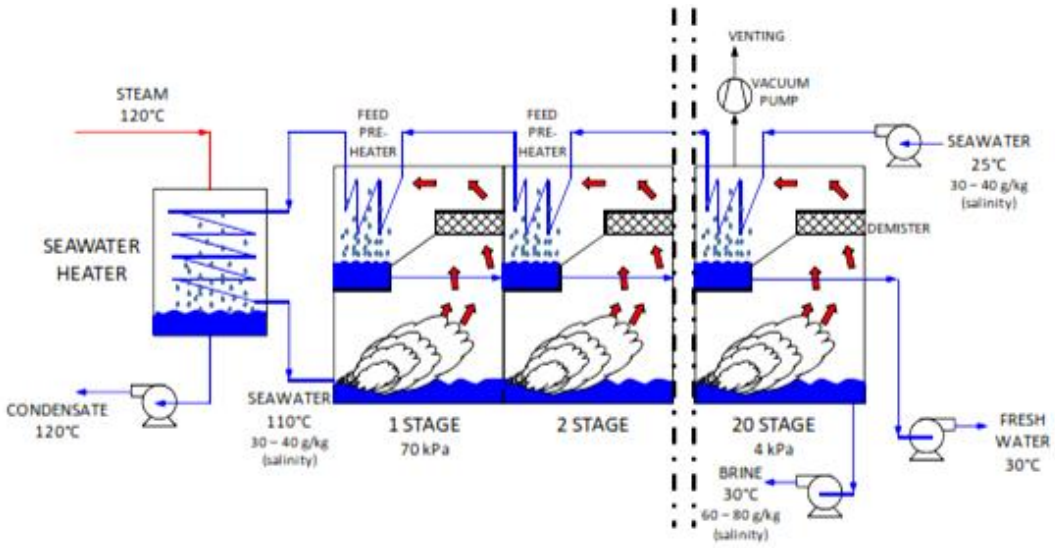

Figure 2.14 Typical process flow schematic of conventional MSF system

The MSF process involves the production of distillation through a number of chambers/stages and each successive chamber/stage operates at progressively lower pressures. The heated feed water is introduced to the first flash chamber where the low pressure of chamber causes rapid evaporation (called flashing) of the portion of water. This process (flashing) of evaporation of a portion of the feed water continues in each successive stage, because the pressure at each stage is lower than in the previous stage. The feed water that passes through the tubes of pre-heaters causes the condensation of vapour produced due to flashing in that chamber [66]. The basic concept of MSF is shown in Figure 2.14. MSF distillation plants can be further

divided into two categories ‘once-through’ or ‘recycled’ process on the basis of feed system [67].

Aly et. al. [68] conducted the thermal performance analysis of MSF system and developed the mathematical modeling for steady state operation. They incorporated all possible factors such as; 1) stage design, 2) correlations/mechanisms for heat transfer and 3) liquid properties variation with salt concentration and temperature. The results of a real MSF plant “Sidi-Krir” at west Alexandria having 17 stages are compared with the model and found to be in good agreement. MSF performance is limited to 10 [69].

Due to serious problems with MED plants such as; severe corrosion and fouling, initially, MSF overtaken desalination market but later researchers developed new anti-corrosive materials and helped MED to gain its position in market again. MED processes are thermodynamically more efficient than MSF processes and they have great potential for large scale plant. However, there are a number of limitations/drawbacks of MED and MSF processes such as; 1) thermal processes are energy intensive, 2) high corrosion and fouling rate due to high heat source temperature, 3) high capital cost due to very big hardware and 4) low recovery ratio [70-73].

In the ***MED-TVC***, MED is used in conjunction with vapor compression (VC) to improve efficiency and performance ratio. Vapor compression processes recompress the vapor produced in the effect to reuse this vapor heat. The vapor produced in one

stage is partially recompressed either with thermal (TVC) or mechanical compressor (MVC) and divert to first cell to use the heat of these compressed vapors. The motive steam at higher pressure is bled from steam turbine for thermal vapor compression [74].

The maximum advantages can be obtained from small to medium installations by incorporating vapour compression processes. The production capacity of MVC units typically ranges in size up to about 3,000m^3/day while TVC units may range in size to 20,000 m^3/day [74]. The thermal performance of MED-TVC system was investigated by M.A. Darwish [75]. This performance model incorporated all necessary parameters such as; 1) evaporator heat transfer area, 2) heat transfer area of heat exchangers, 3) feed temperature, 4) vapors lines pressure drop and 5) evaporator temperatures. Specific energy consumption expression is also proposed in this model.

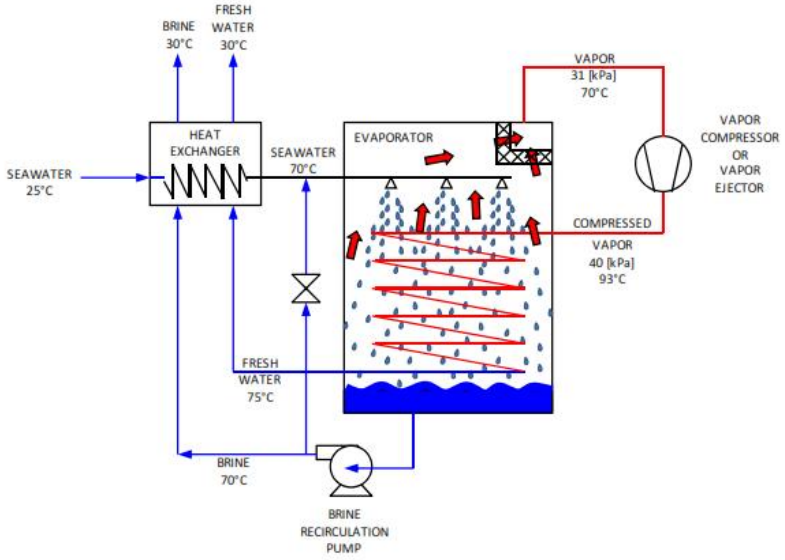

Figure 2.15 Typical process flow schematic of MED-TVC system

The performance ratio of MED is directly related to the number of effects and is always less than the number of effects. Typically the performance ratio of multiple effect desalination plant with 7 or 8 effects is less than 8. This PR of MED can be increased by VC system. By bridging the VC unit to a certain number of effects, the performance ratio will increase to 11: 1 or even higher. The production could be increased 20% higher than nominal rated output by installing VC process [76]. The process diagram is shown in Figure 2.15.

Adsorption processes are introduced by Kayser in 1881 for gases condensation on a free surface [77]. Adsorption is a process of adhesion of gas or liquid atoms or molecules to solid surfaces. These cycles utilize an adsorbate-adsorbent pair. Adsorption desalination (AD) is another thermal desalination method that can overcome the limitations of conventional thermal desalination namely; MED and MSF [78-80]. The AD cycle can produce high grade portable water with lowest specific energy consumption typically ≈ 1.5 KWh/m^3. It utilizes the low grade waste heat, solar or geothermal energy for sorption process that require 45^{o}C – 85^{o}C [81-84]. AD cycles operation is a batch operation with adsorption assisted evaporation and desorption assisted condensation [85, 86].

The adsorption desalination process for low grade waste heat or solar energy has been patented by Ng. et. al [87]. Adsorption desalination was developed to overcome the limitations of conventional thermal desalination systems. Typical AD system consists of four major components namely; 1) the evaporator, 2) silica-gel beds, 3) condenser and 4) pumping unit [88]. AD operation is cyclic steady operation so to

get continuous water production multi-bed scheme is used. Figure 2.16 shows the major components and operation of an AD system. There are many advantages of AD processes namely; 1) low maintenance cost because of no moving parts, 2) low operational cost because of low grade waste heat utilization, 3) less corrosion and fouling chances because of low operational temperature and 4) cooling effect in addition to water production. At chilled water temperature 12^{o}C, AD process can produce 4.7 kg of potable water per kg of silica gel [89].

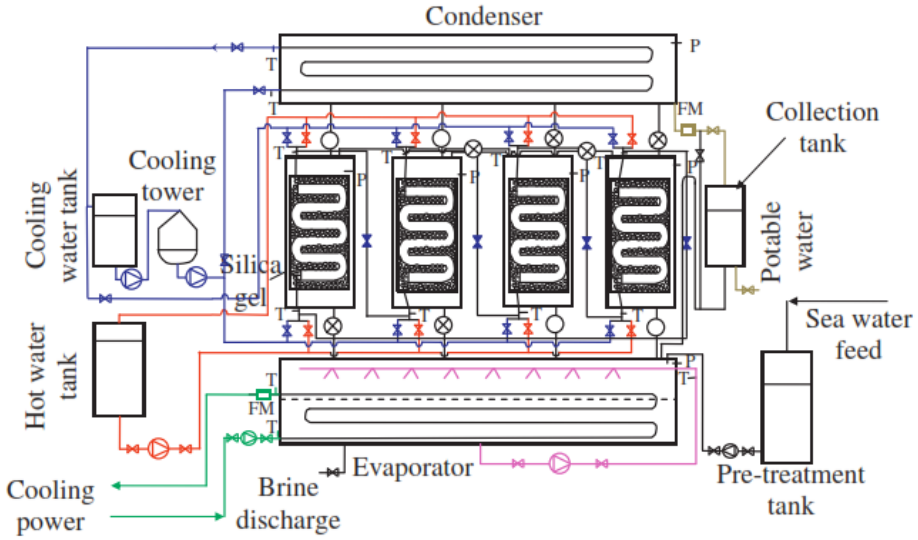

Figure 2.16 Typical AD cycle operational flow schematic [88]

An extensive literature is available on theoretical modeling and simulation of AD cycle [90-94]. Many researchers also conducted the experiments at different heat source temperatures to investigate the performance of AD cycle and to find the optimum operational parameters. The performance analysis based on isotherm, kinetics and energy balance is provided by many researchers [95-97]. They found good agreement of results.

2-Membrane methods:

These processes employ polymeric membranes that filter the dissolved salts when subjected to a pressure gradient or different in electrical potential across the membrane surfaces. Membrane technologies can be subdivided into two broad categories: Reverse Osmosis (RO) and Electrodialysis /Electrodialysis Reversal (ED/EDR).

Reverse Osmosis (RO) processes are dominant in pressure activated desalination. In reverse osmosis (RO) or membrane separation process the pure/drinkable water is recovered from the pressurized saline solution (greater than osmotic pressure) by passing it through semi permeable membrane. The RO membrane filters out the water from pressurized solution keeping the high concentrated solution on other side of membrane. The invention of RO processes was the breakthrough in the desalination industry that changed the whole market because these processes do not require evaporation. The semi-permeable membranes used in RO are made by cellulose acetates, polyamides, polyamides, and poly-sulfones and hold in strong structure.

Most of the energy required for the RO process is for the pressurization of the saline water. Since the osmotic pressure, and hence the pressure required to perform the separation is directly related to the salt concentration, RO is often the method of choice for brackish water, where only low to intermediate pressures are required. The osmotic pressure of seawater is about 25 bars. The RO desalinators operate from 10 – 15 bar pressure for brackish and from 50 to 80 bar pressure for seawater

desalination. As the brine concentration increases the pressure required to recover additional water also increases so the water recovery rate of RO systems tends to be low. Typical, only 40% recovery is possible by RO systems [98].

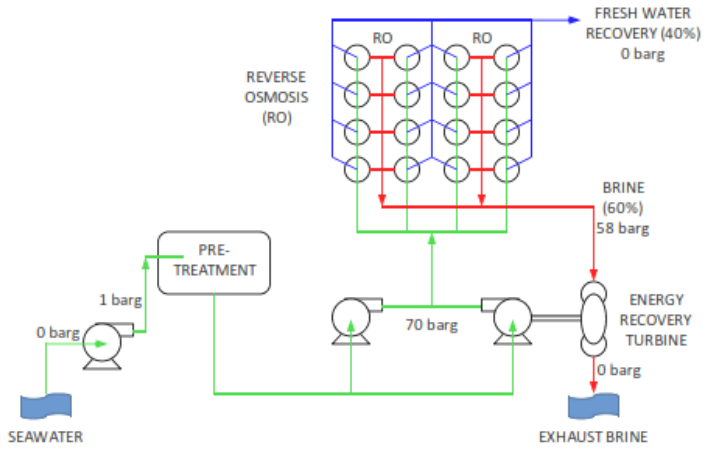

Figure 2.17 Typical RO process flow schematic detail

The main portion of energy supplied is wasted in the form of compressed brine rejection. A device to recover the compression energy from compressed brine is therefore developed and a new RO plant now equipped with these devices to improve the energy efficiency. The pre-treatment of feed water in very important in the RO process because the membranes are very sensitive to pH, oxidizers, a wide range of organics, algae, and bacteria. The cost of the RO process is very much affected by almost 60% discharging of pre-treated water. The process block diagram of RO process is shown in Figure 2.17. RO processes consists pre-treatment, RO membrane and post treatment process. The world largest RO plant in 1969 was a 380m^3/day in Dallas, Texas using brackish water. Today, RO has largest single

capacity of 330,000m^3/day and it consists of 27,000 membrane elements having active surface area about 99ha. This plant total area is equivalent to 132 Olympic size swimming pools and the filter surface area is equivalent to about 200 football fields. These membranes need to replaced 3-7 years [98].

2.6 Global Desalination Installed Capacities Overview

The share of each desalination process in global installed capacities is shown in Figure 2.18. This percentage of share is based on all kind of feed water such as seawater and brackish water. It can be seen that RO is leading with 60% share followed by thermal processes 35% and others as 5% [99, 100].

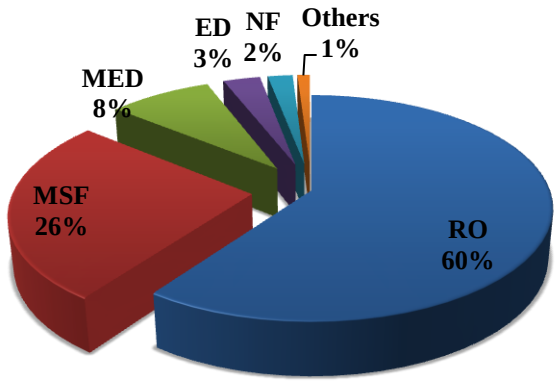

Figure 2.18 Share (by percentage) of different desalination methods in global installed desalination capacities [99, 100]

Although RO processes are dominant, it has certain limitations with respect to local conditions: For example, the frequent maintenance issues from high operating pressure, water quality problems in term of residuals of boron, chlorides and bromides and the severe fluctuations in the seawater intake quality are some of the challenges faced by the RO membranes. In the GCC region, frequent occurrence of

harmful algae blooms (HABs) in the seawater where the microbes of HABs may contain high doses of neuroparalytic and diarrhetic toxins. Such toxins are carried by algae contaminated water that may pass through the pores of membranes, possibly leading to health problems. During an algae event, RO plants face shut down periods up to several weeks leading to severe water shortage as most Gulf Cooperation Council (GCC) countries have water storage of less than a week. Large fluctuations in the feed water quality have direct implications to the operation and maintenance costs of RO plants [101]. Owing to the uncertainty of RO plant operation, thermal desalination are deemed as the dominant processes employed in desalination market in the GCC countries, and more than 70% of water is produced by thermal methods. Table 2.2 shows the desalination capacities in the GCC and non-GCC countries [101-103]. Seawater is the major source of feed for desalination capacities and more than half of installed desalination capacities (58%) are using seawater as feed water s shown in Figure 2.8. Thermal desalination processes are leading with 61% share in seawater desalination market in the world followed by RO with 35% share as shown in Figure 2.19 [104, 105].

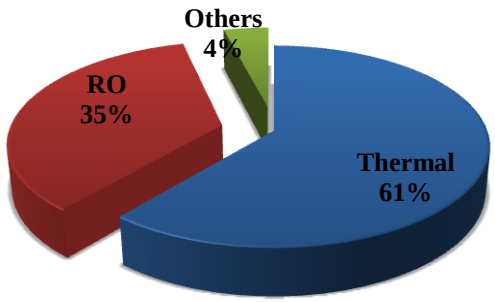

Figure 2.19 **Share (by percentage) of different desalination methods in global desalination capacities on the basis of seawater as a feed [105]**

A bird eye's view of global desalination installations on the basis of feed water type is shown in Figure 2.20 and Table 2.3 list the desalination plant size according to capacities and their share in installed capacities [104, 105].

Table 2.2 Overview of desalination capacities in GCC and non-GCC countries [101]

Year	SWRO (Mm3/day)		Thermal (Mm3/day)		Total (Mm3/day)
	GCC	Non-GCC	GCC	Non-GCC	
1950	-	-	0.03	0.01	0.04
1960	-	0.005	0.06	0.03	0.1
1970	-	0.04	0.13	0.12	0.29
1980	0.1	0.65	1.9	1.4	4.05
1990	0.6	1.6	6.45	2.0	10.65
2000	1.0	2.1	8.3	2.95	14.35
2010	4.3	13.2	17.2	4.1	28.80

Table 2.3 Desalination plant capacity according to daily production [105]

Plant size	Production (m3/day)	% share in market
Very large plant (XL-sized)	XL ≥ 50,000	49%
Large plant (L-sized)	50,000 ≤ L ≥ 10,000	25%
Medium plant (M-sized)	10,000 ≤ M ≥ 1,000	22%
Small plant	S ≤ 1,000 m^3/day	4%

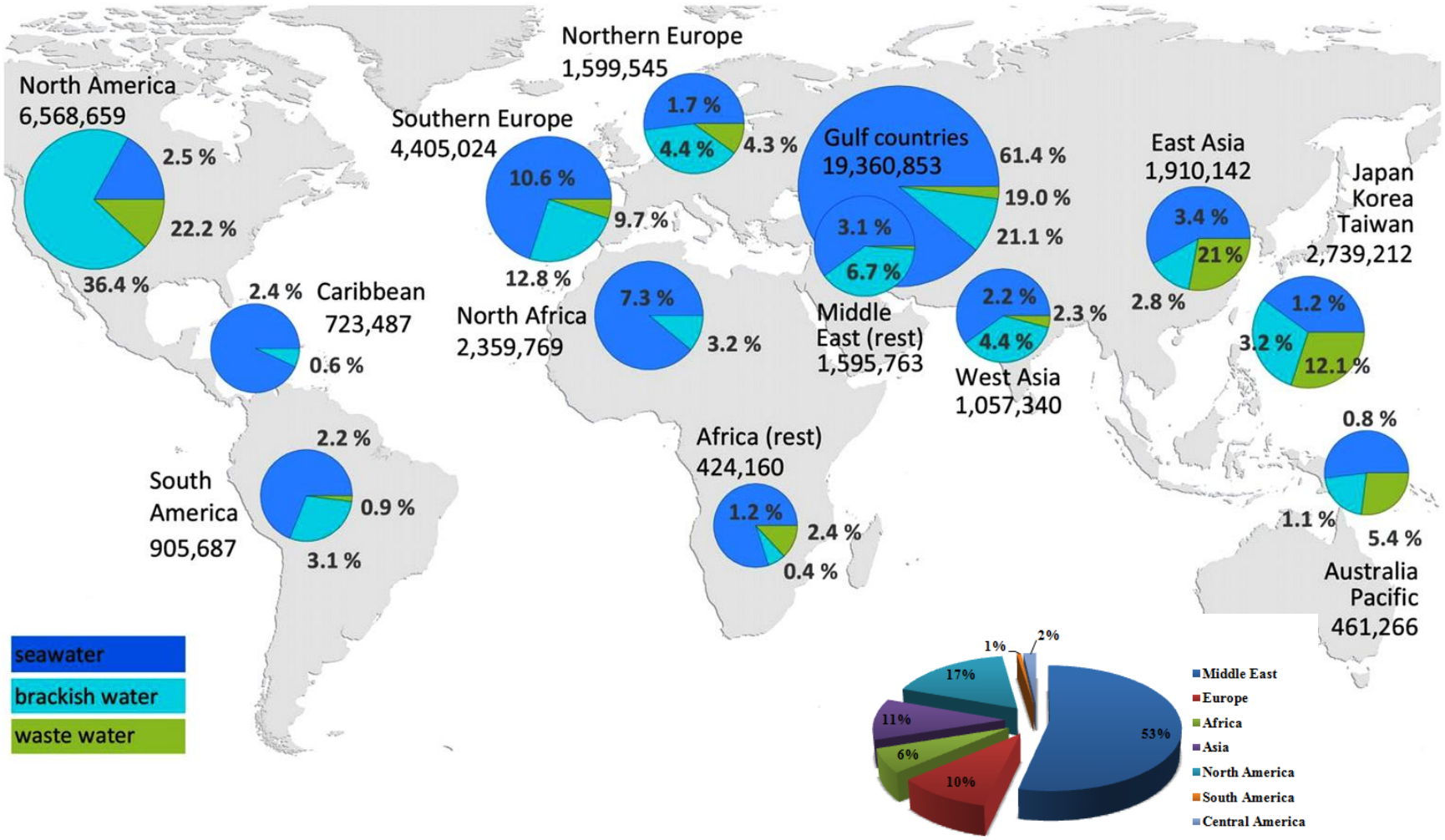

Figure 2.20 **Global desalination capacities overview and share (by percentage) in different parts of the world (Desalination production given in m^3/day using all water sources. The percentage given is the share of desalination capacity with feed water sources) [104,105]**

(Source: IDA and GWI., IDA Worldwide Desalting Plant Inventory Report No. 20 in MS Excel Format, Media Analytics Ltd., Oxford, UK, 2008)

2.7 Desalination Processes Energy Demand

In the last few decades, the desalination market expanded due to high water demand and attracted innovators and research organizations to improve desalination methods to reduce production costs. Figure 2.21 shows the trend of desalination cost reduction and tremendous change can be seen in the last 20 years in thermal desalination up to a factor 10 [106].

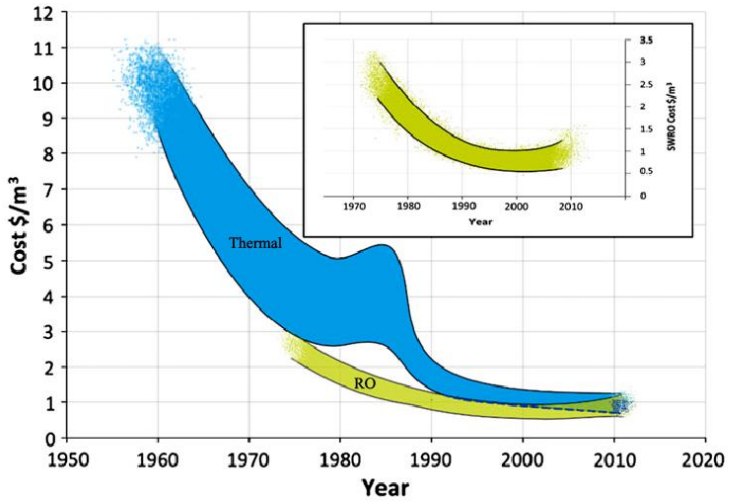

Figure 2.21 Desalination cost trend of thermal and RO processes [106]

Technological development, hybridization and company's competition are the major factors of desalination cost reduction in last two decades. Table 2.4 summarizes the technological developments in the last two decades causes the desalination cost reduction in thermal desalination processes [107, 108]. Even though 20 year's development has great impact on desalination production cost, still all processes are energy intensive (0.70KWh$_e$/m^3). Table 2.5 shows the energy consumption data of desalination processes [106, 109-119]. It can be seen that MSF consumes the most

energy followed by MED system. RO processes are the most developed in the desalination market but still they consume 3-10 times the theoretical minimum energy.

Table 2.4 Technological development in thermal systems [107, 108]

MED	MSF
• Typical unit size increased from 3800 to 22,700 m3/day • Improvement in heat transfer surfaces such as cross end tubes • Improvement in process configuration • Horizontal tubes falling film heat exchangers introduction • Use of TVC • High top brine temperature with NF at upstream • Material development • Hybridization	• Typical unit size increased from 19,000 to 90,000 m3/day • Individual equipment and design configuration improvement • Top brine temperature increase to 120oC • Low cost material development • Hybridization of the system • Installation cost reduction • Improved plant reliability and thermal performance

It is important to consider that, RO plants utilize electrical energy while thermal systems (MSF & MED) utilize thermal energy directly. The power plant efficiency for thermal energy to electrical energy conversion is only 35%, therefore, for fair comparison all the energies are converted to basic fuel energy by considering the conversion system efficiency. It can be seen that on the basis of basic fuel energy, the specific primary energy consumption of RO is about 20-30 times than minimum desalination energy required.

Renewable energies such as 1) solar thermal, 2) wind and 3) geothermal energy are also introduced for desalination process to lower down the cost of water production and detail can be found in the articles published [120-123].

Table 2.5 Desalination processes energy requirements [106, 109-119]

Method of Desalination	Thermal energy Consumed (kWh_t/m^3)	Electric energy Consumed (kWh_e/m^3)	Total primary fuel energy (kWh_{pe}/m^3) η_b=0.94, η_{th}=0.35	Investment cost $/$m^3$/day
Multi-stage Flash (MSF)	19.4	5.2	35.50	1200-2500
Multi-effect Distillation (MED)	16.4	3.8	28.30	900-2000
Vapor compression (VC)	-	11.1	31.71	-
Reverse Osmosis (RO) – single	-	5.5	15.71	900-2500
Reverse Osmosis (RO) – double	-	7.5	21.40	300-1200

There are many factors affecting the per unit water production. Depending on desalination process, these factors have different percentage of share in total cost. Cost breakdown for major desalination processes is given in Figure 2.22. The costing elements include; 1) energy, 2) labor, 3) chemicals and 4) parts cost [105, 124-126]. The reference plant size is 100,000m^3/day.

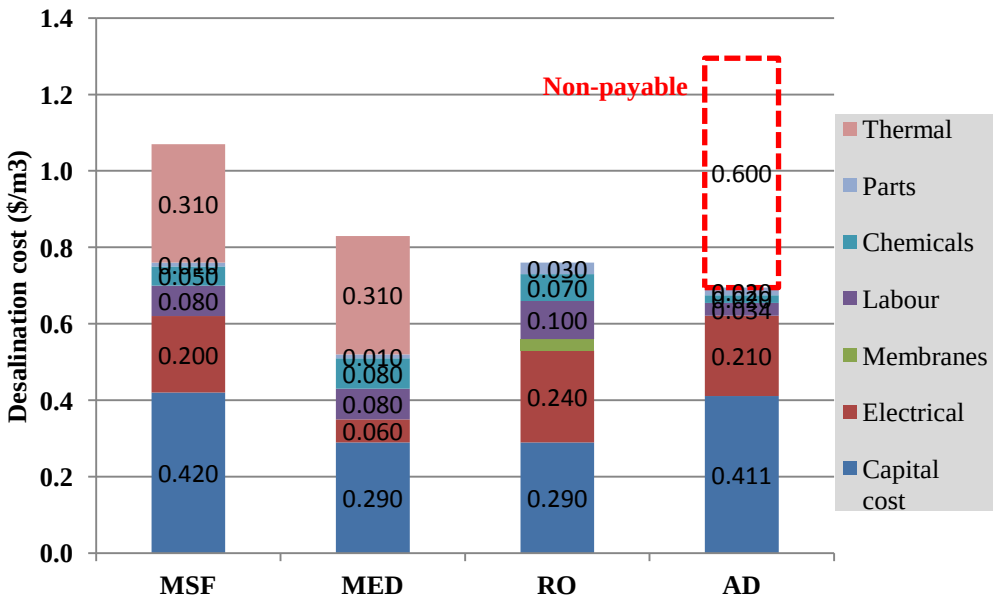

Figure 2.22 Relative water production cost of main desalination methods [124-126]

Energy consumption has a major contribution in desalination costing. This energy can be payable (high grade electrical energy) or non-payable (low grade waste heat or renewable energy). Other examples of non-payable energy are the natural water cycle, where the energy from the Sun affects the evaporation from the surfaces of oceans and transpiration of plants (from photosynthesis). Energy prices are increasing and may increase the desalination cost in future again. It can be seen that RO is the more energetic and efficient process for desalination but due to the above mentioned limitations/drawbacks, thermal process are preferable in GCC countries. Another reason for thermal method attraction in GULF region is feed water that is 100% from sea. Thermal processes are more efficient for seawater desalination.

Although remarkable developments are observed in thermal processes but still there is need for development to overcome the limitations with conventional thermal systems. The main limitation with MED system is its limited operational temperature gap because of top brine temperature (typically 70^{o}C) and lower brine temperature (typically 40^{o}C). Because of this operational gap limitation the numbers of vapor heat recoveries are fixed. MED systems can be superior thermodynamically and energetically if this operational temperature ranges can be extended by breaking upper and lower temperature limits. Ng. et al [127] proposed a hybrid desalination method called MEDAD or ADMED. This novel desalination method can overcome the shortcoming of conventional desalination methods by breaking the temperature limit (top brine temperature and lat stage temperature) barrier. MEDAD method has great potential for future high grade portable water production with energy

consumption less than the bench mark of 1.5kWh/m^3. A brief summary of this novel method is discussed in following section.

2.8 MEDAD Desalination Cycle Overview

This novel desalination cycle is a hybrid of the conventional multi effect distillation (MED) and the adsorption cycle (AD). MED system is robust and thermodynamically more efficient than MSF while AD cycle is new in desalination market. AD has a high attraction in the last few decades because of the different kinds of adsorbents developed such as; 1) silica gel, 2) activated carbon, 3) zeolite and 4) alumina. AD cycle can operate below ambient temperature and that's why it can also produce cooling effect from last stages as an additional benefit. Adsorption cycle based chillers have been commercialized in Japan for two decades [128-132] and many researchers have investigated the different adsoebant-adsorbate pairs [133, 134]. AD working pairs includes; 1) silica gel-water, 2) activated carbon-methanol, 3) activated carbon-ammonia and 4) zeolite-water [135-138].

Adsorption based desalination is investigated by many researchers and reported that optimal specific daily water production (SDWP) for four bed scheme is about 4.7 kg/kg silica gel [139-142]. Adsorption desalination based on low grade waste heat utilization is patented by Ng. et. al. They installed the first adsorption desalination plant in the National University of Singapore (NUS) which consists of four silica gel beds. They investigated the processes using chilled water at 12.5^{o}C and demonstrated that the specific water production of 4.7 kg/kg of silica gel is possible [142].

Ng et al. introduced and patented a novel hybrid desalination method "MEDAD cycle" that is a combination of conventional MED and AD cycle. This novel desalination cycle can mitigate the limitations of conventional MED system to increase the system performance. This combination allows the MED last stage to operate below ambient temperature typically at 5^{o}C as compared to traditional MED at 40^{o}C. This not only reduces the corrosion chances but also increases the distillate production to almost 2-3 folds as compared to traditional MED systems. Kyaw Thu at.el. [143] conducted the simulation of MEDAD cycle and compared the results of MEDAD cycle with conventional MED system. They found that with same heat input, water production increased up to two folds by hybridization of MED with AD.

The advantages of MEDAD system can be summarized as follows:

- It breaks the bottom brine temperature (BBT) temperature limit of conventional MED last stage from 40^{o}C to 5^{o}C. This increase in temperature gap between heat source and last stage helps to insert more number of stages that increase distillate production to almost three fold.
- Water production increased 2.5 to 3 fold as compared to the conventional MED desalination plant.
- Low grade waste heat can be utilized to operate the system.
- Ambient energy can be harnessed in the last stages operating below ambient temperature.

- Salt concentration can be as high as 120,000ppm in the last stages of MED because of the low operating temperature.
- Significant increase in system performance.

Although this novel desalination cycle has great potential for future desalination, there is a dearth of literature data about it. Only a few articles based on simulation results are available. There is no real experimental data available to confirm the simulation results. It is very important to investigate the performance of the system in detail and provide the data for future installations. In this thesis the detailed design and experimental results are presented of a three stage MEDAD hybrid desalination system. This system is installed in the National University of Singapore and details of the setup are discussed in the following chapters of the thesis.

Chapter 3 Falling Film Heat Transfer Coefficient Correlation Development

In process industries such as the refineries, food and desalination plants, the need of high performance evaporators is paramount to minimize irreversibilities due to high heat transfer as well as to reduce footprint area of associated components. A falling film evaporator is one of the key design components which are associated with not only high heat transfer rates but also being immune to change in feed qualities. In particular, for present desalination application, the falling film evaporative process could augment heat transfer rates involving brines which inherently reduce the equipment cost because of compact design.

In this chapter, a horizontal tube falling film evaporator is studied for low temperature applications particularly for the desalination industry. The first part of this chapter focuses on advantages of horizontal tube falling film evaporators over flooded evaporators and vertical tube evaporators and its applications. In the second part of the chapter, a literature review on falling film evaporation heat transfer coefficient (FFHTC) to the extent necessary for this work is provided. A novel FFHTC for low temperature (below ambient) applications and for different salt concentrations is developed in the third part of this chapter. The comparison of proposed correlation with traditional Han and Fletcher [144] correlation and the effect of different operational parameters on heat transfer is discussed in the last section of the chapter.

3.1 Background

Flooded evaporators have been used in desalination industry for long time. Recently, there is a thrust of horizontal tubes falling film evaporators over the flooded evaporators because of their advantages. They also replaced the vertical tube evaporators because of its unique characteristics. Falling film evaporators in general, are highly responsive to operational parameters such as energy supply, pressure levels, feed rate and salt concentrations in the feed. The fact that falling film evaporators can be operated across small temperature differences make them amenable to the application in multiple effect configurations. The advantages of falling film evaporators are outlined in the section below.

3.2 Advantages of Falling Film Evaporators

The main advantages of falling film evaporators over flooded evaporators are:

1. High heat transfer coefficient and resulting compact design.
2. More uniform overall heat transfer coefficient value across the tube bundle.
3. Reduction in working fluid requirement to about 1/3 as compared to flooded evaporators.
4. Short product contact times, typically just a few seconds per pass.
5. Minimization of salt deposition on tubes surface that helps in cleaning the tubes.

The potential advantages of horizontal tube evaporators over vertical tubes evaporators are:

1. Heat transfer coefficients for horizontal tubes are higher than those for vertical tubes since the heated flow length is much shorter.

2. External enhancements are available for tubes in copper, copper-nickel and stainless steel etc. for up to a 10 fold increase in evaporation coefficient.
3. A horizontal tube bundle can have multiple tube passes of the heating fluid to significantly increase its heat transfer coefficient as compared to vertical tubes evaporators with single pass.
4. A larger L/D ratio horizontal shell evaporator can be designed as compared to small L/D ratio of vertical evaporator that helps to prevent the dry out and flooding in the tubes.
5. The two pass (U-tube) design in horizontal tube evaporators is much more efficient, cheaper and easier to maintain compared to the single pass floating head in vertical tubes.
6. Flow length of liquid film in a horizontal tube evaporator minimises the liquid holdup time and residence time during operation.
7. Horizontal tubes bundle arrangement reduces the unit height that helps to reduce the piping work.
8. Horizontal arrangement reduces the footprint for large capacity plant because the evaporators can be arranged in double tier arrangement.

Although the horizontal tubes falling film evaporators have advantages over flooded and vertical tubes evaporators, the main limitation is the lack of heat transfer data particularly at low temperature i.e. below 323 K.

3.3 Heat Transfer Review for Falling Film Evaporators

A critical appreciation of the thermal performance is essential for the optimum design of falling film horizontal tube evaporators especially for desalination industry. A large number of empirical and theoretical heat transfer coefficients correlations are available in literature. The majority of those available correlations are for different refrigerants and few of them are for pure water and limited to saturation temperatures more than 323 K.

Many researchers provided the detailed overview of available correlations. A critical review is published by Ribatski and Jacobi [145] who tabulated the heat transfer correlations in terms of dimensionless numbers as developed by many researchers. They also provided heat transfer coefficient values for water and different refrigerants with single tube and multi tube evaporators. They concluded that every correlation has a limited validation governed by operating parameters under which they developed and efforts are needed to generalize these correlations. Adib et. al. [146] conducted the experiment with vertical tube falling film evaporator and they calculated the heat transfer coefficient value using correlation available in literature [147-151] and found good agreement with experimental results. Uche et al. [152] compared the heat transfer correlations at different inlet brine temperatures and for different mass velocities for horizontal and vertical tube evaporators. They also compared their results with different available correlations [144,153-157] and found that Parken correlation can be used for non-boiling conditions and Han and Fletcher's correlation is good for boiling conditions. A falling film evaporation analytical

model is developed by Fujita et. al. [158-160] using R-11 and they analysed the drip pattern, droplets and sheet modes. They found that accuracy of their model is within ±20%.

Table 3.1 summaries heat transfer correlations of many researchers found in the literature. This table also highlights the limitations of applications of these correlations such as the types of working fluids, pressures and the temperature ranges and evaporator geometry.

Since operational and design parameters are the key factors to maximize the evaporator performance, so researches are provided an extensive data on it. Film modes are controlled by Film Reynolds numbers and different heat transfer coefficient behaviours are noticed by researchers for smooth tubes as Reynolds number changes [161-165]. They observed three kinds of behaviour such as: 1) heat transfer coefficient decrease to its minimum value and then increase again, 2) it increase with Reynolds number and 3) heat transfer coefficient increases to its maximum value and then drop. Lorenz and Yung [166] investigated that film evaporation on a single tube is different to an array of tubes and it may be due to turbulence of inter-tube evaporation. They also found that critical Reynolds number affects the evaporation heat transfer and for below 300, the heat transfer coefficient value for a single tube is higher as compared to an array of tubes. Thome et. al. [167] conducted the experiments for falling film heat transfer coefficient for four types of tubes such as plain, turbo-BII HP, Gewa-B, and high-flux tubes. They concluded that

for different inter-tube flow modes there is no discernible difference in heat transfer coefficients in respective flow zone. Fujita et al. [168] investigated that the heat transfer value is low on the top row of tubes which is due to direct expose to feed supply. They also investigated the effect of feeder type on heat transfer coefficient. They used refrigerant R-11 on horizontal tube evaporators. Liu et al. [169] performed falling film heat transfer experiments for different tubes surfaces and they concluded that the value is 3 to 4 folds higher for roll-worked tubes as compared to smooth tubes. They also found that both the flow conditions and tubes spacing has negligible effect on the heat transfer coefficient. G. Aly et al. [170] conducted the tests for deposit film thickness effects and they found drastic decrease in heat transfer with increase in deposition thickness. Moeykens et al. and Chang et. al. [171-173] performed falling film experiment tests for R-123, R-134a, R-22 and R-141b and they found that it can be enhanced by adding the collection tray under each tube row. The falling film correlations developed by researchers [174-177] for refrigerants R-22, R-123, R-134a and R-141b is having uncertainty of 20-25% by using four different apparatuses. K. Bourouni et at. [178] performed the experiments with aero-evaporator and they reported that increase in characteristic dimensions of heat exchanger results in a significant increase in the evaporative performance. Yang & Shen [179] found that the heat transfer coefficient is a strong function of heat input and increases with heat input. The vapor flow effect due to liquid drag and dry out of tubes is studied by Ribatski and Jacobi [180]. The effect of dynamics of film on heat transfer is investigated by Xu et al. [181] and Yang and Shen [182]. They found that increase in liquid load causes perturbation in film that enhances the heat

transfer. They also reported that increase in tube diameter does not favor heat transfer which can be due to more turbulence in film on smaller diameter tubes. For horizontal tubes falling film evaporators, Han & Fletcher [144] is the most famous correlation where as Chun & Seban [183] is used for vertical tube. Both of these famous correlations are for pure water and for saturation temperatures of 322K or more.

Table 3.1 **Review of heat transfer coefficient correlations for different evaporator design and operation conditions**

References	Correlation
Xu et al. [184]	$h_{evaporation} = 05.169\times10^{-11}.\left[\frac{h_{fg}.g.\rho_l^2.D^2}{\Delta t^2.\mu_l}\right]^{-0.333}\left(\frac{\bar{\delta}}{D}\right)^{-0.422\Delta t^{0.503}}.\left(1+\frac{\delta_{max}-\delta_{min}}{\bar{\delta}}\right)^{5.708}$ Deionized water, 50 ^{0}C, Horizontal copper tubes evaporator.
Fujita et al. [185]	for 1st tube: $Nu = \left(\left(\mathrm{Re}_f\right)^{-2/3} + 0.008\left(\mathrm{Re}_f\right)^{0.3}\left(\mathrm{Pr}\right)^{0.25}\right)^{1/2}$ For 2nd to 5th tubes: $Nu = \left(\left(\mathrm{Re}_f\right)^{-2/3} + 0.01\left(\mathrm{Re}_f\right)^{0.3}\left(\mathrm{Pr}\right)^{0.25}\right)^{1/2}$ Freon R-11, Electrically heated five horizontal copper tubes , OD-25mm
Han and Fletcher [144]	$h_{evaporation} = 0.0028.\left[\frac{\mu_l^2}{g.\rho_l^2.k_l^3}\right]^{-0.333}\left(\mathrm{Re}_\Gamma\right)^{0.5}\left(\mathrm{Pr}\right)^{0.85}$ Pure water, 49 to 127 ^{0}C, Electrically heated single horizontal tube, OD-50.8 mm, thickness-1.7 mm, Length-254 mm
Bourouni et al. [178]	$h_f = 2.2.\left[\frac{\nu_f^2}{g..k_l^3}\right]^{-0.333}.\left(\frac{H}{OD}\right)^{0.1}.\left(\mathrm{Re}_f\right)^{-0.333}$ Pure water, 60 and 90 ^{0}C, Polypropylene horizontal tubes aero-evaporator , OD-25.4 mm,

Chun and Seban [183]	$$h_{film} = 0.821.\left[\frac{\mu_l^2}{g.\rho_l^2.k_l^3}\right]^{-0.333}(\mathrm{Re}_\Gamma)^{-0.22}$$ Pure water, 46 to 118 ^{0}C, Electrically heated single vertical tube, OD-28.58 mm, thickness-0.1 mm, Length-292 mm
Alhusseini et al. [186]	For laminar region: $$h^*_{laminar} = 2.65.(\mathrm{Re})^{-0.158}(Ka)^{0.0563}$$ For combine: $$h^* = \left(h^5_{laminar} + h^5_{turbulent}\right)^{1/5}$$ Propylene glycol and water
Shmerler et al. [187]	$$h^*_E = 0.0038.(\mathrm{Re}_\Gamma)^{0.35}(\mathrm{Pr})^{0.95}$$ Pure water, Electrically heated single vertical tube, OD-25.40 mm, Length-781 mm
Chien et al. [188]	$$Nu_{cv} = 0.0386.(\mathrm{Re}_\Gamma)^{0.09}.(\mathrm{Re}_\Gamma)^{0.986}$$ R245fa, 5 and 20 ^{0}C, Horizontal smooth tubes.

It can be seen from the above discussion that Han and Fletcher's correlation is most frequently used for film boiling on horizontal tubes. This correlation is developed with pure water evaporating at temperatures 322 K and above. There is a lack of data for evaporative film boiling typically below ambient condition. The boiling data pertaining to saline solution of 15000–90000 mg/l or ppm is also scarce, and yet these conditions are particularly important for the designing of falling film evaporators for desalination plants such as: multi effect desalination (MED) and multi stage flash evaporation (MSF). Many manufacturers of MED and MSF plants, perhaps due to competition reason, are not revealing their proprietary film boiling data at these conditions. Thus, there is motivation to develop a new correlation for horizontal tube falling film evaporators operating at low pressures, typically from

0.93 to 3.60 kPa where the corresponding saturation temperatures are 279 to 300 K. This lacuna sets the agenda for the work reported in here.

3.4 Falling Film Heat Transfer Coefficient Development

The methodology used here is to adopt Han and Fletcher's correlation for film boiling on horizontal tubes and to enhance its use by incorporating the effects of salinity and by expanding the range of temperatures of its application for horizontal tubes falling film evaporation.

3.4.1 Theoretical Model

The non-dimensional terms in Han and Fletcher correlation model namely: the Reynolds, Prandtl and Nusselt numbers are adequate to describe the surface evaporation from liquid film due to thermal effect. At low saturation pressures the vapor specific volume rapidly increases and this could possibly leads to enhancement of heat transfer. Han and Fletcher model is revisited to capture this additional heat transfer enhancement phenomenon. At a low saturation temperature the micro bubble generated at tube surface can lift up quickly because of high specific volume and break through the thermal barrier within liquid film. The traditional heat transfer models are unable to define this augmentation of heat transfer enhancement by buoyancy fortified bubble agitation.

The Han and Fletcher correlation given in Table 1 can also be expressed in a more familiar form as shown in Equation 3.1:

$$\frac{h_{evap}\left(\frac{\mu_l^2}{g\rho_l^2}\right)^{1/3}}{k_l} = Nu = 0.0028\left(\mathrm{Re}_{\Gamma}\right)^{0.5}\left(\mathrm{Pr}\right)^{0.85} \tag{3.1}$$

where indices and the constant term are found for the boundary conditions of film boiling. For the determination of the overall heat transfer coefficient, the total heat transfer is computed via heat transferred to circulating water, i.e.,

$$Q_{in} = \dot{m}_{ch,w}\, Cp_{ch,w}\left(T_{ch,w}^{o} - T_{ch,w}^{i}\right) \tag{3.2}$$

Using the concept of log mean temperature difference (LMTD) and the saturation temperature of evaporator, the overall heat transfer coefficient ($U_{overall}$) of the evaporator can be expressed as:

$$UA_{overall} = \frac{\dot{m}_{ch,w}\, Cp_{ch,w}\left(T_{ch,w}^{out} - T_{ch,w}^{in}\right)}{\left\{\frac{(T_{ch,w}^{out} - T_{sat}) - (T_{ch,w}^{in} - T_{sat})}{\ln\frac{(T_{ch,w}^{out} - T_{sat})}{(T_{ch,w}^{in} - T_{sat})}}\right\}} \tag{3.3}$$

The local falling film heat transfer coefficient on film side (h) is deduced from the knowledge of the resistance due to chilled water flow inside the tubes which is calculated by the Dittus-Boelter correlation given in Equation 3.4.

$$Nu = 0.023\,\mathrm{Re}^{0.25}\,\mathrm{Pr}^{n} \tag{3.4}$$

The pipe wall resistance (stainless steel 316) is negligible due to small thickness (0.7 mm). The evaporation heat transfer coefficient is calculated by using overall heat transfer coefficient given in Equation 3.5.

$$\frac{1}{UA} = \left(\frac{1}{hA}\right)_{tubeside} + R_{wall} + \left(\frac{1}{hA}\right)_{outside} \tag{3.5}$$

The experimental program is planned for capturing the two unknown parameters in above Equation 3.5.

3.5 Experimentation

3.5.1 Experimental Apparatus

Adsorption desalination (AD) plant existing in Air-conditioning Laboratory is used to conduct the experiments. Figures 3.1 and 3.2 show the AD plant installed in NUS and plant operational schematic.

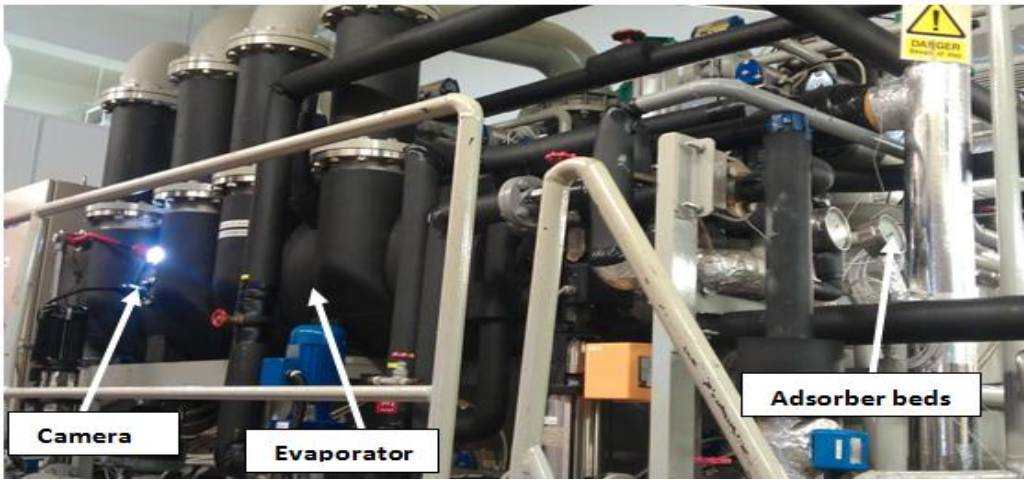

Figure 3.1 Pictorial view of adsorption desalination plant installed in NUS

There are five main components of AD plant namely: 1) evaporator, 2) adsorber/desorber beds, 3) condenser, 4) conditioning facility and 5) pre-treatment facility. The evaporator shell and tubes are fabricated with stainless steel and are arranged horizontally details of which is shown in Figure 3.3.

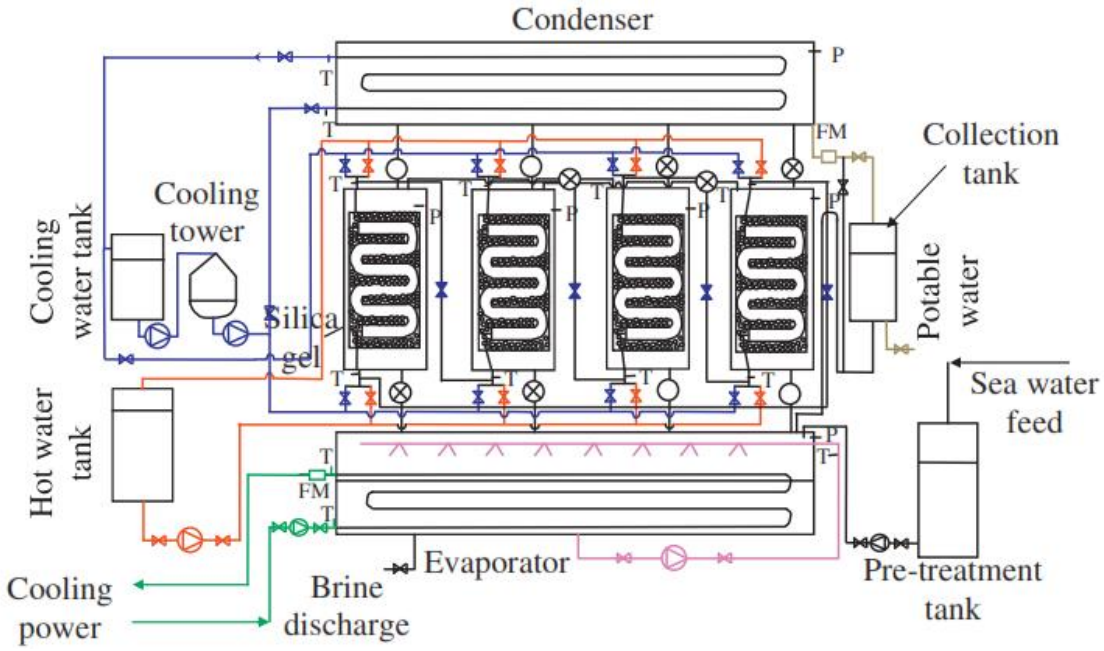

Figure 3.2 Detailed operational schematic of adsorption desalination plant

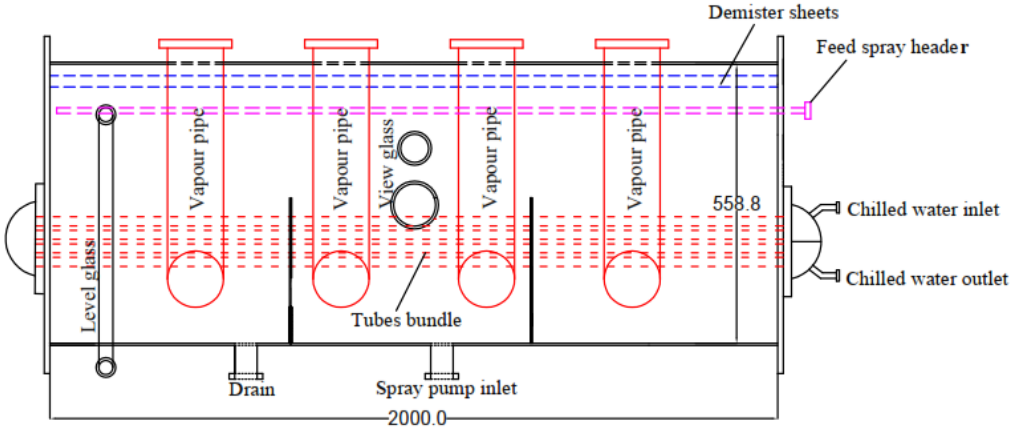

Figure 3.3 Adsorption desalination cycle evaporator detailed design

The evaporator tubes are arranged in four rows with 12 tubes in each row. This evaporator is 4-pass using a "water box" arrangement at the ends of the heat exchanger. Special profiled tubes are used in evaporator to enhance the heat transfer. The details of the tube are shown in Figure 3.4.

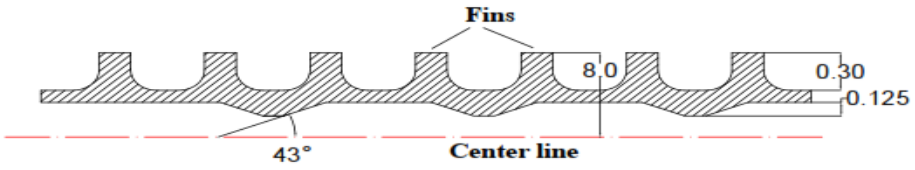

Figure 3.4 **Cross section of end-cross tube used in evaporator of adsorption desalination plant**

A precise electrical thyriator controller is installed to supply the chilled water to evaporator at constant inlet temperature. This thyristor maintains the temperature fluctuations at inlet of coolant water to less than ±0.15K. The chilled water supply is regulated at 48 l/min. Since experiments are conducted at different salt concentrations and constant salt concentration condition in evaporator is maintained by re-circulation the condensate back to evaporator via U-tube. To maintain a constant liquid film on tube surface, a spray pump is used to discharge fine water droplets (nominally 0.1 to 0.15 mm diameter) through nozzles on top of tube bundle. The design parameters of evaporator are given in Table 3.2.

Table 3.2 **Design parameters of adsorption desalination system evaporator**

Parameters	Values	Units
Number of tubes	48	
Length of each tube	1900	mm
Tube outer diameter	16	mm
Tube thickness	0.7	mm
No of passes	4	
Shell diameter	558.8	mm
Shell length	2000	mm

3.5.2 Experimental Procedure

Experimental procedure can be categorized into operation of individual components namely: 1) evaporator, 2) Vacuum system, 3) adsorber/desorber and 4) condenser.

The evaporator operation can be divided into two circuits namely: 1) feed water circuit and 2) chilled water circuit.

Feed water circuit: The seawater/feed first enters into a pre-treatment facility to remove particulates and suspensions and then to the de-aeration tank to de-aerate. In the de-aeration tank, the dissolved non-condensable are removed before the feed enters to AD evaporator. The de-aerated feed is then pumped into the evaporator via feed pump. A spray pump is installed with evaporator to spray the feed on to the tube bundle via spray nozzles. This is special magnetic pump that can operate in vacuum environment. The reflux from condenser maintains the salt concentration level inside the evaporator. This feed water line is provided with flow meter and valve to regulate the feed flow.

Chilled water circuit: The chilled water is the heat source that is circulated inside the tubes of evaporator. An electrical heater is installed to maintain the coolant temperature. This heater is controlled by a thyristor controller to maintain its inlet temperature. Chilled water circuit is equipped with regulating valve and flow meter to adjust the flow rate such that the evaporator can be operated under different conditions. The operation parameters are given in Table 3.3.

Vacuum system: A water vapour tolerant vacuum pump is necessary since the operation of AD system is under vacuum. Prior running an experiment vacuum holding capacity of the system is tested for 36 hours and it is found that the vacuum leak is negligible. During an experiment vacuum pump helps to maintain the desired

saturation pressure inside the evaporator by pulling the air in case if ingress into the system. To ensure that the film on the tube surface is evaporating all the time, it is imminent to maintain the saturation temperature which is always lower than chilled water temperature inside the tubes.

Table 3.3 Operational parameters of adsorption desalination cycle

Parameters	Values	Units
Chilled water flow rate	48	LPM
Sea water flow rate (Γ)	1.1	LPM/m of tube length
Evaporator saturation temperature	279–300	K
Evaporator saturation pressure	0.93 – 3.60	kPa
Feed water salinity range	15,000 – 90,000	ppm

Adsorber/desorber bed operation: The evaporator is connected to adsorber bed filled with silica gel via pneumatic valves to adsorb the water vapor. The adsorption of water vapor sustains the continuous evaporation in the evaporator. The heat of adsorption is removed by circulation of cooling water inside the adsorber coolant flow channel.

Similarly a desorber bed is connected to a condenser and heat of desorption is supplied by a heater controlled by a thyristor controller.

Condenser operation: The desorber bed is connected to a condenser where the desorbed vapors are condensed on shell side. The cooling water circulated through the tubes of condenser is regenerated in a cooling tower at roof top.

The apparatus is fully instrumented to capture all required data. A Yokogawa pressure transmitter of range 0-60 KPa abs. (accuracy ±0.25%) is installed on the

evaporator for saturation pressure readings. The OMEGA 5kΩ type thermistors (accuracy ±0.15 K) are used for all temperature measurements. The KROHNE Flow meters (accuracy ±0.5% of reading) are used for flow measurements. All temperature, pressure and flow readings are continuously monitored by a data logger unit at intervals of one minute.

A high speed camera is installed on the evaporator to observe the film behavior over the tubes. It is observed that there is ample turbulence in liquid film on the tubes due to bubble formation on tube surface. The evidence of film turbulence is captured by camera shown in Figure 3.5 and more clear explanation by a film model is also presented.

There is a natural temperature gradient within liquid film on the tubes and the micro-bubble generation on tube surface agitates the liquid film when it tries to break through the thermal barrier. The micro-bubble generation and agitation phenomenon is explained in Figure 3.6. This bubble agitation has two useful effects: firstly, it breaks the thermal barrier between the liquid film and tube surface that enhances the local heat transfer coefficient and secondly, when a micro-bubble moves up to the tube surface due to its very high specific volume it also draw the heat from tube surface which further helps to enhance the heat transfer. An additional benefit is agitation within the liquid film due to the bubble movement.

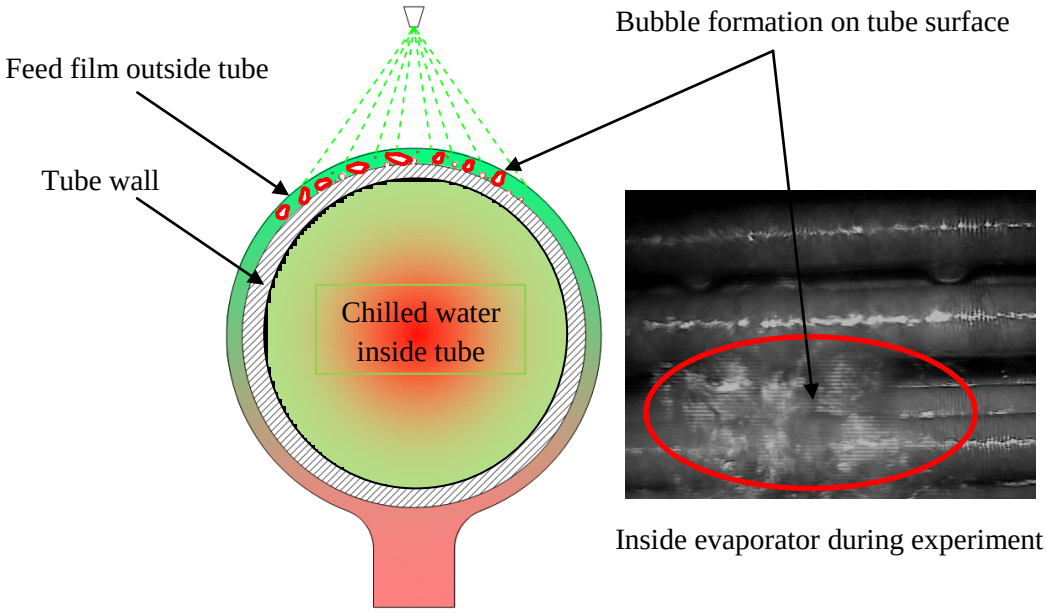

Figure 3.5 **Bubbles formation in liquid film on tube surfaces and film agitation effect captured by camera**

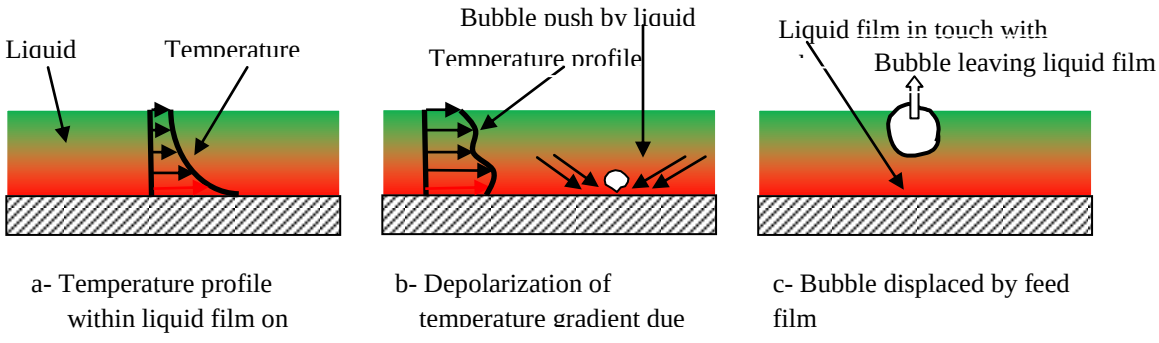

Figure 3.6 **Film agitations due to bubbles movement and effect on conventional thermal gradient**

3.6 Results and Discussion

Figure 3.7 shows the experimental overall heat transfer coefficient values. The heat source temperatures vary from 10 to 40^{0}C and salt concentration is 45000 ppm. It can be seen from the results that overall heat transfer first drop with increase in chilled water temperature and then increase again at 40^{0}C. A similar overall heat transfer trend is observed for 60000ppm (60ppt) salt concentration as shown in Figure 2.8.

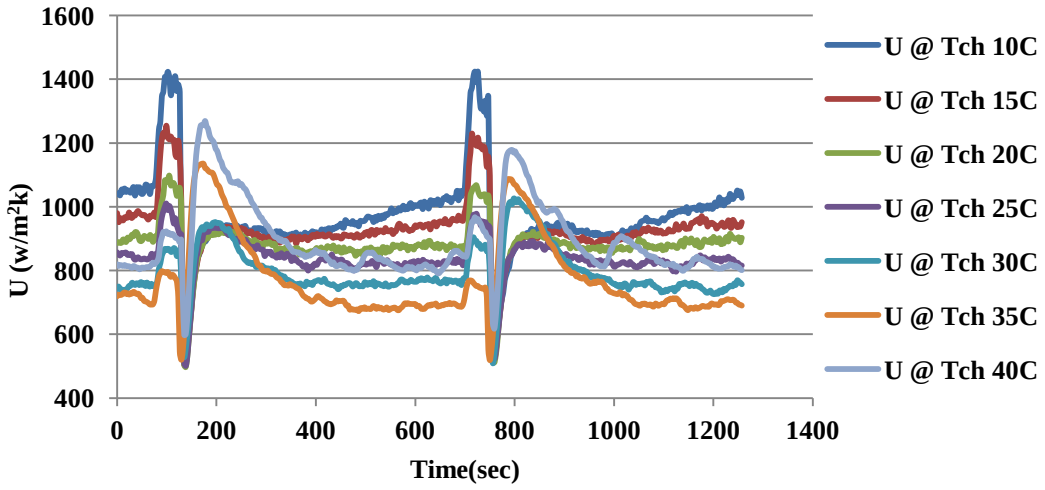

Figure 3.7 **Typical experimental overall heat transfer coefficient profiles at 45000 ppm salt concentration**

.

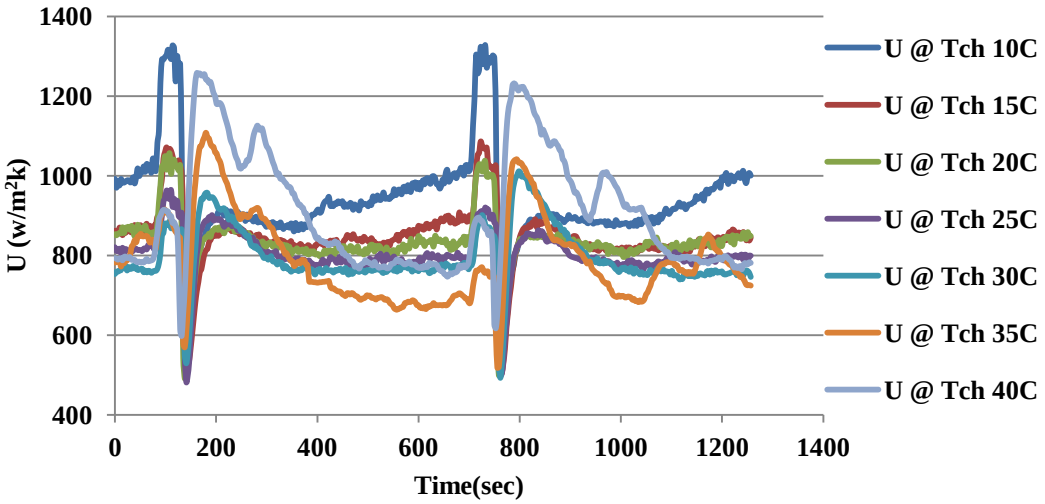

Figure 3.8 **Typical experimental overall heat transfer coefficient profiles at 60000 ppm salt concentration**

The saturation temperature of evaporator and overall heat transfer coefficient values from experimental data at different chilled water inlet temperature and at different salt concentration are tabulated as shown in Table 3.4.

Table 3.4 Experimental overall heat transfer coefficient values and different saturation temperatures and at different salt concentrations

Salinity	$T_{ch,in}$ C	T_{evap} C	U W/m^2K	Salinity	$T_{ch,in}$ C	T_{evap} C	U W/m^2K
15000	**10**	5.9	1025.45	**60000**	**10**	5.9	937.61
	20	13.1	953.28		**20**	13.3	833.69
	30	20.3	885.17		**30**	19.7	776.62
	40	27.3	963.33		**40**	26.2	896.47
30000	**10**	5.9	998.31	**75000**	**10**	5.9	848.06
	20	13.1	920.78		**20**	13.0	751.47
	30	19.7	853.40		**30**	19.6	733.78
	40	25.7	906.96		**40**	26.9	893.53
45000	**10**	5.6	970.78	**90000**	**10**	5.5	815.94
	20	12.9	881.81		**20**	12.9	728.17
	30	19.3	798.17		**30**	19.3	694.79
	40	25.1	895.15		**40**	27.3	898.97

The evaporative heat transfer coefficient is calculated from experimental overall heat transfer coefficient by formulation as explained in theoretical model section. Figure 3.9 shows the three dimensional plot of evaporative heat transfer coefficients for assorted evaporator saturation temperatures and salinity level.

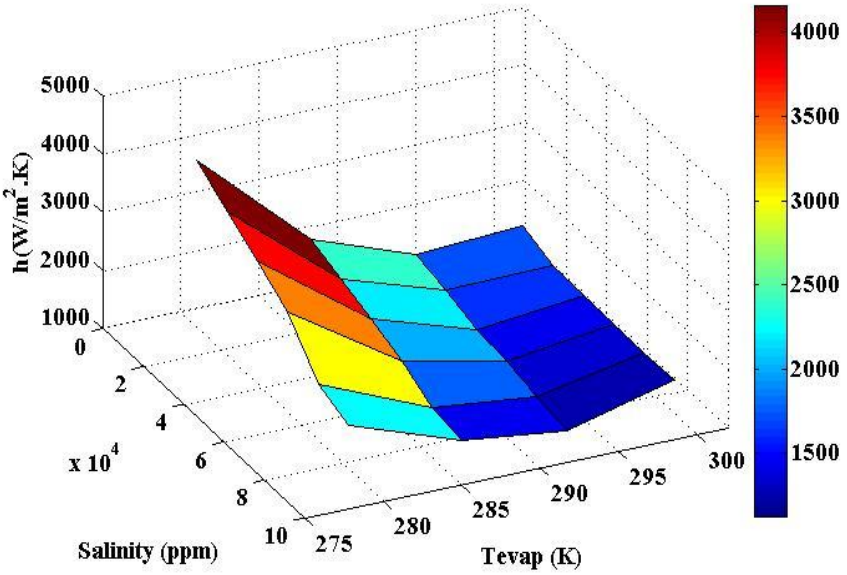

Figure 3.9 **Experimental film evaporation heat transfer coefficient profiles at different saturation temperature and different salt concentrations**

It can be seen from the plot that the heat transfer coefficient varies with saturation temperature and with salt concentration. It can be observed that at any salt concentration, it approaches the minimum value at 295 K and then with further decrease in saturation temperature the evaporation heat transfer coefficient value increase very sharply. It is also observed that specific volume of vapor increases very rapidly below at 295 K and above that temperature the change in specific volume of vapor is very small as shown in Figure 3.10.

It can be concluded that the sharp increase in evaporator heat transfer coefficient below 295K may be due to bubble agitation. The micro-bubble produced on the tube surface from within the liquid film moves up quickly due to its very high specific volume and breaks the thermal barrier due to film agitation. This unique phenomenon is called “bubble assisted evaporation”.

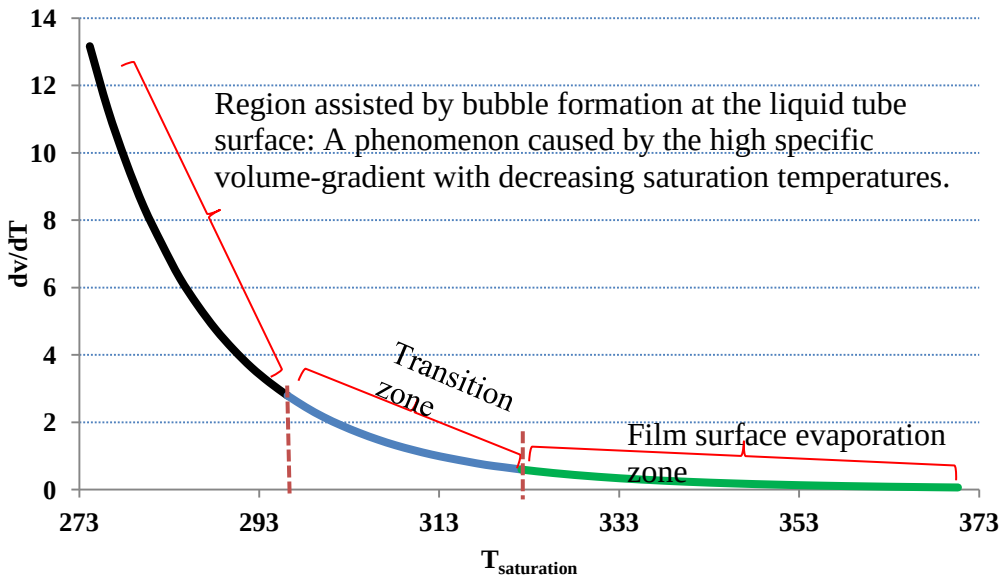

Figure 3.10 Change in vapor specific volume with saturation temperature

In film evaporation, "micro-bubble agitation" plays an important role to enhance the heat transfer by reducing the thermal resistance between the liquid and tube surface barrier (model is shown in Figure 3.6). The traditional falling film evaporation heat transfer coefficient correlations (i.e. Han and Fletcher) do not capture this unique phenomenon and only capture the thermal driven film evaporation at saturation temperatures greater than 322 K.

A new falling film heat transfer coefficient with inclusion of "bubble assisted evaporation" for application at low saturation temperatures is proposed based on the experimental data. The operational parameters namely: film velocity, salt concentration and heat flux are also included as additional parameters in the new correlation. In addition, to capture the effect of vapor specific volume, the gas volume term is also incorporated. The new correlation is given in Equation 3.6.

Figure 3.11 shows a comparison of Equation 3.6 against the experimental data. It can be seen that new correlation has good agreement with experimental result. The measured heat transfer coefficient from experimental data has uncertainty of less than 8%. The RMS error of regressed data is 3.5%. The additional terms used in the proposed correlation permit the limits of salinity and temperature to be accounted for, and a reference temperature, T_{ref} is taken as the reference temperature to match the region of Han and Fletcher.

Thermally driven evaporation

$$h_{evap} = \left[0.277 \left[\frac{\mu_l^2}{g.\rho_l^2.k_l^3} \right]^{-0.333} (\mathrm{Re}_\Gamma)^{-2.11} (\mathrm{Pr})^{4.55} \left[2.\exp\left(\frac{S}{S_{ref}} \right) - 1 \right]^{-0.41} \left(\frac{T_{sat}}{T_{ref}} \right)^{14.70} \right] + \underbrace{\left[0.885. \left(\frac{q}{\Delta T} \right)^{1} . \left(\frac{v_g}{v_{ref}} \right)^{-0.34} \right]}_{\text{Bubble assisted evaporation}} \tag{3.6}$$

The above correlation is suitable for sub-atmospheric conditions from 0.93 to 3.60 kPa (corresponding to saturation temperatures 279 to 300 K) and feed water salinity ranges from 15,000 to 90,000 ppm. The film Reynolds number ranges 45< Reᴦ <90 and Prandtl number ranges 5< Pr <10. In proposed superposition of effects in correlation, the first term is for film surface evaporation thermally driven and the second term is due to enhancement by the bubble assisted boiling effect.

The proposed falling film heat transfer coefficient is compared with Han and Fletcher correlation extrapolated to a region outside its validation range. The Han and Fletcher correlation is for pure water. It can be seen from Figure 3.12 that Han & Fletcher correlation is only suitable for thermally driven surface evaporation for saturation temperature 322 K and above.

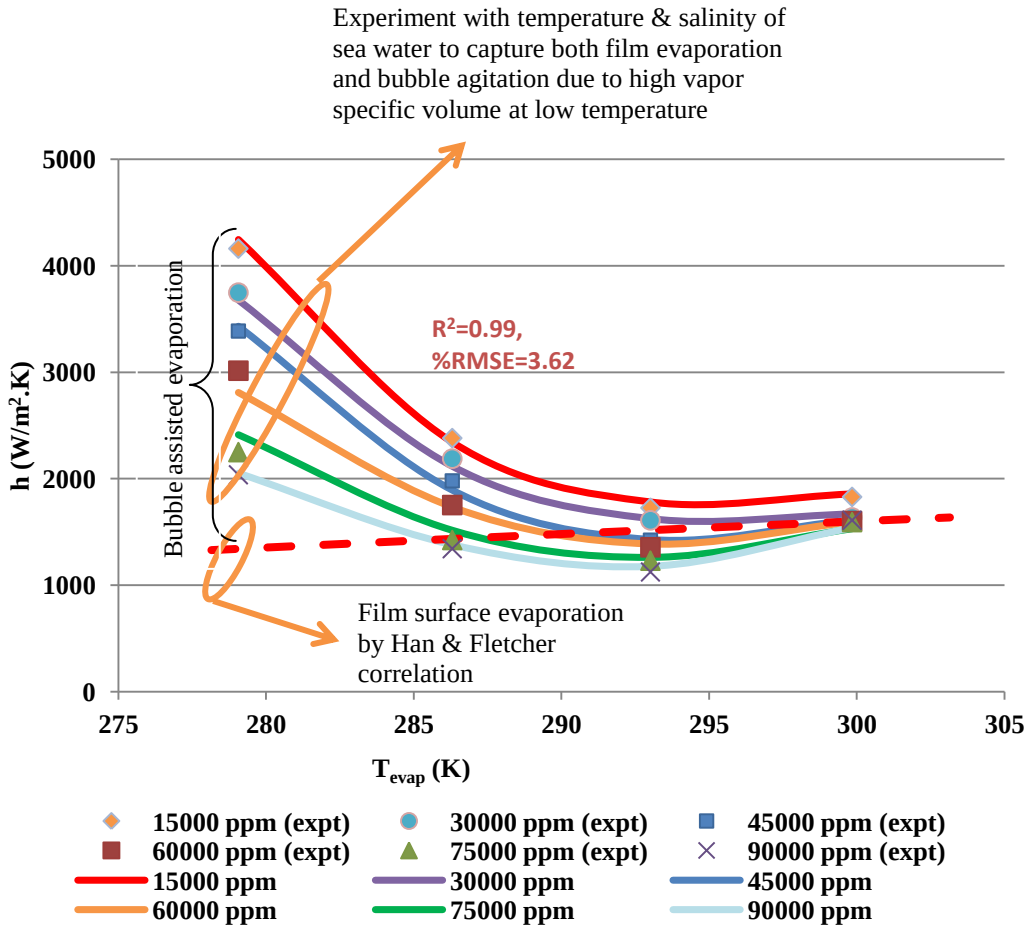

Figure 3.11 Falling film heat transfer coefficients values: experimental and proposed correlation

A unique feature of the present correlation is the capture of "bubble assisted evaporation" which boosts the heat transfer coefficient by two to three folds at low saturation temperature. This additional effect seems to be significant only at a low

saturation temperature 295K or below. As a consequence, for situations where cooling and desalination are required simultaneously the design of such an evaporator is likely to be more compact than at present.

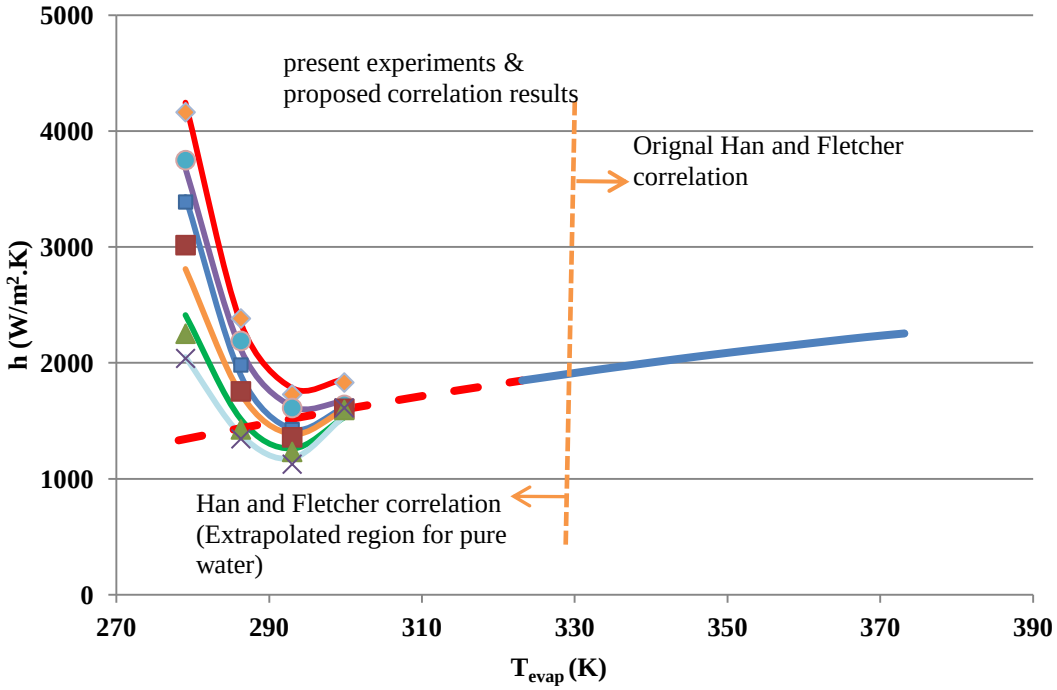

Figure 3.12 **Falling film heat transfer coefficient values: experimental and proposed correlation compared with Han and Fletcher correlation extrapolated region**

This proposed falling film heat transfer coefficient is very useful for design in the desalination industry. MED horizontal tubes falling film evaporators for low saturation temperature operation now can be designed using proposed correlation for better efficiency. This will be used in following chapters for MED theoretical model and experimental facility design to endorse the validity of correlation.

The effect of operational parameters namely: 1) salt concentration and 2) saturation temperature on heat input and LMTD are also investigated. Figure 3.13 shows the effect of these parameters on heat input. It can be seen that heat input increases with saturation temperature and it is due to increase in temperature difference of heat source. It can also be observed that salt concentration effect is negligible on heat input. Figure 3.14 shows the effect of saturation temperature and salt concentration on LMTD. It can be observed that LMTD also increases with saturation temperature which is due to higher temperature differences at high saturation temperatures.

The salt concentration effect is minimal as can be seen from plot. The measured accuracy of log mean temperature difference (LMTD) and the heat input (Q) is 8%.

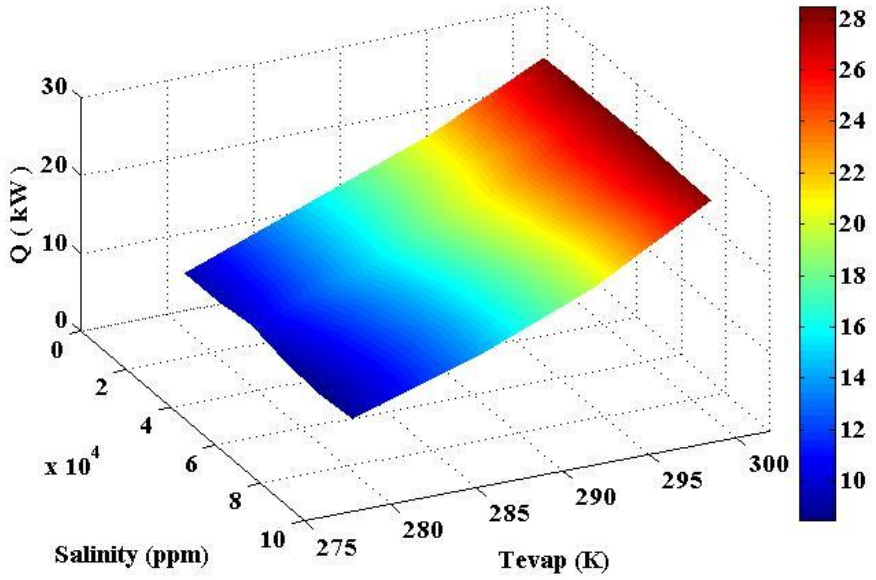

Figure 3.13 Effect of evaporator saturation temperature and feed salt concentration on heat input to evaporator

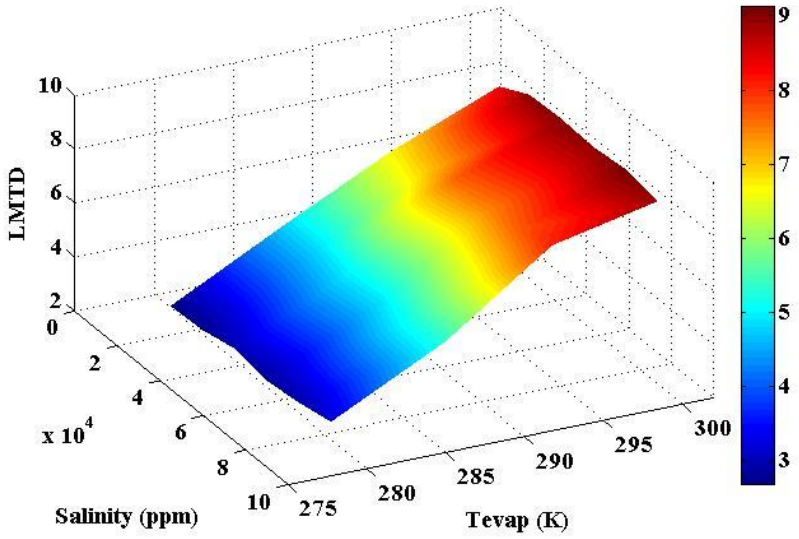

Figure 3.14 **Effect of evaporator saturation temperature and feed salt concentration on LMTD**

Summary of Chapter 3

Horizontal tube falling film evaporators can replace flooded and vertical tube evaporators because of their inherent advantages. Although horizontal falling film evaporators are advantageous, there is a lack of research data related to the heat transfer coefficient especially at low saturation temperatures less than 323 K. The heat transfer coefficient for low saturation temperature (typically in the zone of below ambient) and for a horizontal tube evaporator of special interest to desalination applications is essential.

Experiments are conducted to investigate the heat transfer coefficient for low saturation temperature of 279 to 300 K corresponding to pressure ranges of 0.93 to 3.60 kPa. Salt concentration in the evaporator is investigated in the range of 15,000 to 90,000 ppm. The heat transfer coefficient calculated from experimental data is plotted for different salt concentrations.

At low saturation temperatures, below 298K, the tendency for liquid film to flash into vapor is made easier by the rapid increase in the specific volume of vapor. For a given thermal gradient across the liquid film, the micro-bubble is readily generated at suitable nucleation sites, such as the grooved surfaces on the tubes. This conjecture of “bubble-agitation boiling” is backed up by photographic evidence which indicates the presence of micro-bubble generation beneath the liquid layer. The effect of micro-bubble during film boiling reduces the thermal barrier within liquid film which is responsible for enhancement of heat transfer. At low saturation temperature

the evaporation is by two mechanisms namely: thermally driven evaporation and bubble agitation assisted evaporation. The basic domain of validation of traditional Han and Fletcher correlation is now extended through to capture the bubble assisted evaporation. There is heat transfer enhancement due to bubble assisted evaporation that increases the heat transfer coefficient value from two to four fold.

A new falling film evaporation heat transfer coefficient is proposed with parameter regression including two basic mechanisms observed during experiments. The measured heat transfer coefficient from experimental data has uncertainty of less than 8%. The RMS error of regressed data is 3.5%.

The effects of operational parameters namely: salt concentration and saturation temperature on heat input and LMTD are also investigated.

The proposed correlation can be used for the designing of low pressure horizontal tubes falling film evaporators for process industry. This correlation will be used in following chapters for MED theoretical modeling and system design.

Chapter 4 Multi Effect Desalination: Modelling and Simulation

Multi effect desalination (MED) processes are used to produce potable and process water from sea and brackish water. In thermal desalination, MED processes are the most thermodynamically efficient and economical in terms of primary energy consumption. These processes can even operate with low grade waste heat and solar energy. MED processes are generally employed for medium to large scale capacities.

In this chapter, conventional multi effect desalination (MED) system is studied in detail especially for low temperature applications. An overview of conventional MED system is provided in first part of this chapter. The limitations of conventional plant operation are discussed in second part of this chapter. Comprehensive detail of MED system under investigation is provided in the third part of the chapter. In last part of this chapter mathematical modeling of MED main components namely: steam generator, MED stages, condenser and feed cooler is provided. System studied here is parallel feed, horizontal tube falling film evaporators. The simulation results are also discussed in the last part of this chapter where the system parameters plots are provided.

4.1 Background

Multi effect desalination processes are considered most energy efficient in thermal desalination systems [189, 190]. The other advantages are: 1) lower specific power consumption, 2) no chances of distillate contamination because the pressure of brine side is lower and 3) simple operation. In addition, MED system can also operate as hybrid system as investigated by many researches to enhance the system performance [191-200]. MED system can be categorized on following basis:

4.2 MED System Categories

4.2.1 On the Basis of Feed and Vapor Flow

Depending on the direction of brine and vapor flow, MED system can be classified as:

4.2.1.1 Forward feed system (FF)

4.2.1.2 Backward feed system (BF)

4.2.1.3 Parallel and cross feed system (PF/CF)

Salient features of each system are discussed below. The description of process with flow schematic is also discussed.

4.2.1.1 Forward Feed System (FF)

In the FF configuration, the vapor as well as the brine flow from higher pressure to lower pressure (1^{st} effect to last effect) [199-204] . A schematic of the FF system is shown in Figure 4.1.

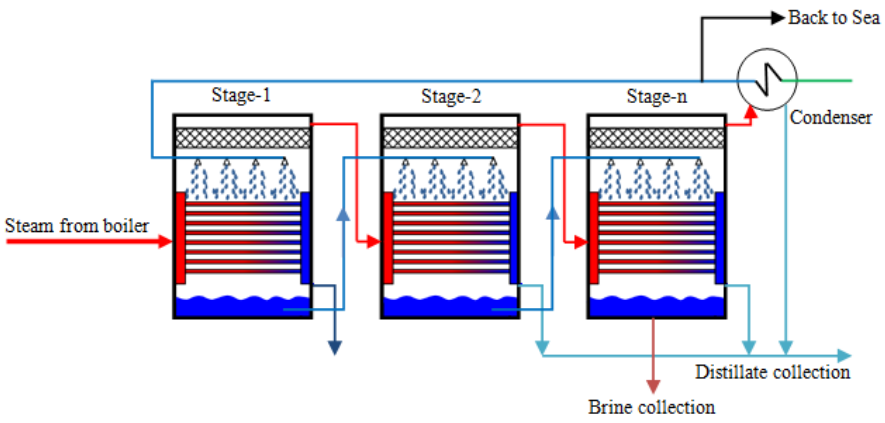

Figure 4.1 Typical flow schematic of forward feed MED system

Limitations of the FF system are: a) total feed has to be pre-heated to the saturation temperature corresponding to the pressure in the first effect before boiling commences that utilize the part of energy of heating steam, b) external heat exchangers for feed pre-heating are essential that increase the maintenance and capital costs and c) inter stage pumps are required to spray the feed to next stage that make the system bulky and complicated.

4.2.1.2-Backward Feed System (BF)

In the BF system, the feed flow is from last effect to 1st effect (i.e., low pressure to high pressure) while vapor flows in opposite direction [199-204]. The feed water flows through successive stages towards the first stage. The successive increase in the pressure and temperature across the effects dictates the use of brine pumping units between the effects. A schematic diagram of BF MED flow is shown in Figure 4.2. Major drawbacks of BF system are: a) inter stage feed pumps are required because the feed flows from low pressure to high pressure, b) the brine with the

highest concentration is subjected to the highest temperature in the system which would causes corrosion and scaling.

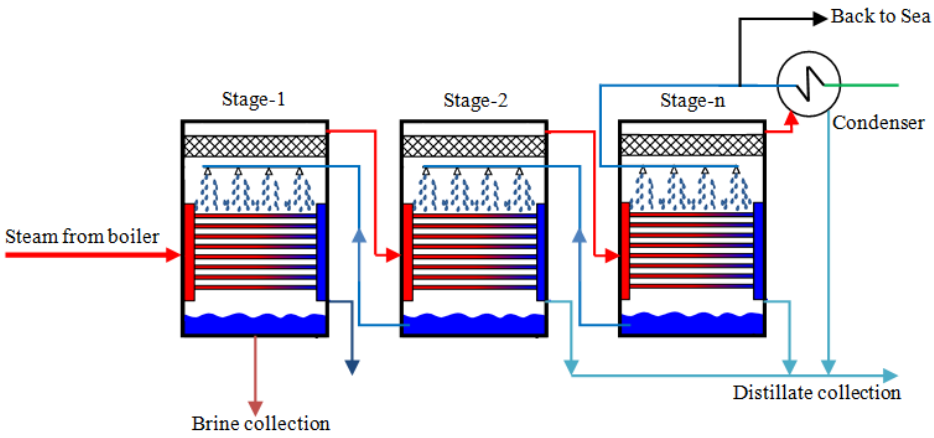

Figure 4.2 Typical flow schematic of backward feed MED system

4.2.1.3-Parallel & Parallel/cross feed system

In the parallel feed system, the vapor flows from 1st effect to last effect (nth effect) in the direction of falling pressure. The feed seawater flows from main header to individual effect in a perpendicular direction as shown in Figure 4.3 [199-204].

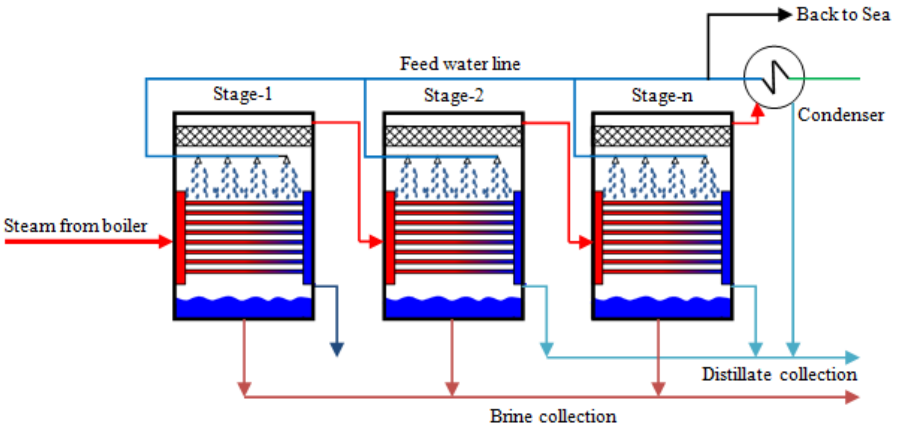

Figure 4.3 Typical flow schematic of parallel feed MED system

In parallel/cross flow, the brine stream leaving the first stage flows to the second, where it flashes and mixes with the feed seawater. The detailed schematic is shown in Figure 4.4.In this scheme intermediate pumps are not required. There is additional flash effect due to mixing of brine feed from previous high pressure effect. In addition, there is no need to pre-heat entire the feed to saturation temperature of 1st effect.

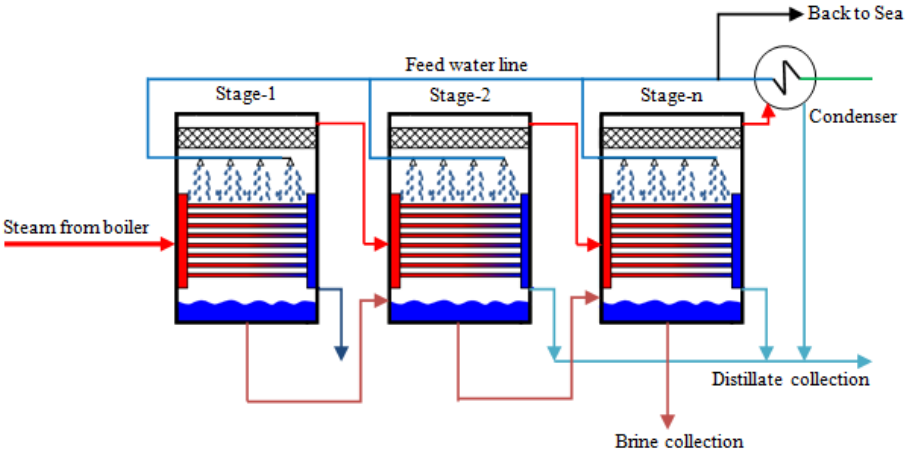

Figure 4.4 Typical flow schematic of parallel/cross feed MED system

4.2.2 On the Basis of Heat Exchanger Arrangement

On the basis of arrangement of heat exchanger, the two configurations have evolved for MED systems [205, 206]:

4.2.2.1 Horizontal stage arrangement

4.2.2.2 Vertically stacked arrangement

MED systems discussed in section 4.2.1 can be arranged horizontally or vertically. Table 4.1 shows the summary of MED configurations. It can be concluded from the above discussion and summary table that parallel feed system is the preferable MED

system as for as scaling and maintenance are concerned. Major MED plants such as: Trapani (8MIGD), Al-Taweelah (3.77MIGD) and Mirfa (2MIGD) are parallel feed arrangements [207].

Table 4.1 Review of MED different configurations advantages, disadvantages and limitations

Parameters for analysis	FF MED system	Backward MED system	Parallel feed MED system	
			Parallel feed system	Parallel/cross feed system
Vapor and brine flow	The flow direction of vapor as well as the brine is from high pressure to low pressure end i.e. from effect 1 to effect n.	The flow direction of vapor is from high pressure to low pressure end (effect 1 to effect n)and the brine flows in the opposite direction (effect n to 1)	The vapor flows from high pressure to low pressure, while the feed seawater flows in a perpendicular direction. The brine stream leaving the first stage does not flow to the second effect. Brine is separately collected from all effects.	The vapor flows from high pressure to low pressure effect, while the feed flows in a perpendicular direction. The brine stream leaving the first stage flows to the second, where it flashes and mixes with the feed.
Operating temperature	It can operate at high top brine temperatures because temperature is higher at one end and salinity higher at other end, El-Dessouky et al. (1998).	This system cannot operate at high top brine temperatures because the highest salinity exposes to highest temperature that increases the chances of corrosion.	The MEE-PF system can operate at high top brine temperatures because temperature is higher at one end and salinity at the other end.	The MEE-PF system can operate at high top brine temperatures because temperature is higher at one end and salinity at the other end.
Inter stage pumping units	Depending upon the arrangement of evaporators, feed pump may be required to pump the feed to next effect.	It requires intermediate pumping units between stages, since the brine flows from the low to the high pressure effects (effect n to effect 1).	Since the brine flows parallel to each effect so intermediate pumping units are not required.	Since the brine flows parallel to each effect so intermediate pumping units are not required.
Feed Pre-heating	All feed need to be pre-heated up to saturation temperature before entering to first effect	Feed enters last stage, no need to pre-heat whole feed up to saturation temperature of first effect.	Feed enter parallel to each effect so no need to pre-heat whole feed to 1st effect saturation temperature.	Feed enter parallel to each effect so no need to pre-heat whole feed to 1st effect saturation temperature.
Pre-heaters	Pre-heaters required pre-heating the feed.	Pre-heaters required pre-heating the feed.	Pre-heaters required pre-heating the feed.	Pre-heaters required for the feed.

Figure 4.5 displays the results of survey of MED plants operating in the World. It can be seen that top brine temperature (TBT) for conventional MED plants ranges from 60~70^{o}C and is limited by the "*soft scaling agents*" in feed water that may cause fouling and corrosion at high temperature [190, 202 and 207].

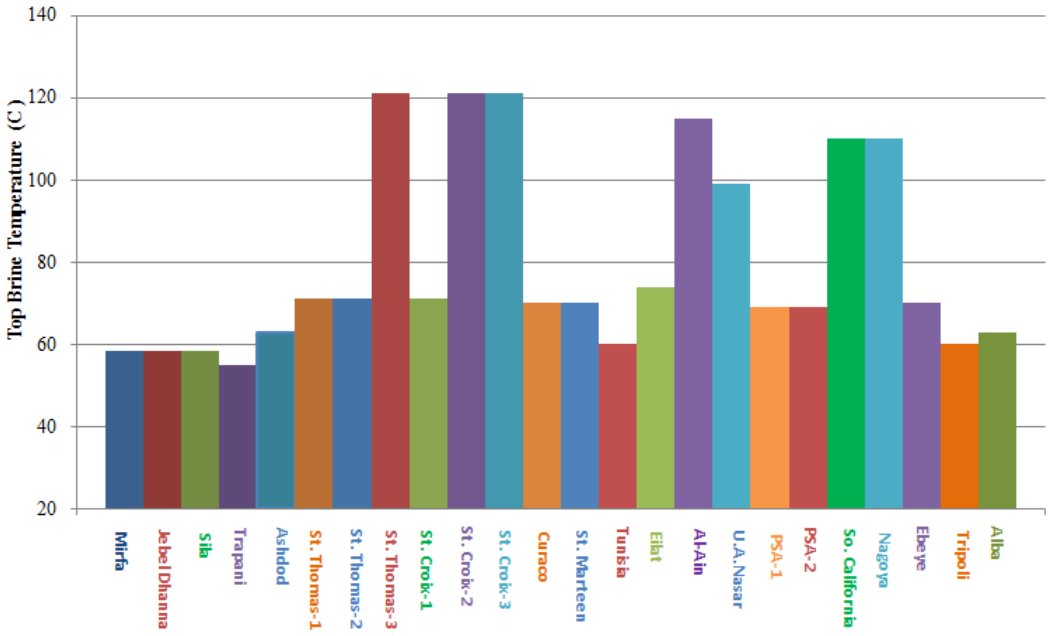

Figure 4.5 Review of top brine temperatures of some conventional MED plants installed in the world

Mittelman et. al [208] reported that specific heat transfer area and specific energy are two parameters affecting TBT of MED. They found that optimal TBT corresponding to minimum heat transfer area is in the range of TBT > 80^{o}C. MED operation above 70^{o}C may increase the capital cost of the system because of expensive material requirement for evaporator fabrication due to soft scaling components those are more active at higher TBT. The limitations of existing traditional MED plants are discussed in following section.

4.3 Conventional MED Limitations

The temperature difference between heat source and last stage is the maximum gap to operate for a conventional thermal desalination systems. In the case of conventional MED system, top brine temperature (TBT) and last stage temperature also called lower brine temperature (LBT) limit the operational temperature gap. This gap actually represents the number of vapor heat recoveries in term of number of stages as inter-stage temperature varies 1.5-3.0^{o}C. The operational gap concept of conventional MED system is shown in Figure 4.6.

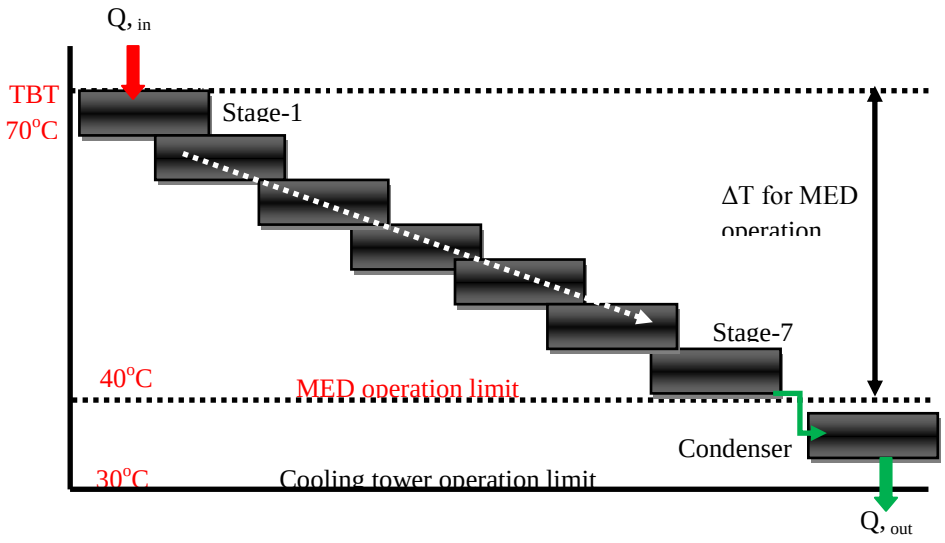

Figure 4.6 Conventional MED system operational limitations: limited operational temperature gap

MED TBT is controlled by dissolved salts also called "*soft scaling components*" that potentially contribute to system corrosion and fouling. Magnesium (Mg++), calcium (Ca++), and sulfate (SO) ions are the most contributing agents in system degradation and limit the MED TBT to 70^{o}C as compared to MSF 120^{o}C. Ca++ and Mg++ can develop calcium carbonate precipitates and magnesium hydroxide at high

TBT and affect the system performance. Researchers found that these "soft scaling" agents can be removed by using nano-filtration (NF) prior to introducing feed into the system. By using NF with MED, TBT can be raised to 130^{o}C [209-211] and this will help to introduce more number of stages with same heat input and hence system water production and performance will enhance.

Even though TBT can be increased by introducing the NF but LBT is limited by condenser operation and conventional MED system cannot operate below 40^{o}C. Figure 4.7 shows the operation temperature v/s salt concentration with respect to salt crystallization or metastable zone at elevated temperature and salt concentration of sea water [189, 202 and 204].

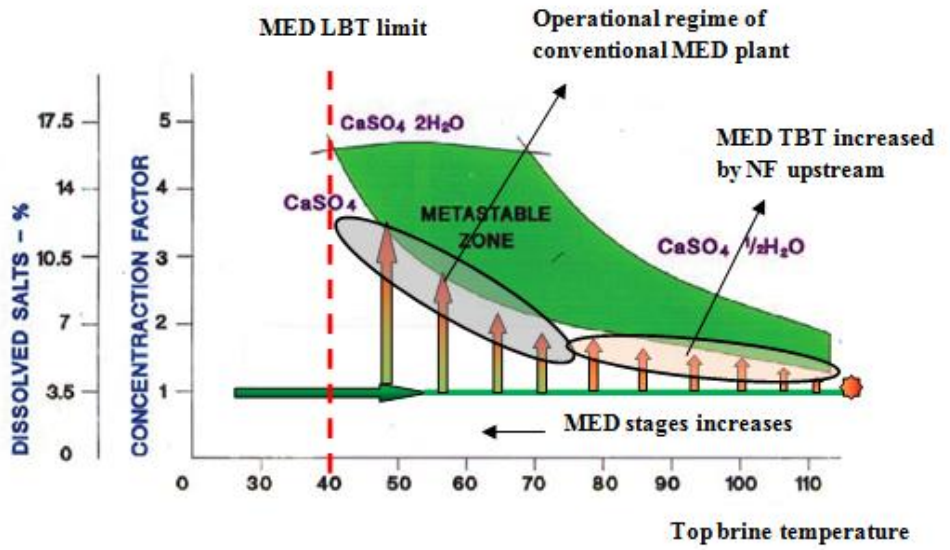

Figure 4.7 **Conventional low temperature MED and high TBT NF-MED operational regimes on salt crystallization curve**

The operational regimes of conventional MED system and MED-NF are highlighted and it can be seen that fouling and scaling is a strong function of temperature and salt concentration. In conventional MED, at steam generator end, concentration factor maximum value 1~2 limits the TBT temperature. On the other end, the last stage temperature is controlled by the cooling water condenser even though the concentration factor can be high due to low temperature. In other words, even when the total feed is pre-heated to the saturation temperature of steam generator, the recovery may still be limited by concentration factor at a higher temperature end and condenser limit at the lower end and hence limiting the system performance.

Due to high attraction of thermal systems especially in the Gulf and MENA region as explained in an earlier chapter, researchers are struggling to improve the thermal desalination system and several approaches have taken towards the improvement of multi effect desalination system. One major development is that of the design of falling film horizontal tube evaporators in order to increase the heat transfer coefficient, which reduces the required heat transfer area as discussed in Chapter 3 in detail. There is need to improve the conventional MED processes and hence, this is the motivation for the present study. Detailed mathematical modeling of 8-stages MED system based on FFHTC developed in last chapter is provided and simulation is completed using FORTRAN linked with international math and state library (IMSL) to solve the differential equations simultaneously. The system under investigation is a parallel feed system and the detailed process description is provided in the following sections.

4.4 MED Process Description

The low temperature MED system includes the following components:

- steam generator
- evaporators
- condenser
- collection tanks
- jet pumps / steam jet ejectors
- cold and hot water circulation pumps
- vacuum pump

A schematic diagram of MED operation is shown in Figure 4.8. The operation of MED system can be subdivided into 1) feed flow, 2) vapor flow, 3) non-condensed vapors flow, 4) distillate flow and 5) brine flow.

4.4.1 Feed flow*:* Parallel feed MED system with horizontal tube falling film evaporator is selected for investigation on the basis of earlier discussion. A Spray nozzle header is installed in each evaporator to distribute atomized feed onto tubes surfaces. The feed is pre-heated in a pre-heater loop provided in each evaporator below the tube bundle to extract the heat from brine pool. A magnetic coupling vacuum pump is used to pump the feed in all three stages at same time. This pump can operate in vacuum suction environment without affecting the vacuum level.

4.4.2 Vapor flow: The initial vapors are produced in the steam generator. Heat source is circulated through the tubes of steam generator and at the same time the brine is sprayed outside the tube through nozzles. The vapors produced due to heat

transfer from hot water to brine are cascaded to the tubes side of next stage (2^{nd} stage). These vapors are condensed inside the tubes due to heat transfer to the brine being sprayed outside the tubes. The latent heat of condensation in the tubes evaporates the outside brine and these vapors directed toward the 3^{rd} stage and condensed inside the tubes. The vapors produced in the last stage are condensed in a condenser where cooling water is supplied from cooling tower.

4.4.3 Non-condensed vapor flow: Low pressure steam jet ejectors are provided in between the MED stages. These ejectors help to extract the non-condensed vapor collected in distillate box. The non-condensed vapor extraction is important to operate the system in stable manner. From the last stage, the non-condensed vapors are send directly to condenser to ensure 100% condensation.

4.4.4 Distillate flow: The U-tubes are used to collect the distillate from each stage distillate box. All U-tubes are connected to a distillate header. This header is connected to a distillate collection tank. High accuracy turbine flow meters are installed on each chamber distillate line to record the distillate production.

4.4.5 Brine flow*:* A brine header is installed to collect brine from all stages. Each stage is connected to brine header via U-tube to maintain the pressure difference between stages. Brine header is then connected to brine collection tank. The feed tank and brine tank are installed in a manner so that required amount of brine can be mixed with feed depending upon the salt concentration to get a higher recovery ratio.

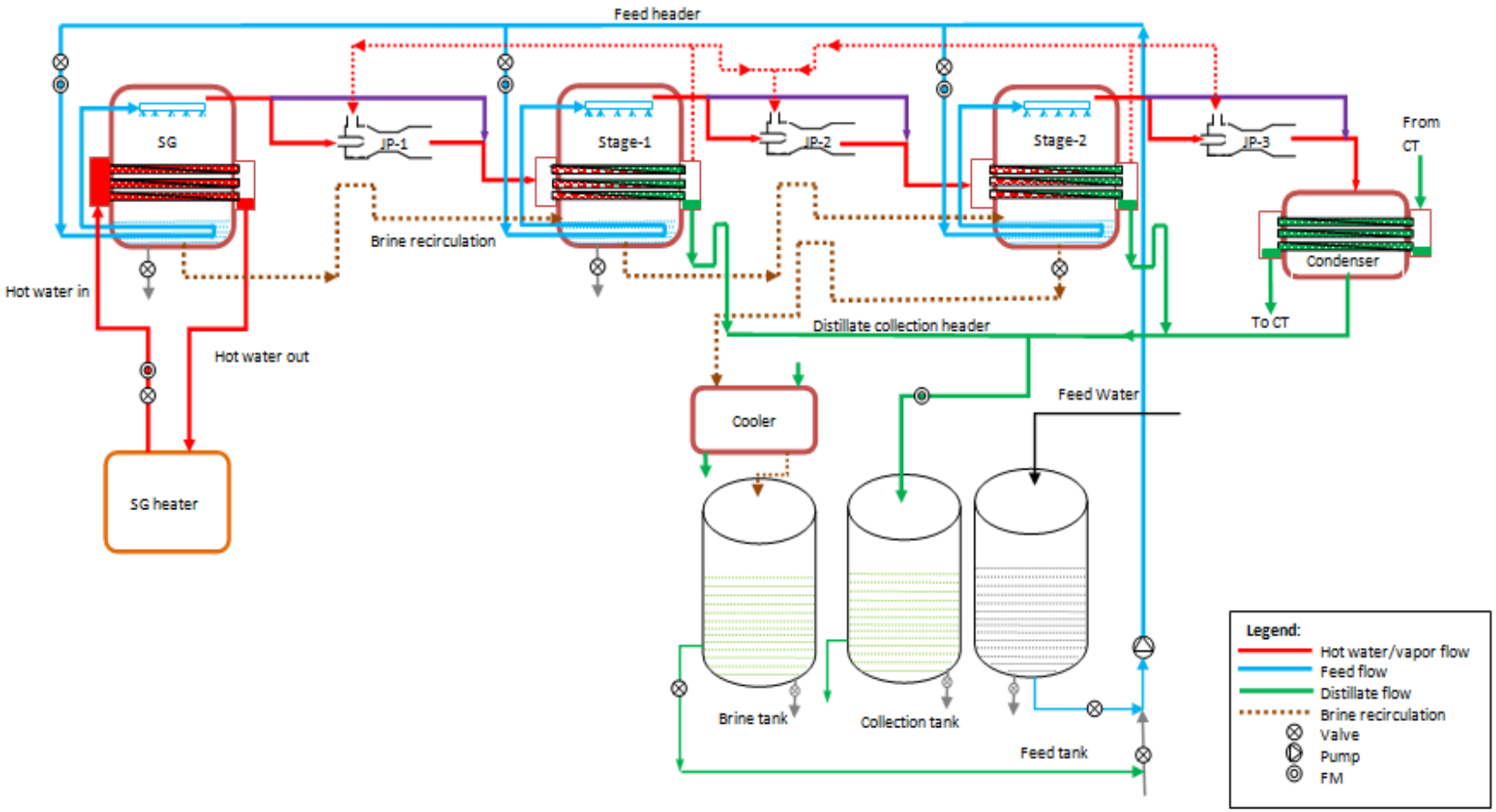

Figure 4.8 Conventional parallel feed MED system flow schematic under investigation

4.5 Mathematical Modeling

A mathematical model is developed based on mass, energy and material balances for main components of MED system. In this distributed modeling, single element of each component is considered to observe the temperature at specific time. The system is a parallel feed system in which feed is supplied parallel to all stages after preheating in pre-heaters in each evaporator. MED system features and assumptions used in the modeling are discussed below.

4.5.1 System Analysis

To make the model closer to a real practical operational plant, some assumptions are made. The main features of MED model are:

1. The heat transfer area of evaporators and feed pre-heaters is assumed to be constant just like common practice in commercial plants.
2. Boiling point elevation (BPE) is calculated for each stage based on saturation temperature and brine concentration. The affect of BPE is considered in calculation of saturation temperature of respective stage.
3. Liquid properties are calculated as a function of salinity, temperature and pressure in each stage to take in to account the effect of these parameters like actual plant.
4. Overall heat transfer coefficient is calculated for each effect individually according to actual conditions during operation.

The following are the assumptions for MED modeling:

1. Vapour is at saturation temperature
2. The heat loss from effects to surrounding is neglected because of low operating temperatures (TBT≈50^{o}C) and insulation.
3. The heat transfer areas of the second to last evaporators are identical.
4. Entire vapours entering the tube side will condense at saturation temperature.
5. The salt concentration in distillate is considered as zero.
6. Scaling and fouling effect is neglected due to low temperature operation.
7. Tubes surface has no contamination due to spray of brine onto the surface.

4.5.2 Mathematical Modelling of Steam Generator (First stage)

The steam generator is used to produce the initial steam for MED system. It is a simple shell and tube heat exchanger in which tubes are arranged horizontally. The hot water is circulated inside the tubes and saline water is sprayed on the tube bundle. The simplified model of steam generator used for modeling is shown Figure 4.9.

Hot water energy balance: Transient temperature of hot water circulated through the tubes can be calculated by using energy balance Equation that can be writing as:

$$\left[\left(M_{HX,i}.Cp_{HX,i}\right)\right]\frac{dT_{hw}}{dt}=\left(\dot{m}_{hw,}\,h_{f,Thw,in}\right)-\left(\dot{m}_{hw}\,h_{f,Thw,out}\right)-h_{in,i}.A_{in,i}\left(T_{hw}-T_{tube,i}\right) \quad (4.1)$$

where T_{hw} is hot water temperature, $M_{HX,i}$ is thermal mass, $Cp_{HX,i}$ is specific heat capacity of tube material, m_{hw} hot water mass flow rate, $h_{f,Thw}$ is enthalpy of hot

water, $h_{in,i}$ is tube side heat transfer coefficient, $A_{in,i}$ is tube side heat transfer area and $T_{tube,i}$ is tube surface temperature. Hot water outlet temperature can be calculated by using the log mean temperature equation that can be re-arranges as:

$$T_{hw,out} = T_{v,i} + (T_{hw,in} - T_{v,i}) \exp\left\{ \frac{U_i A_i}{\dot{m}_{hw} C_{P,Thw}} \right\} \tag{4.2}$$

where, $T_{v,i}$ vapor space temperature, $T_{hw,in}$ is hot water inlet temperature, U_i is overall heat transfer coefficient and A_i is heat transfer area of evaporator.

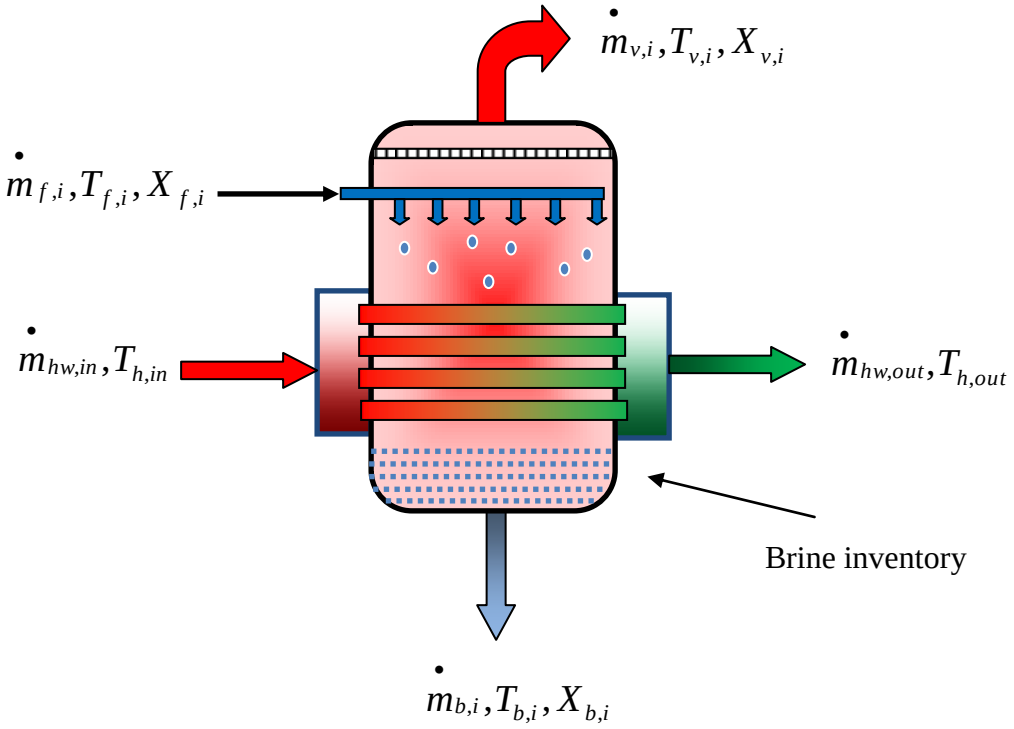

.

Figure 4.9 MED steam generator's model

Tube material energy balance: Heat energy is transferred through the tube material to the falling film. The energy balance for tube material can be writing as:

$$\left[\left(M_{HX,i}.Cp_{hx,i}\right)\right]\frac{dT_{tube,i}}{dt} = h_{in,i}.A_{in,i}\left(T_{hw,i} - T_{tube,i}\right) - h_{out,i}.A_{out,i}\left(T_{tube,i} - T_{v,i}\right) \tag{4.3}$$

where $T_{tube,i}$ is tube surface temperature, $h_{in,i}$ tube side heat transfer coefficient and $A_{in,i}$ tube inner heat transfer area, $h_{out,i}$ evaporator side heat transfer coefficient and $A_{out,i}$ tubes outer heat transfer area.

Mass balance: Instantaneous change in liquid balance in chamber can be found by mass balance equation as:

$$\frac{dM_{b,i}}{dt} = \dot{m}_{f,i} - \dot{m}_{b,i} - \dot{m}_{v,i} \tag{4.4}$$

where, $M_{b,i}$ brine inventory in evaporator, $\dot{m}_{f,i}$ feed flow rate, $\dot{m}_{b,i}$ brine flow rate and $\dot{m}_{v,i}$ vapor flow rate.

Evaporator side energy balance: Transient temperature of evaporator side of the system can be calculated by using energy balance equation that can be written as:

$$\left[\left(M_{b,i}.Cp_{b,Tb}\right) + \left(M_{HX,i}.Cp_{HX}\right)\right]\frac{dT_i}{dt} = \left(\dot{m}_{f,i}\, h_{f,Tf}\right) - \left(\dot{m}_{b,i}\, h_{f,Tb}\right) - \left(\dot{m}_{v,i}\, h_{g,Tv}\right) + Q_{in,i} \tag{4.5}$$

where T_i is evaporator temperature. $h_{f,Tf}$, $h_{b,Tb}$ and $h_{g,Tv}$ are the enthalpy values of feed, brine and vapors at respective temperatures. Heat supplied $Q_{in,i}$ can be found as:

$$Q_{in} = h_{out,i} A_i \left(T_{tube,i} - T_{v,i}\right) \tag{4.6}$$

The vapor temperature $T_{v,i}$ can be found by considering the BPE at specific temperature and salt concentration in evaporator. It can be calculated as:

$$T_{v,i} = T_i + BPE_i \tag{4.7}$$

Material/Salt balance: Salt concentration in liquid balance in each stage after evaporation can be found by material balance equation as given below:

$$M_{b,i} \frac{dX_{b,i}}{dt} = \left(\dot{m}_{f,i} X_{f,i}\right) + \left(\dot{m}_{b,i} X_{b,i}\right) - \left(\dot{m}_{v,i} X_{v,i}\right) \tag{4.8}$$

where $X_{b,i}$, $X_{f,i}$ and $X_{v,i}$ are the concentration values of brine inventory, feed and vapors respectively.

Overall heat transfer coefficient: Three resistances are involved in heat transfer from heat source inside the tube to the evaporating media outside the tube namely: 1) inside heat transfer coefficient, 2) tube wall resistance 3) outside tube heat transfer coefficient. These resistances are calculated by using the following equations.

Tube side heat transfer coefficient: Hot water is flowing through the tubes of steam generator to provide the heat for evaporation. The tube side heat transfer coefficient is calculated by Dittus-Boelters equation [212] as mentioned below:

$$Nu = \frac{h_{in,i} d_{in,i}}{K_{tube,i}} = 0.023 \mathrm{Re}_l^{0.80} \mathrm{Pr}_l^{0.40} \tag{4.9}$$

where Nu is Nusselt number, $d_{in,i}$ is tube diameter and $K_{tube,i}$ is conductivity of tube material.

Tube wall resistance: Tube wall resistance is calculated as below:

$$R_{wall,i} = \frac{\ln\left(\frac{d_{out,i}}{d_{in,i}}\right)}{2.\pi.K_{tube,i}.L_{tube,i}} \tag{4.10}$$

where R_{wall} is tube wall resistance, $d_{out,i}$ tube outer diameter and $L_{tube,i}$ is tube length.

Evaporation heat transfer coefficient: Feed water is sprayed on outer surface of tubes. The evaporation heat transfer coefficient is calculated using the correlation proposed by Wakil et.al [213] as follows:

$$h_{out,i} = \left[0.00143.\left[\frac{\mu_l^2}{g.\rho_l^2.k_l^3}\right]^{-0.16} \left(\mathrm{Re}_\Gamma\right)^{0.45} \left(\mathrm{Pr}\right)^{3.85} \left[2.\exp\left(\frac{S}{S_{ref}}\right) - 1\right]^{-0.38} \left(\frac{T_{sat}}{T_{ref}}\right)^{-0.89} \right] + \left[2.65.\left(\frac{q}{\Delta T}\right)^{0.84} \left(\frac{v_g}{v_{ref}}\right)^{-0.47} \right] \tag{4.11}$$

where μ_l , ρ_l , k_l are liquid properties at respective temperature. S, S_{ref} is the feed concentration and reference seawater concentration (35000ppm) respectively. T_{sat} , T_{ref} is saturation temperature and reference Han & Fletcher temperature (49^{o}C). q is heat specific heat supplied and ΔT is temperature difference. v_g is vapor specific volume at respective temperature and v_{ref} reference gas specific volume at reference temperature.

The overall heat transfer coefficient is then calculated by using these three resistances as shown below.

$$U_i A_i = \frac{1}{\frac{1}{h_{in,i} A_{in,i}} + R_{wall,i} + \frac{1}{h_{out,i} A_{out,i}}} \tag{4.12}$$

The MED effects or stages design is different than MED steam generator. The mathematical modeling of MED stage/effect is discussed in next section.

4.5.3 Mathematical Modelling of Intermediate MED Stages

The vapors produced in steam generator are condensed inside the tube of next stage (i+1). The heat of condensation is transferred through tube material to evaporate the brine film outside the tube. The vapor generated in intermediate stages of MED is re-used in successive stages to recover its heat of condensation. The intermediate evaporators are also shell and tube heat exchangers with vapor condensation inside and falling film evaporation outside. The simplified model of MED intermediate effects used for modeling is shown in Figure 4.10. For the mentioned model, MED modeling equations are developed for intermediate stages and discussed in the following sections.

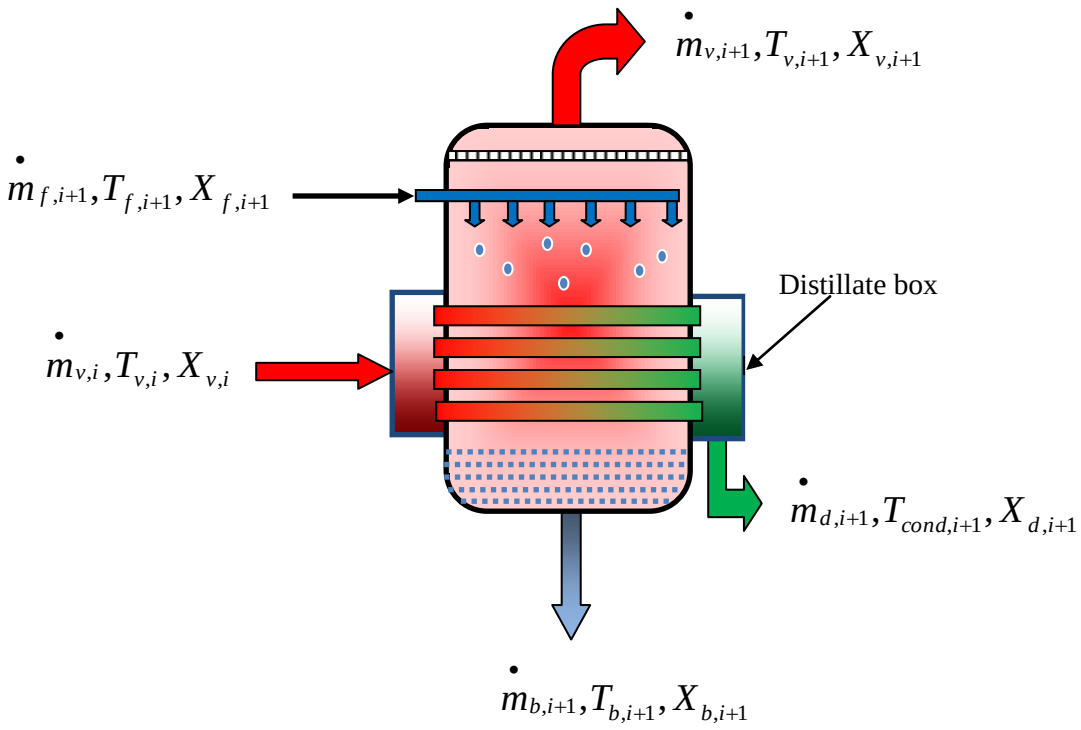

Figure 4.10 MED stage/effect's model

Condenser side (tube side) energy balance: The vapor coming from steam generator condenses in the tubes. The condenser side energy balance can be calculated as:

$$\left[\left(M_{l,i+1}.Cp_{l,Tcond}\right)\right]\frac{dT_{cond,i+1}}{dt}=\left[\dot{m}_{v,}\,h_{fg,Tv}\right]_{i}-\left[h_{in}.A_{in}\left(T_{cond}-T_{tube}\right)\right]_{i+1} \tag{4.13}$$

where T_{cond} is the tube condenser side temperature and T_{tube} is tube wall temperature.

Tube material energy balance: The heat of condensation of vapors transferred thorough tube wall and tube material energy balance can be found as:

$$\left[\left(M_{HX,i+1}.Cp_{hx,i+1}\right)\right]\frac{dT_{tube,i+1}}{dt}=h_{in,i+1}.A_{in,i+1}\left(T_{cond,i+1}-T_{tube,i+1}\right)-$$
$$h_{out,i+1}.A_{out,i+1}\left(T_{tube,i+1}-T_{v,i+1}\right) \tag{4.14}$$

Mass balance: The inventory balance in evaporator chamber can be calculated as:

$$\frac{dM_{b,i+1}}{dt}=\dot{m}_{f,i+1}-\dot{m}_{b,i+1}-\dot{m}_{v,i+1} \tag{4.15}$$

Evaporator side energy balance: The vapor instantaneous temperature within vapor space of evaporator can be calculated by evaporator side energy balance as written below:

$$\left[\left(M_{b,i+1}.Cp_{b}\right)+\left(M_{HX,i+1}.Cp_{HX,i+1}\right)\right]\frac{dT_{i+1}}{dt}=$$
$$\left(\dot{m}_{f,i+1}\,h_{f,Tf}\right)-\left(\dot{m}_{b,i+1}\,h_{f,Tb}\right)-\left(\dot{m}_{v,i+1}\,h_{g,Tv}\right)+Q_{in,i+1} \tag{4.16}$$

Similarly, the vapor temperature can be calculated by using the BPE as explained in Equation 4.7 and heat generation ($Q_{in,i+1}$) can be calculated as:

$$Q_{in,i+1} = h_{out,i+1} A_{i+1} \left(T_{tube,i+1} - T_{v,i+1} \right) \tag{4.17}$$

Material/Salt balance: There is increase in salt concentration in evaporator liquid inventory after evaporation of portion of feed. This can be calculated by material balance equation as explained below:

$$M_{b,i+1} \frac{dX_{b,i+1}}{dt} = \left(\dot{m}_{f,i+1} X_{f,i+1} \right) - \left(\dot{m}_{b,i+1} X_{b,i+1} \right) - \left(\dot{m}_{v,i+1} X_{v,i+1} \right) \tag{4.18}$$

Overall heat transfer coefficient: Falling film heat transfer coefficient and tube resistance calculation is the same as that described in steam generator modeling. Since vapors are condensing inside the tubes so tube side heat transfer coefficient is calculated by condensation correlation as discussed below.

Tube side condensation heat transfer coefficient: Nusselt condensation correlation [214] is used to calculate the condensation heat transfer coefficient inside the intermediate MED effects. The correlation can be written as:

$$Nu = \frac{h_{in,i+1} L_{i+1}}{K_{tube,i+1}} = 0.728 \left[\frac{g h_{fg,Tcond} \rho_{l,Tcond} \left(\rho_l - \rho_v \right)_{Tcond} K_{l,Tcond}^3}{\mu_{l,Tcond} d_i \left(T_{v,i+1} - T_{tube,i+1} \right)} \right]^{1/4} \tag{4.19}$$

The overall heat transfer coefficient is then calculated by using the same approach as described in Equation 4.12 in steam generator modeling section.

4.5.4 Mathematical Modelling of Steam Jet Ejector

In this MED system, the steam jet ejectors are provided to remove the non-condensable gases and un-condensed vapor. The portion of vapor produced in a stage is used as a primary steam and secondary steam side is connected to distillate box. This inter stage ejector combination makes this system different from conventional MED plant. The un-condensed steam will condense in next stage resulting in improvement of the production. Non-condensable gases are extracted out of condenser with a vacuum pump to run system smoothly. The mathematical modeling for low pressure steam jet ejector model shown in Figure 4.11 as discussed in the sections below.

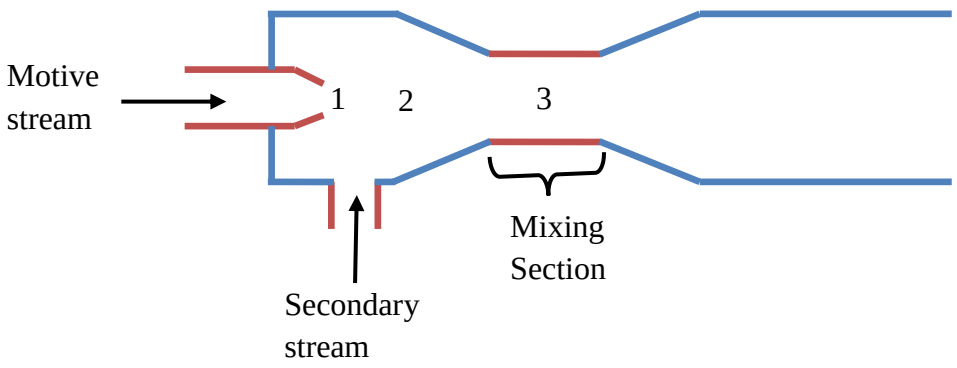

Figure 4.11 MED steam jet ejector's model

Ejector throat pressure: The pressure drop of primary stream at throat to extract the secondary stream can be calculated by the equation written as:

$$\frac{P_{throat}}{P_{motive}} = \left[\frac{2}{n+1}\right]^{\frac{n}{n-1}} \tag{4.20}$$

For saturated steam n=1.135.

Throat area for maximum flow: The throat area for maximum flow through ejector is given as:

$$\frac{m}{A_{throat}} = \left\{ n\left(\frac{2}{n+1}\right)^{\frac{n+1}{n-1}} \frac{p_{motive}}{v_{motive}} \right\} \tag{4.21}$$

Using above equation, throat diameter (d_{throat}) can be calculated from throat area.

Maximum/Critical flow velocity: The critical specific volume at critical pressure is calculated as:

$$\frac{v_{critical}}{v_{motive}} = \left(\frac{P_{motive}}{P_{critical}}\right)^{1/n} \tag{4.22}$$

And then critical velocity is calculated as:

$$C_{critical} = \sqrt{nP_{critical}v_{critical}} \tag{4.23}$$

By using critical volume and critical velocity, critical area can be re-calculated as:

$$A_{critical} = A_{throat} = \frac{\dot{m}\, v_{critical}}{C_{critical}} \tag{4.24}$$

To find out the mixing section parameters (diameter and velocity), mass, momentum and energy balance equations are developed. These equations are explained below.

Mass balance: The mass balance for above given model can be written as:

$$\dot{m}_1 + \dot{m}_2 = \dot{m}_3 \tag{4.25}$$

$$\rho_1 A_1 C_1 + \rho_2 A_2 C_2 = \rho_3 A_3 C_3 \tag{4.26}$$

$$\frac{\rho_1}{\rho_3} A_1 C_1 + \frac{\rho_2}{\rho_3} A_2 C_2 = A_3 C_3 \tag{4.27}$$

Ejector momentum balance The momentum balance for above ejector model can be described as:

$$\dot{m}_1 C_1 + \dot{m}_2 C_2 = \dot{m}_3 C_3 \tag{4.28}$$

$$\rho_1 A_1 C_1^{\,2} + \rho_2 A_2 C_2^{\,2} = \rho_3 A_3 C_3^{\,2} \tag{4.29}$$

By (4.27) & (4.28)

$$\rho_1 A_1 C_1^{\,2} + \rho_2 A_2 C_2^{\,2} = \rho_3 C_3 \left[\frac{\rho_1}{\rho_3} A_1 C_1 + \frac{\rho_2}{\rho_3} A_2 C_2 \right] \tag{4.30}$$

$$\rho_1 A_1 C_1^{\,2} + \rho_2 A_2 C_2^{\,2} = C_3 \left[\rho_1 A_1 C_1 + \rho_2 A_2 C_2 \right] \tag{4.31}$$

Ejector energy balance: The energy balance for ejector can be written as:

$$\dot{m}_1 h_1 + \dot{m}_2 h_2 = \dot{m}_3 h_3 \tag{4.32}$$

$$\rho_1 A_1 C_1 h_1 + \rho_2 A_2 C_2 h_2 = \rho_3 A_3 C_3 h_3 \tag{4.33}$$

By (4.27) & (4.33):

$$\rho_1 A_1 C_1 h_1 + \rho_2 A_2 C_2 h_2 = \rho_3 \left[\frac{\rho_1}{\rho_3} A_1 C_1 + \frac{\rho_2}{\rho_3} A_2 C_2 \right] h_3 \tag{4.34}$$

$$\rho_1 A_1 C_1 h_1 + \rho_2 A_2 C_2 h_2 = \left[\rho_1 A_1 C_1 + \rho_2 A_2 C_2 \right] h_3 \tag{4.35}$$

By using above modeling equations, steam jet ejector parameters can be calculated for required operation.

4.6 Performance Indicator for MED system

The hot water is supplied to steam generator to generate the initial steam. An electric heater is used to maintain the temperature of hot water. The distillate production from each stage can be calculated as:

$$\dot{m}_{d,i} = \frac{h_{out,i} A_i \left(T_{tube,i} - T_{v,i}\right)_i}{h_{fg,Tv,i}} \tag{4.36}$$

The performance ratio (PR) is used as a performance indicator of MED system. For multiple effect systems the PR is directly related to the number of effects.

$$PR = \frac{\dot{m}_{d,total}(kg/\sec).h_{fg,Tsat}(kJ/kg)}{TPE} \tag{4.37}$$

Where TPE is total primary energy and can be calculate by:

$$TPE = \left(\frac{Q_{thermal,payable}}{\eta_{boiler}}\right) + \left(\frac{Q_{electric}}{\eta_{pp}}\right) \tag{4.38}$$

Boiler efficiency is taken as 95% and power plant conversion efficiency is taken as 42%.

Water and steam properties:

The saline water properties are calculated by using the formulation developed by Wagner and Kruse [215], Sieder and Peters [216] and Lienhard [217]. All properties are functions of temperature, pressure and salinity. The steam properties are also

calculated by using the same formulation as a function of pressure and temperature of system. The steam is assumed to be free from salt.

The values and parameters used for MED simulation are given in Table 4.2.

Table 4.2 Parameters used for parallel feed MED system simulation

MED Steam Generator Design Parameters		
Capacity	10.0	KW
Area of heat transfer	4.0	m^2
Tube outer diameter	16.0	mm
Tube thickness	0.7	mm
Single tube length	1300	mm
Tube matrix detail (tubes in a row x rows)	8 x 8	
Evaporator shell inside diameter	500	mm
Evaporator shell length	1300	mm
Operation Parameters		
Hot water flow rate	48	LPM
Hot water inlet temperature	50	^oC
Feed water salinity	35000	ppm
MED Stage Design Parameters		
Area of heat transfer	4.0	m^2
Tube outer diameter	25.4	mm
Tube thickness	0.7	mm
Single tube length	1300	mm
Tube matrix detail (tubes in a row x rows)	8 x 4	
Evaporator shell inside diameter	500	mm
Evaporator shell length	1300	mm

These modeling equations are written in FORTRAN user defines sub-routine and solved simultaneously using IMSL library functions.

4.7 Solution Algorithm

The mathematical model developed above for parallel feed system is interlinked and an iterative solution is used to calculate the system parameters. Initial values used to start solution algorithm are:

a) Hot water temperature (Thw,in): 50^{o}C

b) Feed water temperature (Tfeed): 30^{o}C

c) Feed water concentration (S): 35,000ppm

The solution algorithm is shown in Figure 4.12. The differential equations are solved simultaneously to calculate the following parameters:

a) Hot water outlet temperature.

b) Evaporator space, tube surface and condenser side temperatures for each stage.

c) Pre-heater outlet temperature in each stage.

d) Overall heat transfer coefficient for each stage.

e) Salt concentration in each stage.

f) Vapor generation in each stage.

g) Cooling water outlet temperature.

Gear's BDF method is used to solve differential equations simultaneously. Convergence of solution is depends on initial values guess and 1x10^{-7} tolerance value is used.

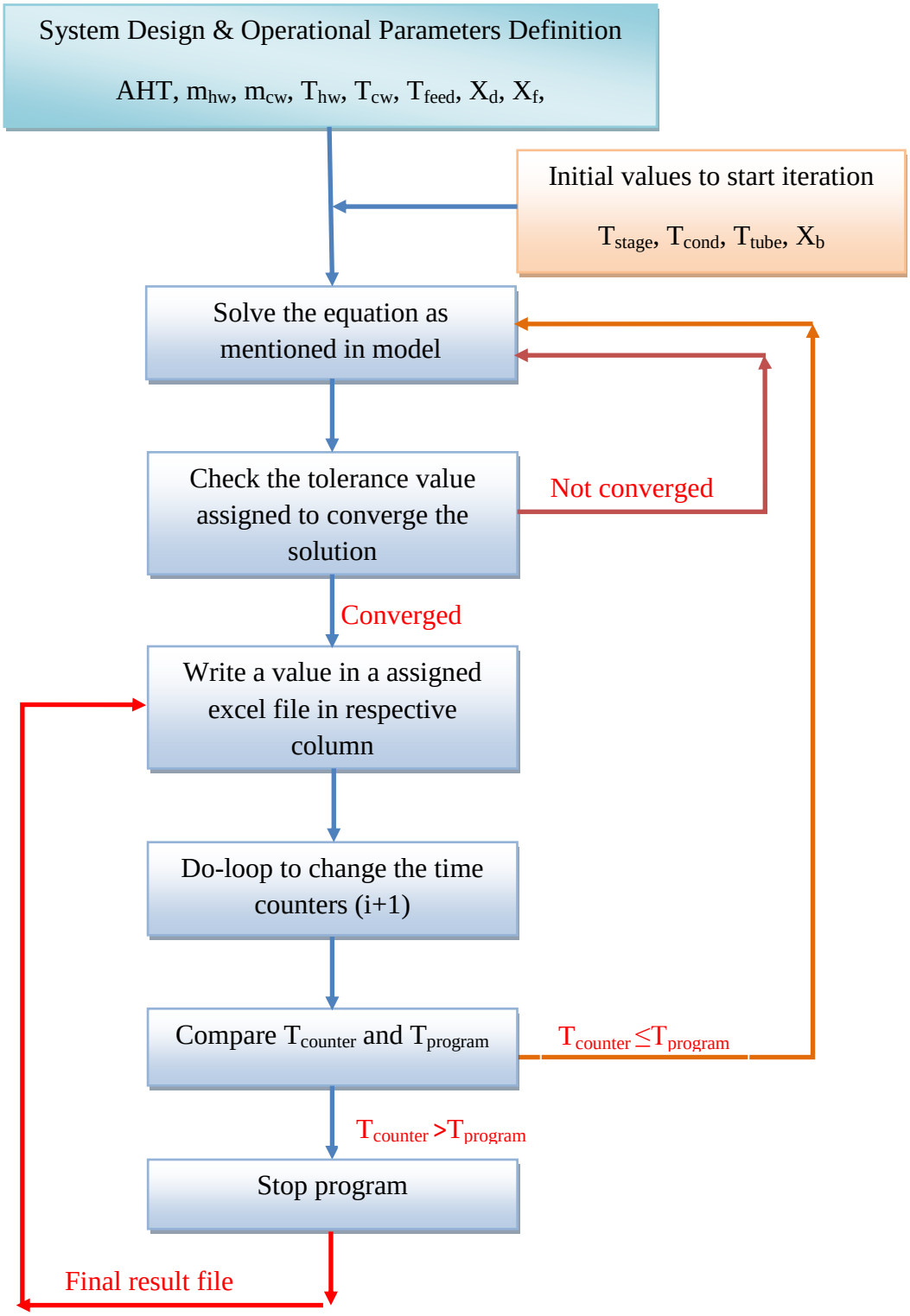

Figure 4.12 FORTRAN simulation solutions algorithm

4.8 Results and Discussion

MED 8-stages distributed simulation is completed by using above modeling equations and parameters. User defined subroutine is written in FORTRAN and IMSL is linked to solve the equation simultaneously.

Figure 4.13 shows the temperature profiles for each stage. The heat source temperature is maintained at 50°C. Condenser side, tube wall and evaporator space temperature profiles are plotted for each stage.

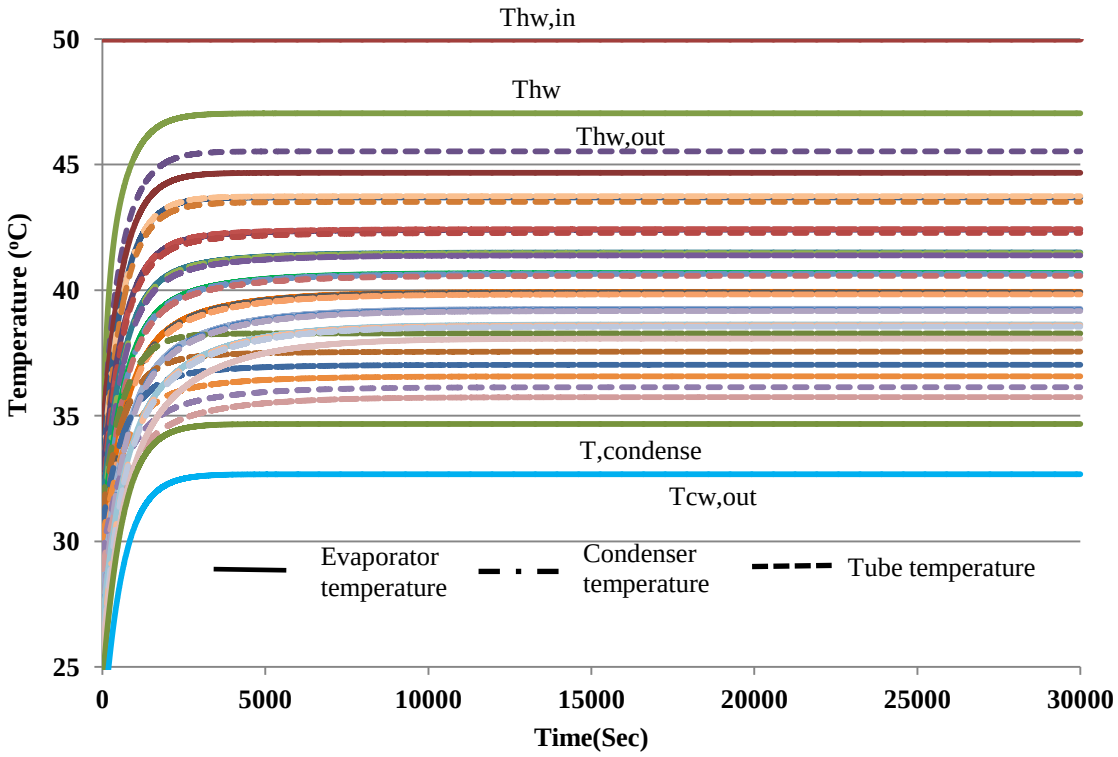

Figure 4.13 Typical temperature profiles of parallel feed MED components at heat source 50°C

It can be seen that heat source temperature difference is about 5°C that have good agreement with real experimental plants data. The temperature difference between cooling water inlet and condenser is also about 5°C as in real plants.

The steady state temperatures of all MED components are plotted in Figure 4.14. It can be seen that the temperature drop between stages varies from 1 to 2°C. This temperature drop has good agreement with some of existing plants as mentioned in literature [207]. BPE for each stage is calculated by using the corresponding stage salt concentration and saturation temperature and used to find the vapor temperatures.

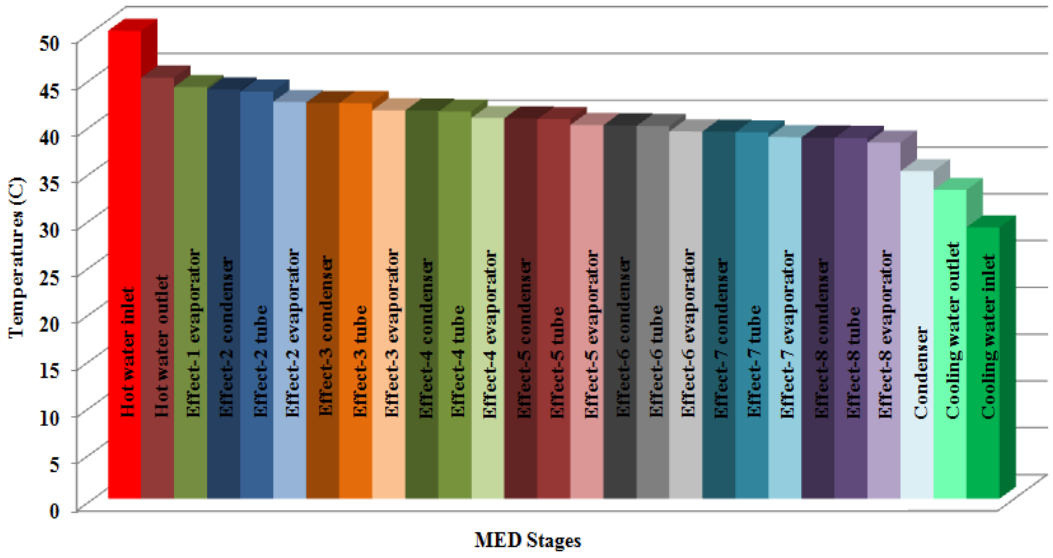

Figure 4.14 MED components steady state temperatures values at 50°C heat source temperature

The vapor pressure losses are calculated by Darcy equation [218] to accommodate the vapor pressure drop in vapor line of actual plants.

Figure 4.15 shows the feed pre-heating in each MED evaporator. There is a heat exchanger loop in the brine pool in each evaporator to recover the energy from brine before rejection as explained that in MED system operation. Feed is supplied at 30°C

but before it enters the spray header it is passed through the pre-heater loop to pre-heat the feed.

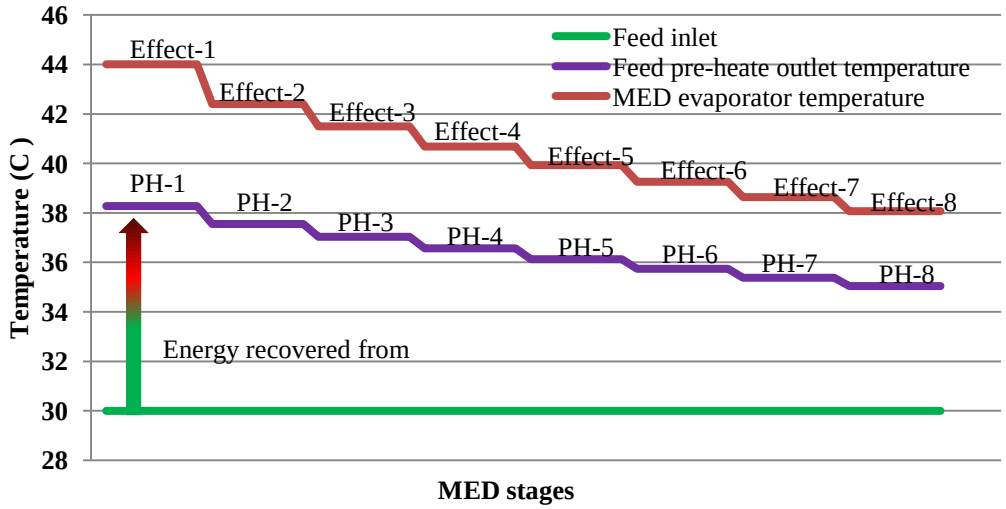

Figure 4.15 Energy recovered from brine pool via built-in pre-heaters to pre-heat the feed

Energy recovered by the pre-heaters is quite substantial which is otherwise wasted if not recovered from brine. Pre-heated feed helps to save energy to pre-heat in evaporate up to saturation temperature from ambient condition (30^{o}C). This in other words increases the performance ratio of MED system. The feed temperature increase in each stage pre-heater can be seen from the Figure 4.15. It can be seen that in successive stages the pre-heater outlet temperature is dropping and this is due to decrease in temperature difference between brine pool and feed inlet temperature.

Figure 4.16 show the values of overall heat transfer coefficient for each stage. It can be seen that first MED stage overall heat transfer coefficient is different from other stages because of different resistances. In the first effect, inside the tubes hot water is circulated and outside the tubes there is saline water spray. In other all stages inside

the tubes there is vapor condensation and outside is seawater spray. From second stage to last stage the overall heat transfer coefficient drops due to drop in temperature in successive stages and changes in thermo-physical properties of fluids.

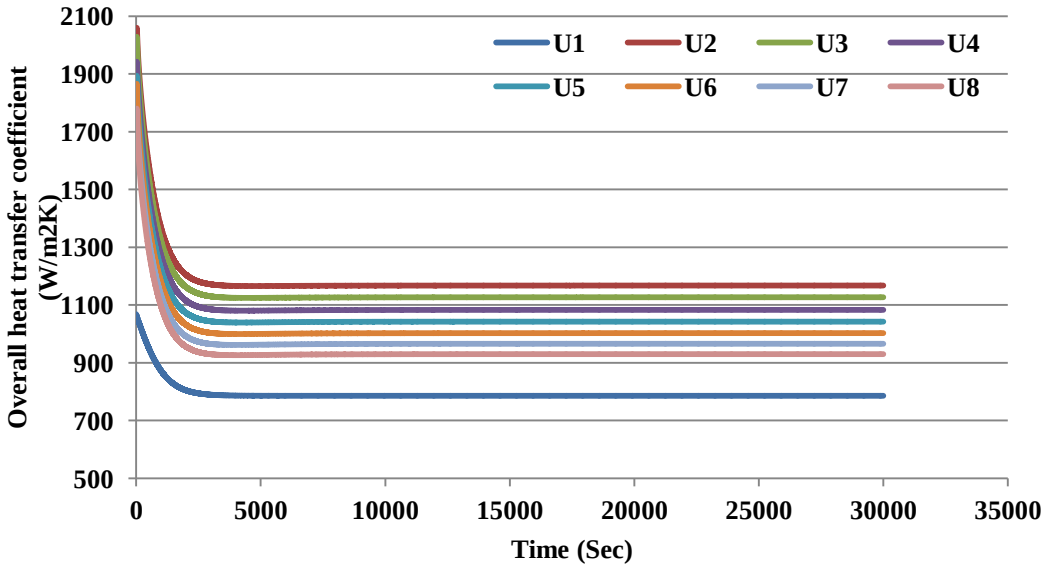

Figure 4.16 Overall heat transfer coefficients profiles of each stage of MED

It can also be observed that the overall heat transfer coefficients are in good agreement with the reported literature (typically 1000~1500 W/m^{2}K) [219] for falling film evaporators.

Figure 4.17 shows the distillate production in each stage. It can be observed that the distillate production decreases in successive stages and it may be due to decrease in saturation temperature and pressure that can affect the heat transfer coefficient. Figure 4.18 shows the total production from 8-stages and system performance (PR) calculated on the basis of formula discussed in modeling section. The system performance normally depends on number heat recoveries or stages (n) and

theoretically it is less than n in case of conventional MED systems. It can be seen that the PR for 8-stages MED is 6.5 also in good agreement with the data reported in the literature [220].

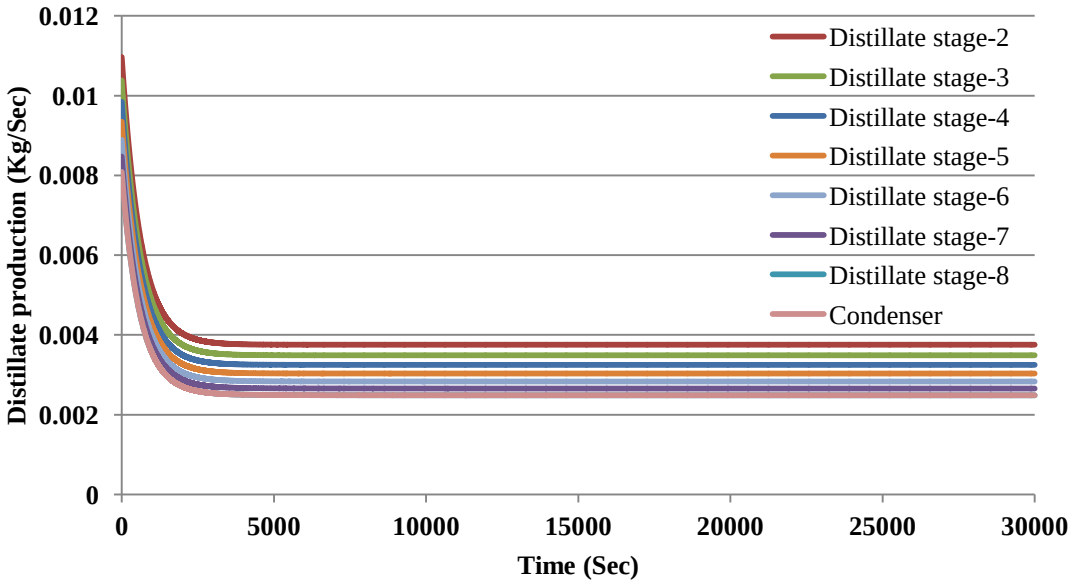

Figure 4.17 Distillate production profiles from each stage of MED

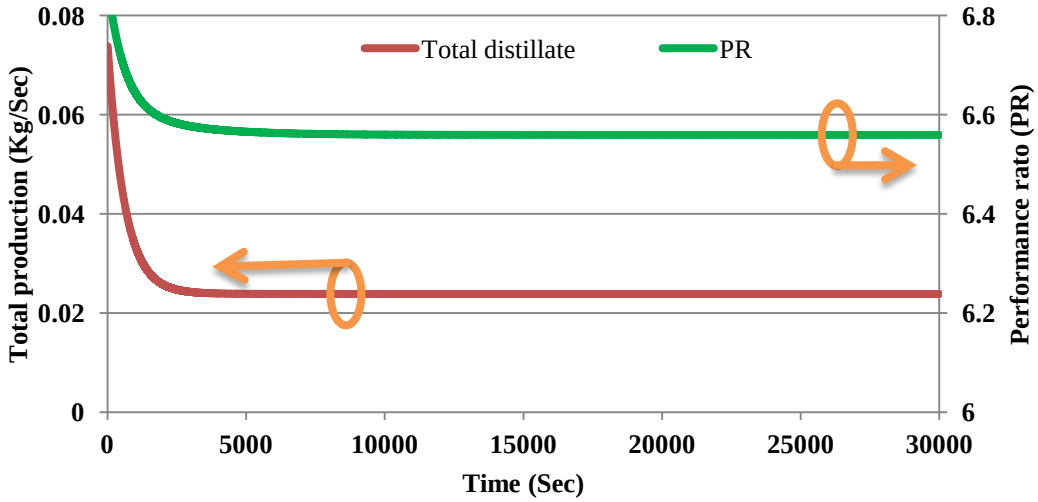

Figure 4.18 8-stages MED total production and system performance ratio

Summary of Chapter 4

Multi effect desalination is the most preferred method to produce fresh water especially in desert and Gulf region. MED has different configurations basis on vapour and brine flow. They can also be categories on the basis of heat exchanger arrangement. It is concluded that parallel/cross feed system configuration with horizontal falling film evaporator is the best configuration. Traditionally, MED operation temperature varies from 65-70^{o}C. MED TBT can be increased to 110^{o}C by introducing the NF at up-stream of MED. Although MED is very famous, there are some limitations/drawbacks: fouling and corrosion at high TBT and condenser barrier at low temperature end. With these limitations, MED operation region is limited.

To enhance the MED system performance and to find the optimum operational parameters, a 8-stages MED system is investigated. Parallel feed flow system is considered for investigation. The process flow is discussed in detail with process schematic diagram. This system is unique as compared to traditional MED systems because low pressure inter stage steam jet ejector are introduced to pull un-condensed vapour and non-condensable. This helps to run the whole system smoothly.

Detailed mathematical modelling is developed for the main components of the system namely: 1) steam generator, 2) MED stages and 3) steam jet ejector. Overall

heat transfer coefficient is calculated by using the FFHTC developed in Chapter 3. The distributed modelling equations are developed by considering the single element of different components to investigate the different parameters at specific location and at specific time. The performance of the system is investigated by indicator "PR".

On the basis of modelling equations developed, the simulation code is written in FORTRAN in user defined sub-routine. IMSL math library is linked to run the equations simultaneously. The tolerance value $1x10^{-7}$ is used to converge the solution. The required parameters of the MED system are simulated namely: 1) system temperatures include condenser side, tube and evaporator, 2) pre-heaters temperatures, 3) stages overall heat transfer coefficient, 4) stages production and 5) system performance. It is found the simulated values have good agreement with data of existing operational plants as reported in the literature.

Chapter 5 Experimental Investigation of 3-Stages Multi Effect Desalination System

The desalination market in MENA and Gulf region is reversing the desalination processes trend to MED installations, as a most efficient thermal desalination system. Although, MED processes are not new but still there is need to develop more energetic processes in terms of kWh/m^3 energy consumption and environmental friendly systems. Performance investigation of multi effect desalination (MED) at assorted heat source temperature 70^{o}C- 38^{o}C (maximum operational gap for conventional MED plant) is important because of lack of real experimental data for full range. This experimentation investigation will not only provide the full picture of MED processes but also help to investigate the possibility of hybridization of MED systems to enhance the system performance.

A 3-stage MED experimental facility is designed, fabricated and installed in air-conditioning laboratory at NUS. In this chapter, the detailed analysis of MED facility is provided. In the first part of the chapter, the detail designs of MED main components namely: steam generator, MED stages, condenser, feed cooler and storage tanks is provided. Detailed P & ID of the system and operational strategy is discussed in the second part of the chapter. In the third part of the chapter, experiments and results are discussed. The comparison of simulation and experimental results is provided in the last part of the chapter.

5.1 Background

Recently, it is noticed that RO processes are facing severe problems of fouling and HABs treatment especially in semi arid region. These limitations are reversing the trend of desalination installations to thermal desalination systems. Availability of industrial low grade waste heat due to industrialization and solar energy in these countries motivated the researchers to investigate the performance of MED system for these applications. This will not only provide the reference data for conventional MED system design and performance at assorted waste heat temperature but will also highlight the understanding for possible MED hybrid desalination cycle to enhance the system performance. A 3-stages MED system is designed, fabricated and installed to investigate the necessary parameters and to provide the data for future reference. The details of the test facility are discussed in the following sections.

5.2 Design of MED System

The MED system investigated here is horizontal tubes falling film evaporators with parallel feed spray. The first stage also called steam generator design is different than the next two stages. In first stage, the hot water is circulated through the tubes and feed is sprayed on the tube bundle. In second and third stages, there is vapor condensation inside the tubes those are generated in the previous stage and feed is sprayed on to the tube bundle. Standard procedure is followed to design the system parameters. In first step, area of heat transfer is calculated by using literature values of some input parameters namely: overall heat transfer coefficient (U) and log mean

temperature difference (LMTD). In the second step also called the verification step, all input values are calculated by using standard correlations and are compared with literature values. In last step, area of heat transfer is calculated on the basis of second step calculations and compared with first step value. The design procedure is shown in Figure 5.1 and verification procedure is shown Figure 5.2.

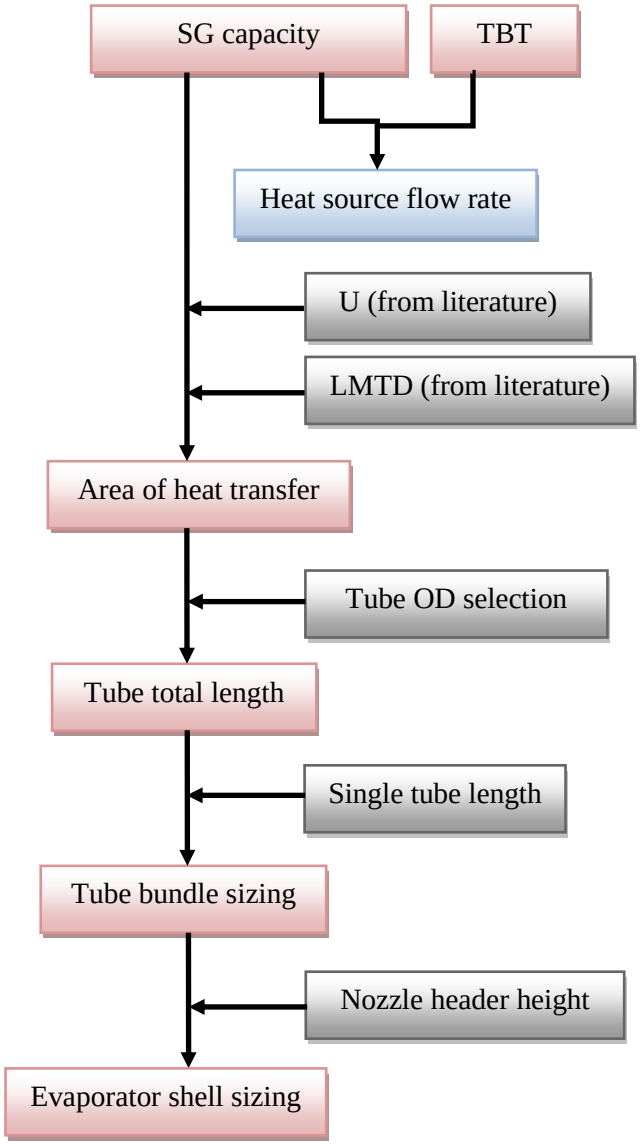

Figure 5.1 MED evaporator's design procedure steps

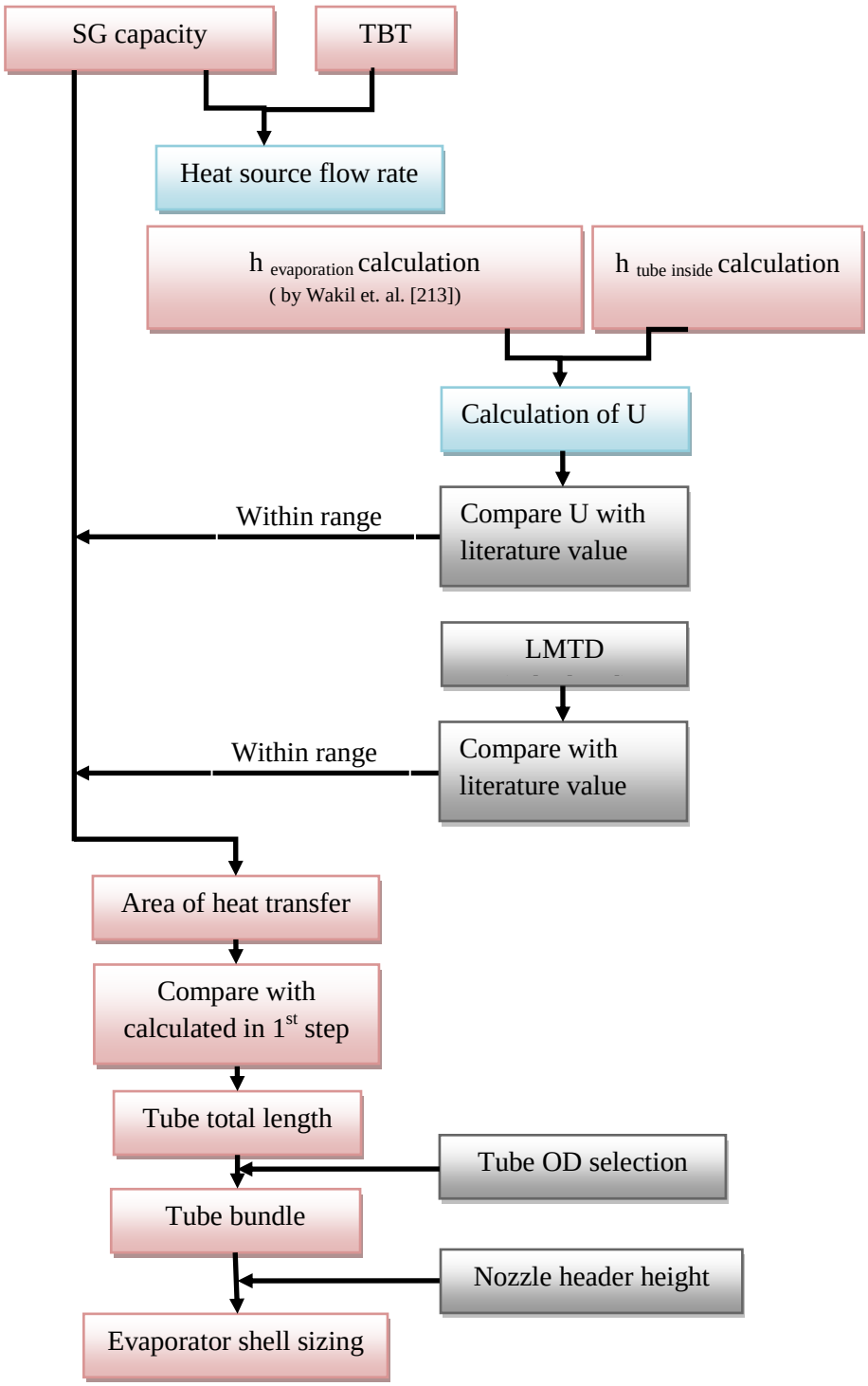

Figure 5.2 MED evaporator's design verification procedure steps

5.2.1 MED Steam Generator Design

Steam generator is designed for 10KW capacity with operating temperature 50^{o}C. The standard design steps are followed for parameters design as discussed above. The detail design sheets are attached in Appendices A1 and A2. Detailed AutoCAD design is shown in Figure 5.3.

5.2.2 MED Stage Design

MED stages are also designed for 10KW capacity with operating temperature 47^{o}C ~48^{o}C. It is because the inter stage ΔT varies 2^{o}C ~3^{o}C as mentioned in literature of real plant data [221, 222]. The same standard design steps are also followed for parameters design of MED stages. The detail design sheets are attached in Appendices B1 and B2. Detailed AutoCAD design is shown in Figure 5.4.

5.2.3 MED Storage Tanks Design

Storage tanks for distillate and brine collection are designed with 120L capacity. This capacity is enough to run experiments with steady state condition for sufficient long time (4~5 hours). A separate feed tank is installed to supply the feed to spray pump. The brine can also be mixed and re-circulate through the system depending upon brine concentration to increase the recovery ratio of the system. Detailed AutoCAD design is shown in Figure 5.5.

5.2.4 MED Steam Jet Ejector Design

A low pressure steam jet ejector is designed and fabricated for inter-stage operation. The design is based on thermodynamic equations explained in modeling section in Chapter-04. The detailed design sheet and sample calculations are attached in Appendices C1 and C2. Detailed AutoCAD design is shown in Figure 5.6.

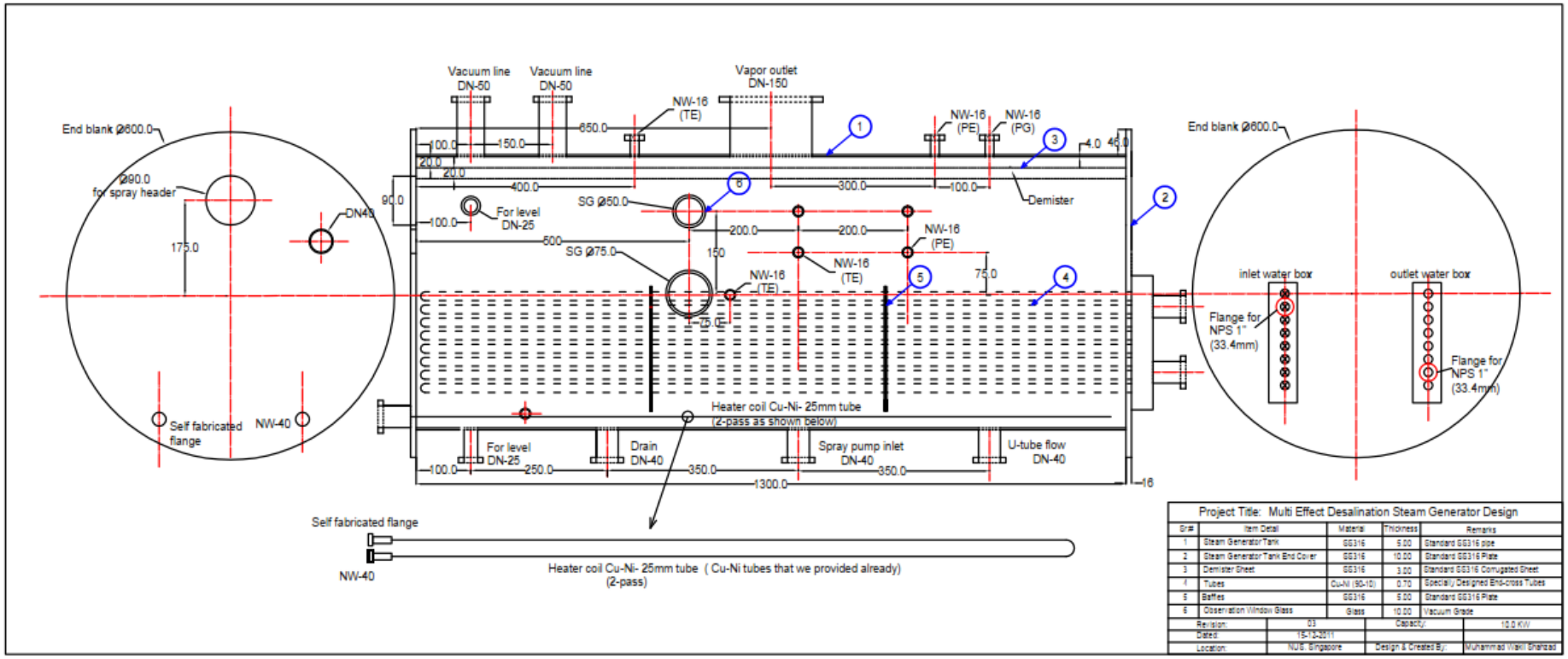

Figure 5.3 MED steam generator detail design AutoCAD model

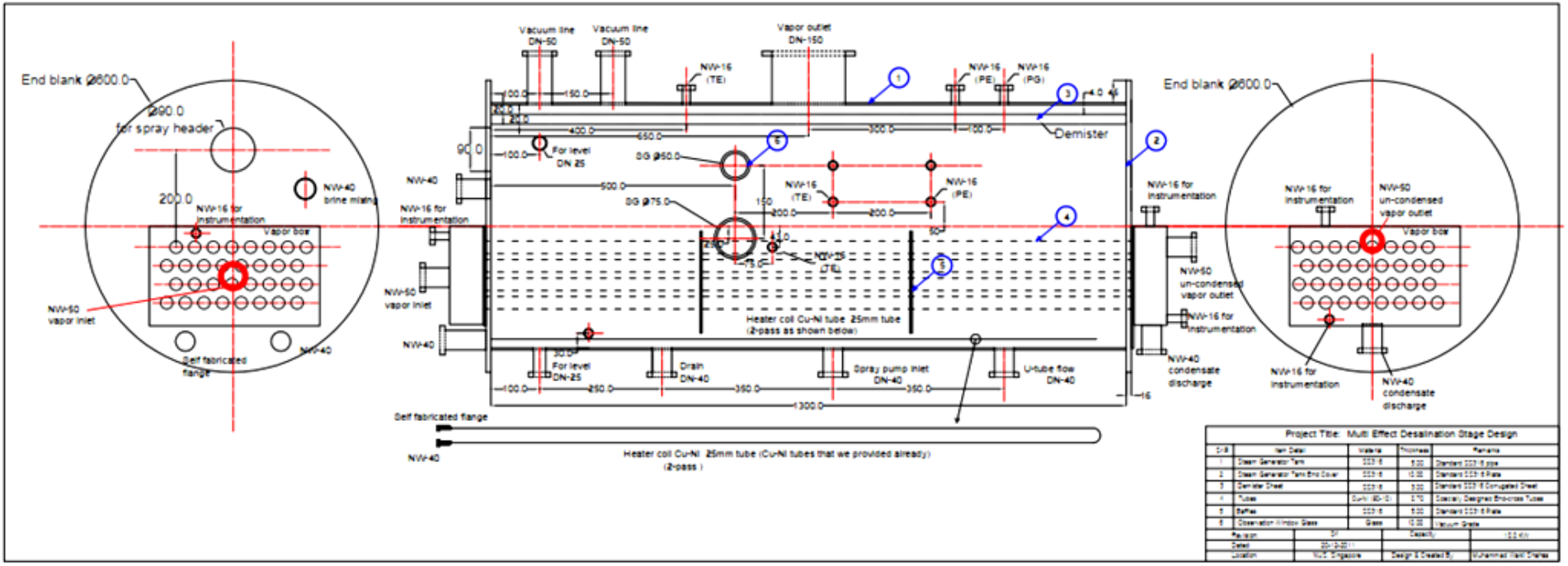

Figure 5.4 MED stages detail design AutoCAD model

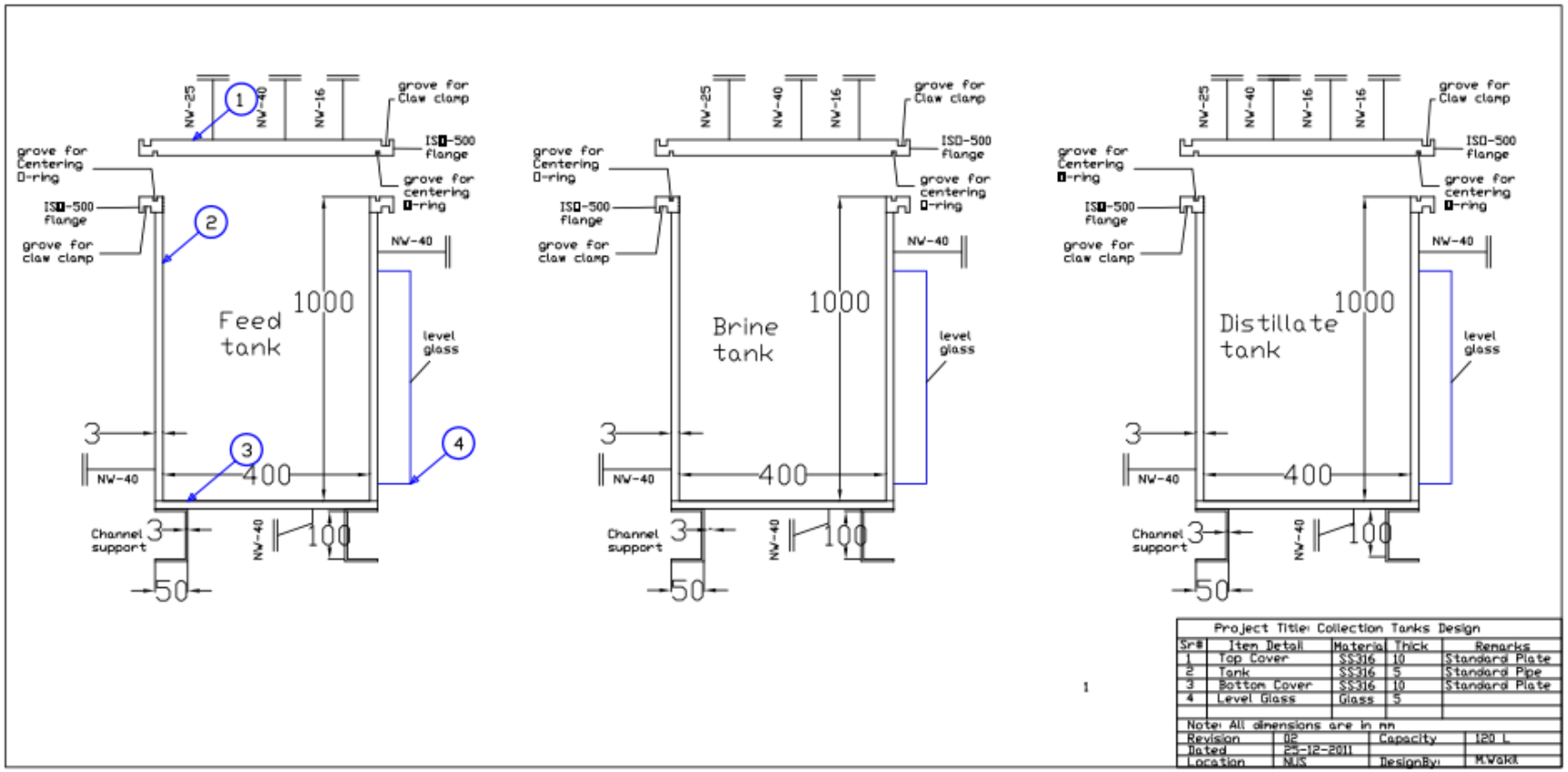

Figure 5.5 MED storage tanks detail design AutoCAD model

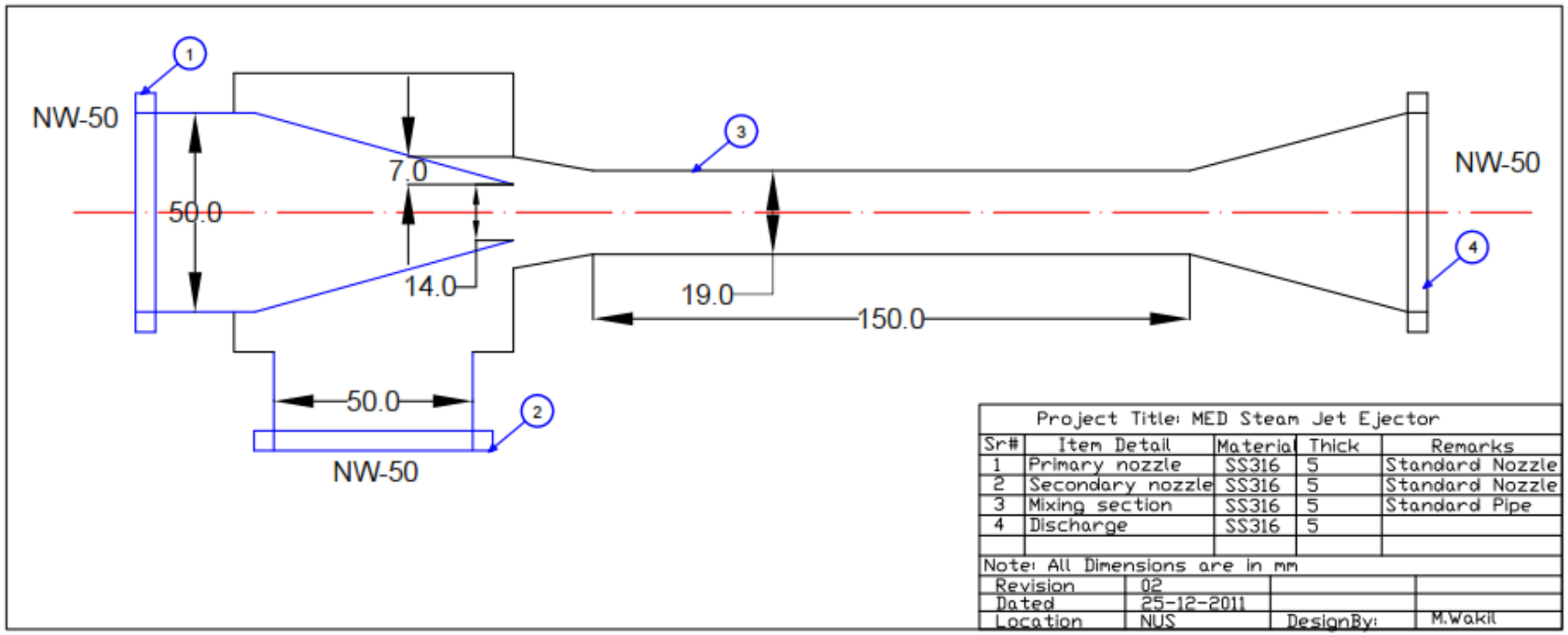

Project Title: MED Steam Jet Ejector

Sr#	Item Detail	Material	Thick	Remarks
1	Primary nozzle	SS316	5	Standard Nozzle
2	Secondary nozzle	SS316	5	Standard Nozzle
3	Mixing section	SS316	5	Standard Pipe
4	Discharge	SS316	5	

Note: All Dimensions are in mm

Revision	02		
Dated	25-12-2011		
Location	NUS	DesignBy:	M.Wakil

Figure 5.6 MED steam jet ejector detail design AutoCAD model

5.3 MED System Installation and Piping

The 3-stage MED system is installed on plate form and auxiliary storage tanks below the plate form. System can operate with parallel feed system with and without brine cascading. An additional facility of brine re-circulation is also provided to run with fresh water for performance parameter testing. A cooling tower is installed on the roof top for cooling the condenser water supply. Although the operating temperature is very low, heat losses are minimized by insulating with armor flux. Pipes are fabricated section by section and vacuum conditions are tested before installation. A typical vapor pipe line section is shown in Figure 5.7. For different pipe sections joining, vacuum flanges are used with special centering o-ring.

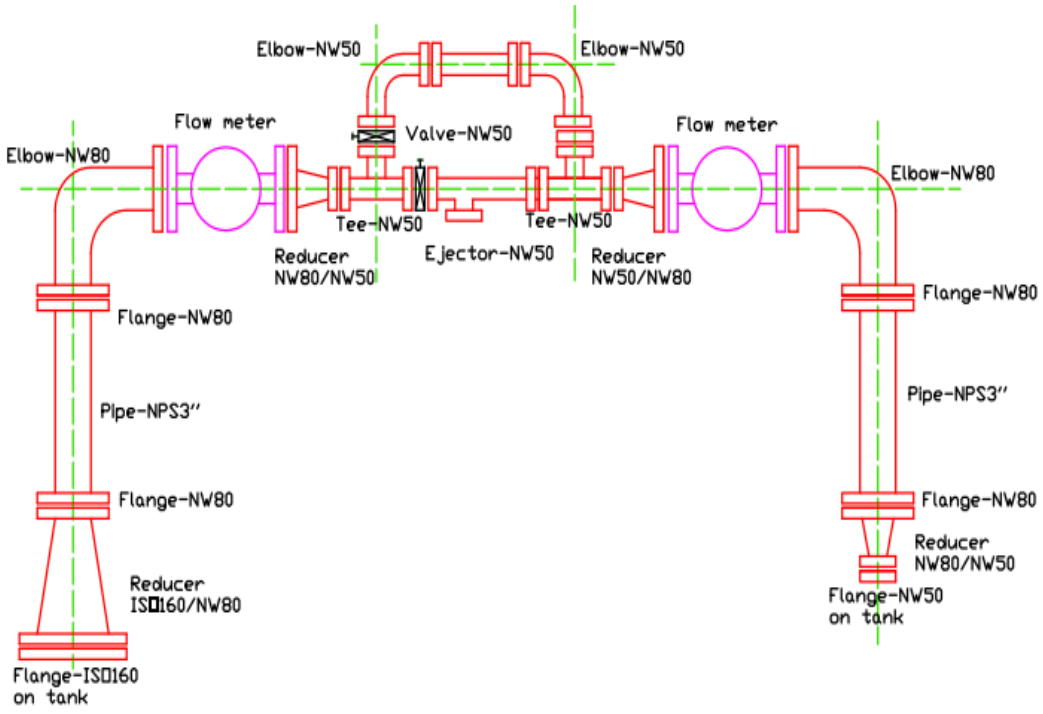

Figure 5.7 **MED plant inter-stage connection vapor pipe line: instruments arrangement**

5.4 Operational Strategy of MED System

The major components of 3-stage MED system installed in NUS are: 1) MED steam generator, 2) MED stages, 3) condenser, 4) cooling tower, 5) brine cooler, 6) steam generator heater bank, 7) collection tanks, 8) pumps and 9) control panel.

Steam generator heat source is provided by thyristor controller electrical heaters with accuracy of ±0.15^{o}C. Hot water pump circulate the hot water inside the tubes of steam generator in close loop manner. Seawater feed is supplied parallel to all the stages. Special spray nozzles are used to spray the feed on to the tubes bundle. A magnetic coupling pump is used to pump the feed from feed tank to feed header in each evaporator. Feed rate is controlled with throttling valve and special magnetic pickup turbine flow meter. The energy is transferred from hot water to the spray film and this heat transfer evaporates a portion of the feed supplied. Feed is always supplied more than the capacity of steam generator to prevent dry out patches. The vapors generated in steam generator also called as 1st stage is transferred to the tube side of next stage called 2nd stage. These vapors are condensed inside the tube due to spray of feed outside the tube bundle. This condensate is distill water and collected via U-tube to a distillation collection header. Heat of condensation again evaporates the portion of feed sprayed onto the tube bundle. Additional vapor are also produced by flashing effect when the leftover brine is transferred from the previous stage (1st stage) to next stage (2nd stage) via U-tube due to pressure difference. The total vapors are then transferred to the tube side of the next stage also called the 3rd stage where they again condense due to heat of condensation taken away by feed spray. Distillate

is again collected via U-tube to collection header. Similarly brine from the 2nd stage is directed toward the 3rd stage via U-tube to get additional flashing effect. The vapors produced in last stage (3rd stage) are then sent to the condenser. Cooling tower is installed at roof top to provide the cooling water to the condenser to condense the last stage vapors and distillate is send to distillate header. The brine inventory is collected to brine collection tank. Brine collection tank is also connected to feed pump to re-circulate the portion of brine to mix with fresh feed to increase the recovery ratio depending on brine concentration. The distillate header is connected to distillate collection tank to collect the distillate from all stages. A special high accuracy turbine flow meter is installed to measure and record the distillate production rate. Since the operation of MED is at low temperature (70^{o}C – 38^{o}C) so to maintain the saturation pressure a vacuum pump is installed. Vacuum holding capacity of all MED components is tested for 48hours before experiment start. The detailed process flow diagram is shown in Figure 5.8 and the experimental 3-stage system installed in NUS is shown in Figure 5.9(a, b). The valves sequence and condition is very important for stable operation and MED system valves condition during normal operation is shown in Figure 5.10.

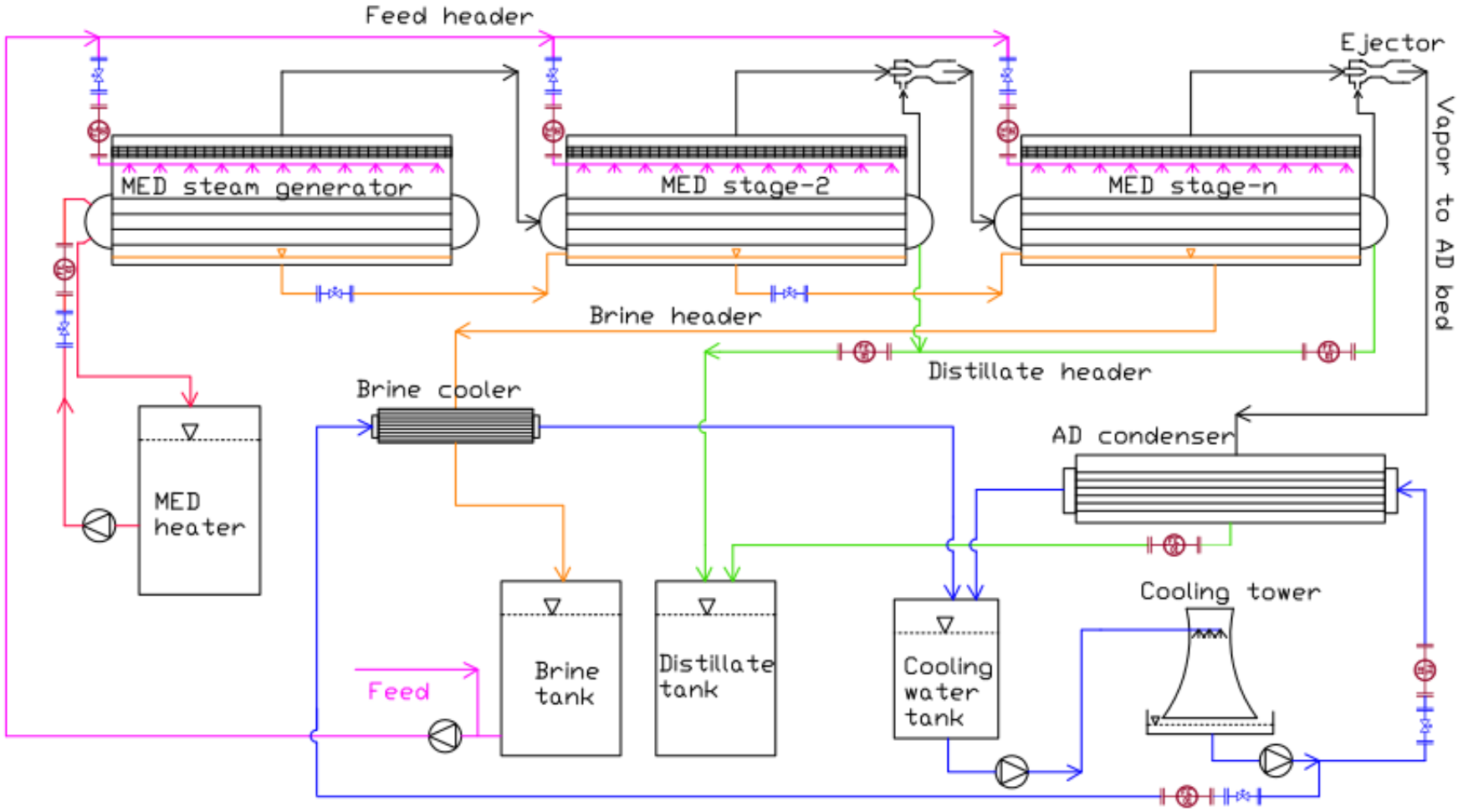

Figure 5.8 Schematic diagram of conventional MED cycle

(a)

(b)

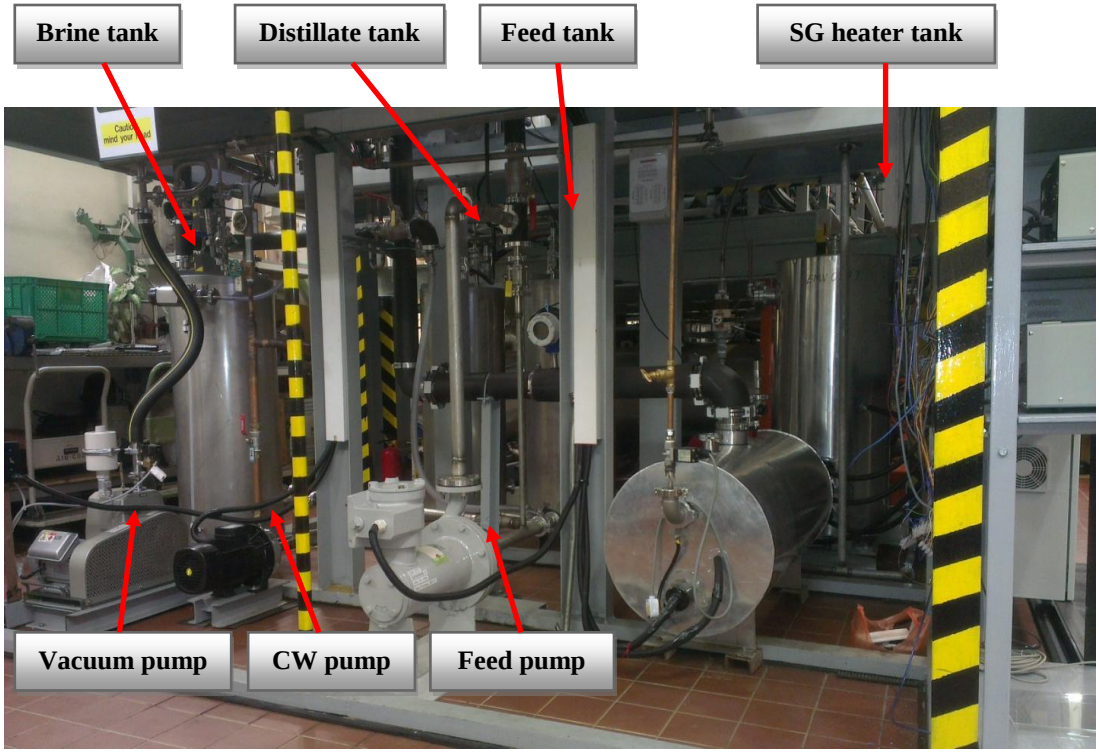

Figure 5.9 **Pictorial view of 3-stages MED system installed in NUS (a) showing the stages and control panel (b) showing the storage tanks and circulation pumps**

Steam Generator			Stage-2			Stage-3			Condenser		
Valve #	Status	Comments	Valve #	Status	Comments	Valve #	Status	Comments	Valve #	Status	Comments
101		Main vapor line	201		Main vapor line	301		Main vapor line	401		Main vapor line
102		JP vapor line	202		JP vapor line	302		JP vapor line	402		Cooling water in
103		JP bypass vapor line	203		JP bypass vapor line	303		JP bypass vapor line	403		Cooling water out
104		Brine line	204		Brine line	304		Brine line			
105		Feed line	205		Feed line	305		Feed line			
106		Hot water line	206		Vacuum line	306		Vacuum line			
107		Vacuum line									
Brine Tank			**Distillate Tank**			**Feed Tank**			**Nomenclature**		
501		Brine inlet	601		Distillate header	701		Feed line			Fully Open
502		Feed pump	602		Balance line to condenser	702		Feed pump			Fully closed
503		Feed line	603		Flow meter bypass	703		Brine mix line			Throttled
504		Vacuum line	604		Vacuum line	704		Vacuum line			Situation depend
505		Condenser balance line	605		Drain line	705		Drain line			
506		Drain line									

Figure 5.10 Valves condition during conventional MED experiment operation

5.4.1 MED System Instrumentation

MED system is fully instrumented to read and record all necessary parameters. Since system is working in vacuum condition so all instrument used are vacuum grade. Table 5.1 shows the detail of instruments used on MED test facility.

Table 5.1 Detail of Instruments used on MED experimental system for data recording

	Instrument	Technical detail	Accuracy	Manufacturer
1	**Pressure measurement**			
	Pressure transducers	Range: 0-60kPa 4-20mA output, 2wire, 1/4''NPT male, wetted part SS316	0.5% FS	General Electric (GE)
2	**Temperature measurement**			
	Thermistor probe sensors	Range: -80^{o}C to 150^{o}C 6'' long, 1/8''diameter, 10kΩ	±0.1^{o}C	OMEGA Engineering Ltd., UK
	Thermistor button sensors	Range: -80^{o}C to 150^{o}C, kΩ	±0.1^{o}C	OMEGA Engineering Ltd., UK
3	**Flow measurements**			
	Turbine flow meter for feed flow	Magnetic pick-up type, 1.1-11LPM, -40 to 85^{o}C, 1/2''NPT FM, 4-20mA output, wetted part SS316	±1.0%	OMEGA Engineering Ltd., UK
	Turbine flow meter for hot and cooling water	3.8-60LPM, -7 to 107^{o}C, 1''NPT FM, 4-20mA output, wetted part SS316	±1.0%	OMEGA Engineering Ltd., UK
	Turbine flow meter for distillate flow	ND05-PATAAC, 0.0-3LPM, 0 to 70^{o}C, 4-20mA output	±1.0%RS	Aichi Tokei Denki Co., Ltd, Japan
	Turbine flow meter for vapor flow	Magnetic pick-up type, 15-200m^{3}/h, -30 to 100^{o}C, 4-20mA output	±1.0%	Sure Instrument, China

MED system P & ID is provided in appendix D where the position of instruments of test facility can be seen clearly. Figure 5.11 shows the MED stage with temperature and pressure sensors location.

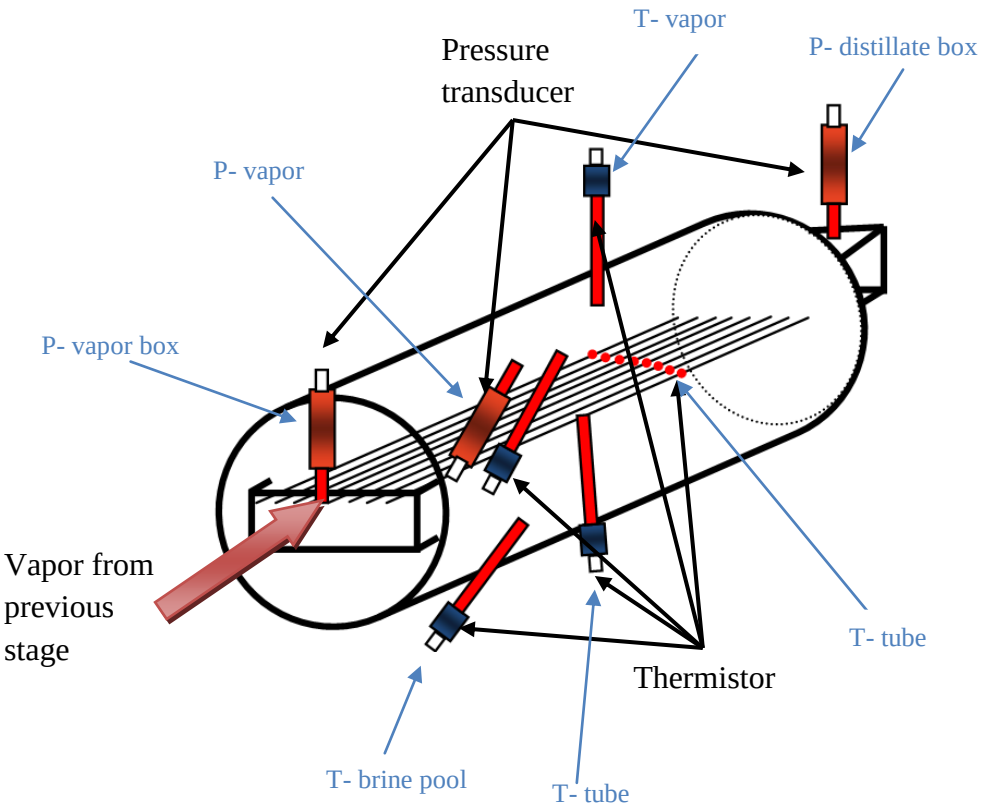

Figure 5.11 **Position of temperature and pressure sensors on MED evaporator for data logging**

Agilent data logging system is used to record the experimental data. All sensors are connected to data logger through to intermediate terminal boxes. All stages sensors detail is provided in appendices E1-E3 and terminal boxes to data logger connections detail is provided in appendices D1-D3.

5.5 Results and Discussion

Experiments were conducted with heat source temperature varies from 70^{o}C to 38^{o}C. The results are discussed below:

MED components temperature distribution

Figure 5.12 shows typical start-up temperature profiles of MED stages at a heat source temperature of 38^{o}C. Steady state events (minimum temperature fluctuations) are seen after 1 hour into the start-up and MED experiments for distillate collection are continued for 4 to 5 hours. From these traces, it is observed that the temperature differences between the stages were less than 1^{o}C, despite the effects from salinity depression of saturation temperatures. This low temperature difference may be because of specially designed (end-cross) high heat transfer tubes used in evaporator. The steam generator has a temperature gap between the source inlet and outlet of 2-3^{o}C whilst the temperature difference between condenser and cooling water outlet is about 5^{o}C. This indicates that a slightly undersized condenser has been used. Similar temperature profiles are observed for other heat source temperatures.

Figure 5.13 shows the steady state temperature values of MED all components for heat source temperature varies from 70^{o}C to 38^{o}C. It can be noticed that in all cases, inter-stage temperature difference is less than 1^{o}C. The temperature difference of heat source for steam generator is 2-3^{o}C and the temperature difference between cooling water inlet and outlet is about 5^{o}C.

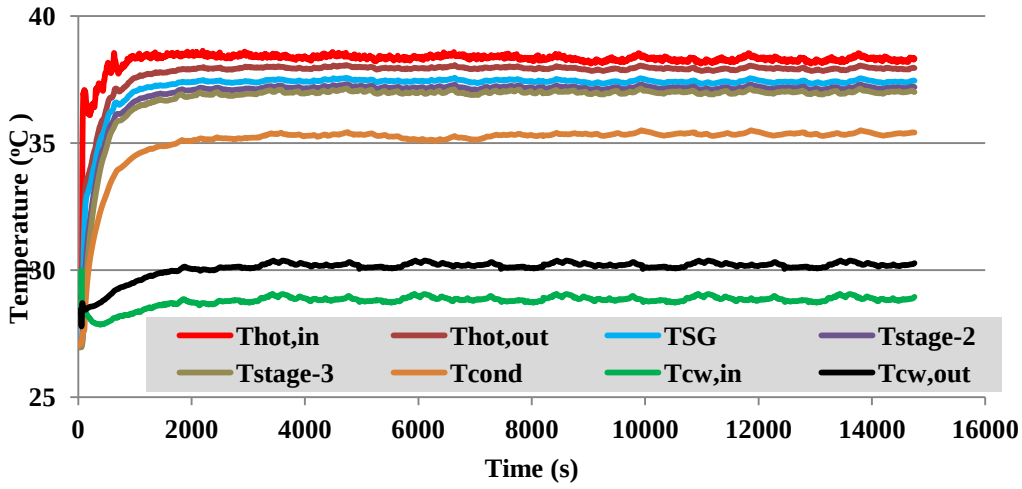

Figure 5.12 **A typical components temperature profiles for the start-up of the 3-stage MED plant at heat source temperature 38°C**

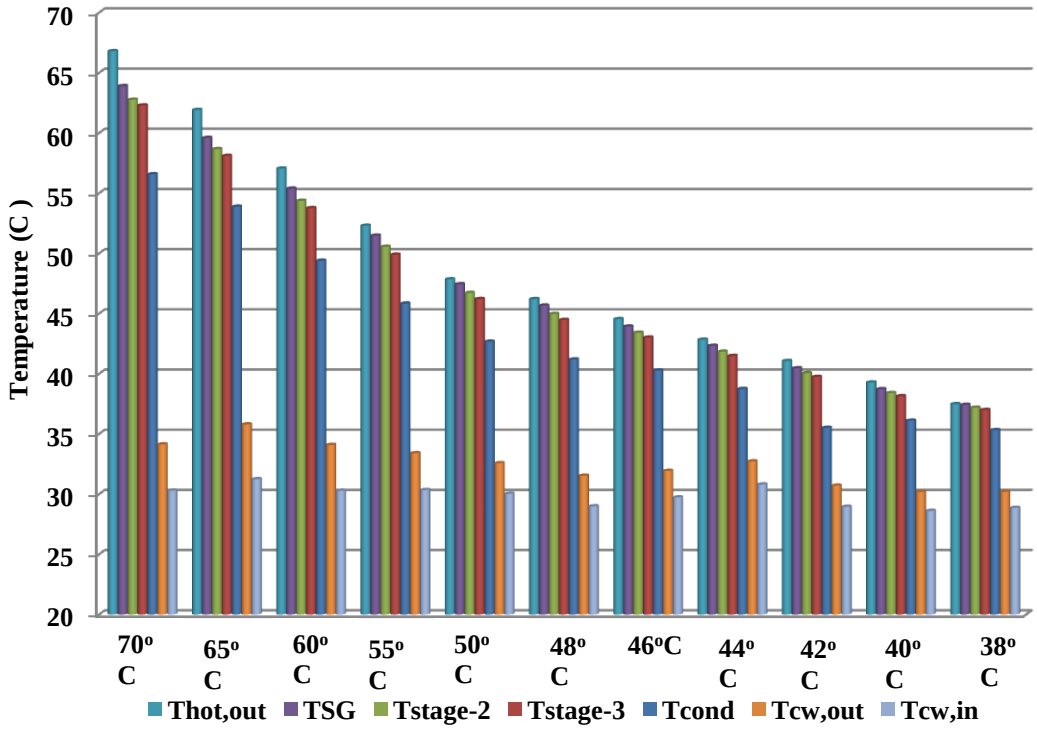

Figure 5.13 **3-stage MED components steady state temperature values at different heat source temperatures**

MED components pressure distribution

Figure 5.14 shows the typical start-up pressure profiles of MED stages at a low heat source temperature of 38^{o}C. Similarly, in pressure traces, steady state events (minimum temperature fluctuations) are also been observed after 1 hour from start-up and MED experiments for distillate collection are continued for 4 to 5 hours. It is observed from the pressure traces that the pressure differences between the stages were less than 1 kPa. Similar steady state profiles are observed for other heat source temperatures. Small fluctuations are observed in saturation pressures and it may be due to feed spray fluctuations. The U-tube is provided between the stages to maintain the pressure difference. It can also be observed that the pressure loss in the vapor pipe line is very small.

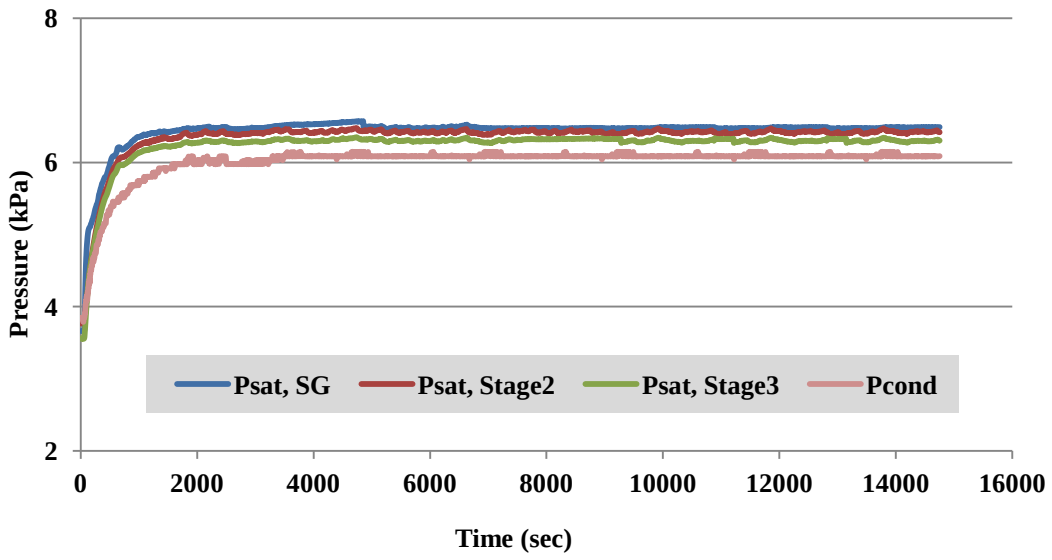

Figure 5.14 A typical components pressure profiles for the start-up of the 3-stage MED plant at heat source temperature 38^{o}C

Figure 5.15 shows the steady state pressure values of MED components at different heat source temperatures. It can be observed that in all cases the pressure difference between stages is less than 1 kPa.

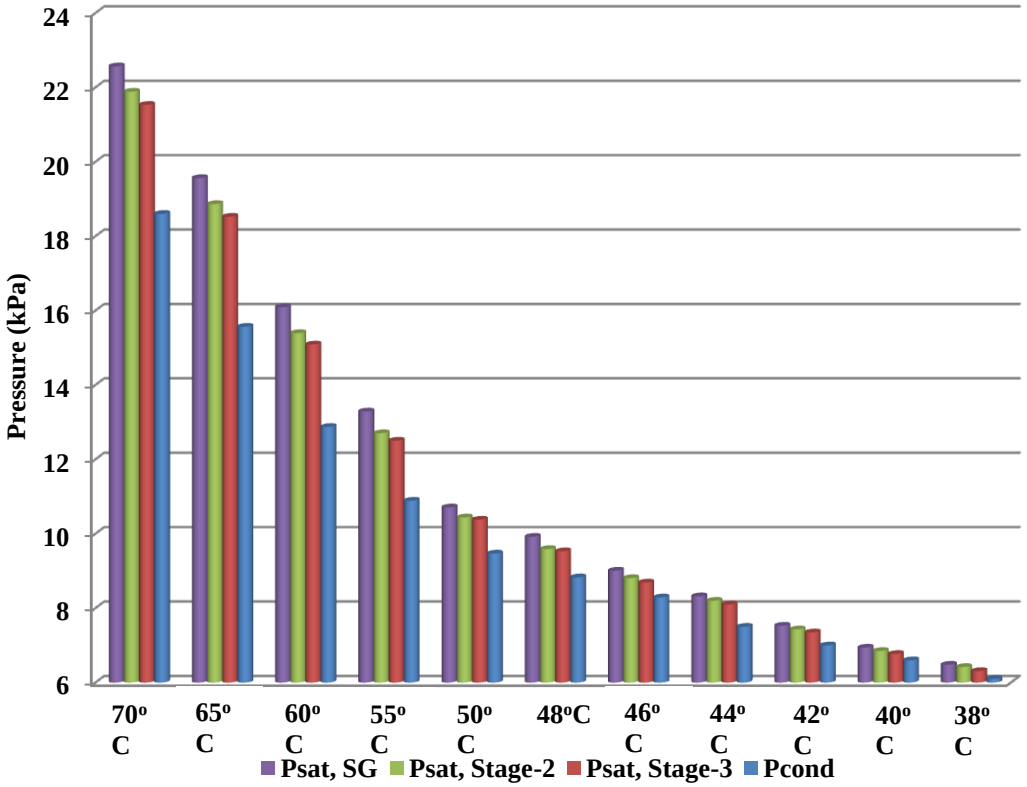

Figure 5.15 **3-stage MED components steady state pressure values at different heat source temperatures**

MED performance

Figure 5.16 shows the power consumption profile during 38°C heat source temperature. High quality thyristor controller is used to control the heat source temperature with accuracy ±0.15°C.

The fluctuations in electric power taken by heater are due to heater cut-in and cut-out during operation to maintain the temperature. The average power is also calculated and plotted in the graph. Figure 5.17 shows the average values of power for heat source temperature varies from 70°C to 38°C.

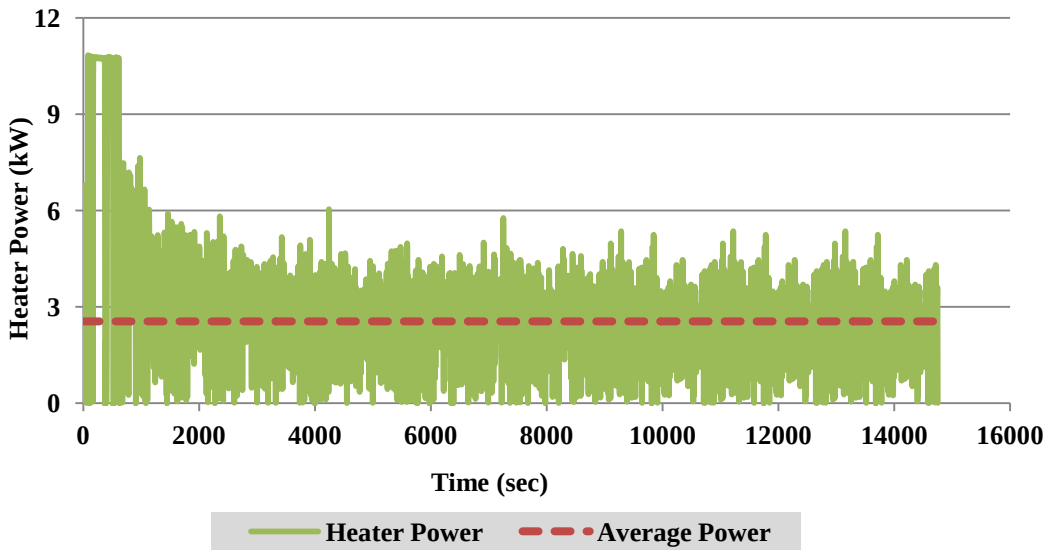

Figure 5.16 3-stage MED instantaneous and average thermal power consumption profiles at heat source temperature 38°C

Figure 5.18 shows the total distillate production trace at heat source 38oC. There are small fluctuations in water production rate and it may be due to fluctuation in spray of feed that affect the condensation rate. Figure 5.19 shows the average water production at different heat source temperatures

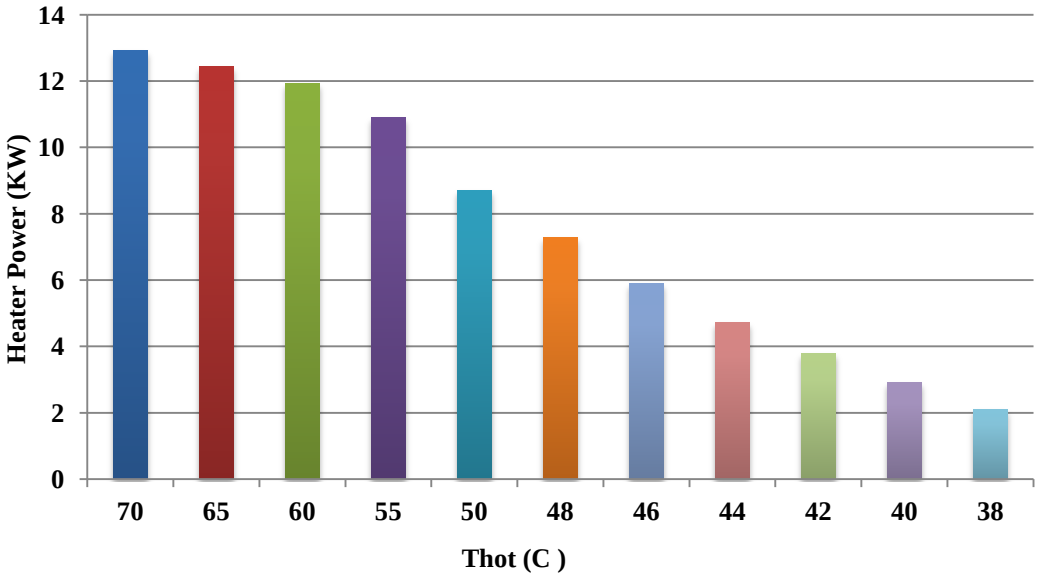

Figure 5.17 **3-stage MED steady state thermal power consumption values at different heat source temperatures**

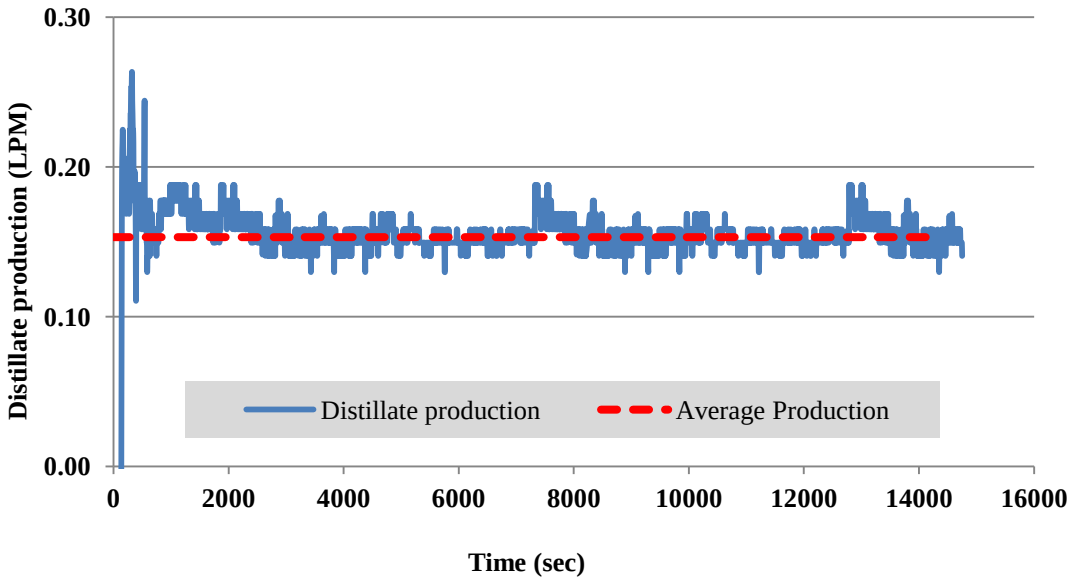

Figure 5.18 **3-stage MED instantaneous and average distillate production profiles at heat source temperature 38°C**

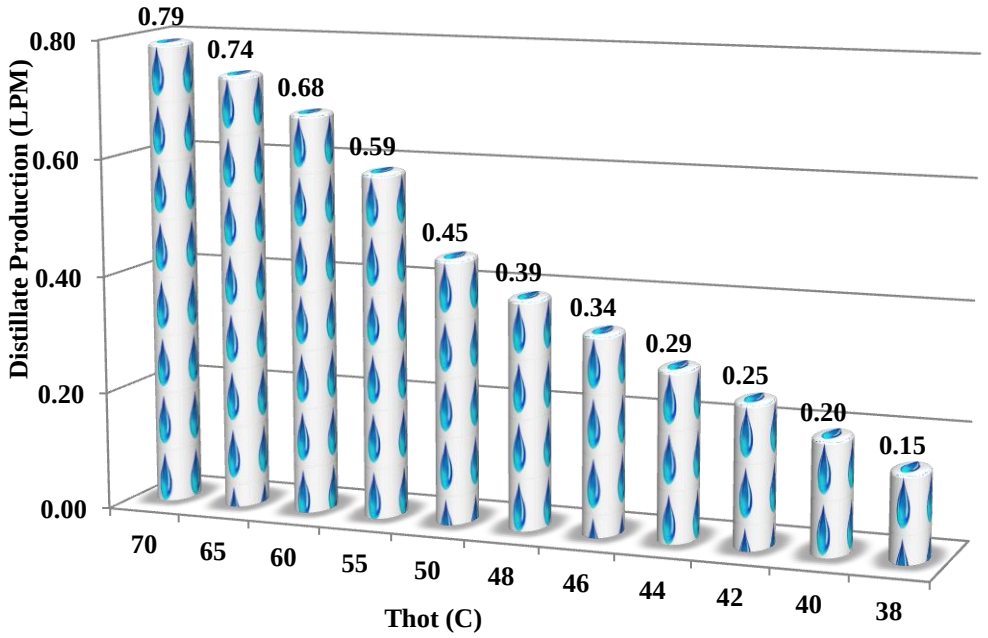

Figure 5.19 3-stage MED steady state distillate production values at different heat source temperatures

Performance ratio (PR) is used as a performance indicator of MED system. It can be defined as:

$$PR = \frac{\dot{m}_{d,total}(kg/\sec).h_{fg,Tsat}(kJ/kg)}{TPE}$$

Figure 5.20 shows the MED 3-stages total distillate production, power consumption and performance ratio at heat source temperature 70°C -38°C. It can be seen that power consumption is increasing with increase in heat source temperature to main required temperature. This increase in power consumption with increase in heat source temperature is due to increase in ΔT of hot water inlet and outlet.

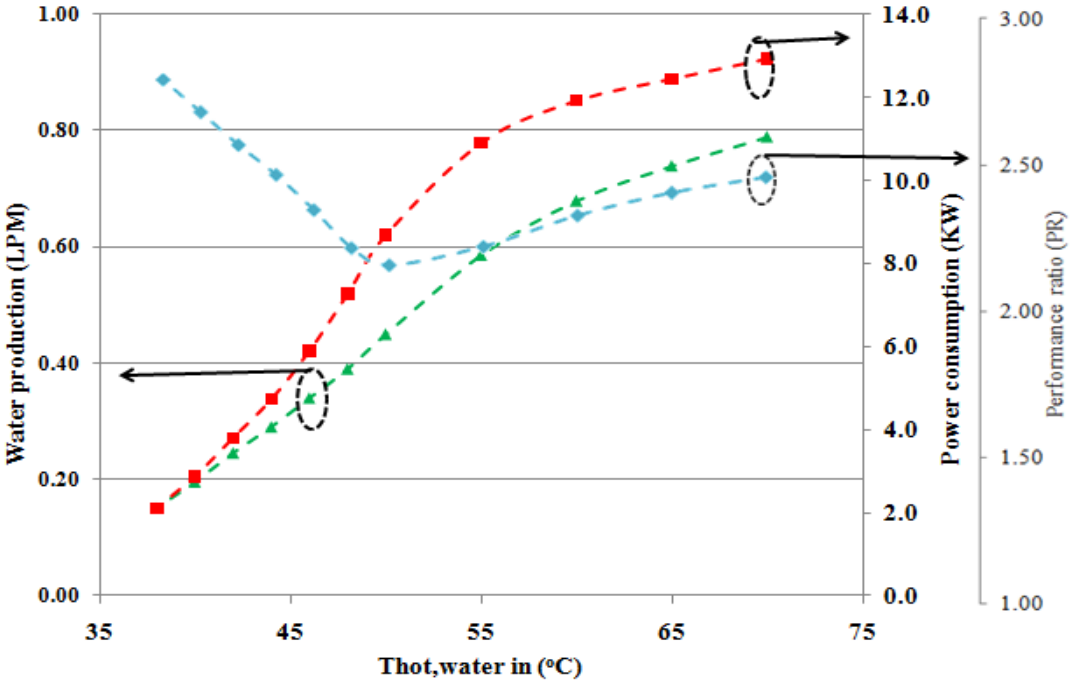

Figure 5.20 **MED system water productions, thermal power consumption and performance ratio at different heat source temperatures**

It can also be seen that production increases with increase in heat source temperature and it drop with heat source temperature drop. The drop in water production at low heat source temperature is due to low saturation pressure. As a conventional MED system, 38^{o}C is the lowest most temperature to operate because of condenser operation temperature limit (35^{o}C).

It can also be seen that PR is increases with increase in heat source temperature and it is due to the increase in water production. Even though the power consumption is also increasing, the increase in water production compensates resulting in a higher PR of the system. High performance ratio at low temperature is attributed to low power consumption.

Table 5.2 summaries the MED operation parameters at different heat source temperatures. The variation in thermal power and PR with heat source temperature can be clearly observed from the table.

Table 5.2 MED experimental output parameters (components temperatures, water production, thermal power and performance) at different heat source

Heating source temperature (^{o}C)	T-SG (Vapor sat) (^{o}C)	T-S2 (vapor sat) (^{o}C)	T-S3 (vapor sat) (^{o}C)	MED water production (LPM)	TPE (kW)	MED PR
38	37.42	37.18	36.99	0.15	2.10	2.92
40	38.72	38.4	38.14	0.20	2.91	2.74
42	40.46	40.05	39.74	0.25	3.80	2.63
44	42.32	41.84	41.48	0.29	4.73	2.50
46	43.93	43.41	43.01	0.34	5.90	2.35
48	45.67	44.97	44.47	0.39	7.27	2.19
50	47.44	46.72	46.21	0.45	8.69	2.12
55	51.47	50.54	49.90	0.59	10.91	2.20
60	55.38	54.37	53.37	0.68	11.92	2.33
65	59.59	58.66	58.10	0.74	12.45	2.43
70	63.90	62.76	62.29	0.79	12.93	2.49

5.6 Validation of Simulation Results

The 3-stage MED system simulation is conducted at assorted heat source temperature and experimental results are compared with simulation results. MED simulation code is written in FORTRAN and linked with IMSL to solve differential equations simultaneously. Even though MED test facility was designed at 50^{o}C heat source temperature but simulation is conducted at wide range of heat source temperature to investigate the system parameters. Table 5.3 shows the parameters used in simulation code of MED.

Table 5.3 MED parameters used in simulation

Parameters	Values	Units
Heat source temperature ($T_{hw,in}$)	40 ~ 60	^{o}C
Heat source flow rate	58	LPM
Heat transfer area	4	m^2
SG tube cluster specification	16x0.7x1300x64	mm
MED stages cluster specification	25x0.7x1300x32	mm
Feed temperature	30	^{o}C
Cooling water inlet temperature	30	^{o}C
Cooling water flow rate	60	LPM

The water properties are calculated by using the formulation developed by Wagner and Kruse [215], Sieder and Peters [216] and Lienhard [217]. All properties are functions of temperature, pressure and salinity. The steam properties are also calculated by using the same formulation as a function of pressure and temperature of system. The steam is assumed to be free from salt.

Figure 5.21 shows the temperature profile of different MED components at heat source temperature 50°C. The solid line shows the simulation results and experimental results are plotted with dotted line. It can be seen clearly that at design condition, all components are operating very well and have good agreement between simulation and experiment results.

The MED system takes some time (almost one hour) for stable operation because of thermal mass, so, this causes the slight deviation from the expected behavior at the start of the experiment. During stable operation (almost after one hour) the results have good agreement with experimental values.

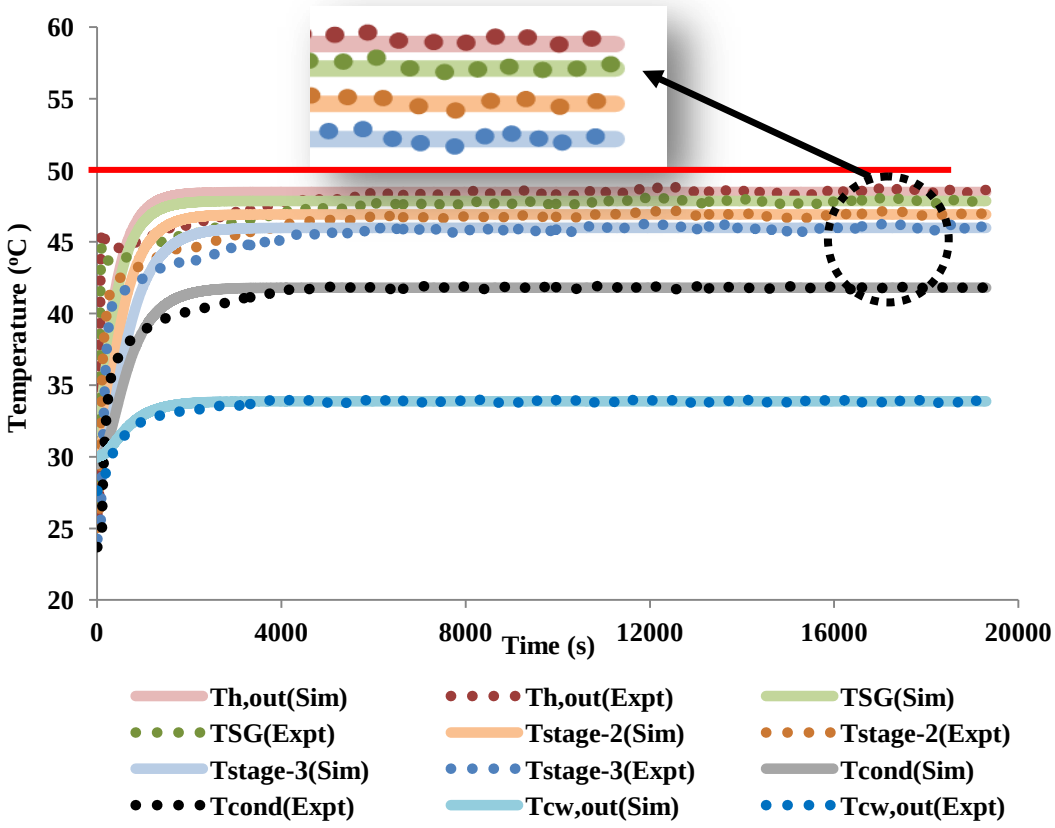

Figure 5.21 **A comparison of MED components temperature profiles: simulation & experiment**

Since saturation pressure follows the temperature, it is also observed good agreement between simulated pressure profiles with experimental results. The similar trends are observed for other heat source temperatures. The comparison of simulation results and experimental results of MED components temperature is given in Table 5.4.

Table 5.4 A comparison of MED components steady state temperature values: simulation & experiments

Heat source		Thot out	SG	Stage-2	Stage-3	Cond	Tcw, out	Tcw, in
60°C	Experimental	57.1	55.4	54.4	53.8	49.4	34.1	30.3
	Simulation	57.8	57.2	56.18	55.0	48.5	36.0	30.0
55°C	Experimental	52.3	51.5	50.5	49.9	45.8	33.4	30.3
	Simulation	53.3	52.6	51.6	50.5	45.2	35.0	30.0
50°C	Experimental	47.8	47.4	46.7	46.2	42.6	32.6	30.0
	Simulation	48.2	47.6	46.7	45.8	41.6	33.8	30.0
45°C	Experimental	44.5	43.9	43.4	43.0	40.27	31.9	29.7
	Simulation	44.7	44.1	43.2	42.5	39.3	33.0	30.0
40°C	Experimental	39.3	38.7	38.4	38.1	36.1	30.2	28.6
	Simulation	39.2	38.5	37.7	37.0	35.2	32.0	30.0

It can be seen that there is good agreement within ±5% between simulation and experimental values not only at design condition as well as at all other heat source conditions.

It shows that the system design is robust and has ability to operate with a wide range of heat source conditions to investigate the system performance.

Table 5.5 shows the comparison of performance parameters of MED system at wide range of heat source temperature. It can be seen that there is good agreement between simulation results and experimental results not only at design as well as at other condition. These results show that system can operate at wide range of heat source efficiently.

Table 5.5 A comparison of MED performance parameters (water production, thermal power and PR): simulation & experiments

Heat source		Distillate production	Power consumption	PR
60°C	Experimental	0.68	11.92	2.33
	Simulation	0.70	12.16	2.35
55°C	Experimental	0.59	10.91	2.20
	Simulation	0.60	11.18	2.19
50°C	Experimental	0.45	8.69	2.12
	Simulation	0.43	8.20	2.14
45°C	Experimental	0.34	5.90	2.35
	Simulation	0.35	5.35	2.45
40°C	Experimental	0.20	2.91	2.74
	Simulation	0.23	3.26	2.79

MED system performance parameters comparison of simulation and experimental results are shown in Figure 5.22, 5.23 and 5.24. It can be seen that there is good agreement between simulation and experimental results within ±5% in all cases.

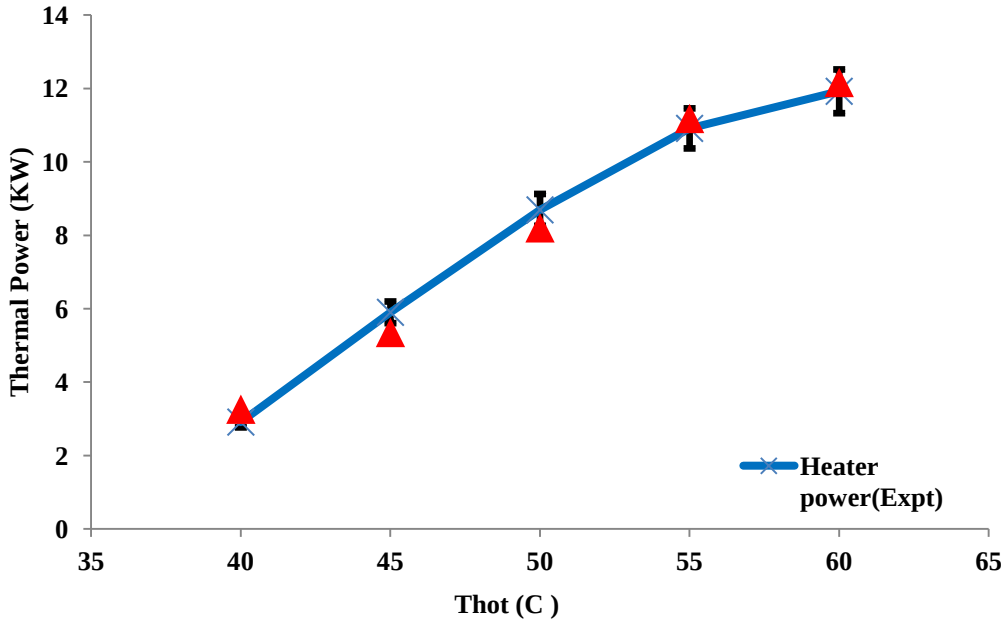

Figure 5.22 Experimental thermal power consumption comparisons with simulation results at different heat source temperatures

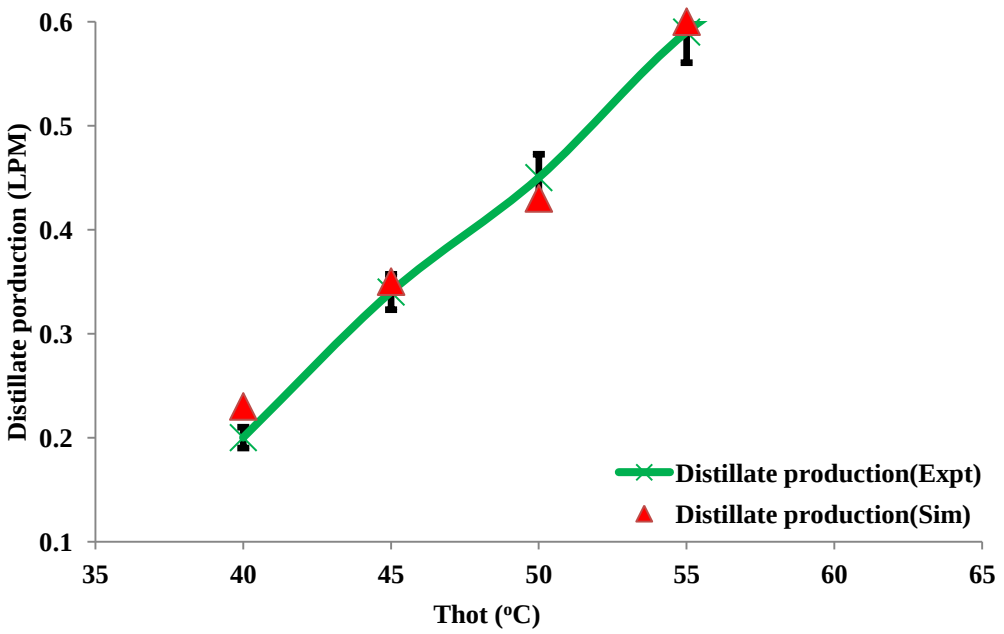

Figure 5.23 **Experimental total water production comparisons with simulation results at different heat source temperatures**

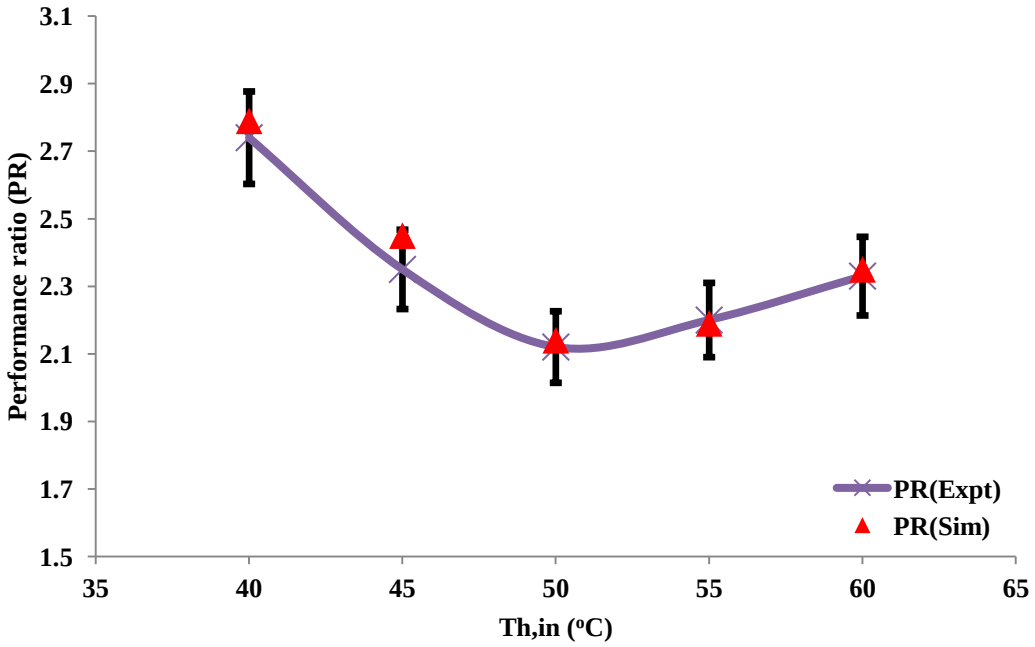

Figure 5.24 **Experimental system performance comparisons with simulation results at different heat source temperatures**

Summary of Chapter 5

A 3-stage Multi effect desalination system is designed with horizontal tubes evaporators. In the first step, area of heat transfer is calculated using values of overall heat transfer coefficient and LMTD reported in the literature. In second step, the verification step, area of heat transfer is calculated by using standard correlations for heat transfer coefficient and compared with the area calculated in 1st step. Evaporator sizing and other parameters are calculated on the basis of calculated area of heat transfer. After designing, fabrication drawings are prepared using AUTOCAD to fabricate the setup. MED components are fabricated and then installed in air-conditioning laboratory in NUS according to process flow diagram. High quality instruments are installed and experimental rig is than commissioned.

The MED system vacuum is tested for 48 hours and then experiments are started. Even though the system was designed at heat source 50^{o}C, but set-up is tested for a wide range of heat source 38^{o}C to 70^{o}C to estimate the system performance. System components operational parameters (temperature, pressure etc.) are plotted and found good tolerance between stages. System performance parameters (Distillate, PR etc.) are measured on the basis of experimental data and are presented. It is found that system performance is very good and very near to theoretical maximum value.

Lastly, system simulation is conducted using experimental operational parameters to verify with experimental results. It is found that simulation results have good agreement within ±5% with experimental results for a wide range of heat source

temperatures. This shows that system designed well and operating efficiently. MED falling film evaporators were designed on the basis of FFHTC correlation developed in chapter 3, so in other words, system efficient operation also validated the strength of proposed correlation.

Chapter 6 Multi-Effect Desalination – Adsorption Desalination (MEDAD) System

Although MED is currently the most efficient thermal system and has advantages over RO in specific locations, its performance is limited by many parameters. Hybridization of thermal desalination systems is a novel technique to overcome the system limitations to enhance performance. It is predicted that hybridization can increase the water production many-fold with same heat input as compared to conventional operation of desalination plants. It is also predicted that hybridization of thermal systems can meet the energy consumption values of RO in terms of KWh/m^3 and can get the large share in world desalination industry. Investigation of thermal hybrid system is very important because of dearth of literature data. Detailed mathematical modeling and simulation of a proposed hybrid thermal desalination system (MEDAD) is provided for better understanding of hybridization and for future desalination industry references.

The proposed hybrid MEDAD system is discussed here in detail. In the first part of the chapter, adsorption desalination (AD) system is discussed in detail. In the second part, detailed discussion on MEDAD system and its hybridization concept is provided. In the third part of the chapter, detailed mathematical modeling of MED, AD and MEDAD system is provided. In the last part of this chapter, MEDAD results are discussed and compared with conventional MED system.

6.1 Background

Even though thermally driven desalination cycles are well developed but still thermodynamically not very efficient in terms of KWh/m^3. The next step in their development is systems integration as researchers has been realized. MED is most energy efficient thermal desalination system and AD is an emerging low cost cycle. Integration or hybridization of these two thermal desalination cycle (MEDAD) is proposed to investigate the system performance as compared to conventional MED system. Detailed mathematical modeling is developed and simulation code is constructed in FORTRAN. The detail of MEDAD system is discussed in following sections.

6.2 Overview of Adsorption Desalination System (AD)

Adsorption Desalination cycle is based on sorption principles in which the water vapors are adsorbed during adsorption processes and regenerated during desorption processes. The adsorbent used for the AD processes are activated carbon, silica gel and zeolite having high pore surface area typically more than 500m^2/g. There are five main components of AD system namely: i) evaporator, ii) adsorption/desorption reactor beds, iii) condenser, iv) pumps and v) pre-treatment facility. The detailed process diagram is shown in Figure 6.1 [222-225]. The AD operation involves two main processes:

i) adsorption-assisted-evaporation: in which the vapors generated in AD evaporator are adsorbed on the pore surface area of adsorbent. The heat source is circulated through the tubes of evaporator and seawater is sprayed on the tube bundle. It is

observed that the evaporation is initiated by heat source but during adsorption process the high affinity of water vapor of adsorbent drop the evaporator pressure and contribute in evaporation.

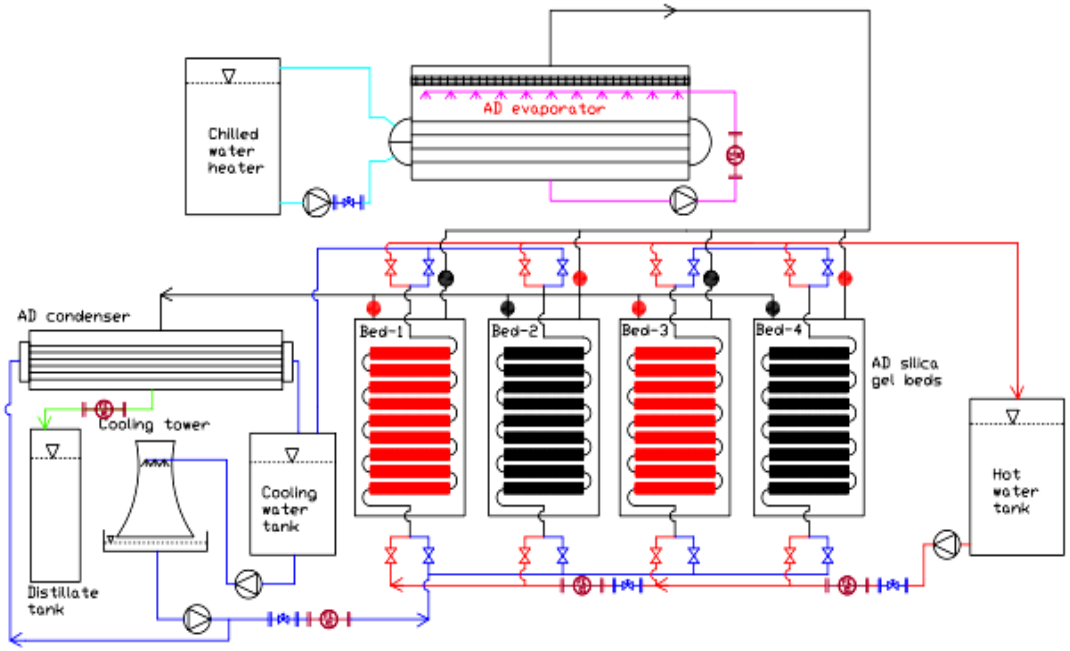

Figure 6.1 Detailed schematic of Adsorption desalination cycle

The AD evaporator operation temperature can be controlled by heat source temperature that is normally circulated in term of chilled water. The AD evaporator can operate at a wide range of chilled water temperature varies from 5^{o}C to 30^{o}C to produce the cooling effect as well at low temperature operation. The vapor adsorption process is continues until the adsorbent bed reach to a saturation state.

ii) desorption-activated-condensation: in which saturated adsorbent is regenerated using the low grade industrial waste heat or renewable energy (desorption

temperature varies from 55 °C to 85 °C) and desorbed vapors are condensed in a water cooled condenser and collected as a distillate water [226-230].

It can be seen that two useful effects produced by AD cycle are the cooling effect by the first process "adsorption-assisted-evaporation" and fresh water by converting the seawater by second process "desorption-activated-condensation". Useful effects which are cooling and water production can be produced simultaneously by introducing the multi-bed technique [231-235].

In multi-bed AD system, the operation and switching technique is used. During operation, one or pair of adsorbent reactor beds undergo the adsorption process and at same time one or pair of adsorbent reactor beds execute the desorption process. The time for adsorbent reactor beds operation either adsorption or desorption is depends on the heat source temperature and silica gel quantity packed in a bed [235]. Prior to changing the reactor duties, there is a short time interval called switching in which the adsorber bed pre-heated whilst the desorber bed pre-cooled to enhance the performance of cycle. In AD cycles, the operation (adsorption and desorption) and switching processes are controlled by automated control scheme that can open and close the respective bed hot/cold water valves. During switching operation, all vapor valves are closed so there is no adsorption or desorption taking place.

6.3 Multi Effect Desalination-Adsorption Desalination Systems (MEDAD)

6.3.1 MED+AD Cycles Hybridization Concept.

MEDAD is a hybrid of two thermal systems namely; multi-effect desalination system and adsorption cycle. The main components of this novel thermal hybrid system are: 1) multi-effect distillation (MED) system, 2) adsorption desalination (AD) cycle and 3) auxiliary equipments. In this hybridization system, the last stage of the MED is connected to adsorption beds of AD cycle for the direct vapor communication to adsorption beds. The basic concept of MEDAD cycle is shown in Figure 6.2(a) & 6.2(b) in comparison with conventional MED system. It can be seen that in conventional MED system, number of stages are restricted by TBT (70^{o}C) and LBT (40^{o}C) and hence the system performance due to limited number of heat recoveries in terms of vapor condensation. In thermal desalination systems, TBT is limited by soft scaling agents namely; magnesium (Mg++), calcium (Ca++), and sulfate (SO_4^{2-}) and these agents are more active above 70^{o}C and cause system degradation. The last stage temperature limit (40^{o}C) is due to condenser that operating with cooling tower water. The ambient conditions of cooling tower limit the last stage temperature and cannot be extended below 40^{o}C.

In solution to above limitations, researchers found that by introducing the nano filtration (NF) or anti-scalant prior to introduction the feed into MED, “soft scaling” agents can be removed and TBT can be raised to 130^{o}C [236-238]. The inter stage temperature and the last stage operating temperature barrier can be broken by hybridization with adsorption cycle. AD cycle can operate below ambient condition typically at 5^{o}C due high affinity of water vapors of adsorbent (silica gel). MED last

stage temperature can be lower down to 5^{o}C by introducing the AD at downstream. Conventional MED and proposed MEDAD operation concept is shown in Figure 6(a) and Figure 6(b).

It can be seen that by hybridization, the overall operational gap increased from 70^{o}C – 40^{o}C to 70^{o}C – 5^{o}C. The overall larger operational temperature gap help to install more number of stages with same heat input that increase the number of heat recoveries or in other words the water production and hence system performance.

The other commonly used membrane hybrid technologies are; MED-RO, MSF-RO, NF-RO, RO-FO etc [239-248]. All these hybridization schemes help to improve the system performance in term of kWh/m^{3}.

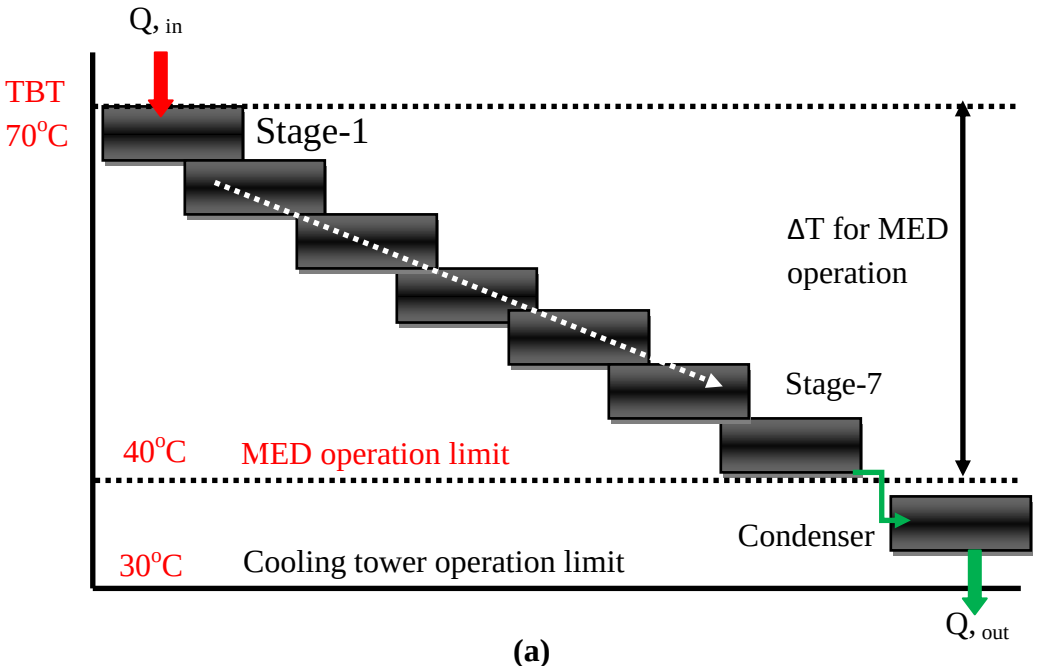

(a)

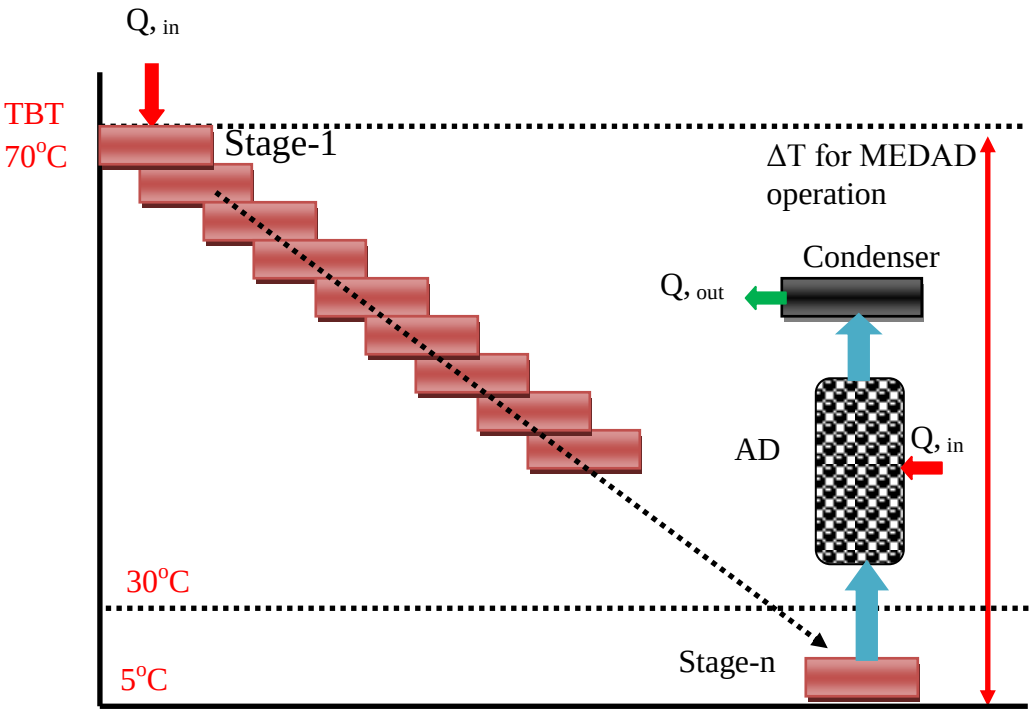

(b)

Figure 6.2 **Basic concept of hybrid MEDAD operation (a): MED operation regime and limiting BBT 40°C, (b): MEDAD operational regime and limiting BBT 5°C**

The operation zone of conventional MED, hybrid MEDAD and NF-MEDAD on salt crystallization curve is shown is shown in Figure 6.3. It can also be seen that at higher temperature nano filtration (NF) can remove the soft scaling components at upstream of plant before entering the feed into system and prevent the system from scaling and fouling. While at downstream, the LBT range is extended to 5°C due to AD integration. Proposed MEDAD is the most thermal efficient system because of its larger operational gap and large number of additional heat recoveries.

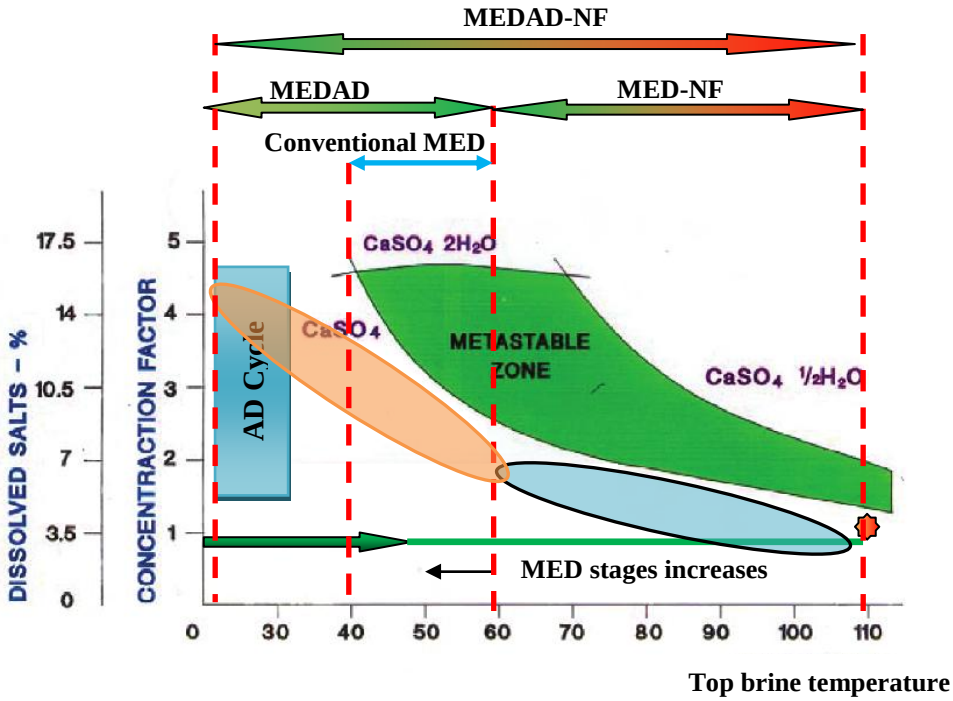

Figure 6.3 **A comparison of MED, AD and hybrid MEDAD operation zone on salt metastable curve**

The detailed operational strategy of MEDAD system is discussed in following section.

6.3.2 MEDAD Operational Strategy

Hybrid desalination cycle or in short called as MEDAD desalination process is shown in Figure 6.4. In this investigation, a parallel feed MED system is coupled with an AD cycle to break the last stage temperature barrier as in conventional MED system. The pseudo-effect i.e., AD evaporator is replaced by the last stage of MED for integration of these two thermal systems. The temperature and pressure of this stage is controlled by two factors: (i) the condensation energy of water vapor from the preceding effect and (ii) the vapor uptake of the adsorbent in the AD cycle.

In MED stages, vapor emanation from feed seawater is achieved by falling film-evaporation process. Evaporation energy is recovered by series of re-utilization of vapor condensing energy in successive stage those are produced in preceding stages. Process of vapor production and energy recovery by condensation continues until the last stage of MED. The vapors from the last stage are than directed towards AD beds where they adsorbed on the adsorbent surface. Adsorbent high affinity for water vapor drops the pressure and hence the saturation temperature of last stages below ambient typically up to 5^{o}C. It is believed that this drop in pressure and temperature of last stage will also affect the parameters of the few proceeding stages.

Hot water is circulated through MED steam generator as a heat source. Being a parallel feed MED, seawater feed is supplied individually to all stages via nozzle header installed in each stage. The vapor produced in the steam generator is condensed in the tube side of the next MED stage where the latent heat of

condensation is transferred to the spray feed water through heat exchanger tubes. In this way, the latent heat of condensation is recovered in successive stages multiple times for vapor generation across the stages with lowering saturation pressures and temperatures. Inventory brine from each stage is collected via U-tubes to a brine collection header and then to the brine collection tank. The condensate from each stage condensate box is collected to a condensate collection header via U-tubes. This condensate is than measured and collected to a distillate tank as a drinking water.

In a hybrid design, the AD reactor beds can be designed so that the mass transfer by the adsorbent provides sufficient cooling energy to accommodate several additional effects operating at below ambient temperatures. AD cycles normally operate in batch manner so for continuous operation multi-bed scheme is utilized [225-227]. During adsorption process the adsorber reactor has direct communication with MED last evaporator to adsorb the last stage vapors whilst the desorber bed valve is opened to condenser for desorbed vapor condensation.

Being an exothermic process, adsorption process is maintained by circulating the cooling water through the adsorber bed to reject the heat of adsorption whilst heat source is circulated through the desorber bed to provide the heat of desorption. In AD cycles, silica gel regeneration temperature varies from 55°C to 85°C. Simple valve controlling scheme is used to changeover the duties of reactor beds from adsorption to desorption or vice versa. However, a sufficient time interval called switching time is provided to preheat the adsorber bed and to pre-cool the desorber bed to attain the condensation and evaporation pressures respectively prior to interchanging their roles.

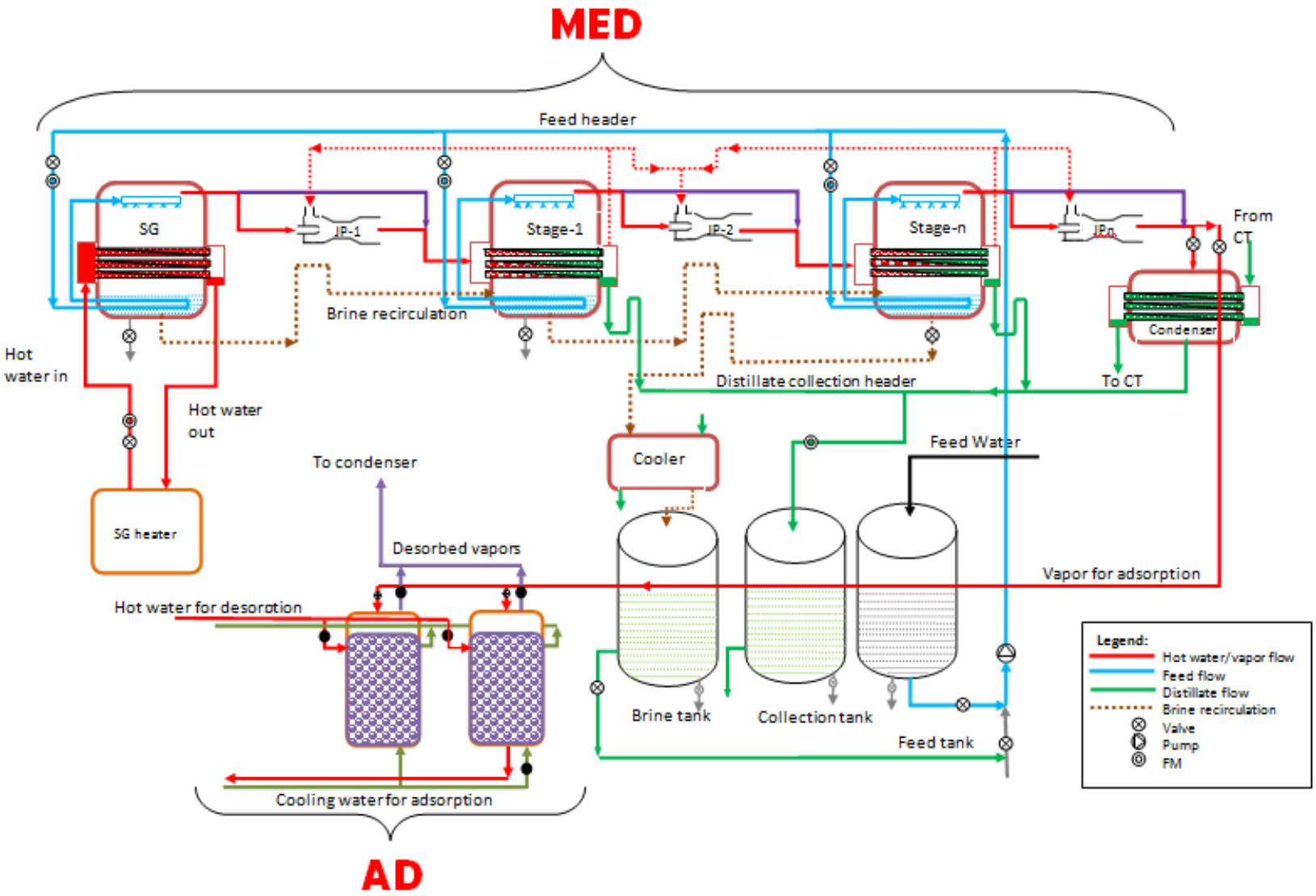

Figure 6.4 Detailed schematic of Hybrid MEDAD cycle

Four reactor beds are employed in present investigation and system is operating in a two bed mode. The reason for this configuration is rigorously validation of mathematical model and simulation results for various operating conditions [249-252]. Both thermal systems MED and AD are arranged in such a manner that the can also operate as a standalone systems. These operating conditions can easily obtained just by changing the valve conditions. In standalone condition, AD can produced two useful effects cooling and desalination [224, 229] whereas MED can produce desalinated water. In the present study, the performance of the hybrid MEDAD cycle is compared with a conventional MED cycle for the same heat source temperatures to investigate the performance improvement as a result of hybridization.

6.4 MEDAD System Mathematical Modeling

Mathematical modeling of hybrid MEDAD system with a parallel feed MED configuration and adsorption desalination (AD) cycle is formulated using the mass, energy and concentration balances. For sorption characteristics, silica gel-water pair model is incorporated. The assumptions considered are: i) the homogenous temperature in the MED stage ii) full water vapor condensation in side of all the effects including final condenser, iii) due to low temperature, heat leak to/from the ambient is negligible and iv) no non-condensable gases in feed water due to de-aeration. Transient modeling for the MED system is developed in order to synchronize the operation of the MED with the cyclic-steady state behavior of the AD cycle.

6.4.1 MED System Mathematical Modelling

MED components mathematical modeling is developed using mass, concentration and energy balances. Feed seawater is supplied to MED stages in parallel manner. Before spraying onto the tubes, feed is pre-heated in build-in pre-heater in evaporators. The motive vapor is generated in steam generator utilizing hot water as heat source. The vapors produced in preceding stages are used as a heat source in successive stages. All MED stages essentially a shell and tube heat exchanger with the heating liquid in the tube side. Thermodynamic model equations for the simulation of the MED plant are summarized in Table 6.1.

Table 6.1 Mathematical modeling equations of MED components

Equation	Remarks	
Modeling equations for steam generator		
$\left[\left(M_{hw}.Cp_{hw}\right)\right]\frac{dT_{hw}}{dt}=\left(\dot{m}_{hw,}\ h_{f,Thw,in}\right)-\left(\dot{m}_{hw}\ h_{f,Thw,out}\right)-h_{in,i}.A_{in,i}\left(T_{hw}-T_{tube,i}\right)$	Energy balance for the hot water flowing inside the tubes of brine heater.	(6.1)
$\left[\left(M_{HX,i}.Cp_{hx,i}\right)\right]\frac{dT_{tube,i}}{dt}=h_{in,i}.A_{in,i}\left(T_{hw,i}-T_{tube,i}\right)-h_{out,i}.A_{out,i}\left(T_{tube,i}-T_{v,i}\right)$	Energy balance for metal tubes.	(6.2)
$\frac{dM_{b,i}}{dt}=\dot{m}_{f,i}-\dot{m}_{b,i}-\dot{m}_{v,i}$	Mass balance for the seawater inventory in the evaporator side of the brine heater.	(6.3)
$\left[\left(M_{b,i}.Cp_{b,Tb}\right)+\left(M_{HX,i}.Cp_{HX}\right)\right]\frac{dT_i}{dt}=\left(\dot{m}_{f,i}\ h_{f,Tf}\right)-\left(\dot{m}_{b,i}\ h_{f,Tb}\right)-\left(\dot{m}_{v,i}\ h_{g,Tv}\right)+Q_{in,i}$ $Q_{in}=h_{out,i}A_i\left(T_{tube}-T_{v,i}\right)$	Energy balance for the evaporator side of the steam generator.	(6.4) (6.5)
$M_{b,i}\frac{dX_{b,i}}{dt}=\left(\dot{m}_{f,i}\ X_{f,i}\right)+\left(\dot{m}_{b,i}\ X_{b,i}\right)-\left(\dot{m}_{v,i}\ X_{v,i}\right)$	Material/concentration balance	(6.6)
$Nu=\frac{h_{in,i}d_{in,i}}{K_{tube,i}}=0.023\mathrm{Re}_l^{0.80}\ \mathrm{Pr}_l^{0.40}$	Convective heat transfer coefficient equation [231]	(6.7)
$R_{wall,i}=\frac{\ln\left(\frac{d_{out,i}}{d_{in,i}}\right)}{2.\pi.K_{tube,i}.L_{tube,i}}$	Tube wall resistance	(6.8)

$$h_{out,i}=\left[0.00143.\left[\frac{\mu_l^2}{g.\rho_l^2.k_l^3}\right]^{-0.16}(\mathrm{Re}_\Gamma)^{0.45}(\mathrm{Pr})^{3.85}\left[2.\exp\left(\frac{S}{S_{ref}}\right)-1\right]^{-0.38}\left(\frac{T_{sat}}{T_{ref}}\right)^{-0.89}\right]+\left[2.65.\left(\frac{q}{\Delta T}\right)^{0.84}\left(\frac{v_g}{v_{ref}}\right)^{-0.47}\right]$$	Falling film evaporation heat transfer coefficient	(6.9)
$$h_{out,i}\left(\frac{v^2}{k^3 g}\right)=0.0007\,\mathrm{Re}^{0.2}\,\mathrm{Pr}^{0.65}\,q^{0.4}$$	Falling film evaporation heat transfer coefficient, Han and Fletcher's correlation [232].	(6.10)
$$U_i A_i=\frac{1}{\frac{1}{h_{in,i}A_{in,i}}+R_{wall,i}+\frac{1}{h_{out,i}A_{out,i}}}$$	Overall heat transfer coefficient	(6.11)
Modeling equations for intermediate stages		
$$\left[\left(M_{l,i+1}.Cp_{l,Tcond}\right)\right]\frac{dT_{cond,i+1}}{dt}=\left[\dot{m}_{v,}\,h_{fg,Tv}\right]_i-\left[h_{in}.A_{in}\left(T_{cond}-T_{tube}\right)\right]_{i+1}$$	Energy balance for the condenser side of the ith effect.	(6.12)
$$\left[\left(M_{HX,i+1}.Cp_{hx,i+1}\right)\right]\frac{dT_{tube,i+1}}{dt}=h_{in,i+1}.A_{in,i+1}\left(T_{cond,i+1}-T_{tube,i+1}\right)-h_{out,i+1}.A_{out,i+1}\left(T_{tube,i+1}-T_{v,i+1}\right)$$	Energy balance for tube metal	(6.13)
$$\frac{dM_{b,i+1}}{dt}=\dot{m}_{f,i+1}-\dot{m}_{b,i+1}-\dot{m}_{v,i+1}$$	Brine inventory balance	(6.14)

$\left[\left(M_{b,i+1}.Cp_b\right)+\left(M_{HX,i+1}.Cp_{HX,i+1}\right)\right]\frac{dT_{i+1}}{dt}=\left(\dot{m}_{f,i+!}\,h_{f,Tf}\right)-\left(\dot{m}_{b,i+1}\,h_{f,Tb}\right)-\left(\dot{m}_{v,i+1}\,h_{g,Tv}\right)+Q_{in,i+1}$ $Q_{in,i+1}=h_{out,i+1}A_{i+1}\left(T_{tube,i+1}-T_{v,i+1}\right)$	Energy balance for evaporator side	(6.15) (6.16)
$M_{b,i+1}\frac{dX_{b,i+1}}{dt}=\left(\dot{m}_{f,i+1}\,X_{f,i+!}\right)-\left(\dot{m}_{b,i+1}\,X_{b,i+1}\right)-\left(\dot{m}_{v,i+!}\,X_{v,i+!}\right)$	Material/ concentration balance	(6.17)
$Nu=\frac{h_{in,i+1}L_{i+1}}{K_{tube,i+1}}=0.728\left[\frac{gh_{fg,Tcond}\rho_{l,Tcond}\left(\rho_l-\rho_v\right)_{Tcond}K_{l,Tcond}^3}{\mu_{l,Tcond}d_i\left(T_{v,i+1}-T_{tube,i+1}\right)}\right]^{1/4}$	Nusselt film condensation correlation for the calculation of the heat transfer coefficient inside the condenser tubes [233]	(6.18)
$U_iA_i=\frac{1}{\frac{1}{h_{in,i}A_{in,i}}+R_{wall,i}+\frac{1}{h_{out,i}A_{out,i}}}$	Overall heat transfer coefficient equation.	(6.19)
MED last stage connected with AD beds		
$\left[\left(M_{b,n}.Cp_b\right)+\left(M_{HX,n}.Cp_{HX,n}\right)\right]\frac{dT_n}{dt}=\left(\dot{m}_{f,n}\,h_{f,Tf}\right)-\left(\dot{m}_{b,n}\,h_{f,Tb}\right)-\left(M_{sg}h_{g,Tv}\right)\frac{dq_{ads}}{dt}+Q_{in,n}$	Energy balance for the condenser side of the i[th] effect.	(6.20)
$Q_{in,n}=h_{out,n}A_n\left(T_{tube,n}-T_{v,n}\right)$		(6.20a)

6.4.2 AD System Mathematical Modelling

In thermal cycle integration, the adsorption cycle reactor bed is coupled to the last effect of MED to absorb the water vapors. Saturated adsorber bed is then regenerated using low grade waster heat. The regenerated water vapors are condensed using a water-cooled condenser. The performance or sorption characteristic of the adsorbent is governed by the equilibrium uptake and kinetic behavior of the silica gel-water pair. The thermo-physical properties and adsorption model of silica gel - water vapor pair sorption in the AD cycle are adopted from Thu et al.[35]. AD cycle mathematical modeling equations are given below.

Water vapors uptake: Toth isotherm equation is used for calculation of water vapors uptake by silica gel and can be written as:

$$q^* = \frac{k_0 \exp\{\Delta H_{ads}/(RT)\}P}{\left[1+\left\{\frac{k_0}{q_\infty}\exp\{\Delta H_{ads}/(RT)\}P\right\}^t\right]^{1/t}} \tag{6.21}$$

Where, q_∞, k_0 and t are the constants.

Transient uptake: transient uptake is calculated by linear driving force equation expressed by Suzuki and Sakoda as shown below.

$$\frac{dq}{dt} = \frac{15 D_{SO} \exp\left(\frac{-E_a}{RT}\right)}{R_P^2}\left(q^* - q\right) \tag{6.22}$$

Where, q^* is the equilibrium uptake calculated by Toth equation, D_{s0} is pre-exponential factor of the efficient water diffusivity in the adsorbent and R_p is the average radius of the adsorbent grains.

Heat of adsorption: isosteric heat of adsorption as function of uptake, temperature and pressure is calculated as:

$$Q_{st} = h_{fg} - E \times \left\{ -ln\left(\frac{q}{q^0} \right) \right\}^{1/n} + T \times v_g \times \left(\frac{\partial P}{\partial T} \right)_g \tag{6.23}$$

Adsorber energy balance: energy balance for adsorber beds connected to MED evaporator is calculated as:

$$\left(M_{sg} C_{P,sg} + M_{HX} C_{P,HX} + M_{abe} C_{P,abe} \right) \frac{dT_{ads}}{dt} = \Delta H_{ads}\left(T_{ads}, P_{ads} \right) . M_{sg} \frac{dq_{ads}}{dt}$$
$$+ \dot{m}_{cw} C_{P\,cw}\left(T_{ads}, P_{ads} \right)\left(T_{cw,in} - T_{cw,out} \right) \tag{6.24}$$

The first term in the left hand side represents the thermal mass by the adsorbent materials, the second term represent the heat exchanger thermal mass and the last term denotes the thermal mass contributed by the adsorbed phase.

Desorber energy balance: energy balance for desorber beds connected to condenser can be written as:

$$\left(M_{sg} C_{P,sg} + M_{HX} C_{P,HX} + M_{abe} C_{P,abe} \right) \frac{dT_{des}}{dt} = -\Delta H_{des}\left(T_{des}, P_{des} \right) . M_{sg} \frac{dq_{des}}{dt}$$
$$+ \dot{m}_{hw} C_{P\,hw}\left(T_{des}, P_{des} \right)\left(T_{hw,in} - T_{hw,out} \right) \tag{6.25}$$

Condenser energy balance: energy balance for condenser connected to desorber beds can be calculated as.

$$\left(M_{cw}C_{P,CW}+M_{HX}C_{P,HX}\right)\frac{dT_{cond}}{dt}=-h_f\left(T_{cond}\right).\frac{dm_d}{dt}+M_{sg}h_g\frac{dq_{des}}{dt}$$
$$+\dot{m}_{cw,cond}C_P\left(T_{cond}\right)\left(T_{cw,in}-T_{cw,out}\right) \quad (6.26)$$

Heat capacity: Specific heat capacity of the adsorbed phase vapors can be found as.

$$C_{P,ads}=C_{P,g}+\left\{\frac{1}{T}-\frac{1}{v_g}\left(\frac{\partial v_g}{\partial T}\right)_P\right\}Q_{st}-\left(\frac{\partial Q_{st}}{\partial T}\right)_p \quad (6.27)$$

Outlet temperature: outlet temperature of the heating or cooling fluid can be calculated by log mean temperature difference approach as shown below.

$$T_{cw/hw,out}=T_O+\left(T_{cw/hw,in}-T_O\right)\exp\left[\frac{-UA}{\dot{m}_{cw/hw}C_{p,TO}}\right] \quad (6.28)$$

Evaporator energy balance: AD evaporator is replaced by last stage of MED in case of hybridization and vapor space temperature can be found by the equation 6.20.

Parameters used in the simulation are provided in Table 6.22.

Table 6.2 Parameters used for MEDAD cycle simulations

MED Steam Generator		
Design Parameters		
Capacity	10.0	KW
Area of heat transfer	4.0	m^2
Tube outer diameter	16.0	mm
Tube thickness	0.7	mm
Single tube length	1300	mm
Tube matrix detail (tubes in a row x rows)	8 x 8	
Evaporator shell inside diameter	500	mm
Evaporator shell length	1300	mm
Operation Parameters		
Hot water flow rate	48	LPM
Hot water inlet temperature	50	^oC
Cooling water inlet temperature	30	^oC
Feed water salinity	35000	ppm
MED Stage Design Parameters		
Area of heat transfer	4.0	m^2
Tube outer diameter	25.4	mm
Tube thickness	0.7	mm
Single tube length	1300	mm
Tube matrix detail (tubes in a row x rows)	8 x 4	
Evaporator shell inside diameter	500	mm
Evaporator shell length	1300	mm
AD Cycle parameters		
Heat of adsorption ($H_{ads/des}$)	2693.0	kJ/kg
Maximum adsorbed amount (q_e)	0.45	kg/kg of SG
Constant (Ko)	$7.3x10^{-13}$	kg/kgPa
Constant (t)	12	
Kinetic constant (Dso)	$2.54x10^{-4}$	m^2/sec
Activation energy (Ea)	$4.2x10^{-4}$	kJ/kg
Average radius of SG particles (Rp)	0.40	mm
Specific heat of SG (Cp,sg)	921	J/kgk
Mass of SG per bed (Msg)	100	kg
Thermal mass of beds (M_{HX})	284.1	kJ/k
Water flow rate	1.52	kg/sec
Cooling water temperature	30	^0C
Hot water temperature	85	^0C

6.4.3 MEDAD System Performance Modelling

In MEDAD cycle operation, hot water is circulated through the steam generator and desorber beds to supply the heat to the system. Cooling water is circulated through the desorber beds and condenser to extract the heat of adsorption and condensation and rejected to ambient through cooling tower. In proposed hybrid desalination MEDAD cycle, the heat supplied to MED steam generator is rejected to adsorber beds during adsorption process in contrast to a conventional MED cycle where the input heat energy is rejected at condenser via cooling water circulation. In AD cycle, the granular silica gel adsorbent is packed on a heat exchanger where the hot/cooling water is circulated to supply the heat of desorption or to reject the heat of adsorption. Heat supplied or rejected in AD cycle is calculated by water inlet and outlet temperatures. The hybrid MEDAD desalination system performance modeling is discussed below.

MED-SG heat input: hot water is circulated through the MED steam generator to produce initial vapors. Energy supplied to the steam generator can be calculated by:

$$Q_{SG} = \dot{m}_{hw,SG}\, C_{p,Thw}\left(T_{hw,SG,in} - T_{hw,SG,out}\right) \tag{6.30}$$

Heat of desorption: hot water is circulated through the desorber bed heat exchanger to supply the heat of desorption. Energy supplied to the desorber bed is given by:

$$Q_{des} = \dot{m}_{hw,bed}\, C_{p,Tdes}\left(T_{hw,bed,in} - T_{hw,bed,out}\right) \tag{6.31}$$

Heat rejection at adsorber: heat rejected by cooling water from the adsorber bed can be calculated as:

$$Q_{ads} = \dot{m}_{cw,bed}\, C_{p,Tads}\left(T_{cw,bed,out} - T_{cw,bed,in}\right) \tag{6.32}$$

Heat rejection at condenser: cooling water is circulated through the condenser tubes to reject the heat of condensation and can be calculated as:

$$Q_{cond} = \dot{m}_{cw,cond}\, C_{p,Tcond}\left(T_{cw,cond,out} - T_{cw,cond,in}\right) \tag{6.33}$$

Water produced from AD: desorbed vapors are condensed in the AD condenser and can be calculated as:

$$\dot{m}_{distillate,AD,cond} = UA\left(\frac{LMTD}{h_{fg,Tcond}}\right) \tag{6.34}$$

Water production from MED: water produced from each stage of MED can be calculated as:

$$\dot{m}_{distillate,MED,i} = \left(\frac{h_{out,i} A_i .(T_{tube} - T_{v,i})}{h_{fg,Tvi}}\right) \tag{6.35}$$

Total water production: Total water production from MEDAD is than calculated as:

$$\dot{m}_{disittale,total} = \sum_{i=1}^{n} \dot{m}_{MED,i} + \dot{m}_{AD,cond}$$

(6.36)

Performance indicator: performance ratio (PR) is used as a performance indicator of MEDAD and calculated as:

$$PR = \frac{\dot{m}_{distillate,total}\, h_{fg}}{TPE} \tag{6.37}$$

Where TPE is total primary energy and can be calculate by:

$$TPE = \left(\frac{Q_{thermal,payable}}{\eta_{boiler}} \right) + \left(\frac{Q_{electric}}{\eta_{pp}} \right) \tag{6.38}$$

Boiler efficiency is taken to be 95% and power plant conversion efficiency is taken to be 42%. Modeling equations are written in FORTRAN subroutine and solved using IMSL. Simulation results are discussed in following sections.

6.5 MEDAD System Simulation Results and Discussion

MEDAD distributed simulation is completed by using above modeling equations and parameters. An 8-stages MED is coupled with an AD cycle to investigate the hybrid system performance. User defined subroutine is written in FORTRAN and IMSL is linked to solve the equation simultaneously.

Figure 6.5 shows the temperature profiles for each MED stage. The heat source temperature is maintained at 50^{o}C. Condenser side, tube wall and evaporator space temperature profiles are plotted for each stage.

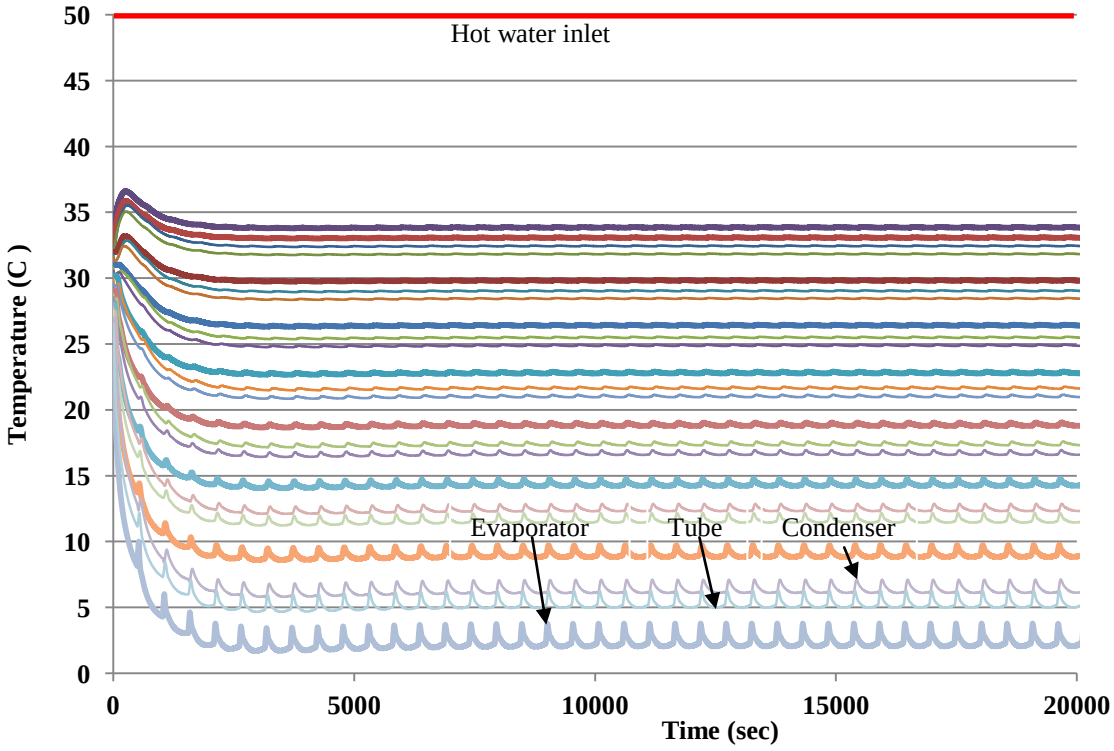

Figure 6.5 **Hybrid MEDAD components temperature profiles: Condenser, tube surface and evaporator side temperatures**

For hybrid system there are two main drivers namely; the MED steam generator at upstream and AD reactor at downstream. Three main points observed here are: ***Firstly***, the temperature of the last stage of MED is below ambient (≈3^{o}C) as compared to conventional MED (≈40^{o}C) and this is only possible by addition of AD. Adsorbent can pull the last stage of MED temperature below ambient. Adsorption power even can be seen up to steam generator. In the first two stages, temperature increases first due to heat input but after some time it is dropped by the adsorption effect and then operates at stable condition. It can be seen that after 4-5 cycles, the system reaches its stable condition. ***Secondly***, cyclic temperature profile of MED stages can also be observed and it is because of AD cyclic operation. These temperature fluctuations can be seen clearly in last 3-4 stages and then it is damping down due to upstream driver effect. ***Lastly,*** the inter stage temperature difference is varies from 2^{o}C to 3^{o}C as compared to 1^{o}C in conventional MED system. This higher temperature difference increases the water production due to cooler condenser temperature in each stage and also helps to insert more number of stages with same heat input. These extra number of stages increases the heat recoveries that also increase the water production and hence the system performance. It can be observed clearly that the overall operating temperature range is increased from 50^{o}C-38^{o}C in conventional MED system to 50^{o}C-3^{o}C in hybrid system with same operating parameters.

Figure 6.6 shows the temperature profiles of adsorber and desorber reactors during operation. Heat source is supplied at 85^{o}C to desorber reactor to provide the heat of

desorption and cooling water is circulated at 30°C to adsorber reactor to reject the heat of adsorption. At near saturation, before changeover of their duties, there is a switching period to prepare the reactors for the next operation. During the AD bed changeover the water valves also operate accordingly to supply hot and cooling water to respect beds.

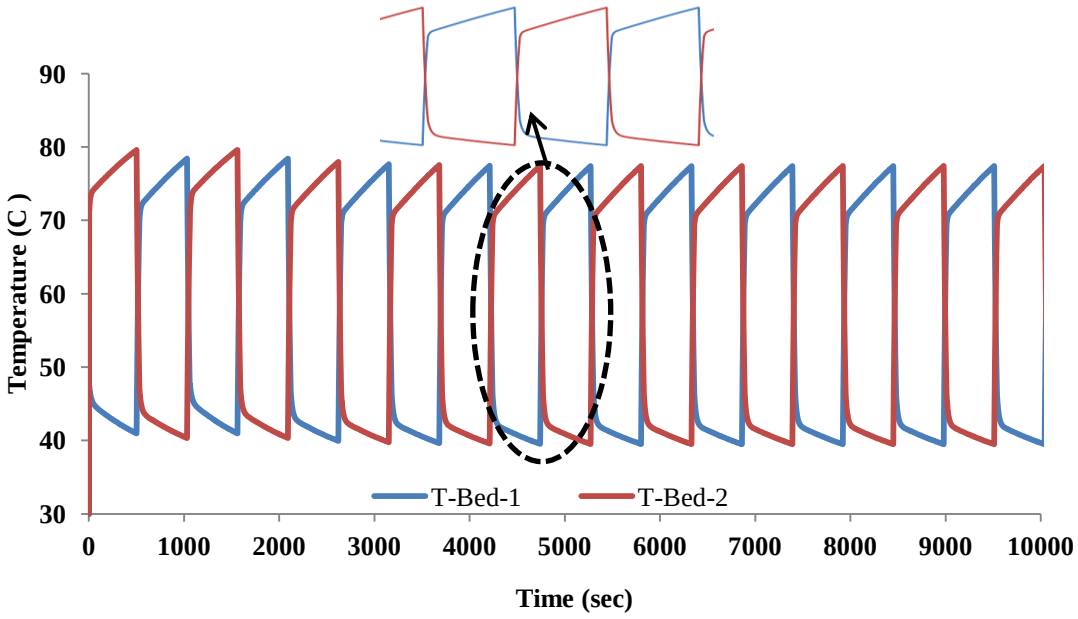

Figure 6.6 AD adsorber and desorber reactors instantaneous temperature profiles

Figure 6.7 shows the water production from hybrid MEDAD system. It can be seen that water production in MED successive stages is dropping and it is due to drop in saturation pressure. It is also observed that the water production in last stage of MED that is coupled with AD reactor beds is higher than the preceding effect and it is because the last stages have two drivers namely; i) heat of condensation of vapors from previous stage and ii) high affinity of adsorbent for water vapors. The last stages of MED in hybrid cycle were expected to have effect of adsorption pulling and it is proved here in terms of water production. Adsorbent effect damps down

towards the first effect or steam generator as can be seen clearly. It can also be seen that water production from AD evaporator is higher at the start of desorption process and decreasing with time. During switching it is zero as there is no desorption during switching time.

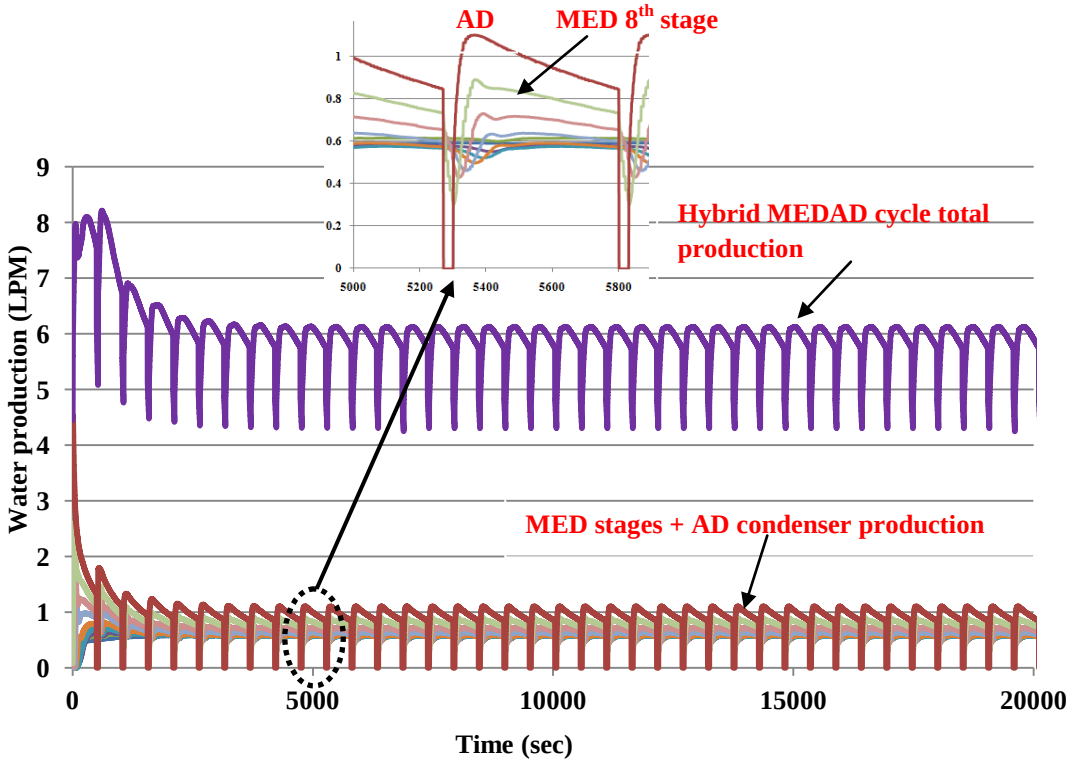

Figure 6.7 MED stages, AD condenser and total MEDAD cycle water production profiles

Figure 6.8 shows the total primary energy consumption, performance ratio and total water production of hybrid MEDAD system. Total primary energy is calculated by considering the thermal power plant and boiler efficiencies. This is total payable energy for hybrid MEDAD desalination cycle while the thermal energy required for

adsorbent regeneration is considered as a non-payable energy such as industrial process waste heat or solar energy.

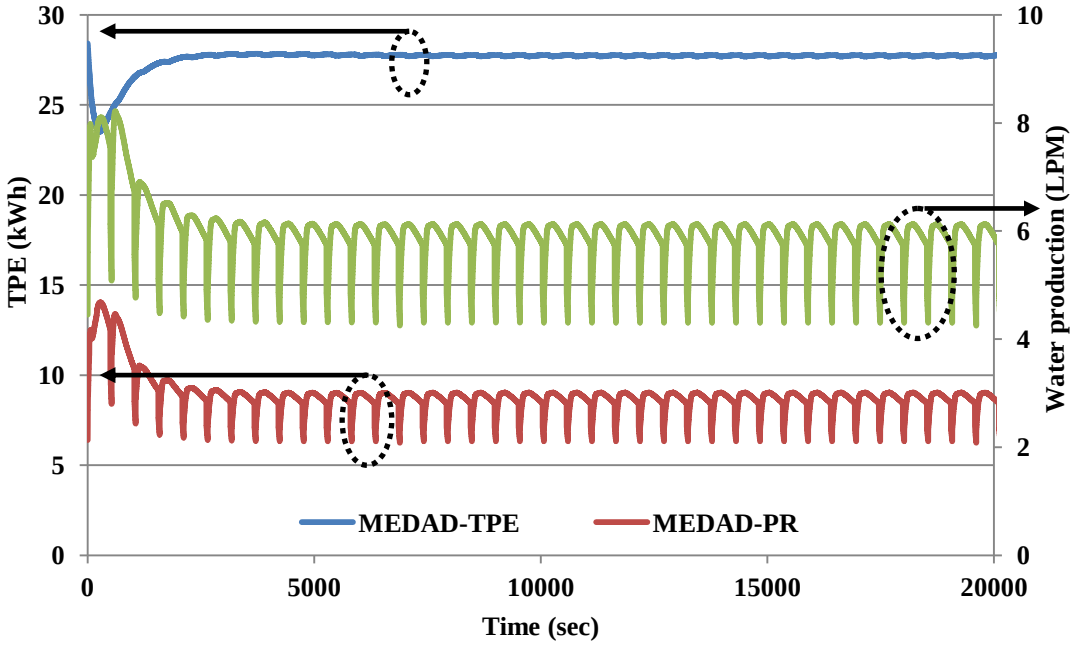

Figure 6.8 Hybrid MEDAD total water production, primary energy and performance ratio profiles

It can observed that the simplest hybridization without any additional effect (only with pseudo evaporator of the AD cycle) provides water production rate increment about 3-4 fold as compared to the MED plant. This hybridization scheme can be applicable to an existing MED plant by coupling an AD cycle to boost water production with minimum additional modifications. However, being the last temperature down below ambient conditions, it is possible to implement addition effects. It should also be noted that the hybrid MEDAD cycle offers operational

flexibilities to switch the operation mode between the desalination plant and the desalination cum cooling power production with simple valve control arrangement through programmable logic control (PLC) tweet.

6.6 MEDAD and MED System Comparison

Hybrid MEDAD simulation results as discussed in this chapter are compared with conventional MED results as discussed in Chapter 4. It can be seen that the MEDAD inter stage temperature varies 3°C to 4°C (as shown in Figure 6.5) as compared to 1°C in case of conventional MED system (as shown in Figure 4.13). This higher temperature difference boosts the evaporation and hence the water production.

Figure 6.9 shows the comparison of water production of conventional MED and hybrid MEDAD system. It can be seen that with same heat input the hybrid MEDAD system production is 2.5 to 3 times higher as compared to conventional MED system.

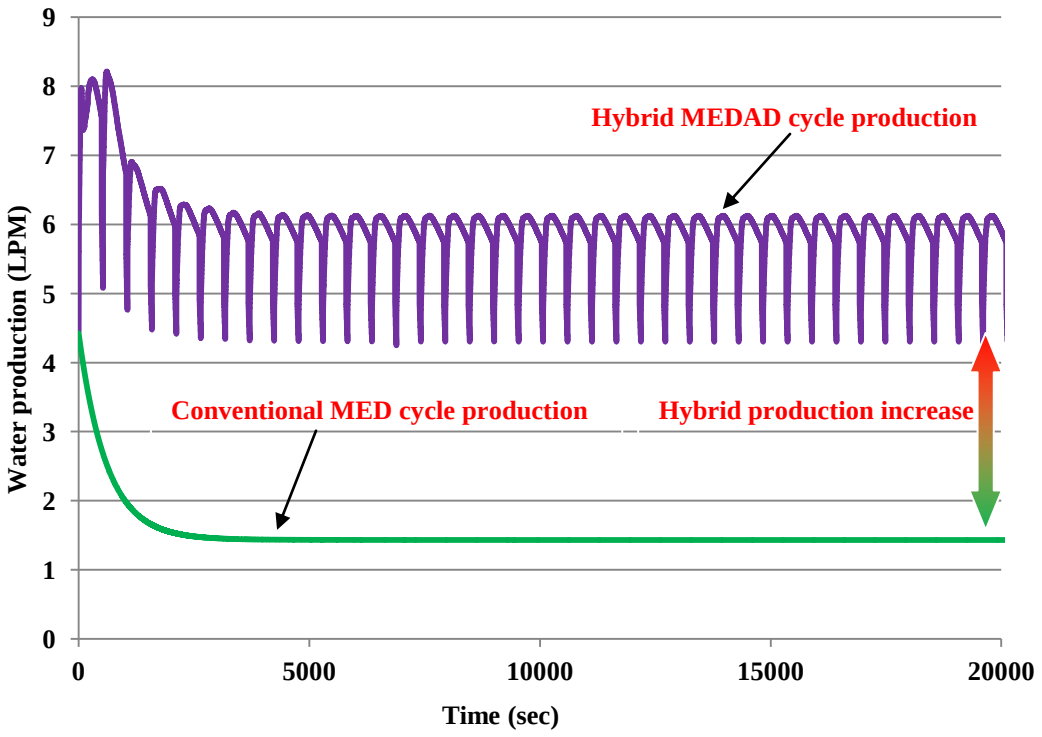

Figure 6.9 **Hybrid MEDAD total water production compared with conventional MED total water production with same heat input**

Another noticeable point is, in case of conventional MED, the last stage is restricted to 40^{o}C because of cooling tower operation but, in MEDAD the last stage temperature can be as low as 5^{o}C. This higher operational temperature gap increase the number of stages and hence the system performance.

Summary of Chapter 6

Hybrid desalination cycle called "MEDAD" cycle is proposed to overcome the limitations of conventional MED system and to enhance the thermal system performance. It is a combination of two thermal systems namely; i) MED and ii) AD. Adsorption desalination system components and its operation are discussed in detail. The limitations of conventional MED system and its hybridization with AD cycle are discussed in detail. The operational strategy of hybrid MEDAD system is explained in detailed with process flow diagram and its advantages are also highlighted.

A detailed mathematical model is developed for MED, AD and hybrid MEDAD system. MED steam generator is operated by hot water circulation and heat source temperature is maintained by electrical heater. The MED last stage is integrated with AD reactor beds and its modelling equations are also discussed.

Detailed simulations codes are developed and written in the user defined subroutine in FORTRAN. To solve all the differential equations simultaneously, IMSL is linked with FORTRAN. Initial values for solution are provided and tolerance 1x10-7 is provided to converge the solution.

The required parameters of hybrid MEDAD system such as i) system component temperature distribution, ii) water production, iii) total primary energy consumption and iv) performance ratio are simulated. The following remarkable improvements are observed:

1- Last stage of MED temperature can be as low as 3^{o}C.

2- Inter stage temperature is 3-4^{o}C as compared to 1^{o}C in conventional MED system.

3- Overall operational temperature gap in increased as compared to conventional MED system that will help to insert more number of stages.

4- Water production boosted by 2.5 to 3 folds with same heat input.

5- Cooling can produce from last stages operating below ambient temperature as additional benefits.

6- Ambient energy can be harnessed in last stages operating below ambient temperature.

Chapter 7 Experimental Investigation of Hybrid MEDAD Desalination System

Desalination hybridization is an emerging technique to enhance the system performance in term of water production and cost (kWh/m^3). Hybridization of thermal systems can increase the water production up to 3 folds as proved by the simulation results in previous chapter. There is no single hybrid cycle experimental results are available to endorse the simulation results. This experimentation will provide the wide range of real data of hybrid MEDAD operation for future plant design reference.

A 3-stage MED experimental facility discussed in Chapter 5, is integrated with the adsorption desalination cycle to test as a hybrid MEDAD cycle. In this chapter the detailed analysis of experimental facility of MEDAD system is provided. In the first part of the chapter, the detailed overview of experimental facility of hybrid MEDAD cycle is provided. Experimentation detail is provided in second part of the chapter. MEDAD experimental results are discussed the third part of the chapter. Simulation results are verified with experimental results in fourth part of the chapter. The comparison of Hybrid MEDAD desalination cycle and conventional MED system is provided in the last part of the chapter.

7.1 Background

Hybridization of two thermal desalination systems namely: Multi effect desalination and adsorption desalination can improve water production by many-fold as compared to the conventional MED system as proved by system simulation in Chapter 6. This novel system has a great potential in future desalination market to fulfill the supply-demand gap of fresh water. Up till now, there is no single hybrid experimental system is build to validate the simulation results to provide the confidence to desalination industry. To endorse the simulation results, a thermal hybrid (MEDAD) desalination test facility is installed in NUS and tested for wide range of heat input to provide the reference data for desalination industry. The detail of hybrid cycle and experimental facility is provided in following sections.

7.2 Hybrid MEDAD Cycle Experimentation

A 3-stage MED experimental system installed in NUS as described in Chapter 5 is integrated with existing AD system to test as a hybrid MEDAD cycle. The system is designed and installed in such a manner that it can operate as a hybrid MEDAD and also as a two stand alone MED and AD desalination cycles. This operational switchover can easily get by changing few valve conditions.

For hybrid MEDAD experimentations, initially both cycles MED and AD run separately according to developed standard operating procedure (SOP) as explained in detail in Chapters 5 and 6. Once the both systems are in stable condition, MED last stage to condenser connection pipe line valve will be closed and bypassed the condenser and the last stage integration to AD silica gel beds pipe line valve will be

opened. In this scheme, the vapors from last stage of MED will adsorb on silica gel packed in the forms of cake in the beds. MED and AD experimental set-up installed in NUS, integration pipe line and integration valve are shown in Figures 7.1, 7.2 and 7.3 respectively.

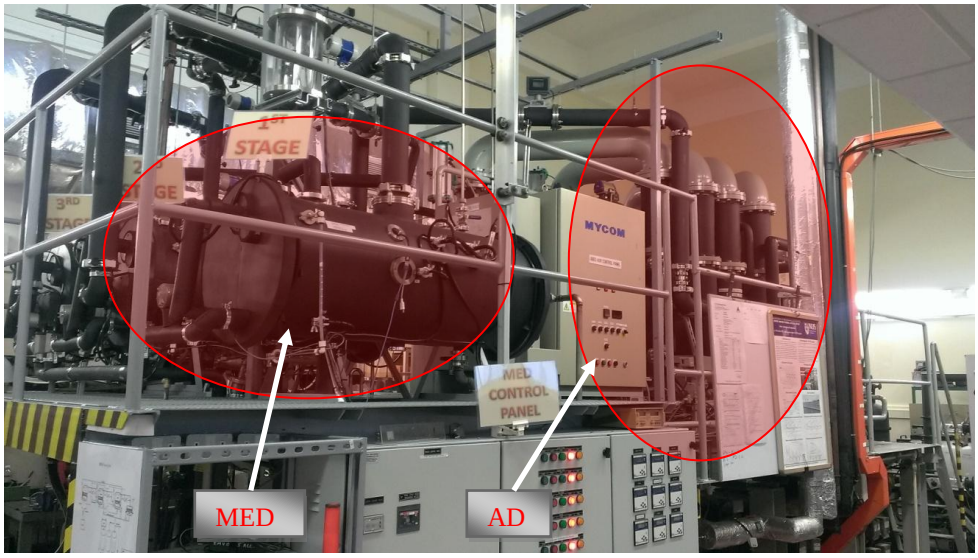

Figure 7.1 **Pictorial view of conventional MED and AD experimental set-up installed in NUS**

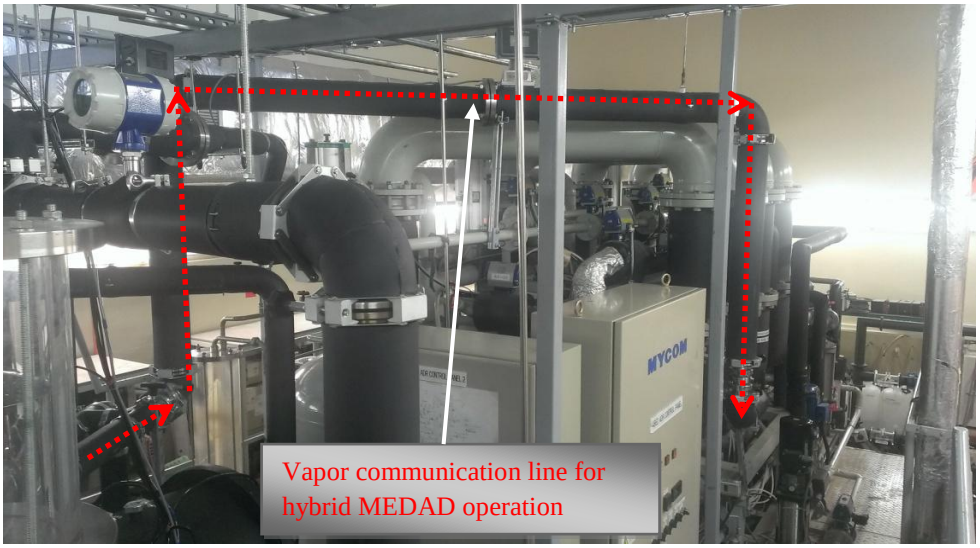

Figure 7.2 **Integration pipe line from last stage of MED to AD beds for last stage vapor adsorption**

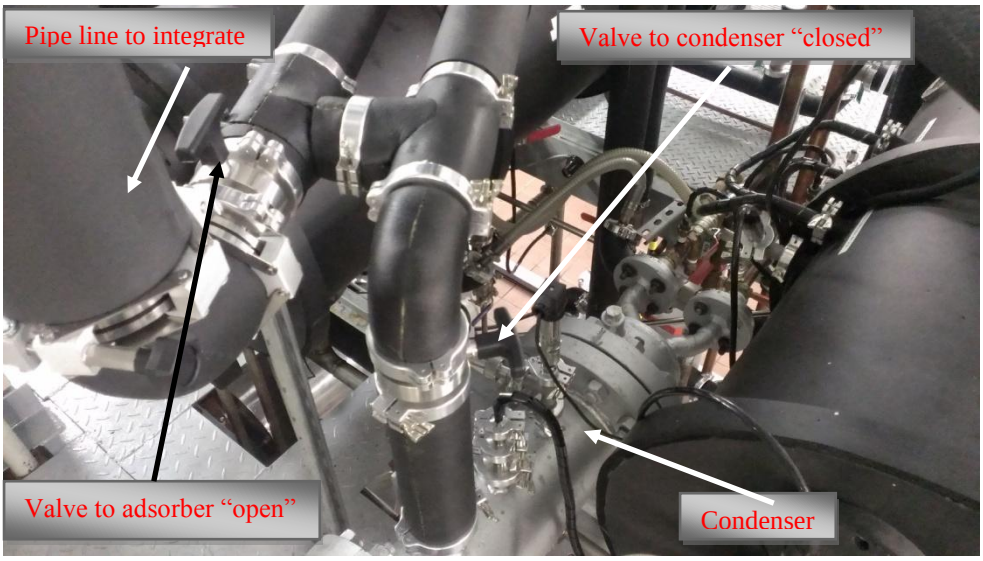

Figure 7.3 **Condenser valve scheme for integration of MED and AD to operate as hybrid MEDAD system**

The detailed flow schematic is shown in Figure 7.4. The desorbed vapors from AD silica gel beds are than condensed in water cooled condenser.

The operation is standard as MED and AD stand alone operation except MED condenser and AD evaporator by-pass. The heat supplied to MED steam generator and desorber beds is rejected to cooling water in AD condenser. Detailed 3-D model of MEDAD integration is shown in Figure 7.5 (a) and (b) where the piping can be seen clearly.

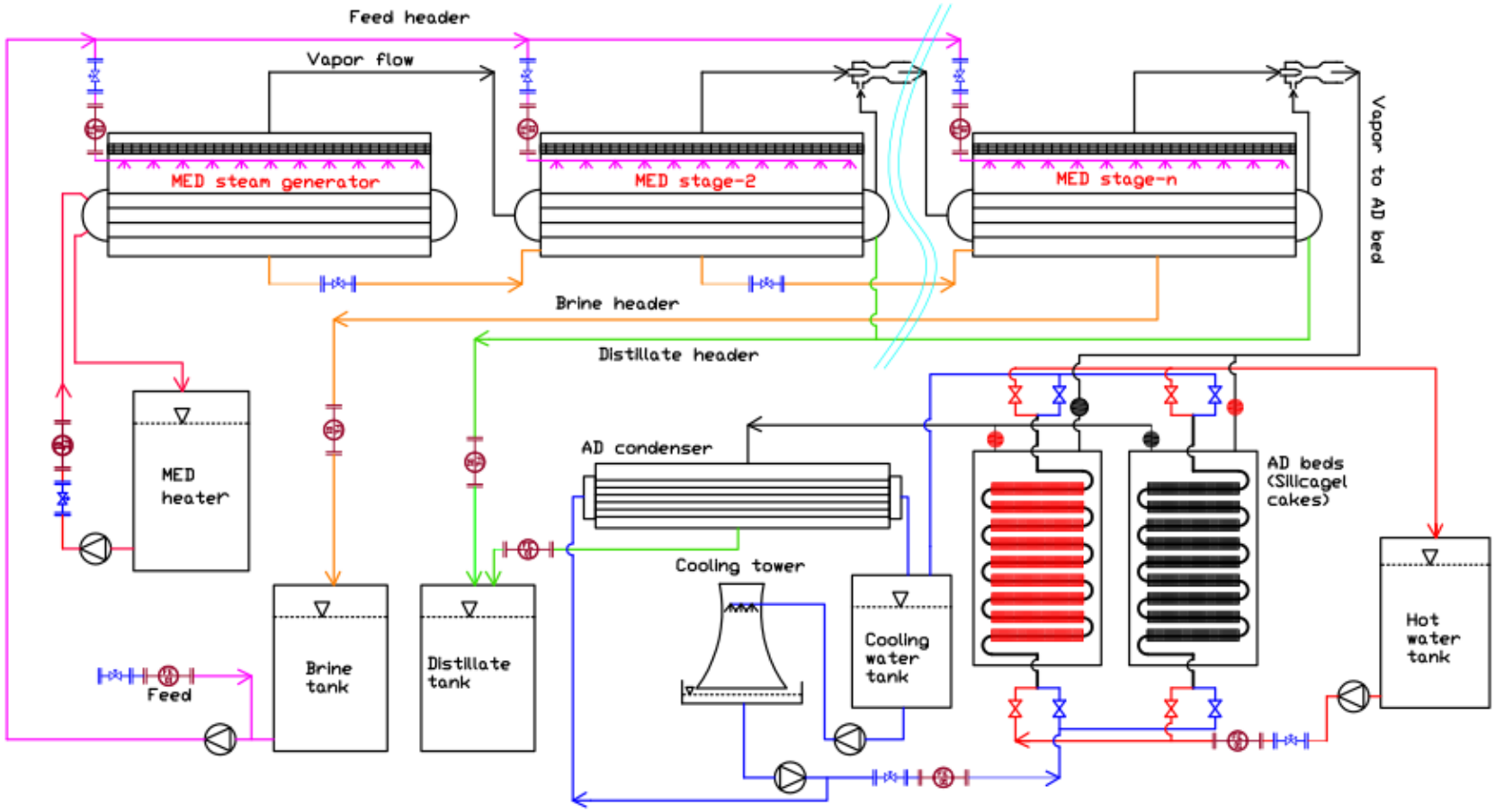

Figure 7.4 MEDAD detailed operational flow schematic

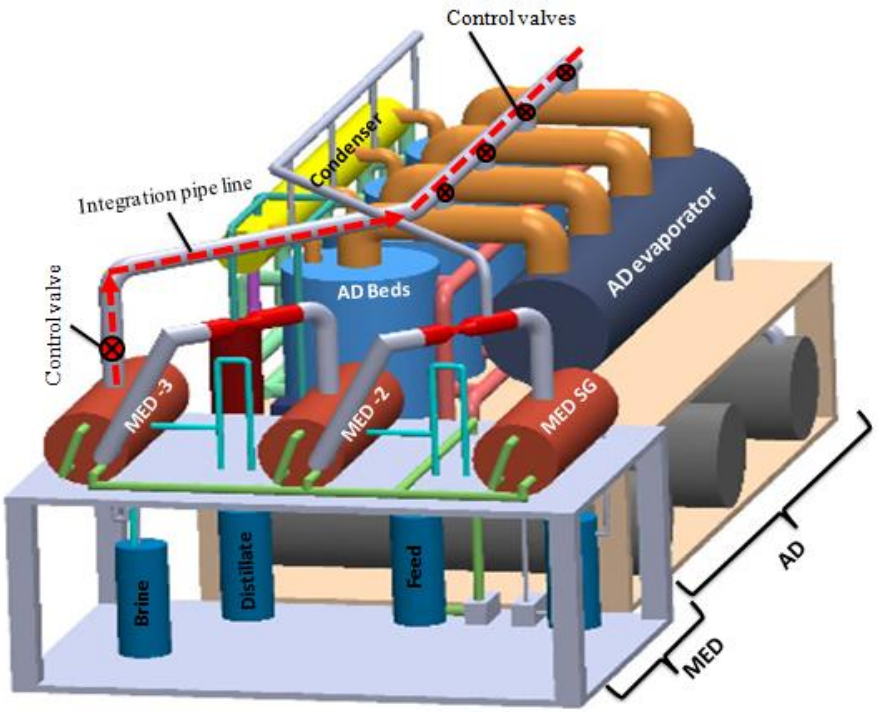

(a)

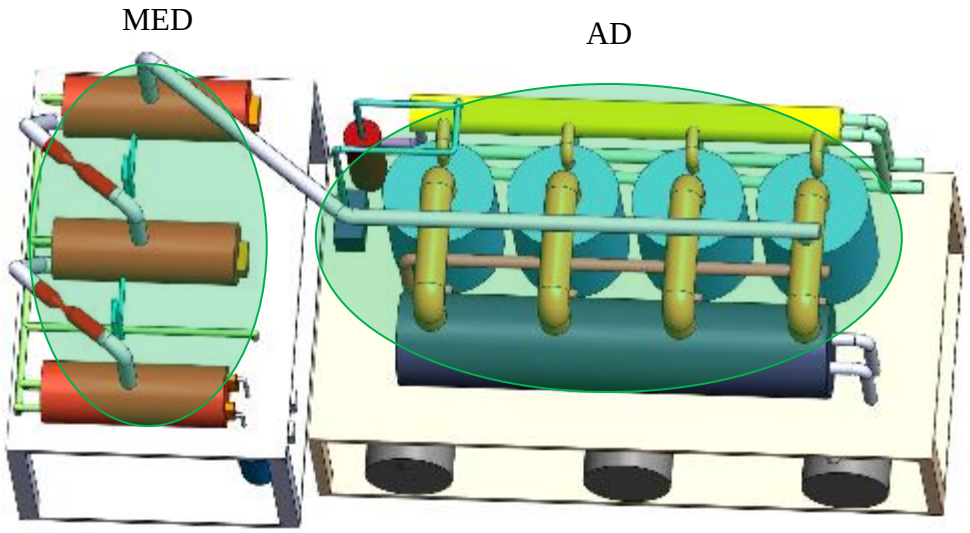

(b)

Figure 7.5 **MEDAD equipments arrangement and piping 3D model, (a) showing MEDAD main components and integration pipe line, (b) showing the top view of installation**

7.3 Results and Discussion

Experiments were conducted with heat source a temperature varies from 15°C to 70°C. The results are discussed below:

MEDAD components temperature distribution:

Figure 7.6 shows the instantaneous temperatures of MEDAD components at heat source temperature of 38°C. It can be seen that steady state events (minimum temperature fluctuations) occur after 1 hour from start-up and experiments for distillate collection are continued for 4 to 5 hours. It can be seen clearly that the inter-stage temperature difference (ΔT) is more than twice per stage as compared to the conventional MED stages (as shown in chapter 5): This is attributed to the vapor uptake by the adsorbent of AD cycle, resulting in the increase of vapor production. The MED+AD cycle yields a stage ΔT from 3°C to 4°C as compared to 1°C or less in the case of MED alone.

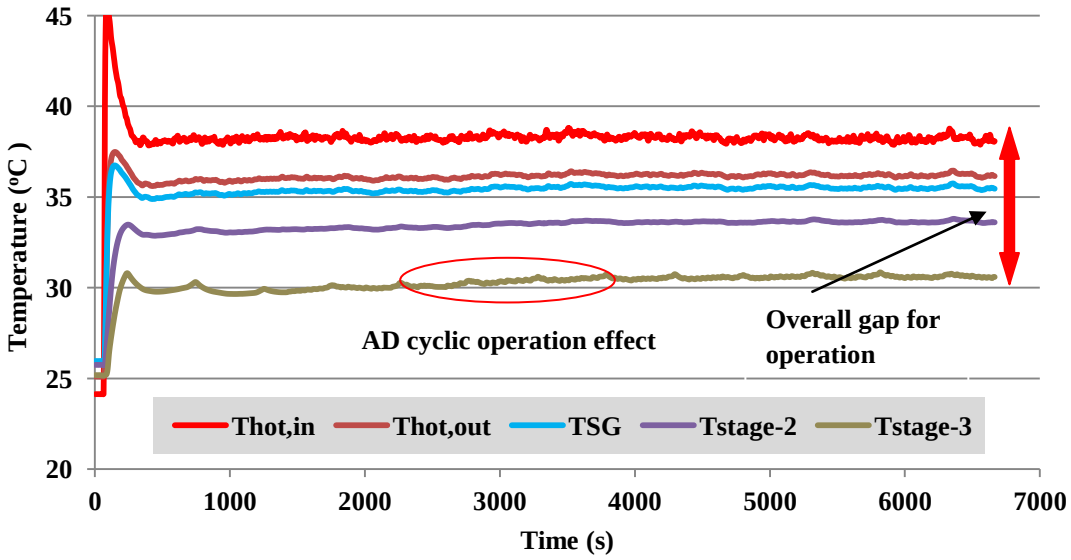

Figure 7.6 **Typical experimental start-up temperature profiles of the hybrid MEDAD components at heat source temperature 38°C**

At a heat source of 38^{o}C, the 3rd or last stage temperature of MED in the hybrid cycle is 30^{o}C, which is 4 degree lower than the case of MED alone. Since the AD cycle is batch operated, only the temperature profile of the last MED stage is affected in a cyclical manner, and such cyclical behavior is expected to diminish on the upper stages. In general, the operating conditions of MEDAD hybrid can be varied to a large extend by controlling the adsorbent vapor uptake, an intrinsic design feature of the hybrid cycle. As it can be seen that the last stage temperature is 30^{o}C and it is due to only 3-stages but in reality it can be as low as 5^{o}C if more number of stages can be provided.

The inter stage temperature difference (ΔT) and profile pattern has good agreement with the simulated results as explained in Chapter 6.

Figure 7.7 shows the steady state temperature values of MEDAD all components for heat source temperatures vary from 15^{o}C to 70^{o}C. It can be observed that in all cases, inter-stage temperature varies from 3^{o}C to 4^{o}C. The ambient energy scavenging effect can also be seen at 15^{o}C and 20^{o}C heat source temperature where the heat source outlet temperature is higher. It is predicted that in full scale 40-50 stages plant, the ambient energy can be scavenged in last few stages working below ambient temperature. An additional cooling effect can also extracted from the stages working below ambient temperatures. Even with only 3-stages of MED, the hybridization effect can be seen clearly in term of inter stage temperature distribution.

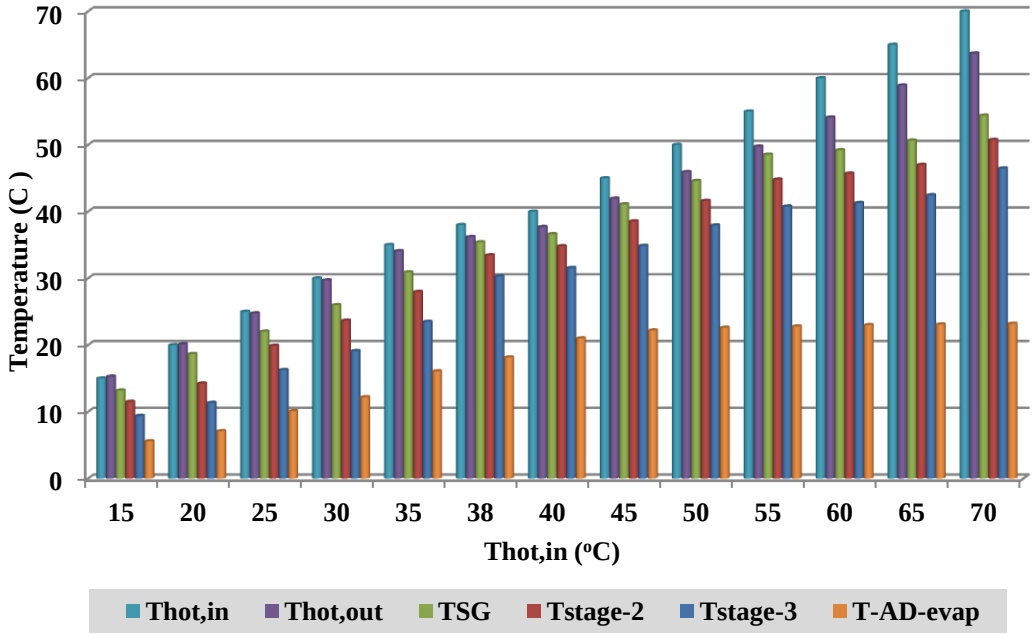

Figure 7.7 **Steady state temperatures of MEDAD components at different heat source temperatures**

MEDAD components pressure distribution:

Figure 7.8 shows the typical start-up pressure profiles of MEDAD stages at a low heat source temperature of 38^{o}C. Similarly, in pressure traces, system is almost stable after 1 hour but experiment is continued for 4 to 5 hours. It is observed from the pressure traces that the pressure differences between the stages is 1-2 kPa as compared to conventional MED less than 1 kPa. In the last stage the cyclic fluctuations are also observed in saturation pressures and it is due to cyclic operation of AD cycle and these fluctuations are damped down toward steam generator (first stage).

Figure 7.9 shows the steady state pressure values of MEDAD components at different heat source temperatures. It can be observed that in all cases the pressure difference between stages is varies from 1-2 kPa.

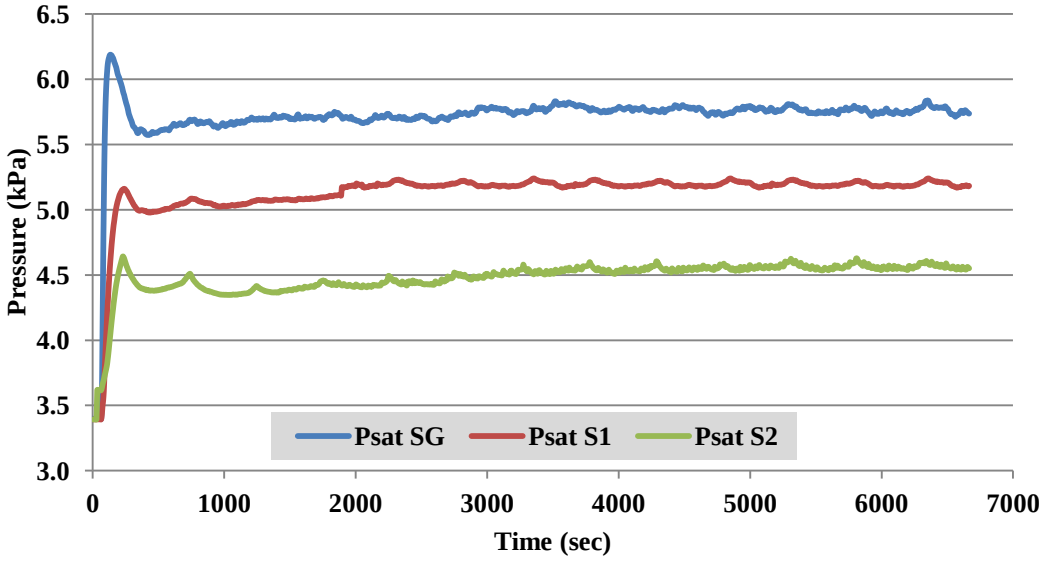

Figure 7.8 **Experimental start-up pressure profiles of MEDAD components at heat source temperature 38°C**

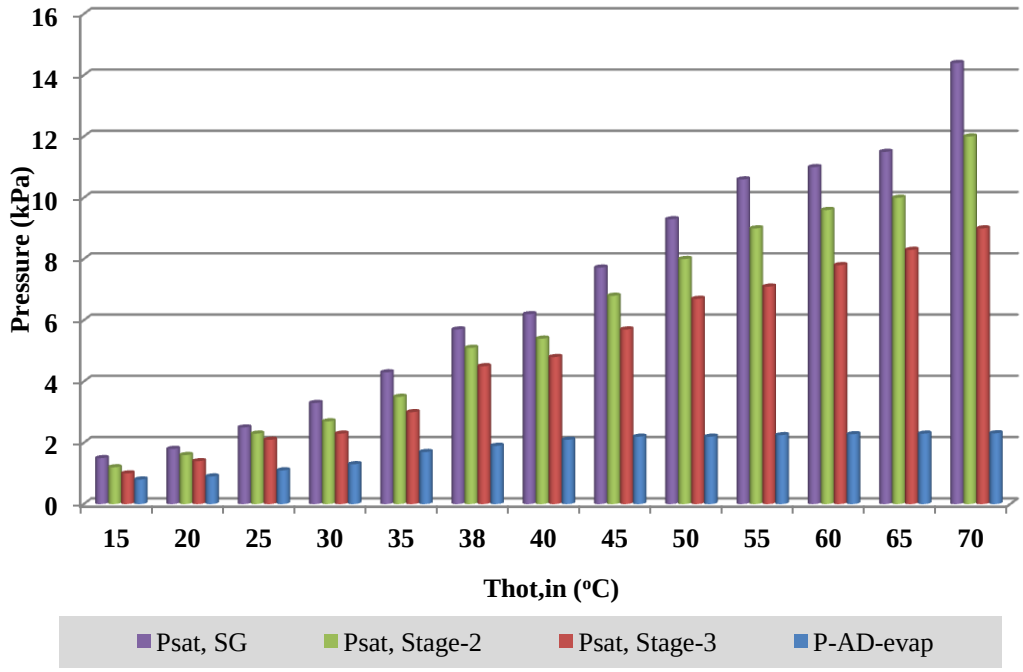

Figure 7.9 **Hybrid MEDAD cycle components steady state pressure values at different heat source temperature**

MEDAD performance:

Figure 7.10 shows the thermal power consumption profile during 38°C heat source temperature. High accuracy thyristor controller is used to control the heat source temperature within ±0.15°C. The fluctuations in electric power taken by heater are due to heater cut-in and cut-out during operation to maintain the temperature. The average power is also calculated and plotted in the graph.

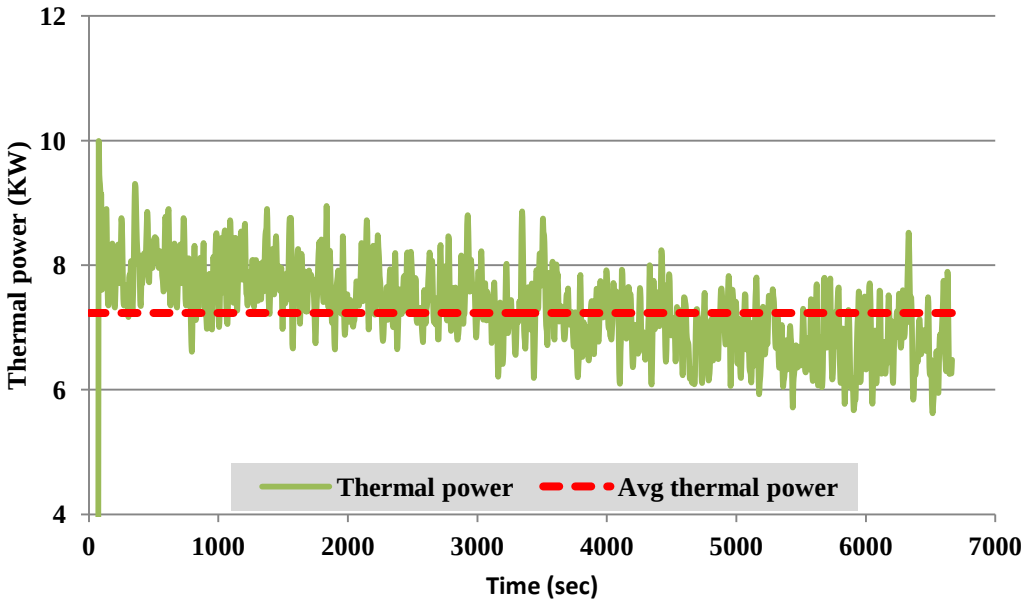

Figure 7.10 MEDAD experimental instantaneous and average thermal power consumption profiles at heat source 38°C

Figure 7.11 shows the average values of power for heat source temperature varies from 15°C to 70°C. It can be seen that the power consumption is higher for same heat source temperature as compared to conventional MED and it is due to higher ΔT between heat source inlet and outlet attributed to AD effect that bring down the saturation temperature of stages. It can also be seen clearly that while operating at

20°C and 15°C, the power calculated is in –ve and it shows that energy is scavenged from ambient due to below ambient temperature operation. In other words it shows that in practical full scale plant (19-stage), the last few stage (7-10 stages) operating below ambient temperature can harness the ambient energy and can operate with ambient energy only.

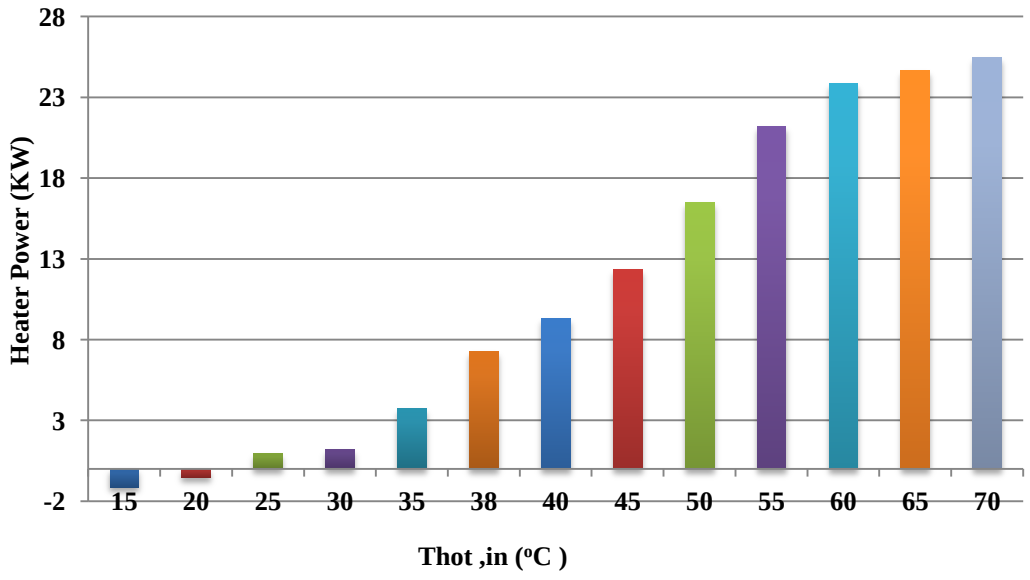

Figure 7.11 **MEDAD experimental average thermal power consumptions at different heat source temperature**

MED stages distillate production is collected in MED collection tank and AD condenser production is in another tank. Both side productions are measured by high accuracy turbine flow meter. Figure 7.12 shows the distillate production trace at heat source 38°C from MED stages, AD condenser and combined. The batch operated AD production can be seen clearly. At the start of desorption the production is higher and it drops with time to zero during the switching period while MED stages production is quite stable. Small fluctuations in MED water production may be due

to the fluctuations in the spray of the feed that affect the condensation rate. Water production profiles are similar as explained in simulated results

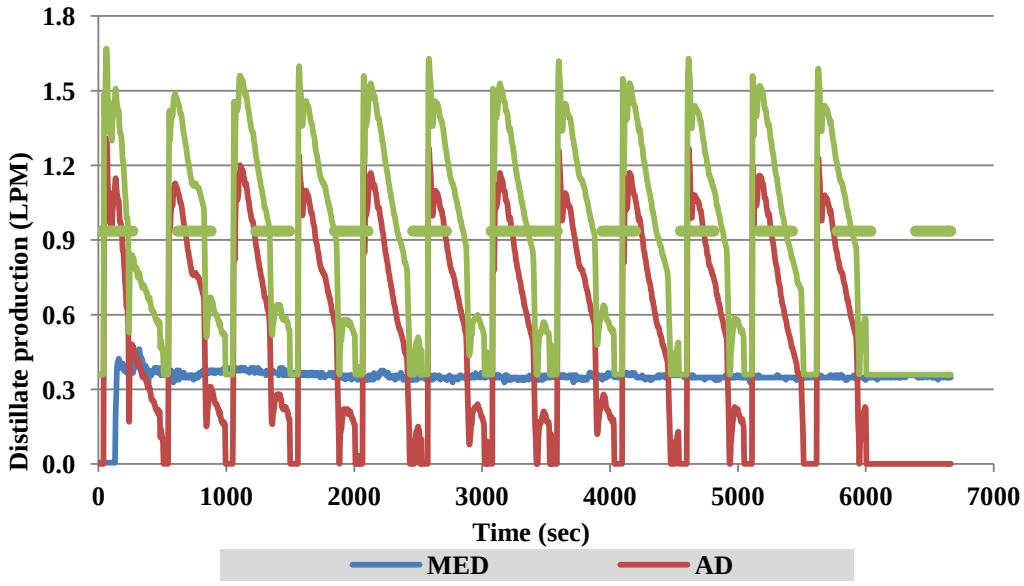

Figure 7.12 **MED, AD and hybrid MEDAD experimental instantaneous distillate production profiles at heat source temperature 38°C.**

Experiments are conducted for 4-5 hours for stable distillate production measurement. Figure 7.13 shows the average water production at heat source temperature varies from 15°C to 70°C. The drop in production with lowering the heat source temperature is due to drop in saturation temperature and hence the saturation pressure. Even though the last stage production is lower but it is still feasible due to energy harvesting from ambient. Another useful effect from last stage operating below ambient condition is cooling that can be produced simultaneously with water production. This additional benefit cannot be obtained from conventional MED systems

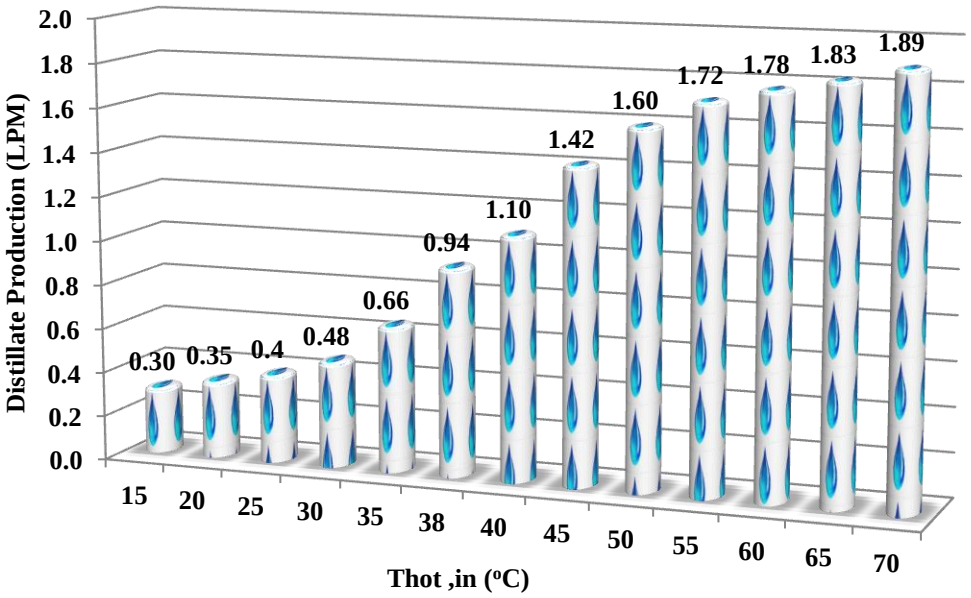

Figure 7.13 **Hybrid MEDAD experimental total average distillate production at different heat source temperatures**

Total primary energy consumption (TPE) is calculated from thermal energy by considering the boiler efficiency (95%) and power plant conversion efficiency (42%) to convert it as basic fuel energy for fair comparison with any kind of desalination processes. The system performance (PR) is then calculated on the basis of TPE. Figure 7.14 shows the TPE and PR_{TPE} of the system at heat source varies from 15°C to 70°C. System performance can be even higher if more number of stages can be installed for more recoveries. System under investigation has only 3-stages that have only two recoveries.

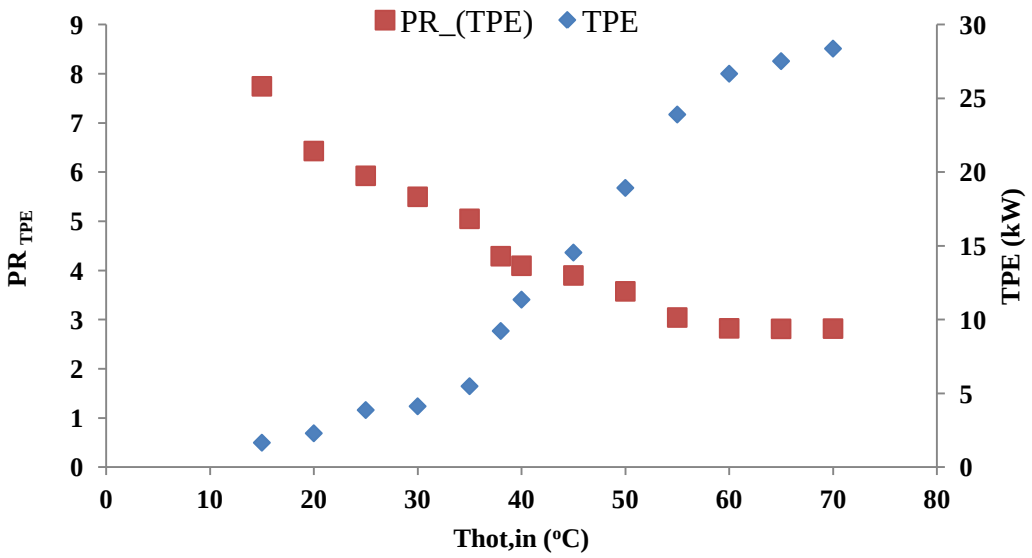

Figure 7.14 **Hybrid MEDAD system performance (PR_{TPE}) and total primary energy consumption (TPE) profiles at different heat source**

7.4 Validation of Simulation Results

The experimental results of a 3-stage MEDAD system at heat source temperature 38^{o}C are compared with simulation results. MEDAD simulation code is written in FORTRAN and linked with IMSL to solve differential equations simultaneously as mentioned in Chapter 6. Table 7.1 shows the experimental parameters used for simulation code of MEDAD.

Table 7.1 MEDAD parameters used in simulation

Parameters	Values	Units
MED		
Heat source temperature ($T_{hw,in}$)	38^{o}C	^{o}C
Heat source flow rate	58	LPM
Heat transfer area	4	m^2
SG tube cluster specification	16x0.7x1300x64	mm
MED stages cluster specification	25x0.7x1300x32	mm
Feed temperature	30	^{o}C
AD		
Mass of silicagel	72	kg
Hot water bed flow rate	48	LPM
Cooling water bed flow rate	48	LPM
Cooling water condenser flow rate	120	
Cycle time	480	Sec
Switching time	60	Sec

Figure 7.15 shows simulated and experimental temperature profiles of MEDAD components at heat source temperature 38^{o}C. Simulation results are plotted with dotted line while solid line shows the experimental results. It can be seen clearly that during steady state condition there is good agreement between simulation and experiment results within ±5% deviation.

During the experiment, the heat source is first heated up to 38°C and then the measurements were made, thus there is sharp rise of all system components temperatures at the start of experiment. In case of simulation, there is a time delay due to thermal mass that's why at start simulation results are different then experimental results.

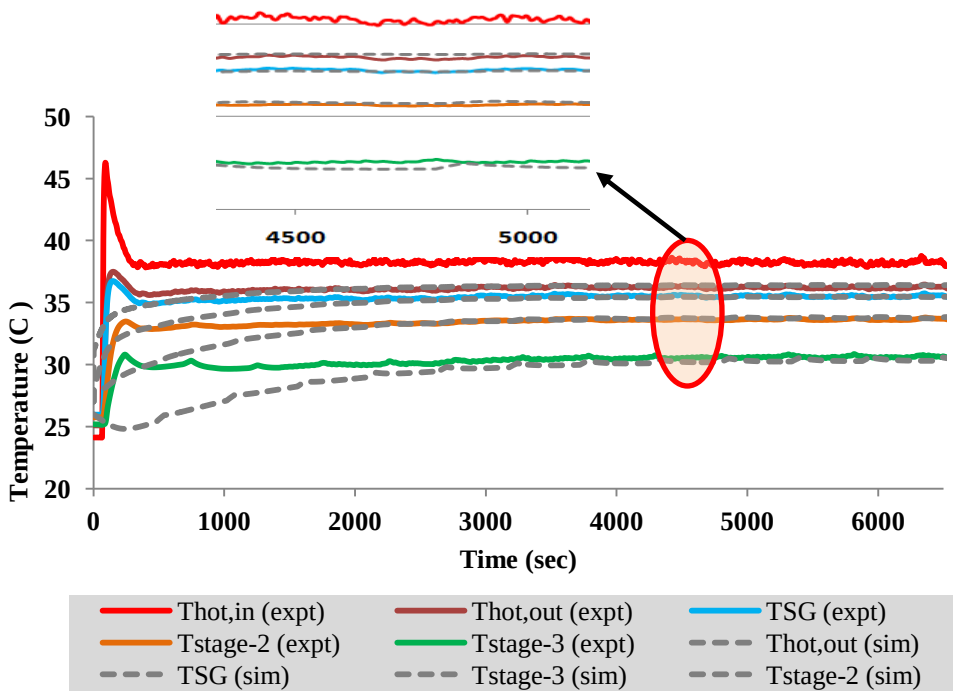

Figure 7.15 A comparison of MEDAD components temperature profiles: simulation & experiment at heat source temperature 38°C

The average distillate production comparison of simulation and experimental results is shown in Figure 7.16. It can be seen clearly that there is good agreement of simulation and experimental results within average production has good ±5% deviation.

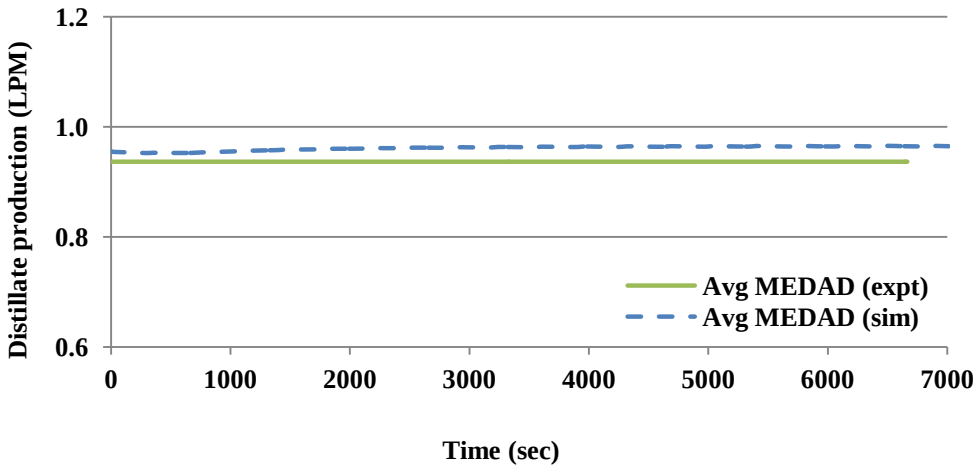

Figure 7.16 **A comparison of MEDAD average production: simulation & experiment at heat source temperature 38°C**

Figure 7.17 to Figure 19 shows the comparison of simulation and experimental results of distillate production, total primary energy consumption and system performance respectively at assorted heat source temperatures.

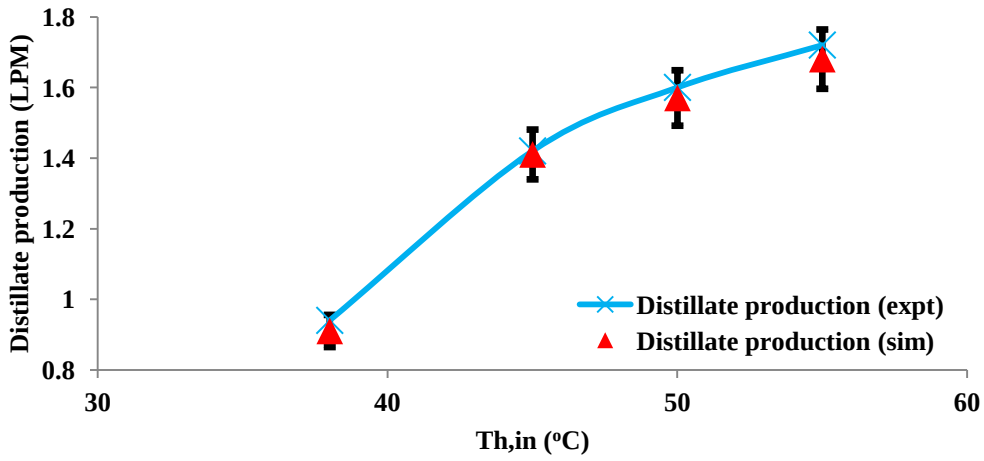

Figure 7.17 **Experimental system average production comparisons with simulation results at different heat source temperatures**

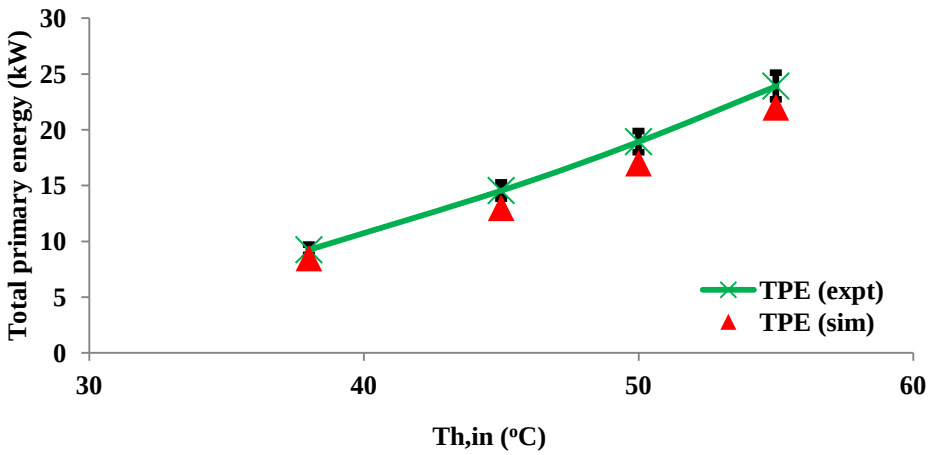

Figure 7.18 **Experimental system total primary energy consumption comparisons with simulation results at different heat source temperatures**

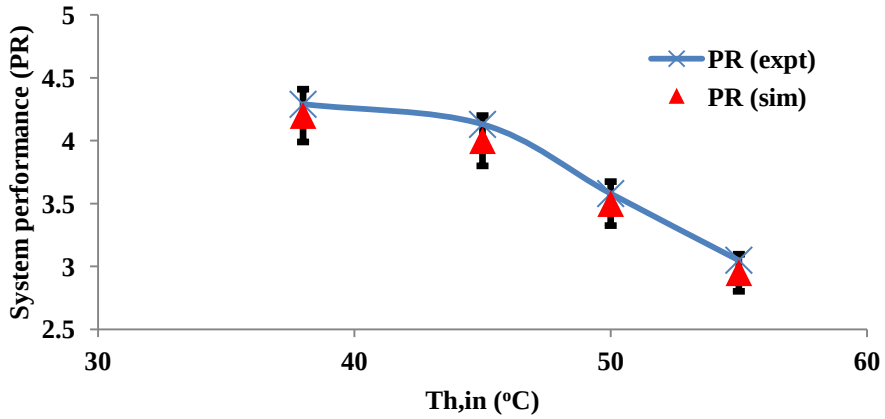

Figure 7.19 **Experimental system performance (PR) comparisons with simulation results at different heat source temperatures**

It can be seen that 3-stage MEDAD simulation results have good agreement with experimental results within ±5% deviation at all heat source temperatures.

7.5 Hybrid MEDAD cycle and MED system Comparison

Proposed hybrid MEDAD cycle experimental results are compared with conventional MED system to show the system performance enhancement due to hybridization. Table 7.2 shows the MEDAD components temperature values compared with conventional MED system. The difference of inter-stage temperatures of MED and MEDAD can be observed clearly.

Table 7.2 A comparison of conventional MED and hybrid MEDAD systems components temperatures at different heat source temperatures

Heat source temperature (°C)	MED SG	MEDAD SG	MED Stage-2	MEDAD Stage-2	MED Stage-3	MEDAD Stage-3	MED condenser	AD evaporator
70	63.9	54.4	62.8	50.8	62.3	46.7	56.6	26.1
65	59.6	50.7	58.7	47.0	58.1	42.5	53.9	25.8
60	55.4	49.2	54.4	45.7	53.8	41.3	49.4	25.5
55	51.5	48.5	50.5	44.8	49.9	40.8	45.8	25.1
50	47.4	44.6	46.7	41.6	46.2	37.9	42.7	23.2
45	43.9	41.1	43.4	38.6	43.0	34.9	40.3	22.4
40	38.7	36.6	38.4	34.8	38.1	31.6	36.1	21.0
38	37.4	35.4	37.2	33.5	37.0	30.3	35.3	18.2
Operating limit of Conventional MED. Lower operational points are from MEDAD Hybrids								
35	-	30.9	-	27.9	-	23.5	-	16.1
30	-	26.0	-	23.7	-	19.1	-	12.2
25	-	22.1	-	19.9	-	16.3	-	10.1
20	-	18.1	-	14.2	-	11.3	-	7.1
15	-	13.2	-	11.5	-	9.4	-	5.6

For all heat source temperatures, more than three times inter stage temperature difference in MEDAD hybrid system is observed as compared to conventional MED system. Higher inter stage temperature difference is due to adsorbent affinity for water vapors that bring down the temperature of MED stages. This higher temperature difference enhance the water production due to higher heat flux and hence system performance.

It can also be seen that in case of hybrid MEDAD cycle, at same heat input, operational temperature gap is larger even with only 3-stages as compared to conventional MED system and more number of stages can be inserted to increase the water production and hence the system performance. For conventional MED system, last stage temperature can drop only up to 38^{o}C because of condenser operation. In case of hybrid MEDAD cycle the last stage temperature can be as low as 5^{o}C because of integration of AD shown from the table.

The effect of water production due to hybridization is observed in Figure 7.20, where the contributions from the MED stages and from the AD cycle can be seen. With hybridization, the improvement in water production in the same MED stages is almost doubled owing to the higher heat fluxes from a higher ΔT on the film evaporation processes. Concomitantly, the batch-operated AD water production is also seen and the combined water production boosted a production yield of 2.5 to 3 folds. The synergetic effect of hybridization is obvious and it represents a breakthrough for water production for thermal processes of desalination industry. It is also noted that the lower boiling temperature of the MED stages of hybrid cycle would give lesser fouling and scalling tendency on the surfaces of tubes.

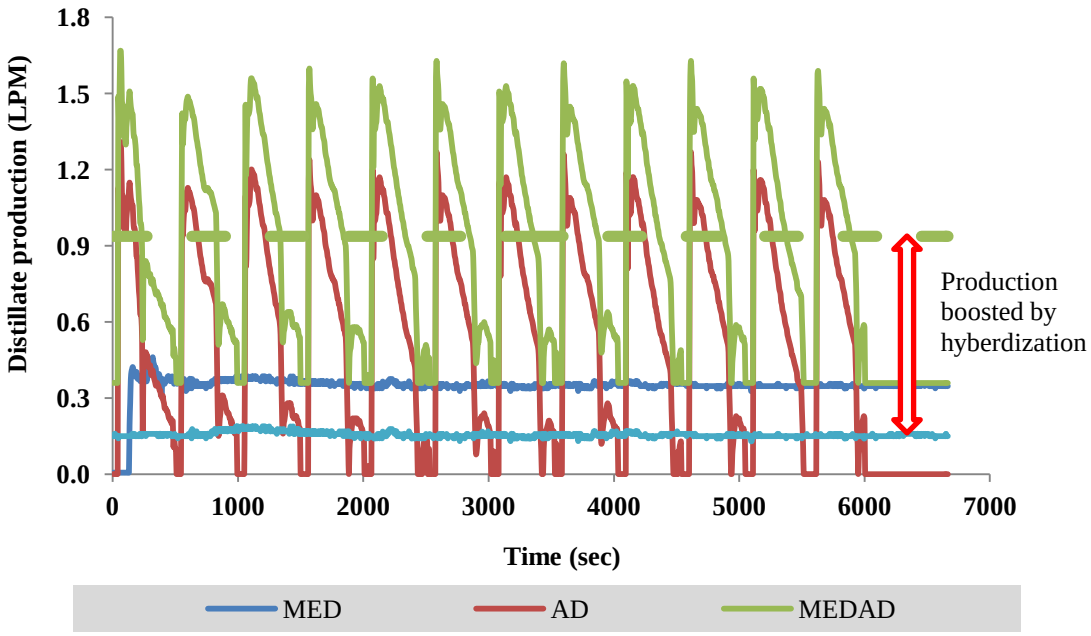

Figure 7.20 **Typical experimental water production profiles of 3-stage MED and hybrid MEDAD at heat source temperature 38°C**

Although the experimental facility has only 3 stages, experiments were conducted in a piece-wise manner where the saturation temperature of the last stage is reproduced as the input temperature to the steam generator. In this succession manner, it is possible to collate the performances of the MEDAD hybrid as though the AD cycle is integrated to many stages of MED, a design concept akin to what can be permitted by the available ΔT between the top-brine to the bottom brine stages. Figure 7.21 shows the water production measured from both the 3-stage MED and from MEDAD hybrid (same 3-stage) for assorted range of stage temperatures. At each steam generator temperature, a marked improvement to the water production is observed with 2 to 3 folds quantum jump.

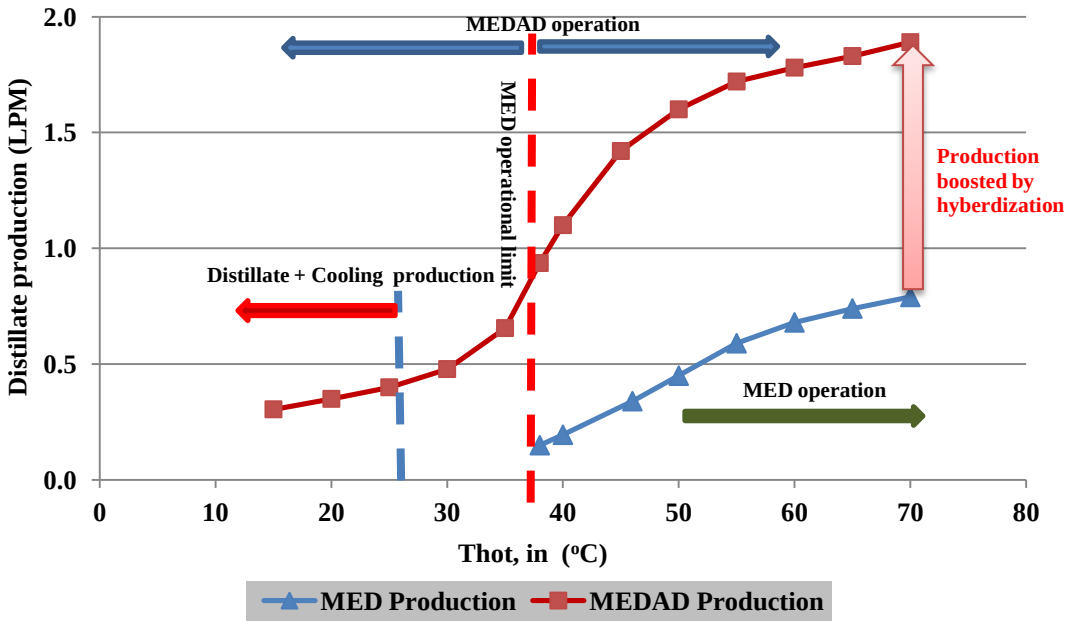

Figure 7.21 **A comparison of conventional 3-stage MED and hybrid MEDAD water production rates at different heat source temperatures**

Assuming that the MED stages can be configured in a piece-wise manner, the expected total available stages for MED is 10 whilst for the MEDAD operation can be stretched to 18. The hybrid cycle has the advantage of not limited by the local ambient temperature where the lower brine temperature (LBT) is constrained. The AD cycle has the ability to lower the LBT to as low as 5°C to 10°C. Based on an extrapolation of the total stages in the MED (about 10 stages) and MEDAD hybrid (18 stages), the respective water production is estimated to be 2.17 l/min versus 5.67 l/min, and a quantum improvement by more than two fold can be realized, as shown in Table 7.3.

Table 7.3 **A comparison of cumulative production of MED & MEDAD cycles operating piece-wise manner**

Cycle	TBT	LBT	Total number of stages	Total production
MEDAD	70^{o}C	8^{o}C	18	5.67 LPM
MED	70^{o}C	40^{o}C	10	2.02 LPM

Hybridization of the MED cycle not only improves the water production or the performance ratio, it can also minimize fouling and scalling on the tube surfaces at low brine temperatures. Such integrated designs with the proven thermal desalination methods can rival the membrane based RO method, both in terms of the specific energy efficiency as well as simpler and less susceptible operation to harmful algae blooms (HABs) of feed water.

Summary of Chapter 7

A 3-stage Multi effect desalination system is integrated with AD cycle to test as a hybrid MEDAD system. Experimentation detail of hybrid system is discussed. Valve scheme to operate two standalone systems MED and AD and a hybrid system MEDAD is highlighted. Flow schematic is provided and discussed in detail.

Hybrid MEDAD system experimental results are provided and discussed for a wide range of heat source temperature. All necessary parameters (i.e pressure, temperature and distillate flow rate) are measured and presented. It is observed that inter stage temperature and pressure is gap quite large as compared to conventional MED system. It is also noted that the ambient energy is harnessed by the system in the stages operating below ambient temperature. System performance is calculated on the basis of thermal energy and total primary energy. It is observed that system performance can be increased by inserting more number of stages as large operation temperature gap is available. It is also observed that simulation results have good agreement with experimental results with ±5% deviation.

Proposed hybrid MEDAD experimental results are compared with conventional MED system results. Inter stage temperature varies from 3^{o}C to 4^{o}C and pressure varies from 1-2kPa. It is noted that production increased by 2 to 3 folds by hybridization at same heat source temperature. Two main reasons for production boosting can be high film evaporation rate and cooler condenser side temperature that boost the condensation rate.

Experimental set up consist only 3-MED stages but in actual it can be many stages (>15) which can boosted the production by many folds and hence the system performance. The superiority of hybridisation can even realize with only 3-stages MED in terms of distillate production increase and system performance. MEDAD cycle can produce two useful effects namely; distillate production and cooling.

Chapter 8 Economic Analysis of Desalination Systems

Unit water production cost is the major factor for process selection and project decision of a desalination installation. Primary fuel cost is the major contributor after capital cost and different methods are adopted to estimate the fuel cost for unit production for stand alone and for integrated plant with power generation facility. Almost all methods based on energy apportioning costing, and in dual purpose plants it is not fair cost distribution. A new exergy based model is proposed for cost apportioning on the basis of "quality" of energy utilized by the process in dual purpose plants. This exergy model will provide the real cost apportioning guide lines for dual plant where desalination is integrated with power generation.

The proposed exergy model is discussed in detail in the following sections. In the first part of the chapter, the main costing factors and their calculation methods are discussed. The detailed exergy model is presented in the second part of the chapter. The benefits of integration of power plant with desalination are discussed in third part of the chapter. The unit distillate production cost ($/m^3) of MEDAD compared with all desalination systems and CO_2 savings are presented in the last part of the chapter.

8.1 Background

In project decisions, process selection and unit production cost are the major factors. Integration of a desalination plant with power plant (PP) is most adopted scheme to optimize both processes. The primary fuel cost is a major cost factor in unit water production cost. The fair cost distribution of primary fuel supplied to PP boiler is very important in the case of integrated installations. In general, cost apportionment on the basis on energy utilized by the PP and desalination plant is used for primary fuel cost distribution. It is realized that this is not a fair distribution and the desalination industry charges more even low grade energy is utilized from the last stages of low pressure turbines. This cost apportioning must be on the basis of "quality" of energy used by the processes. For dual purpose plants, exergy based cost apportionment is proposed as exergy is defined by the quality of energy. Exergy based costing is the real apportionment of primary fuel for PP and desalination processes on the basis of quality of energy they utilized. The detail of exergy model is provided in the sections below.

8.2 Factors Affecting the Cost of Desalination

Most of the factors affecting the desalination costing are generic to all desalination plants but some factors are specific to process and site. Other than thermal energy requirements for thermal processes, the most important and affecting factor for desalination plants are listed in Table 8.1.

Table 8.1 Overview of factors affecting the desalination costing

no	Factor affect cost	Remarks
1	**Plant life**	Affects the amortization period and hence the capital costs of the plant.
2	**Technology and plant size**	Most important decision factor for investment in terms of plant size and unit cost.
3	**Interest rates**	Total investment and capital cost is influenced by this factor.
4	**Inflation rates**	Unit production cost is affected by this factor.
5	**Site costs**	This is capital cost that depends on site condition and footprint of project
6	**Feed intake and brine discharge**	Plant distance from sea intake is important to reduce the piping and pumping cost
7	**Feed water quality**	Water production cost is directly affected by feed quality especially in RO. It also affects the pre-treatment processes.
8	**Output water quality**	In case of RO, the required output water quality is a important cost factor because membrane replacement cost has significant effect on unit production cost. But for thermal processes this factor may not be a controlling parameter as they can produce very high quality water with concentration is about 15ppm.
9	**Energy sources**	Energy is basic needed for all desalination processed for desalting the seawater. The source (renewable or non-renewable) and type (high grade or low grade) of energy is an important cost factor. Renewable energy sources and industrial waste heat sources are getting attraction now a days for many desalination processes such as low temperature MED and AD cycles.
10	**Pretreatment cost**	Feed pre-treatment is a necessary step to reduce the system degradation and has substantial contribution to the cost of the thermal unit and membrane unit production.
11	**Chemical costs**	Chemicals have a major contribution to cost in membrane unit production and also have some effect in thermal production units. It can vary with location based on feed water quality.

8.3 Costing Heads Estimation

The major heads in total cost of any desalination process are; i) capital, ii) operational, iii) maintenance, iv) labor, v) pre-treatment and vi) energy requirement. Desalination plant life based on process type and plant capacity can affect the annualized capital cost via the amortization period (n) and interest rate (i) through a capital recovery factor (CRF), i.e., the product between initial investment and the CRF. Desalination plant operational cost includes fuel and electricity contribution and in some cases maintenance, labor and pre-treatment cost is also dump into it. Inflation rates (j), arising from the cost of primary fuel, electricity price fluctuations, etc can also affect the operational costs. Inflation weighted factor (IWF) is used to incorporate the increases over a period of time into the future. Different cost factor calculations are discussed in the following sections in detail.

Inflation weighted factor (IWF): Inflation weighted factor (IWF) is defined as:

$$IWF = \frac{CRF(i,n)}{CRF(i^{'},n)} \tag{8.1}$$

Unit desalination cost: life-cycle approach is used to find the unit desalination cost based on key variables and can be defined as:

$$C = \left(\sum_{a=1}^{n} C_{capital} (CRF(i,n))_k \right) + \left(\sum_{b=1}^{m} C_{operational} \left(\frac{(CRF(i,n))}{(CRF(i^{'},n))} \right) \right) \tag{8.2}$$

where C is unit volume production cost ($/m^3), n & m are capital investment items and operational cost items. Operational cost includes all the factors or items namely; a) electricity cost, b) maintenance cost, c) labor cost, d) chemical cost, e) pre-

treatment cost, f) equipment replacement cost and g) interest cost factor. The detailed analysis of cost factors involved in a typical desalination plant is discussed in below section.

Direct-capital cost ($C_{capital}$)**:** based on plant life span and total distillate production, the direct capital cost can be calculated as:

$$C_{capital} = \frac{S_{direct-capital} \cdot \beta}{D} \tag{8.3}$$

where $S_{direct-capital}$ is direct capital cost, β is amortization factor and D is distillate produce per annum by plant. In general, the direct capital cost is involved mainly the equipment costs. In MEDAD the major components are; MED stages, AD beds, adsorbent heat exchangers, AD condenser and cooling tower. Moreover feed pre-treatment facility items and circulation pumps also included in capital cost. The amortization factor also called capital recovery factor β can be calculated as:

$$\beta = \frac{i(i+1)^n}{(i+1)^n - 1} \tag{8.4}$$

where i is the interest rate and n is plant life.

Electricity cost ($C_{electrical}$)*:* in thermal or membrane desalination, the circulation pumps are the main user of electricity. Pump work input can be calculated as:

$$W_{pump}(kW) = \sum \frac{\Delta P_{across-circuit} \cdot V_{liquid-flow}}{\eta_{pump}} \tag{8.5}$$

where ΔP (KPa) is the pressure drop in the pipe circuit, V (m^3/sec) is the volume handled by pump and η_{pump} is pump efficiency. On the basis of pump work input, hourly electricity cost can be calculated as:

$$C_{hourly-pump}(\$/h) = W_{pump}(kW).R_{electricity}(\$/kWh) \tag{8.6}$$

Total electricity cost can be calculated on the basis of distillate produced as follows:

$$C_{electrical} = \frac{C_{pump-hourly}.yearly - operatin - hour}{D} \tag{8.6}$$

Maintenance cost $(C_{maintenance})$*:* generally, the maintenance cost of a desalination plant is given by the percentage of direct capital cost and can be calculated as:

$$M(\$/yr) = S_{capital}.\alpha.\beta \tag{8.7}$$

Where the M is the maintenance cost per year and α is the percentage of capital cost. The total maintenance cost based on distillate production can be calculated as:

$$C_{maintenance} = \frac{M(\$/yr)}{D(m^3/yr)} \tag{8.8}$$

The key advantage of MEDAD plant is low operational temperature that reduces the chances of corrosion and fouling results low level of maintenance cost. The AD maintenance cost is 0.01% of direct capital cost. Hence it is practical to assume maintenance cost of MEDAD is at 0.02% of direct capital cost.

Chemical cost $(C_{chemical})$*:* feed water treatment is required to prevent corrosion and fouling problems in desalination plant. Chemical treatment cost varies with desalination process and with operating conditions. In membrane processes (RO) unit chemical treatment cost varies from \$0.025/m^3 to \$0.035/m^3 [253, 254]. In case of hybrid MEDAD, almost no chemical treatment is required because of low temperature operation and robust evaporative system. Thus, contribution of chemical cost is assumed negligible in hybrid MEDAD system.

Pre-treatment cost $(C_{pre-treatment})$*:* this involves the cost of materials and equipments installed for feed pre-treatment process. It has substantial contribution in case of RO and high temperature evaporative processes such as MSF. In the case of hybrid MEDAD, pre-treatment cost is very low because only de-aeration tank is required for pre-treatment.

Labor cost (C_{labor})*:* this cost is related to personals working at plant and it depends on capacity, size and type of plant. Hybrid MEDAD plant operation is very simple and valve scheme is totally automated so very few personals are required to operate the plant. The labor cost to operate hybrid MEDAD system is very minimal.

Membrane replacement cost $(C_{chemical})$*:* these involve membrane and its replacement cost and can be calculated as:

$$C_{membrane} = \frac{S_{membrane}(\$)}{D(m^3)} x \frac{i(i+1)^y}{(i+1)^y - 1} x \frac{n}{y} \tag{8.9}$$

$$C_{membrane-replacement} = \frac{R_{membrane}(\$)}{D(m^3)Y(yr)} \tag{8.10}$$

where $S_{membrane}$ is the membrane cost, Y is the membrane life and $R_{membrane}$ is the membrane replacement cost. Membrane replacement also includes the installation cost.

8.4 Primary Fuel Cost Estimation: An Exergy Analysis Approach

In desalination, the cost of fuel or input energy is a major contribution to overall production cost. Since, desalination processes are energy intensive so they are normally associated with power generation systems as a dual purpose plant.

In dual purpose plants, primary energy apportioning is very important for fair costing of power production and desalination. In the literature, many researchers [255-258] provided a detailed economical analysis but all studies uses energy based cost apportioning. Energy based cost apportionment is not the true cost distribution because desalination plants utilized low grade bleed steam. This low grade bleed steam has very less ability to perform work in turbines but it can produce a substantial work in desalination because of low pressure operation. So in dual purpose, power and desalination plants, consideration of same level energies for cost apportionment is not impartiality with water production systems.

For dual purpose plants, the cost apportioning on the basis of "quality" of energy utilized by process is the true cost distribution. Cost apportioning utilizing exergy analysis shows the real cost of primary fuel energy for power plant and desalination processes since the quality of the energy is differentiated.

Exergy is an extensive thermodynamic function defined as maximum theoretical achievable work from an energy carrier under environmental imposed condition (T_o, P_o) at given amount of chemical element. At environmental state also called as dead state, system exergy is considered as zero. Therefore, the general exergy term includes thermo-mechanical and chemical exergy. The thermo-mechanical exergy is the maximum available work when system conditions (T and P) approaches environmental conditions (T_o, P_o) without changes in chemical composition of process stream. The chemical exergy is defined as the maximum work obtained when the concentration (C_o) of each substance in processes streams changes to that of environmental conditions (T_o, P_o).

The main difference between energy and exergy is that energy always remains conserved in a process according to first law of thermodynamic while exergy is destroyed due to irreversibilities in the process. Exergy destruction or annihilation is caused by entropy generation in a process within each component of the system. In addition, there are some exergy losses to ambient due to temperature difference and it is called effluent exergy losses. Main point of interest is to find the potential of work of flow stream also called specific exergy across each component of the system.

Many researchers [259-279] conducted the detailed exergy analysis for different thermal and membrane desalination processes as a standalone and with dual purpose plant configuration but for costing they used energy apportioning techniques. The method of exergy based cost apportioning is discussed in following sections in detail.

8.4.1 System Description

The standard dual purpose plant considered for analysis is shown in Figure 8.1 [280]. This system consists of high pressure (HP-T) and low pressure turbines (LP-T) with re-heating steam loop. Bleed steam from specific stage of LP-T is utilized as a heat source for MED plant with TVC configuration. Required operational parameters at all points are given for analysis purpose. It can be seen that steam entering at HP-T has high energy (371^{o}C, 104bar) while steam utilized for desalination is of low quality (204^{o}C, 17bar).

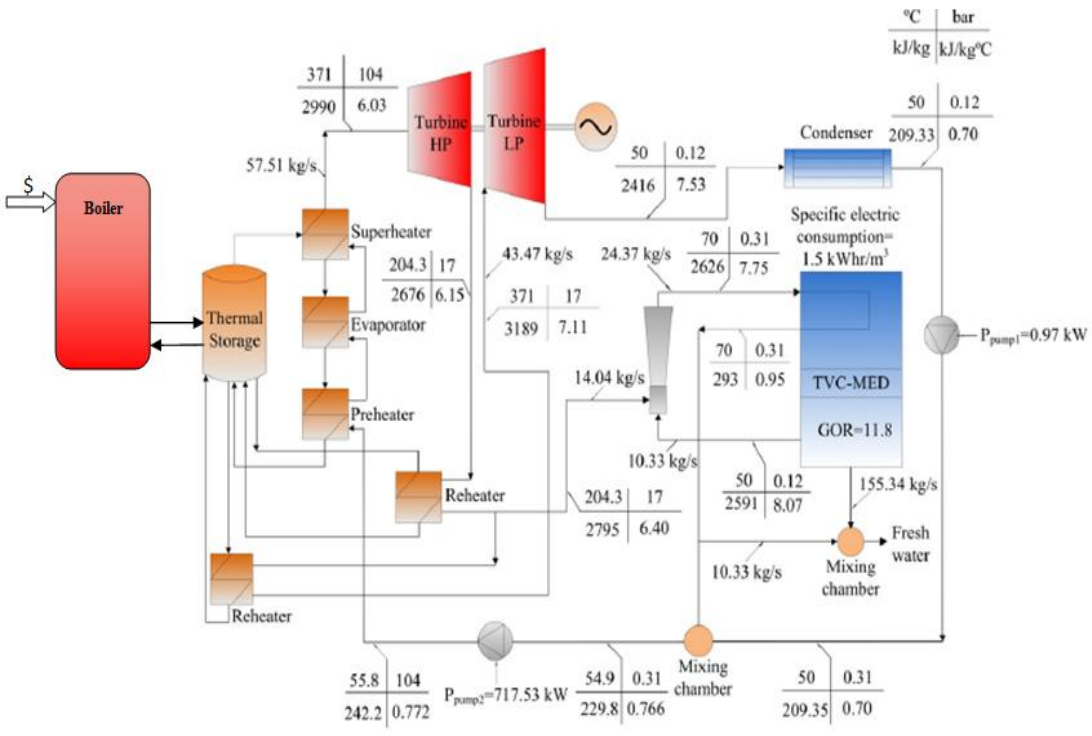

Figure 8.1 **Process flow of dual purpose plant considered for cost apportioning on the basis exergy analysis [280].**

8.4.2 Theoretical Model

The co-generation system as mentioned in earlier section, is simplified for power plant and desalination as PP+MED and PP+MEDAD as shown in Figures 8.2 and 8.3. Steam pressure and temperature conditions are mentioned at each section according to standard plant operation.

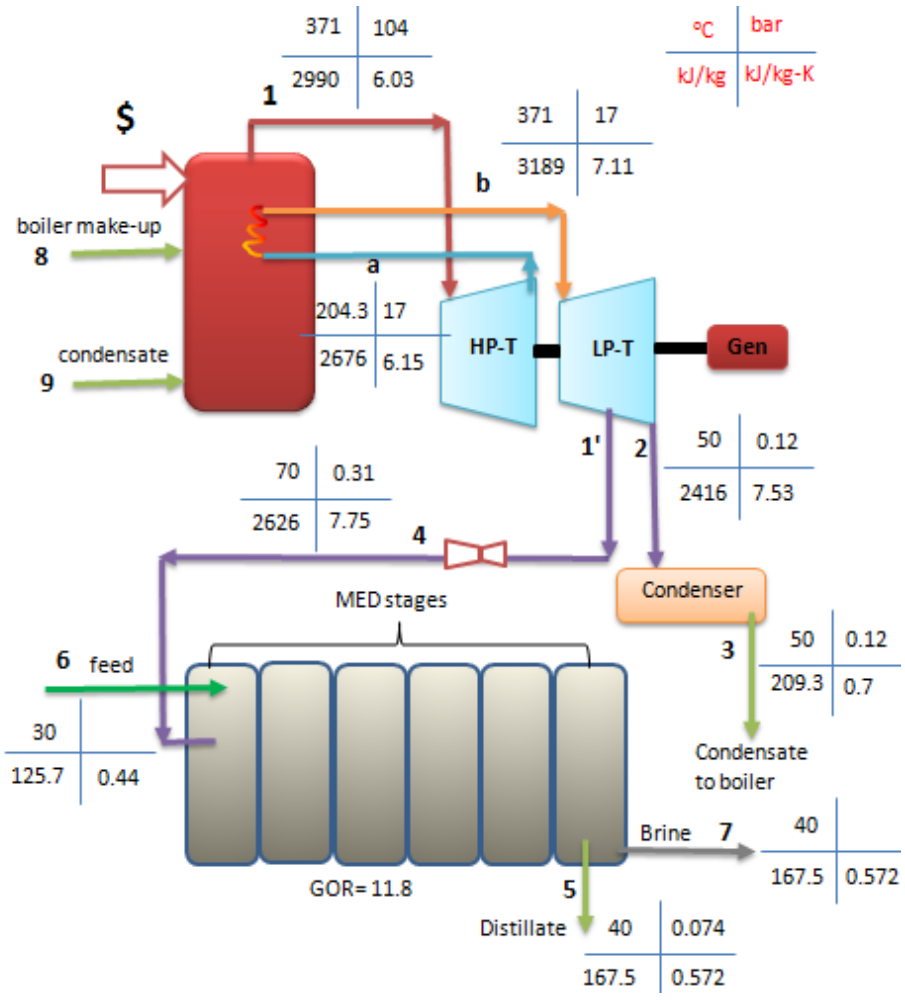

Figure 8.2 Simplified model of dual purpose plant (PP+MED)

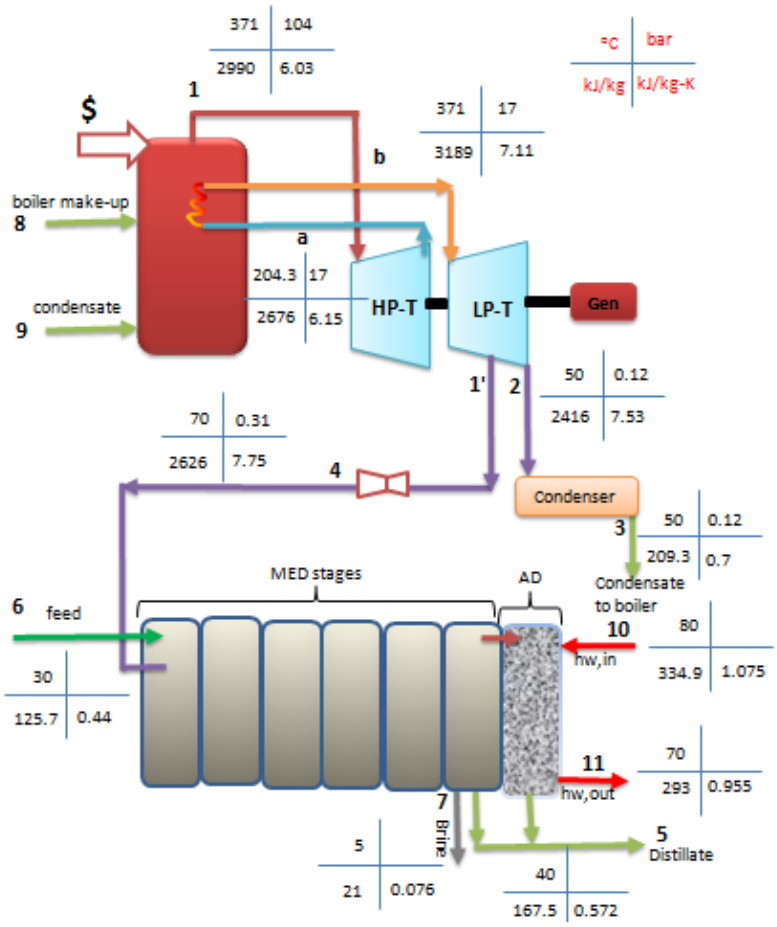

Figure 8.3 Simplified model of dual purpose plant (PP+MEDAD)

The theoretical model is developed and discussed in detail in Tables 8.2 and 8.3 where the properties such as enthalpy (h) and entropy (s) are the functions of temperature and pressure at respective points. Based on model developed, exergy is calculated at each point and then across all components and finally across systems (PP & Desalination). The percentage of total exergy across PP and desalination system is calculated on the basis of total exergy available for whole system.

Table 8.2 Detailed exergy modeling of power plant combined with desalination system

State points	Exergy Calculation	Comments	
1 - a	$E_{1-a} = \dot{m}_1[(h_1 - h_a) - T_o(S_1 - S_a)]$	total available work from HP-T	(8.1)
b-1'	$E_{b-1'} = \dot{m}_1[(h_b - h_{1'}) - T_o(S_b - S_{1'})]$	total available work from LP-T upto bleed point	(8.2)
1' - 2	$E_{1'-2} = \dot{m}_2[(h_{1'} - h_2) - T_o(S_{1'} - S_2)]$ $\dot{m}_2 = \dot{m}_1 - \dot{m}_{1'}$	work available after bleeding point in LP-T	(8.3)
1 - 2 (Turbine)	$E_{T,1-2} = E_{1-a} + E_{b-1'} + E_{1'-2}$	total exergy across power plant	(8.4)
2 - 3 (Cond)	$E_{2-3} = \dot{m}_2[(h_2 - h_3) - T_o(S_2 - S_3)]$	exergy lost across condenser	(8.5)

Table 8.3 Detailed exergy modeling of desalination system combined with power plant

State points	Exergy Calculation	Comments	Desalination system	
4 - 5	$E_{4-5} = A - T_o B$ $B = \left(s_4 x \dot{m}_{1'}\right) - \left(s_5 x \dot{m}_{1'} GOR\right)$ $A = \left(h_4 x \dot{m}_{1'}\right) - \left(h_5 x \dot{m}_{1'} GOR\right)$	exergy across MED stages by steam entring and distillate leaving	MED MEDAD	(8.6)
6-7	$E_{6-7} = C - T_o D$ $C = \left(h_6 x \dot{m}_{feed}\right) - \left(h_7 x \dot{m}_{brine}\right)$ $D = \left(s_6 x \dot{m}_{feed}\right) - \left(s_7 x \dot{m}_{brine}\right)$	exergy across MED by feed entring and brine leaving	MED MEDAD	(8.7)
10-11	$E_{10-11} = \dot{m}_{hw}[(h_{10} - h_{11}) - T_o(S_{10} - S_{11})]$	exergy across AD by h/w entring and c/w leaving	MEDAD	(8.8)
Desalination	$E_{MED} = E_{4-5} + E_{6-7}$ $E_{MEDAD} = E_{4-5} + E_{6-7} + E_{10-11}$	total exergy across desalination plant	MED MEDAD	(8.9) (8.10)

On the basis of total exergy available across whole system, proportion utilized by power plant and desalination system is calculated as presented in Table 8.4.

Table 8.4 Detailed performance modeling for combined power and desalination plant

	Exergy Calculation	Comments	Desalination system	
Exergy$_{total,\ cogen}$	$E_{Total,PP+MED} = \left[E_{T,1-2} + E_{MED}\right]$	dual purpose plant total available exergy (desalination+PP)	MED	(8.11)
	$E_{Total,PP+MEDAD} = \left[E_{T,1-2} + E_{MEDAD}\right]$		MEDAD	(8.12)
% Exe across turbine	$\%E_{PP1} = \frac{E_{T,1-2}}{E_{Total,PP+MED}}$	percentage of exergy utilized by power plant	MED	(8.13)
	$\%E_{PP2} = \frac{E_{T,1-2}}{E_{Total,PP+MEDAD}}$		MEDAD	(8.14)
% Exe across Desalination	$\%E_{MED} = \frac{E_{MED,4-7}}{E_{Total,PP+MED}}$	percentage of exergy utilized by desalination plant	MED	(8.15)
	$\%E_{MEDAD} = \frac{E_{MEDAD}}{E_{Total,PP+MEDAD}}$		MEDAD	(8.16)

8.5 Cost Estimation

Developed exergy model is used to analyze the selected dual plant. Figure 8.4 shows the proportion of exergy utilized by PP and desalination systems in dual purpose power plant at different steam extractions. In general, only 20% to 25% steam is extracted for desalination, but results are presented at 10- 50% extraction for full range of desalination plant sizes.

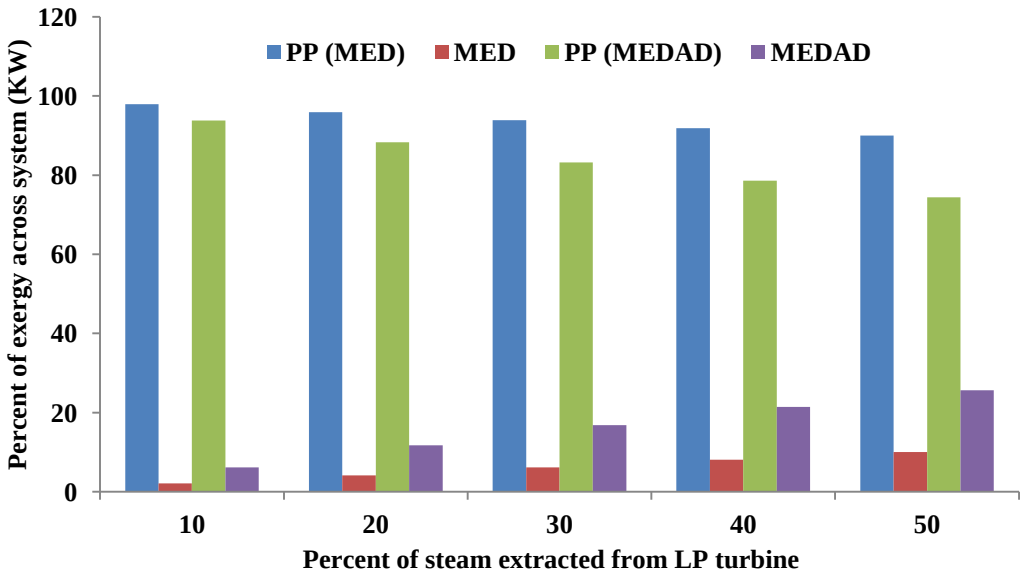

Figure 8.4 Exergy utilized by PP and desalination in dual purpose plant

It can be seen clearly that at 20% steam extraction, MED utilized only 4% of total exergy and MEDAD 12% while at 30% extraction, exergy utilization for desalination is 6% and 17% respectively. This shows the true picture of proportion of energy utilization in dual purpose power plants. Previously, desalination industry experts considered these proportions as 50-50% and it caused over charged to desalination. Here it is very clear that in dual purpose power plants, desalination contribute a small portion in total fuel cost.

Table 8.5 shows the proportions of primary energy utilization on the basis of exergy and energy for PP and desalination at different steam extractions. It can be seen that proportions utilized by desalination systems calculated by exergy methods is far away from energy based calculation and it is because the effect of "quality" that is not captured by energy method. Exergy based proportion analysis showed the true picture of costing on the basis of "quality" of energy utilized.

Table 8.5 **Primary energy utilization on the basis of energy and exergy in PP and desalination systems at different steam extractions.**

Percent of steam extraction for desalination	MED				MEDAD			
	Energy method (%)		Exergy method (%)		Energy method (%)		Exergy method (%)	
	Power production	Water production	Power production	Water production	Power Production	Water production	Power Production	Water Production
10	86.7	13.3	98	2	52.4	47.6	94	6
20	76.1	23.9	96	4	35.1	64.9	88	12
30	67.6	32.4	94	6	26.1	73.9	83	17
40	60.5	39.5	92	8	20.6	79.4	79	21
50	54.5	45.5	90	10	16.9	83.1	74	26

It is clear from table that on the basis of quality of energy utilization, desalination processes contribution is very less in primary fuel input.

Integration of PP with desalination also increases the available work extraction as shown in Figure 8.5. This increase in available work extraction is due to low grade energy utilization in desalination that may not able to produce work in PP. Extracted

low quality steam can be utilized effectively in desalination and can produce more work as compared to if it will be utilized in PP.

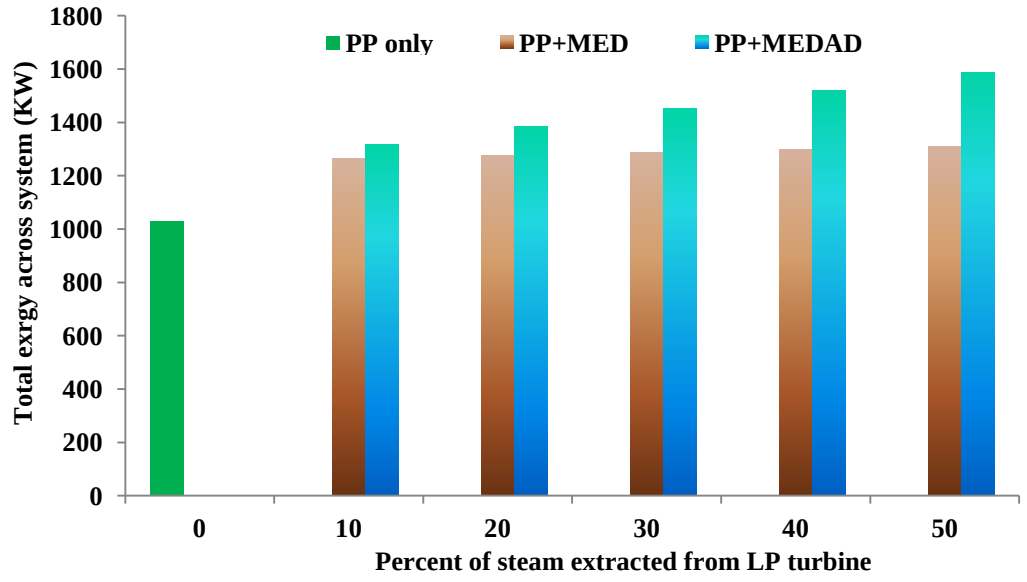

Figure 8.5 **Maximum work extraction with PP, PP+MED and PP+MEDAD cycle**

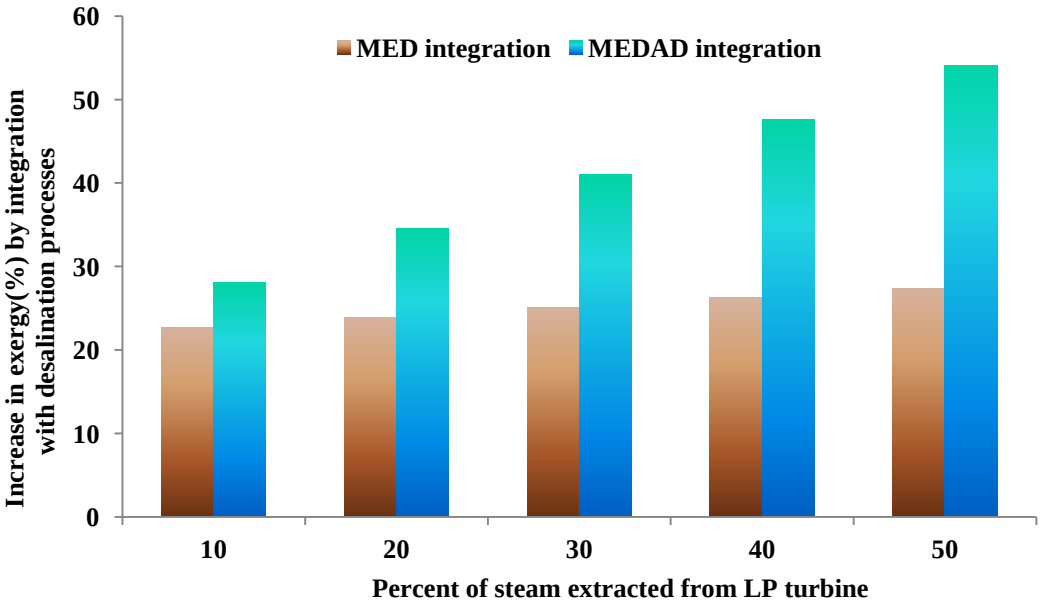

Figure 8.6 **Percent increase in available work by integration of MED and MEDAD**

It can also be noticed that this extraction is even higher in case of hybrid MEDAD system and it is because of lower last stage temperature as compared to conventional MED. This shows that hybrid MEDAD with PP is the best combination to extract maximum work from available. The percent increase in work extraction by integration of conventional MED and hybrid MEDAD is shown in Figure 8.6. It can be seen that at 50% steam extraction, integration of MEDAD increases the work extraction by 55% as compared to conventional MED about 30%.

For Industrial scale plant analysis, it is important to calculate the maximum possible number of stages. To calculate the maximum possible number of stages of MED/MSF systems, the whole system considered as a black box with steam energy entering and distillate is leaving with liquid energies. The theoretical concept of the plant is shown in Figure 8.7.

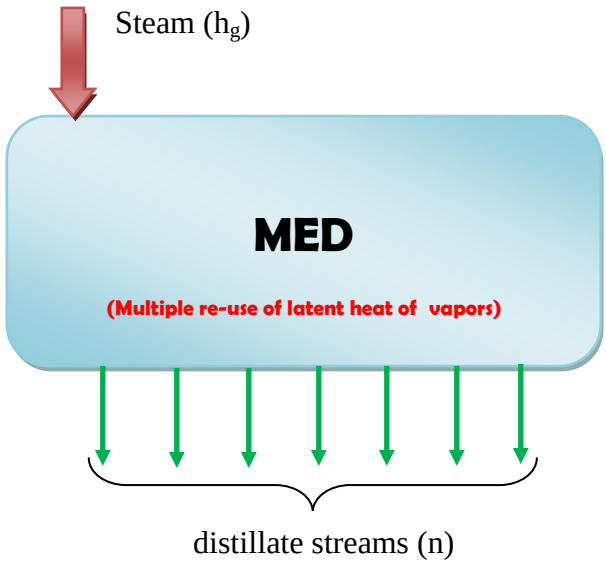

Figure 8.7 Maximum possible numbers of stages of MED (black box analysis)

Theoretical possible number of stages can be calculated as:

$$n = \frac{steam\ energy\ (h_g)}{distillate\ energy(h_f)} - 1$$

For a conventional MED system, if we consider the steam is entering at 70°C with vapor enthalpy 2626 kJ/kg and distillate is leaving at 35°C with enthalpy 146 kJ/kg, than maximum theoretical number of stages can be:

$$n = \frac{2626}{146} - 1 \approx 18$$

It shows that thermodynamic limit the maximum possible number of stages for conventional MED systems at 18. In case of hybrid MEDAD system, maximum number of stages can be even more than 19 because of lower last stage temperature (5°C). By considering the theoretical maximum number of stages (18) and energy proportions, primary fuel cost for thermal and membrane based desalination is calculated as shown in Table 8.6.

Table 8.6 Primary fuel cost for different desalination processes

	Thermal methods (MED/MSF)	**Membrane methods (RO)**
Primary fuel energy (kWh_pe/m^3)	$PE_{MED} = \frac{Q_{th-MED}}{n.\eta_b} + \frac{Q_{elec-MED}}{\eta_{pp}}$ $PE_{MEDAD} = \frac{PE_{MED}}{\alpha}$	$PE_{RO} = \frac{Q_{elec-RO}}{\eta_{pp}}$
Distillate production cost on the basis of exergatic analysis primary fuel energy apportionment	$\$/m^3 = (PE_{MED}.\beta.\$_{PE}) + \left(\frac{Q_{elec-MED}.\$_{PE}}{\eta_{PP}}\right)$	$\$/m^3 = PE_{RO}.\beta.\$_{PE}$

Power plant conversion efficiency (η_{PP}): **35%**

Boiler efficiency (η_b): **96%**

Thermal energy required for MED/MSF (Q_{th-MED}): **624 kWh/m^3**

Electrical energy required for MED/MSF ($Q_{elec-MED}$): **0.5 kWh/m^3**

Electrical energy required for MED/MSF ($Q_{elec-RO}$): **5.0 kWh/m^3**

Exergy factor for cost apportionment (β): **5:95** (PP to MED at 25 % steam extraction)

MED to MEDAD production increased factor (α): **2**

Primary energy cost ($\$_{PE}$): **$5/293kWh**

MED/MSF number of stages (n): **12** (largest MED till today)

Distillate production cost ($/m^3)	**MED**	**MEDAD**	**RO**
	$0.074/m^3	$0.0488/m^3	$0.231/m^3

MED commercially available up to 12 stages, it can be seen that hybrid MEDAD cycle primary fuel cost is lower as compared to RO even with 12 stages. Figure 8.8 shows primary fuel cost of RO system compared with hybrid MEDAD for different number of stages. It can be seen that even with 10 numbers of stages, MEDAD cost is lower than RO system. This shows that on the basis of true cost proportioning, MEDAD system is cost efficient as compared to RO processes.

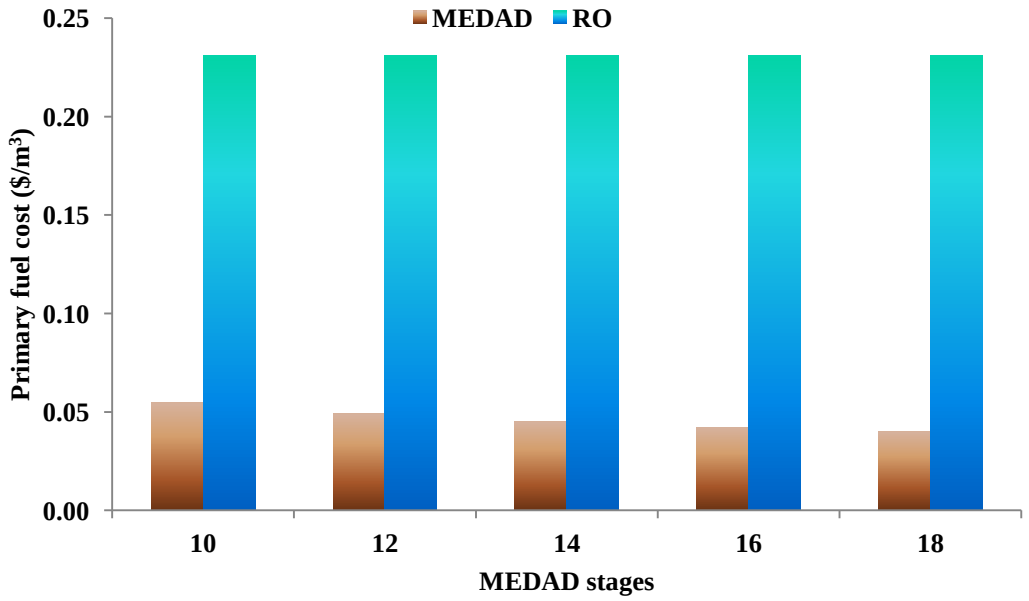

Figure 8.8 A comparison of primary fuel cost of RO and hybrid MEDAD (with different stages)

8.6 Unit Water Production Costing

On the basis of above analysis for primary fuel cost (thermal energy cost) and literature data [281,282] for other cost heads, the total distillate production cost ($/m^3) is calculated for all processes as shown in Figure 8.9. It can be seen that MEDAD unit water production cost is the lowest ($0.50/m^3) as compared to all other processes if energy required for desorption processes considered as non-payable (low grade water heat, solar or geothermal).

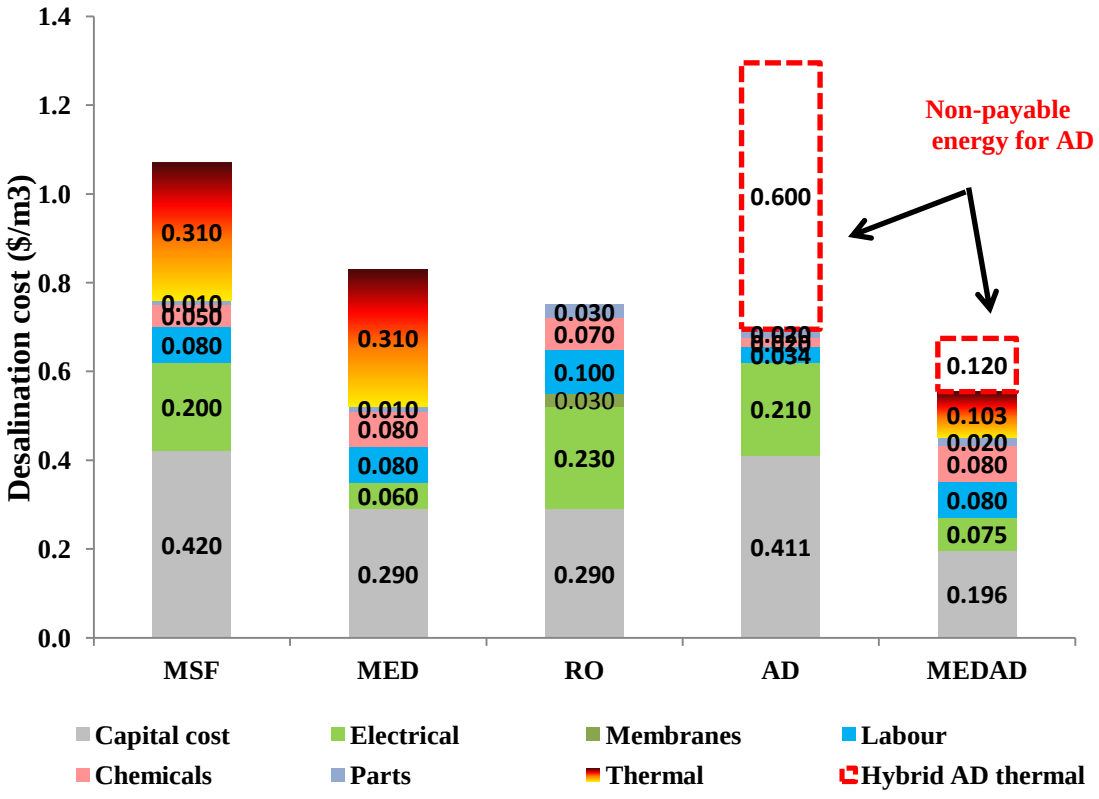

Figure 8.9 **A comparison of unit production cost of different desalination methods on the basis of exergy apportioning primary fuel cost**

It can also be noticed that capital cost of MEDAD system is lower as compared to conventional MED system and it is because of increase in production by hybridization (2.5 to 3 folds) that reduce the hardware footprint.

8.7 CO_2 Emission Savings

CO_2 emission is calculated on the basis of thermal and electrical energy utilization for all desalination processes and presented in Table 8.7.

Table 8.7 **A comparison of CO2 emissions for conventional desalination methods and savings by utilizing hybrid MEDAD cycle (reference plant size is 1000m3/day)**

Desalination Methods	CO_2, from thermal (ton/year)	CO_2, from electrical (ton/year)	CO_2, total (ton/year)	CO_2, savings (ton/year)
MSF	1636.6	875.4	**2511.9**	**1839.5**
MED	1383.5	639.7	**2023.2**	**1350.7**
RO (single-pass)	0	1380.4	**1380.4**	**707.9**
RO (double-pass)	0	1515.0	**1515.1**	**842.6**
MEDAD (AD non-payable)	345.9	326.6	**672.45**	-

Emission factor for CO_2 from natural gas burning is $64.2x10^{-5}$ ton / MJ [283] and for electrical generation is o.642ton/MWh [284, 285]. MEDAD (AD non-payable) is considered as baseline to calculate the CO_2 emission savings.

It can be seen that the hybrid MEDAD cycle CO_2 emission is lower as compared to all other desalination methods i.e. MSF, MED and RO. It shows that for the same amount of water production, CO_2 emission can be as low as four times as compared to the MSF and 2.5 times compared to RO. If MEDAD cycle is utilized for distillate production, CO_2 emission can be reduced and can help to save environment directly.

This analysis shows that MEDAD is not only energy efficient but also environmental friendly.

MEDAD system can be scaled to any size as it is very robust system. It can also be installed on a container skid for portable operation in remote community. The other applications are; 1) on ship and 2) with large engine exhausts.

Desalination requirements are increasing with better growth and development of countries and inserting a huge pressure on energy utilization and environmental emissions. Energy efficient and environment friendly proposed novel hybrid cycle "MEDAD" proved that this technology can fulfill the fresh water requirement gap with energy efficiency and CO_2 emission savings.

These reasons were the motivation for the investigation of this novel hybrid MEDAD cycle theoretically and experimentally.

Summary of Chapter 8

Economic analysis for desalination systems is conducted in detail. All the factors affecting unit production cost are discussed and their formulation for estimation is presented.

A new exergy based model for cost apportioning in dual purpose plant is introduced. This model shows the real primary fuel cost distribution for processes (PP and desalination) on the basis of "quality" of energy. It shows that only 25% of fuel cost belongs to desalination processes in integrated installation and the rest of the 75% must be charged to power generation. Exergy analysis also shows that the total available work extraction is higher in dual purpose plants as compared to PP only due to low grade energy utilization in desalination cycles. It is also observed that this quantity is even higher in the case of hybrid MEDAD as compared to conventional MED plants.

Unit water production cost is calculated by considering all costing factors. It shows that the hybrid MEDAD unit production cost is the lowest ($\$0.58/m^3$) amongst all available desalination processes. This was another reason for the investigation of hybrid MEDAD cycle. Exergy based costing analysis proves that hybrid MEDAD can beat RO energetically and efficiently. CO_2 emission savings analysis is also calculated and it is found that a huge emission can be reduced by utilizing this novel cycle. MEDAD is an environmental friendly technology. It is predicted that MEDAD hybrid cycle will cover the major share in desalination industry in near future.

Chapter 9 Conclusion

9.1 The Major Findings of this Research Work

The thesis pertains to the investigation of the hybridization of an adsorption (AD) cycle and the multi-effect distillation (MED) cycle. To achieve this objective, the following research work has been carried out as described in the earlier thesis chapters;

(1) A new falling film correlation for heat and mass transfer processes on horizontal tubes was investigated. The experiments were conducted with parameters related to MED operation, i.e., low vacuum pressures and at assorted salt concentration in the seawater, patching a knowledge gap for accurate prediction of the film boiling processes on tube surfaces. The available correlations found in the literature were meant for higher temperature and pressure ranges with only pure water.

(2) The next stage of research described in the thesis was to develop a theoretical model for handling the multi-effect desalination, based on thermodynamic properties of seawater such as the enthalpy, density, internal energy, viscosity and heat capacity. A distributed approach is used to enable the prediction of P, T and X (salt concentration) at different tubes surfaces, MED stages, etc. The simulation code is verified by experiments conducted on a 3-stage MED (nominal capacity up to 30 kW) for assorted heat source input to the steam generator stage. This facility was designed, fabricated and commissioned in

the project. The comparison shows that the simulated results are within ± 5% of the measured results in the 3-stage MED plant.

(3) The important part of the research was to integrate the MED cycle to the AD cycle. The hybridization of these cycles demonstrated the synergetic effects from the operation of the MEDAD cycles, resulting in a quantum jump in water production yield up to 2.5 to 3 folds and hence a higher performance ratio. The tests were conducted across the expected top-brine temperatures from a high of 70^{o}C to a low of 15^{o}C, which is below the ambient temperature. A companion distributed simulation code was developed to handle the hybrid MEDAD cycle and performance verification. The simulation code shows good agreement with experimental results within ±5% deviation.

(4) In addition, proposed hybrid MEDAD desalination cycle results were compared with conventional MED system and it was found that inter-stage temperature varies from 3^{o}C to 4^{o}C in hybrid MEDAD operation as compared to 1^{o}C in conventional MED. In hybrid MEDAD cycle, the last stage temperature was observed as low as 7^{o}C to 10^{o}C as compared to 38^{o}C in conventional MED that was restricted by condenser. A remarkable production increase 2.5 to 3 folds was observed due to hybridization at same operating conditions.

(5) Finally, a specific cost analysis was conducted by considering the capital and operational costs of the MEDAD cycle. The approach was to assume the MED cycle forms part of the cogeneration plant where electricity and water

production are generated from the combined plant. An exergy approach was used to apportion the true cost of energy (fuel) input to the desalination processes whilst the AD cycle used the waste exhaust heat source for the regeneration of the adsorbent. As opposed to the conventional energetic approach, the exergy analysis shows that the desalination consumed only 20 to 25 % of the total fuel cost instead of >45% as calculated by energy approach. The exergy based primary fuel apportioning approach predicted a realistic water production cost of less than \$0.6 /m^3 for the MEDAD cycle. It was observed that MEDAD can beat RO processes energetically and efficiently.

CO_2 emission analysis was also conducted and it was found that a huge emission (1000-2000 ton/year) can be reduced by MEDAD cycle utilization for same amount of water production. It was observed that MEDAD in not only an energy efficient method, also an environment friendly cycle.

Finally, the key advantages of the MEDAD cycle have been demonstrated in this research; i.e., higher water production, simple and reliable operation, low operational cost as there is no major moving parts in the plants and environment friendly. It is the author's believe that the hybrid cycles such as MED+AD, MSF+AD or MD+AD, etc., is the genuine way for improving energy efficiency in the desalination industry of the future. The AD technology has the ability to utilize low grade heat energy sources, either from waste exhaust or the renewable sources where the heat source temperatures are in the range of 60^o to 85^o C and these energy sources are available in abundance.

9.2 Recommendations for Future Works

Based on current work, following recommendations are made:

(1) Development of distributed modeling for large scale systems (19 stages) to investigate the industry scale plant performance. Current model can be extended up to maximum number of stages.

(2) Hybrid MEDAD testing with desorbed vapor injection to respective MED stage to increase the re-use of vapors latent heat. This requires vapor pipe line fabrication and instrumentation to inject the required amount of vapors back to MED stage condenser.

(3) Hybrid MEDAD cycle testing with higher heat source temperatures (>70^{o}C). The steam generator heater can be upgraded to supply required heat source temperature and a small NF unit can be installed at feed line to remove the soft scaling agents.

References

[1] http://www.unwater.org/statistics_res.html

[2] World Water Assessment Programme (WWAP) http://www.unwater.org/statistics_use.html

[3] MENA development Report, Renewable Energy Desalination, An Emerging Solution to Close the Water Gap in the Middle East and North Africa, the World Bank Report. (www.worldbank.org/mna/watergap)

[4] http://www.unwater.org/statistics_use.html

[5] http://environment.nationalgeographic.com/environment/freshwater/freshwater-crisis/

[6] Seawater Desalination, Menachem Elimelech, Department of Chemical and Environmental Engineering, Yale University, 2012 NWRI Clarke Prize Conference, Newport Beach, California, November 2, 2012

[7] Mezher, Toufic, Hassan Fath, Zeina Abbas, and Arslan Khaled. Techno-economic assessment and environmental impacts of desalination technologies, Desalination 266 (2011) 263-273.

[8] Noreddine Ghaffour , Thomas M. Missimer and Gary L. Amy, Technical review and evaluation of the economics of water desalination: Current and future challenges for better water supply sustainability, Desalination 309 (2013) 197–207.

[9] Abdel-Nasser A. Mabrouk, Techno-economic analysis of tube bundle orientation for high capacity brine recycle MSF desalination plants, Desalination 320 (2013) 24–32.

[10] Osman A. Hamed, Mohammad A.K. A1-Sofi, Monazir Imam, Ghulam M. Mustafa, Khalid Ba Mardouf, Hamad A1-Washmi, Thermal performance of multi-stage flash distillation plants in Saudi Arabia, Desalination 128 (2000) 281-292.

[11] Toufic Mezher , Hassan Fath, Zeina Abbas, Arslan Khaled, Techno-economic assessment and environmental impacts of desalination technologies, Desalination 266 (2011) 263–273

[12] Kim Choon Ng, Kyaw Thu, Youngdeuk Kim, Anutosh Chakraborty and Gary Amy ,Adsorption desalination: An emerging low-cost thermal desalination method, Desalination 308 (2013) 161–179.

[13] Michael E. McClain, Balancing Water Resources Development and Environmental Sustainability in Africa: A Review of Recent Research Findings and Applications, Ambio. 2013 September; 42(5): 549–565, DOI: 10.1007/s13280-012-0359-1

[14] The United Nation World Water Development Report 4 http://www.zaragoza.es/contenidos/medioambiente/onu/789-eng-ed4-v2.pdf

[15] Sources of fresh water, UNESCO module-7. http://www.unesco.org/education/educprog/ste/pdf_files/sourcebook/module7.pdf

[16] Abdul Ghani I. Dalvi, Radwan A. Al-Rasheed And Mohammad Abdul Javeed, Studied on, Organic Foulants in the Seawater Feed of Reverse Osmosis Plants of SWCC, Research & Development Center, Saline Water Conversion Corporation.
(Technical Report No. TR 3803/APP 95010, November 1999).

[17] Drinking Water Advisory: Consumer Acceptability Advice and Health Effects Analysis on Sodium, U.S. Environmental Protection Agency Office of Water (4304T), Health and Ecological Criteria Division, Washington, DC 20460
www.epa.gov/safewater/ccl/pdf/sodium.pdf

[18] World Health Organization, Guidelines for drinking-water quality [electronic resource]: incorporating first addendum. Vol. 1, Recommendations. – 3rd ed., ISBN 92 4 154696 4

[19] Igor Shiklomanov's chapter "world fresh water resources" Peter H. Gleik (editor) 1993, water in crisis: a guide to the world's fresh water resources.
http://ga.water.usgs.gov/edu/earthwherewater.html

[20] Table of world water distribution, July 20-2008.
http://serc.carleton.edu/details/images/12447.html

[21] World Bank development education program, beyond economic growth.
(http://www.worldbank.org/depweb/beyond/global/chapter3.html)

[22] Ballooning global population adding to water crisis, warns new UN report, UN News Centre, (UN News Service, March 12, 2009), Accessed June 16, 2010.
http://www.un.org/apps/news/story.asp?NewsID=30167&Cr=water&Cr1=supply
http://www.populationinstitute.org/external/files/Fact_Sheets/Water_and_population.pdf

[23] Peter H. Gleick, Dirty Water: Estimated Deaths from Water-Related Disease 2000-2020, Pacific Institute for Studies in Development, Environment, and Security. (www.pacinst.org)

[24] UN World water development report.
(www.unesco.org/water/wwap/wwdr/index.shtml)
http://www.theglobaleducationproject.org/earth/fresh-water.php

[25] A UN report on Majority of world population face water shortages unless action taken.
http://www.un.org/apps/news/story.asp?NewsID=29796&Cr=water&Cr1=agriculture

[26] Water Facts & Water Stories from Across the Globe, The world water organization.
http://www.theworldwater.org/water_facts.php

[27] The Looming Threat of Water Scarcity, World watch institute.
http://www.worldwatch.org/looming-threat-water-scarcity

[28] The world water shortage looks unsolvable, U.S. Agency for International Development (USAID), Dina Fine Maron, Scientific American. http://www.salon.com/2013/08/04/global_water_shortage_is_getting_worse_partner/

[29] Population institute report, July 2010. (http://www.populationinstitute.org/external/files/Fact_Sheets/Water_and_population.pdf)

[30] Global Water Consumption 1900-2025. http://blogs.triplealearning.com/2011/03/diploma/dp_biology/world-water-day-3/

[31] Water in a changing world, The United Nations World Water Development Report 3. http://www.unesco.org/new/fileadmin/MULTIMEDIA/HQ/SC/pdf/WWDR3_Facts_and_Figures.pdf

[32] Kyaw Thu, Anutosh Chakraborty, Young-Deuk Kim, Aung Myat, Bidyut Baran Saha and Kim Choon Ng. Numerical simulation and performance investigation of an advanced adsorption desalination cycle. Desalination 308 (2013) 209-218 .

[33] Kim Choon Ng, Kyaw Thu, Young-Deuk Kim, Anutosh Chakraborty and Grey Amy, Adsorption desalination: An emerging low-cost thermal desalination method, Desalination 308 (2013) 161-179.

[34] http://www.rubiconwater.com/news/869/usa-why-we-need-to-improve-water-use-productivity

[35] A report on charting of our water future, Economic frameworks to inform decision-making, the 2030 Water Resources Group.

[36] Mohamed A. Eltawil, Zhao Zhengming, Liqiang Yuan, A review of renewable energy technologies integrated with desalination systems, Renewable and Sustainable Energy Reviews 13 (2009) 2245–2262

[37] Ebensperger U, Isley P. Review of the current state of desalination, water policy working paper 2005-008. Georgia State University. Environmental policy program, Water Policy Centre; 2005.

[38] Schiffler M. Perspectives and challenges for desalination in the 21st century,
Desalination 165(2004)1–9.

[39] IDA Desalination Yearbook 2012-2013.

[40] IDA Desalination Yearbook 2013-2014.

[41] IDA and GWI, IDA Worldwide Desalting Plant Inventory Report No. 20 in MS Excel Format, Media Analytics Ltd., Oxford, UK, 2008.

[42] Mahmoud Shatat, Mark Worall and Saffa Riffa, Opportunities for solar water desalination worldwide: Review, Sustainable Cities and Society 9 (2013) 67–80.

[43] Lattemann, S., Kennedy, M. D., Schippers, J. C., & Amy, G. (2010). C. E. Isabel, & I. S.Andrea (Eds.), Global desalination situation. Sustainability science and engineering (pp. 7–39). Elsevier. Chapter 2

[44] A.Y.Hoekstra, M.M. Mekonnen, Global water scarcity: the monthly blue water footprint compared to blue water availability for the world's major river basins, Value of water research report series no. 53, UNESCO-IHE Institute for Water Education.

[45] Mohamed A. Dawoud and Mohamed M. Al Mulla Environmental Impacts of Seawater Desalination: Arabian Gulf Case Study, International Journal of Environment and Sustainability, Vol. 1 No. 3, pp. 22-37 (2012)

[46] Mohamed A. Dawoud, The role of desalination in augmentation of water supply in GCC countries, Desalination 186 (2005) 187–198

[47] Hassan Fath, Ashraf Sadik and Toufic Mezher, Present and Future Trend in the Production and Energy Consumption of Desalinated Water in GCC Countries, Int. J. of Thermal & Environmental Engineering, Volume 5, No. 2 (2013) 155-165

[48] Annual Energy Outlook 2009 with Projections to 2030. United States Energy Information Administration (EIA), June 2008 (http://www.eia.doe.gov/)

[49] Tian-xiang He and Li-jun Yan. Application of alternative energy integration technology in seawater desalination. Desalination 249 (2009) 104–108.

[50] Soteris A. Kalogirou, Seawater desalination using renewable energy sources, Progress in Energy and Combustion Science 31 (2005) 242–281.

[51] Xavier Bernat, Oriol Gibert, and Carlos Campos. The economics of desalination for various uses, Chapter 18.

[52] Toufic Mezher, Hassan Fath, Zeina Abbas and Arslan Khaled. Techno-economic assessment and environment impact of desalination technologies. Desalination 266 (2012) 263-273.

[53] Akili D. Khawaji, Ibrahim K. Kutubkhanah, Jong-Mihn Wie, Advances in seawater desalination technologies, Desalination 221 (2008) 47–69.

[54] M. A1-Shammiri, M. Safar, Multi-effect distillation plants: state of the art, Desalination, Vol. 126 pp. 45-59, (1999).

[55] Soteris A. Kalogirou, Seawater desalination using renewable energy sources, Progress in Energy and Combustion Science 31 (2005) 242–281.

[56] H.T. El-Dessouky, H.M. Ettouney, Multiple-effect evaporation desalination systems: thermal analysis, Desalination Vol. 125 pp. 259–276 (1999).

[57] Hisham T. El-De ssouky, Hisham M. Ettouneya, Faisal Mandani, Performance of parallel feed multiple effect evaporation system for seawater desalination, Applied Thermal Engineering, Vol 20 pp. 1679-1706, (2000).

[58] Ali M. E1-Nashar, Amer A. Qamhiyeh, Simulation of the steady-state operation of a multi-effect stack seawater distilla tion plant, desalination, Vol. 101 pp. 231-243, (1995).

[59] Mukhtar M. Ashour, Steady state analysis of the Tripoli West LT-HT-MED plant, Desalination 152 (2002) 191-194

[60] Narmine H. Aly, M.A. Marwan, Dynamic response of multi-effect evaporators, Desalination 114 (1997) 189-196

[61] H.T. El-Des souky, H.M. Ettoune y, Fundamentals of salt water desalination, Elsevier, Amsterdam, the Netherlands, (2002).

[62] Silver R.S., British Patent Application No. 829820, September, (1957).

[63] GWI, 2004 worldwide desalting plants inventory. Global Water Intelligence, (2005).

[64] K.S. Spiegler and Y.M. El-Sayed, A Desalination Primer, Balaban, Desalination Publications, Santa Maria Imbaro, Italy (1994).

[65] M.A. Darwish, N.M. Al-Najem in Energy consumption by multi-stage flash and reverse osmosis desalters, Applied Thermal Engineering, 20 399 (2000).

[66] Akili D. Khawaji, Ibrahim K. Kutubkhanah, Jong-Mihn Wie, Advances in seawater desalination technologies , Desalination 221 (2008) 47–69.

[67] Tian-xiang He, Li-jun Yan, Application of alternative energy integration technology in seawater desalination, Desalination 249 (2009) 104–108.

[68] Narmine H. Aly, Adel K. El-Fiqi, Thermal performance of seawater desalination systems, Desalination, Vol. 158 pp. 127-142 (2003).

[69] M. A1-Shammiri, M. Safar, Multi-effect distillation plants: state of the art, Desalination, Vol. 126 pp. 45-59, (1999).

[70] Bart Van der Bruggen, Carlo Vandecasteele, Distillation vs. Membrane filtration: overview of process evolutions in seawater desalination, Desalination 143 (2002) 207-218.

[71] Hisham T. E1-Dessouky, Hisham M. Ettouney, Plastic /compact heat exchangers for single-effect desalination systems, Desalination Vol. 122 pp.271-289 (1999).

[72] HishamT.El- Dessouky, HishamM.Ettouney, YousefAl-Roumi, Multi-stage flash desalination: present and future outlook, Chemical Engineering Journal Vol. 73 pp. 173 190 (1999).

[73] Mohammad Abdul-Kareem Al-Sofi, Fouling phenomena in multi stage flash (MSF) distillers, Desalination 126 (1999) 61-76.

[74] J.E. Miller, Review of water resources and desalination technologies, SAND 2003 0800.

[75] M.A. Darwish, Thermal Analysis of Vapor Compression Desalination System, Desalination, 69 (1988) 275-295.

[76] Adil Al-Radif, Review of various combinations of a multiple effect desalination plant (MED) and a thermal vapour compression unit, Desalination, 93 (1993) 119-125.

[77] Chi Tien, Adsorption calculation and modeling, Butterworh-Heinemann series in chemical engineering, Boston, 1994.

[78] [X.L. Wang, K.C. Ng, Experimental investigation of an adsorption desalination plant using low-temperature waste heat, Appl. Therm. Eng. 25 (2005) 2780–2789.

[79] X.L. Wang, A. Chakraborty, K.C. Ng, B.B. Saha, How heat and mass recovery strategies impact the performance of adsorption desalination plant: theory and experiments, Heat Transfer Eng. 28 (2) (2007) 147–153.

[80] K.C. Ng, X.L. Wang, L.Z. Gao, A. Chakraborty, B.B. Saha, S. Koyama, A. Akisawa, T.Kashiwagi, Apparatus and method for desalination, WO Patent Number 121414 (2006).

[81] K. Thu, A. Chakraborty, Y.D. Kim, A. Myat, B.B. Saha, K.C. Ng, Numerical simulation and performance investigation of an advanced adsorption desalination cycle, Desalination, (2012).

[82] K. Thu, A. Chakraborty, B.B. Saha, W.G. Chun, K.C. Ng, Life-cycle cost analysis of adsorption cycles for desalination, Desalination and Water Treatment, 20 (2010) 1-10.

[83] K. Thu, Y.-D. Kim, A. Myat, A. Chakraborty, K.C. Ng, Performance investigation of advanced adsorption desalination cycle with condenser–evaporator heat recovery scheme, Desalination and Water Treatment, (2012) 1-14.

[84] K. Thu, K.C. Ng, B.B. Saha, A. Chakraborty, S. Koyama, Operational strategy of adsorption desalination systems, International Journal of Heat and Mass Transfer, 52 (2009) 1811-1816.

[85] K.C. Ng, K. Thu, A. Chakraborty, B.B. Saha, W.G. Chun, Solar-assisted dual-effect adsorption cycle for the production of cooling effect and potable water, International Journal of Low-Carbon Technologies, 4 (2009) 61-67.

[86] K.C. Ng, K. Thu, B.B. Saha, A. Chakraborty, Study on a waste heat-driven adsorption cooling cum desalination cycle, International Journal of Refrigeration, 35 (2012) 685-693.

[87] Ng, K. C., Wang, X.L, Gao, L. Z., Chakraborty, A., Saha, B. B. and Koyama, S., Apparatus and method for desalination, SG Patent application number 200503029-1 (2005) and WO Patent no. 121414A1 (2006).

[88] Kyaw Thu, Kim Choon Ng, Bidyut B. Saha, Anutosh Chakraborty and Shigeru Koyama, Operational strategy of adsorption desalination systems, International Journal of Heat and Mass Transfer 52 (2009) 1811–1816.

[89] X. Wang, K.C. Ng, Experimental investigation of an adsorption desalination plant using low-temperature waste heat, Applied Thermal Engineering, 25 2780–2789 (2005).

[90] Kyaw Thu, Anuthosh Chakraborty, Young-Deuk Kim, Bidyut Baran Saha, Kim Choon Ng, Aung Myat, Numerical simulation and

performance investigation of an advanced adsorption desalination cycle, Desalination 308 (2013) 209–218

[91] Wai Soong Loh, Bidyut Baran Saha, Anutosh Chakraborty, Kim Choon Ng, Wongee Chun, Performance analysis of waste heat driven pressurized adsorption chiller, Journal of thermal science and technology, Volume5, No. 2, 2010.

[92] W.S. Loh, I.I. El-Sharkawy, Kim Choon Ng, Bidyut Baran Saha, ,Adsorption cooling cycles for alternative adsorbent/adsorbate pairs working at partial vacuum and pressurized conditions, Applied Thermal Engineering 29 (2009) 793–798

[93] H.T. Chua, K.C. Ng, W. Wang, C. Yap , X.L. Wang , Transient modeling of a two-bed silica gel–water adsorption chiller, International Journal of Heat and Mass Transfer 47 (2004) 659–669.

[94] H.T. Chua, K.C. Ng, A. Malek, T. Kashiwagi , A. Akisawa and B.B. Saha , Modeling the performance of two-bed, sillica gel-water adsorption chillers, International Journal of Refrigeration 22 (1999) 194–204

[95] X.L. Wang, K.C. Ng, Experimental investigation of an adsorption desalination plant using low-temperature waste heat, Appl. Therm. Eng. 25 (2005) 2780–2789.

[96] X.L. Wang, A. Chakraborty, K.C. Ng, B.B. Saha, How heat and mass recovery strategies impact the performance of adsorption desalination plant: theory and experiments, Heat Transfer Eng. 28 (2) (2007) 147–153.

[97] K.C. Ng, X.L. Wang, L.Z. Gao, A. Chakraborty, B.B. Saha, S. Koyama, A. Akisawa, T. Kashiwagi, Apparatus and method for desalination, WO Patent Number 121414 (2006).

[98] T. Pankratz, Membrane growth takes off, in: T. Pankratz (Ed.), Water Desalination Report, Media Analytics Ltd., Oxford, UK, 2008, in cooperation with Global Water Intelligence, Houston, TX.

[99] Chennan Li,Yogi Goswami and Elias Stefanakos Solar assisted seawater desalination: A review, Renewable and Sustainable Energy Reviews 19 (2013) 136–163.

[100] The IDA Desalination Year book 2011–2012, Water desalination report.

[101] Kim Choon Ng, Kyaw Thu, Youngdeuk Kim, Anutosh Chakraborty and Gary Amy, Adsorption desalination: An emerging low-cost thermal desalination method, Desalination 308 (2013) 161–179.

[102] M.J. Abdulrazzak, Water supplies versus demand in countries of Arabian Peninsula, J. Water Resources Planning Management ASCE, 121(3) (1995) 227–234

[103] Mohamed A. Dawoud, and Mohamed M. Al Mulla, Environmental Impacts of Seawater Desalination: Arabian Gulf Case Study, International Journal of Environment and Sustainability ISSN 1927-9566, Vol. 1 No. 3, pp. 22-37 (2012).

[104] Dr.-Ing. Tobias Bleninger & Prof. G.H. Jirka, Final report on Environmental planning, prediction and management of brine discharges from desalination plants, Middle East Desalination Research Center Muscat, Sultanate of Oman, MEDRC Series of R&D Reports, MEDRC Project: 07-AS-003.

[105] Sabine Lattemann, Maria D. Kennedy, Jan C. Schippers and Gary Amy , Global Desalination Situation, Chapter 2, Sustainability Science and Engineering, Volume 2, ISSN 1871-2711, DOI 10.1016/S1871-2711(09)00202-5

[106] Noreddine Ghaffour, Thomas M. Missimer and Gary L. Amy, Technical review and evaluation of the economics of water desalination: Current and future challenges for better water supply sustainability, Desalination 309 (2013) 197–207

[107] R. Matz, U. Fisher, A comparison of the relative economics of seawater desalination by vapor compression and reverse osmosis for small and medium capacity plants, Desalination 36 (1981) 137–151.

[108] M.A. Darwish, N.M. Al-Najem, Energy consumption and costs of different desalting systems, Desalination 64 (1987) 83–96.

[109] Kyaw Thu, A. Chakraborty, , B.B. Saha, Won Gee Chun and K.C. Ng, Life-cycle cost analysis of adsorption cycles for desalination, Desalination and Water Treatment 20 (2010)1-10

[110] K. Wangnick, IDA Worldwide Desalting Plant Inventory Report No. 18, Wangnick Consulting, Germany, 2004.

[111] Raphael Semiat, Energy issues in desalination processes, Environmental Science & Technology, Vol. 42, No. 22, (2008).

[112] Global Water Intelligence (GWI/IDA DesalData), Market profile and desalination markets, 2009–2012 yearbooks and GWI website, http://www.desaldata.com/.

[113] K. Quteishat, Desalination and Water Affordability, SITeau International Conference, Casablanca, Morocco, January 2009.

[114] K.V. Reddy, N. Ghaffour, Overview of the cost of desalinated water and costing methodologies, Desalination 205 (2007) 340–353.

[115] T. Pankratz, MEDRC workshop on Membrane Technology Used in Desalination and Wastewater Treatment for Reuse, www.medrc.orgMarch 2008(Muscat, Oman).

[116] R. Borsani, S. Rebagliati, Fundamentals and costing of MSF desalination plants and comparison with other technologies, Desalination 182 (2005) 29–37.

[117] C. Sommariva, H. Hogg, K. Callister, Cost reduction and design lifetime thermal desalination plants: thermodynamic and corrosion resistance analysis for heat exchange tubes material selection, Desalination 17–21.

[118] M.A. Darwish, N.M. Al-Najem, Energy consumption and costs of different desalting systems, Desalination 64 (1987) 83–96.

[119] A. Maurel, Seawater/Brackish Water Desalination and Other Non-conventional Processes for Water Supply, 2nd edition book Lavoisier, 2006. (10:2-7430-0890-3).

[120] Raphael Semiat, Energy issues in desalination processes, Environmental Science & Technology, Vol. 42, No. 22, (2008).

[121] E. Tzen, R. Morris, Renewable energy sources for desalination, Solar Energy, 75 (2003) 375–379.

[122] D. Hoffman, The application of solar energy for large-scale seawater desalination, Desalination, 89 (1992) 115–184.

[123] Garcia-Rodriguez L, Gomez-Camacho C. Perspectives of solar desalination, Desalination, 136 (2001) 213–8.

[124] Global Water Intelligence (GWI), Operating cost comparison across major desalination technologies. http://www.globalwaterintel.com/archive/13/10/general/technology-choice-still-open-yanbu-3.html

[125] Ioannis C. Karagiannis, Petros G. Soldatos, Water desalination cost literature: review and assessment, Desalination 223 (2008) 448–456.

[126] Global Water Intelligence (GWI), Energy makes all the difference: desalination operating costs compared. http://www.globalwaterintel.com/archive/8/2/analysis/chart-of-the-month.html

[127] Ng Kim Choon, Kyaw Thu, Gary Amy, Mohammed.Chunggaze, Tawfiq Y AL-GHASHAM, An Advanced ADMED Cycle For Low-Temperature Driven Desalination, US Provisional Application No. 61/450,165.

[128] E.C. Boelman, B. B. Saha, T. Kashiwagi, Experimental investigation of a silica gel–water adsorption refrigeration cycle – the influence of operating conditions on cooling output and COP, ASHRAE Trans. Res. 101 (2) 358–366 (1995).

[129] E.C. Boelman, B.B. Saha, T. Kashiwagi, Parametric study of a silica gel–water adsorption refrigeration cycle – the influence of thermal capacitance and heat exchanger UA-values on cooling capacity, power density and COP, ASHRAE Trans. 103 (1) 139–148 (1997).

[130] K. C. Ng, H.T. Chua, C.Y. Chung, C.H. Loke, T. Kashiwagi, A. Akisawa, B.B. Saha, Experimental investigation of the silic a gel-water adsorption isotherm characteristics, Applied Thermal Engineering, 21, 1631-1642 (2001).

[131] K.C. Ng, H.T. Chua, X.L. Wang, T. Kashiwagi, B.B. Saha, Prototype testing of a novel four-bed regenerative silica gel–water adsorption chiller, International conference of refrigeration, Washington DC, (2003).

[132] Saha BB, Kashiwagi T. Experimental investigation of an advanced adsorption refrigeration cycle. ASHRAE Trans, 103(2):50–58 (1997).

[133] D.C. Wang, Y.H. Li, D. Li, Y.Z. Xia, J.P. Zhang, A review on adsorption refrigeration technology and adsorption deterioration in physical adsorption systems, Renewable and Sustainable Energy Reviews Vol. 14 pp. 344–353 (2010).

[134] Suzuki, M. Adsorption Engineering Elsevier, Amsterdam, the Netherlands, (1990).

[135] Critoph RE, Vogel R. Possible adsorption pairs for use in solar cooling, Ambient Energy Vol. 7 pp. 183–90 (1986).

[136] Meunier F, Douss N. Performance of adsorption heat pumps. Active carbon–methanol a nd zeolite–water pairs, ASHRAE Transactions 2:267–74 (1990).

[137] Wang RZ, Jia JP, Teng Y, Zhu YH, Wu JY, Study on a new solid adsorption refrigeration pair, active carbon fiber–methanol, ASME Journal of Solar Energy Engineering;119:214–8 (1997).

[138] Restuccia G, Cacciola G., Performances of adsorption systems for ambient heating and air conditioning, International Journal of Refrigeration Vol. 22 pp.18–26 (1999).

[139] D.B. Broughton, Continuous desalination process, USPO 4,447,329, May 8, (1984).

[140] D. Zejli, R. Benchrifa, A. Bennouna, O.K. Bouhelal, A solar adsorption desalination device: first simulation results, Desalination Vol. 168 pp. 127-135 (2004).

[141] S. Al-kharabsheh, D.Y. Goswami, Theoretical analysis of a water desalination system using low grade solar heat, Journal of solar energy engineering transactions of the ASME Vol. 126 pp. 774–780 (2004).

[142] X. Wang, K.C. Ng, Experimental investigation of an adsorption desalination plant using low-temperature waste heat, Applied Thermal Engineering, 25 2780–2789 (2005).

[143] Kyaw Thu, Young-Deuk Kim, Gary Amy, Won Gee Chun and Kim Choon Ng, A hybrid multi-effect distillation and adsorption cycle, Applied Energy 104 (2013) 810–82

[144] J. C. Han, and L. S. Fletcher, Falling Film Evaporation and Boiling in Circumferential and Axial Grooves on Horizontal Tubes, Industrial and Engineering Chemistry Process Design and Development 24 (1985) 570-575.

[145] G. Ribatski and A. M. Jacobi, Falling Film Evaporation on Horizontal Tubes-A Critical Review. International journal of refrigeration, 28 (2005) 635-653.

[146] Tarif Ali Adib and Bertrand Heyd, Jean Vasseur , Experimental results and modeling of boiling heat transfer coefficients in falling film evaporator usable for evaporator design, Chemical Engineering and Processing 48 (2009) 961–968

[147] K.R. Chun, R.A. Seban, Heat transfer to evaporating liquid films, Transactions of the ASME: Journal of Heat Transfer 93 C (1971) 391–396.

[148] J.S. Prost, M.T. Gonzaalez, M.J. Urbicain, Determination and correlation of heat transfer coefficients in a falling film evaporator, Journal of Food Engineering 4 (73) (2006) 320–326.

[149] S.Y. Ahmed, R. Kaparthi, Heat transfer studies of falling film heat exchangers, Indian Journal of Technology 1 (1963) 377–381.

[150] W.H. McAdams, T.B. Drew, G.S. Bays, Heat transfer to falling—water films, Transactions of ASME 62 (1940) 627.

[151] L.S. Herbert, U.J. Stern, An experimental investigation of heat transfer to water in film flow, Canadian Journal of Chemical Engineering 46 (1968) 401–407.

[152] Javier Uche, Javier Artal and Luis Serra, Comparison of heat transfer coefficient correlations for thermal desalination units, Desalination 152 (2002) 195-200.

[153] W.H. Parken and L.S. Fletcher, An experimental and analytical investigation of heat transfer to thin water films on horizontal tubes, University of Virginia, Report UVA-526078-MAE, 1977, pp. 77-101.

[154] D. Barba and R. Di Felice, Heat transfer in turbulent flow on a horizontal tube falling film evaporator—a theoretical approach, Desalination, 51 (1984) 325-333.

[155] W. Nusselt, Surface condensation of water vapor, Parts I and II, VDI, 60(27) (1916) 541, 60(28) (1916) 569.

[156] S.S. Kutateladze, Fundamentals of Heat Transfer. Academic Press, New York, 1963.

[157] D.A. Labuntsov, Heat transfer in film condensation of pure steam on vertical surfaces and horizontal tubes, Teploenergetika, 4(7) (1957) 72-79.

[158] Y. Fujita, M. Tsutsui, Experimental investigation of falling film evaporation on horizontal tubes, Heat Transfer-Japanese Research 27 (1998) 609-618.

[159] Y. Fujita, M. Tsutsui, Z.-Z. Zhou, Evaporation heat transfer of falling films on horizontal tube - part 1, analytical study, Heat Transfer-Japanese Research 24 (1995) 1-16.

[160] Y. Fujita, M. Tsutsui, Z.-Z. Zhou, Evaporation heat transfer of falling films on horizontal tube - part 2, experimental study, Heat Transfer-Japanese Research 24 (1995) 17-31.

[161] Z.H. Liu, J. Yi, Falling film evaporation heat transfer of water/salt mixtures from roll-worked enhanced tubes and tube bundle, Appl. Therm. Eng. 22 (1) (2002) 83–95.

[162] Y. Fujita, M. Tsutsui, Experimental investigation of falling film evaporation on horizontal tubes, Heat Transfer Jpn. 27 (1998) 609–618.

[163] L.P. Yang, S.Q. Shen, Experimental study of falling film evaporation heat transfer outside horizontal tubes, in: Conference on Desalination and the Environment, Halkidiki, GREECE, 2007.

[164] W.H. Parken et al., Heat-transfer through falling film evaporation and boiling on horizontal tubes, J. Heat Transfer – Trans. ASME 112 (3) (1990) 744–750.

[165] G. Ribatski, J.R. Thome, Experimental study on the onset of local dryout in an evaporating falling film on horizontal plain tubes, Exp. Thermal Fluid Sci. 31 (6) (2007) 483–493.

[166] J.J. Lorenz, D. Yung, Film breakdown and bundle-depth effects in horizontal tube, falling-film evaporators, J. Heat Transfer – Trans. ASME 104 (3) (1982) 569–571.

[167] J.F. Roques, J.R. Thome, Falling films on arrays of horizontal tubes with R-134a. Part II: Flow visualization, onset of dry out, and heat transfer predictions, Heat Transfer Eng. 28 (5) (2007) 415–434.

[168] Y. Fujita and M. Tsutsui. Experimental Investigation of Falling Film Evaporation on Horizontal Tubes, Heat Transfer-Japenese Research, 27(8), 1998.

[169] Z. H Liu and J. Yi, Falling Film Evaporation Heat Transfer of Water/Salt Mixtures from Roll Worked Enhanced Tubes and Tube Bundle, Applied thermal engineering. 22 (2002) 83-95.

[170] G. Aly, A. Al-Hadda and M. Abdel-Jawad, Parametric Study on Falling Film Seawater Desalination, Desalination. 65 (1897) 43-55.

[171] S. Moeykens, M.B. Pate, Spray evaporation heat transfer performance of R134a on plain tubes, Ashrae Transactions 100 (2) (1994) 173-184.

[172] S. Moeykens, J.E. Kelly, M.B. Pate, Spray evaporation heat transfer performance of R-123 in tube bundles, Ashrae Transactions 102 (2) (1996) 259-272.

[173] T.B. Chang, J.S. Chiou, Spray evaporation heat transfer of R-141b on a horizontal tube bundle, International Journal of Heat and Mass Transfer 42 (1998) 1467-1478.

[174] S. Moeykens, M.B. Pate, The effects of nozzle height and orifice size on spray evaporation heat transfer performance for a low-finned, triangular-pitch tube bundles with R-134a, Ashrae Transactions 101 (2) (1995) 420-433.

[175] S. Moeykens, M.B. Pate, Effect of lubricant on spray evaporation heat transfer performance of R-134a and R-22 in tube bundles, Ashrae Transactions 102 (1) (1996) 410-426.

[176] S. Moeykens, B.J. Newton, M.B. Pate, Effects of surface enhancement, film-feed supply rate, and bundle geometry on spray evaporation heat transfer performance, Ashrae Transactions 101 (2) (1995) 408-419.

[177] S. Moeykens, J.E. Kelly, M.B. Pate, Spray evaporation heat transfer performance of R-123 in tube bundles, Ashrae Transactions 102 (2) (1996) 259-272.

[178] K. Bourouni, R. Martin, L. Tadrist, and H. Tadrist, Modelling of Heat and Mass Transfer in a Horizontal Tube Falling Film Evaporators for Water Desalination, Desalination. 116 (1998) 165-184.

[179] L. Yang and S. Shen, Experimental Study of Falling Film Evaporation Heat Transfer outside Horizontal Tubes, Desalination. 220 (2008) 654-660.

[180] G. Ribatski and A. M. Jacobi, Falling Film Evaporation on Horizontal Tubes-A Critical Review. International journal of refrigeration, 28 (2005) 635-653.

[181] Li Xu, M. Ge, S. Wang and Y. Wang, Heat Transfer Film Coefficients of Falling Film Horizontal Tube Evaporators, Desalination 166 (2004) 223-230.

[182] L. Yang and S. Shen, Experimental Study of Falling Film Evaporation Heat Transfer outside Horizontal Tubes, Desalination. 220 (2008) 654-660.

[183] K. R. Chun, and R. A. Seban, Heat Transfer to Evaporating Liquid Films, ASME Journal of heat transfer, 1971, 11, 391-396.

[184] Li Xu, M. Ge, S. Wang and Y. Wang, Heat Transfer Film Coefficients of Falling Film Horizontal Tube Evaporators, Desalination 166 (2004) 223-230.

[185] Y. Fujita and M. Tsutsui. Experimental Investigation of Falling Film Evaporation on Horizontal Tubes, Heat Transfer-Japenese Research, 27(8), 1998.

[186] A. A. Alhusseini, K. Tuzla and J. C. Chen, Falling Film Evaporation of Single Component Liquids, Int. J. Heat Mass Transfer, Vol. 41, No. 12, pp. 1623-1632, 1998.

[187] J. A. Shmerler and I. Mudawwar, Local Evaporative Heat Transfer Coefficient in Turbulent Free-Falling Liquid Films, Int. J. Heat Mass Transfer, Vol. 31, No. 4, pp. 731-742, 1988.

[188] L. H. Chien and Y. L. Tsai, An Experimental Study of Pool Boiling and Falling Film Evaporation on Horizontal Tubes in R-245fa, Applied Thermal Engineering 31 (2011) 4044-4054.

[189] Ophir A, Lokiec F. Advanced MED process for most economical sea water desalination. Desalination 182 (2005)187–98.

[190] M.Al-Shammiri, M.Safar, Multi effect distillation plants: state of art, Desalination, 126 (1999) 45-59.

[191] Alarcón-Padilla D-C, García-Rodríguez L. Application of absorption heat pumps to multi-effect distillation: a case study of solar desalination. Desalination 212 (2007) 294–302.

[192] Alarcón-Padilla DC, García-Rodríguez L, Blanco-Gálvez J. Experimental assessment of connection of an absorption heat pump to a multi-effect distillation unit. Desalination 250 (2010)500–505.

[193] Alarcón-Padilla DC, García-Rodríguez L, Blanco-Gálvez J. Design recommendations for a multi-effect distillation plant connected to a double effect absorption heat pump: a solar desalination case study. Desalination 2010;262:11–4.

[194] Wang Y, Lior N. Proposal and analysis of a high-efficiency combined desalination and refrigeration system based on the LiBr–HO absorption cycle—Part 1: system configuration and mathematical model. Energy Convers Manage 2011;52:220–7.

[195] Wang Y, Lior N. Proposal and analysis of a high-efficiency combined desalination and refrigeration system based on the LiBr–H O absorption cycle—Part 2: thermal performance analysis and discussions. Energy Convers Manage 2011;52:228–35.

[196] Wang Y, Lior N. Thermoeconomic analysis of a low-temperature multi-effect thermal desalination system coupled with an absorption heat pump. Energy 2011;36:3878–87.

[197] Al-Ansari A, Ettouney H, El-Dessouky H. Water–zeolite adsorption heat pump combined with single effect evaporation desalination process. Renew Energy 2001;24:91–111.

[198] El-Dessouky HT, Ettouney HM. Multiple effect evaporation vapor compression. In: Fundamentals of salt water desalination. Amsterdam: Elsevier Science B.V; 2002 [chapter 5].

[199] Faisal Al-Juwayhel, Hisham T. El-Dessouky, Hisham M. Ettouney, Analysis of single-effect evaporator desalination systems combined with vapour compression heat pump. Desalination 114 (1997) 253-275.

[200] S.E Ally, A study of a new thermal vapour compression/multi-effect stack (TVC/MES) low temperature distillation system. Desalination 103 (1995) 257-263.

[201] A.S. Nafey, H.E.S. Fath, A.A. Mabrouk, Thermo-economic investigation of multi effect evaporation (MEE) and hybrid multi effect evaporation-multi stage evaporation (MEE-MSF) systems. Desalination 201 (2006) 241-254.

[202] Hisham T. El-Dessouky, Hisham M. Ettouney, Faisal Mandani, Performance of parallel feed multi effect evaporation system for seawater desalination. Applied Thermal Engineering 20 (2000) 1679-1706.

[203] Hisham T. El-Dessouky, Hisham M. Ettouney, Multi effect desalination systems: thermal analysis. Desalination 125 (1999) 259-276.

[204] El-Dessouky HT, Ettouney HM. Multiple effect evaporation. In: Fundamentals of salt water desalination. Amsterdam: Elsevier Science B.V; 2002 [chapter 4].

[205] Ali M. El-Nashar, Amer A. Qamhiyah, Simulation of steady state operation of a multi effect stack seawater distillation plant. Desalination 101 (1995) 231-243.

[206] Ali M. El-Nashar, Perdicting part load performance of small MED evaporators- a simple simulation program and its experimental verification. Desalination 130 (2000) 217-234.

[207] A. O. Bin Amer, Development and optimization of ME-TVC desalination system. Desalination 249 (2009) 1315-1331.

[208] Gur Mittelman, Abraham Kribus, Ornit Mouchtar, Abraham Dayan, Water desalination with concentrating photovoltaic/thermal (CPVT) systems, Solar Energy 83 (2009) 1322–1334.

[209] A.N.A. Mabrouk, H.E.-b.S. Fath, Techno-economic analysis of hybrid high performance MSF desalination plant with NF membrane, Desalination and Water Treatment, 51 (2012) 844-856.

[210] O.A. Hamed, A.M. Hassan, K. Al-Shail, M.A. Farooque, Performance analysis of a trihybrid NF/RO/MSF desalination plant, Desalination and Water Treatment, 1 (2009) 215-222.

[211] O.A. Hamed, Lessons learnt from the operational performance of SWCC MSF desalination plants, Desalination and Water Treatment, 18 (2010) 321-326.

[212] Dittus FW, Boelter LMK, Heat transfer in automobile radiators of the tubular type. International Commun Heat Mass Transfer 1985;12:3–22.

[213] Muhammad Wakil Shahzad, Aung Myat, Chun Won Gee and Kim Choon Ng, Bubble-assisted film evaporation correlation for saline water at sub-atmospheric pressures in horizontal-tube evaporator, Applied Thermal Engineering 50 (2013) 670-676.

[214] Collier JG, Thome JGCJR. Convective boiling and condensation. Clarendon Press; 1996.

[215] W. Wagner, A. Kruse, Properties of Water and Steam, Springer-Verlag, New York, 1997.

[216] Siedler and Peters, Physical Properties (general) of Seawater, Numerical data and functional relationships in science and technology, New serves, Oceanography Vol. V/3a , Springler, Berlin, 233-264, 1986.

[217] Mostafa H. Sharqawy, John H. Lienhard V, Syed M. Zubair, Thermophysical properties of seawater: a review of existing correlations and data, Desalination and Water Treatment 16 (2010) 354–380.

[218] http://www.engineeringtoolbox.com/darcy-weisbach-equation-d_646.html

[219] Wilfried Roetzel and Bernhard Spang, Typical Values of Overall Heat Transfer Coefficients, DOI 10.1007/978-3-540-77877-6_6

[220] Dongfeng Zhao , Jianliang Xue, Shi Li, Hui Sun and Qing-dong Zhang, Theoretical analyses of thermal and economical aspects of

multi-effect distillation desalination dealing with high-salinity wastewater, Desalination 273 (2011) 292–298.

[221] A.O. Bin Amer, Development and optimization of ME-TVC desalination system, Desalination 249 (2009) 1315–1331

[222] Chennan Li, D. Yongi Goswami, Andrew Shapiro, Elias K. Stefanakos and Gokmen Demirkaya, A New Combined Power and Desalination System Driven by Low Grade Heat for Concentrated Brine, Energy 46 (2012) 582-595

[223] K. Thu, K.C. Ng, B.B. Saha, A. Chakraborty, S. Koyama, Operational strategy of adsorption desalination systems, International Journal of Heat and Mass Transfer, 52 (2009) 1811-1816.

[224] K.C. Ng, K. Thu, A. Chakraborty, B.B. Saha, W.G. Chun, Solar-assisted dual-effect adsorption cycle for the production of cooling effect and potable water, International Journal of Low-Carbon Technologies, 4 (2009) 61-67.

[225] K.C. Ng, K. Thu, B.B. Saha, A. Chakraborty, Study on a waste heat-driven adsorption cooling cum desalination cycle, International Journal of Refrigeration, 35 (2012) 685-693.

[226] K. THU, Adsorption desalination: Theory & Experiments, (2010).

[227] K. Thu, Y.-D. Kim, A. Myat, W.G. Chun, K.C. NG, Entropy generation analysis of an adsorption cooling cycle, International Journal of Heat and Mass Transfer, 60 (2013) 143-155.

[228] I.I. Ei-Sharkawy, K. Thu, K.C. Ng, B.B. Saha, A. Chakraborty, S. Koyama, Performance improvement of adsorption desalination plant: experimental investigation, Int. Rev. Mech. Eng., 1 (2007) 25-31.

[229] K. Thu, B.B. Saha, A. Chakraborty, W.G. Chun, K.C. Ng, Study on an advanced adsorption desalination cycle with evaporator-condenser heat recovery circuit, International Journal of Heat and Mass Transfer, 54 (2011) 43-51.

[230] A. Chakraborty, K. Thu, K.C. Ng, Advanced adsorption cooling cum desalination cycle: A thermodynamic framework, in, Vol. 4, 2011, pp. 605-610.

[231] F.W. Dittus, L.M.K. Boelter, Heat transfer in automobile radiators of the tubular type, International Communications in Heat and Mass Transfer, 12 (1985) 3-22.

[232] L.F. J. Han, Falling film evaporation and boiling in circumferential and axial grooves on horizontal tubes, Industrial & Engineering Chemistry Process Design and Development, 24 (1985) 570-597.

[233] J.G. Collier, J.G.C.J.R. Thome, Convective Boiling and Condensation, Clarendon Press, 1996.

[234] H.T. El-Dessouky, H.M. Ettouney, F. Mandani, Performance of parallel feed multiple effect evaporation system for seawater desalination, Applied Thermal Engineering, 20 (2000) 1679-1706.

[235] K. Thu, A. Chakraborty, B.B. Saha, K.C. Ng, Thermo-physical properties of silica gel for adsorption desalination cycle, Applied Thermal Engineering, (2011).

[236] A.N.A. Mabrouk, H.E.-b.S. Fath, Techno-economic analysis of hybrid high performance MSF desalination plant with NF membrane, Desalination and Water Treatment, 51 (2012) 844-856.

[237] O.A. Hamed, A.M. Hassan, K. Al-Shail, M.A. Farooque, Performance analysis of a trihybrid NF/RO/MSF desalination plant, Desalination and Water Treatment, 1 (2009) 215-222.

[238] O.A. Hamed, Lessons learnt from the operational performance of SWCC MSF desalination plants, Desalination and Water Treatment, 18 (2010) 321-326.

[239] M.A.K. Al-Sofi, A.M. Hassan, O.A. Hamed, A.G.I. Dalvi, M.N.M. Kither, G.M. Mustafa, K. Bamardouf, Optimization of hybridized seawater desalination process, Desalination, 131 (2000) 147-156.

[240] Y. Ammar, H.N. Li, C. Walsh, P. Thornley, V. Sharifi, A.P. Roskilly, Desalination using low grade heat in the process industry: Challenges and perspectives, Applied Thermal Engineering, 48 (2012) 446-457.

[241] L. Awerbuch, S. May, R. Soo-Hoo, V. van der Mast, Hybrid desalting systems, Desalination, 76 (1989) 189-197.

[242] M.G. Marcovecchio, S.F. Mussati, P.A. Aguirre, N.J. Scenna, Optimization of hybrid desalination processes including multi stage flash and reverse osmosis systems, Desalination, 182 (2005) 111-122.

[243] S. Sarkar, A.K. SenGupta, A new hybrid ion exchange-nanofiltration (HIX-NF) separation process for energy-efficient desalination: Process concept and laboratory evaluation, Journal of Membrane Science, 324 (2008) 76-84.

[244] G. Fosselard, K. Wangnick, Comprehensive study on capital and operational expenditures for different types of seawater desalting plants (RO, MVC, ME, ME-TVC, MSF) rated between 200 m3/d and 3,000 m3/d, Desalination, 76 (1989) 215-240.

[245] W. Li, W.B. Krantz, E.R. Cornelissen, J.W. Post, A.R.D. Verliefde, C.Y. Tang, A novel hybrid process of reverse electrodialysis and reverse osmosis for low energy seawater desalination and brine management, Applied Energy, 104 (2013) 592-602.

[246] O.A. Bamaga, A. Yokochi, B. Zabara, A.S. Babaqi, Hybrid FO/RO desalination system: Preliminary assessment of osmotic energy recovery and designs of new FO membrane module configurations, Desalination, 268 (2011) 163-169.

[247] A.J.N. Khalifa, Evaluation of different hybrid power scenarios to Reverse Osmosis (RO) desalination units in isolated areas in Iraq, Energy for Sustainable Development, 15 (2011) 49-54.

[248] S. Zhao, L. Zou, D. Mulcahy, Brackish water desalination by a hybrid forward osmosis–nanofiltration system using divalent draw solute, Desalination, 284 (2012) 175-181.

[249] M.M. Dubinin, The potential theory of adsorption of gases and vapors for adsorbents with energetically nonuniform surfaces, Chemical Reviews, 60 (1960) 235-241.

[250] K. Thu, A. Chakraborty, Y.D. Kim, A. Myat, B.B. Saha, K.C. Ng, Numerical simulation and performance investigation of an advanced adsorption desalination cycle, Desalination, (2012).

[251] K. Thu, A. Chakraborty, B.B. Saha, W.G. Chun, K.C. Ng, Life-cycle cost analysis of adsorption cycles for desalination, Desalination and Water Treatment, 20 (2010) 1-10.

[252] K. Thu, Y.-D. Kim, A. Myat, A. Chakraborty, K.C. Ng, Performance investigation of advanced adsorption desalination cycle with condenser–evaporator heat recovery scheme, Desalination and Water Treatment, (2012) 1-14.

[253] U. Atikol, Hikmet S. Aybar, Estimation of water production cost in the feasibility analysis of RO systems, Desalination Vol. 184 pp. 253–258 (2005).

[254] G. Fiorenza, V.K. Sharma and G. Braccio, Techno-economic evaluation of a solar powered water desalination plan. Energy Conversion and Management, Vol. 44 pp. 2217–2240 (2003).

[255] Michael J. Moran, Availability Analysis: A Guide to Efficient Energy Use, Prentice Hall, Englewood Cliffs, N. J., 1981

[256] T J Kotas, The exergy method of thermal plant analysis, Krieger, Malabar, Florida, 1995.

[257] M. Tribus, R. B. Evans and G. L. Crellin, Principles of desalination, K.W. Spiegler edition, academic press, New York, 1966.

[258] Richard A. Gaggioli, Second Law Analysis for Process and Energy Engineering, ACS Symposium Series; American Chemical Society: Washington, DC, 1983.

[259] F.A. Al-Sulaiman, B. Ismail, Exergy analysis of major re-circulating multi-stage flash desalting plants in Saudi Arabia, Desalination 103 (1995) 265e270.

[260] O.A. Hamed, A.M. Zamamir, S. Aly, N. Lior, Thermal performance and exergy analysis of a thermal vapor compression desalination system, Energy Conversion and Management 37 (4) (1996) 379e387.

[261] K.S. Spliegler, Y.M. E1-Sayed, The energetics of desalination processes, Desalination 134 (2001) 109e128.

[262] M.H. Sharqawy, J.H. Lienhard V, S.M. Zubair, Formulation of Seawater Flow Exergy Using Accurate Thermodynamic Data, Proceeding of the International Mechanical Engineering Congress and Exposition IMECE-2010, November 12-18, 2010, Vancouver, British Columbia, Canada.

[263] Y. Cerci, Improving the thermodynamic and economic efficiencies of desalination plants, Ph.D. Dissertation, Mechanical Engineering, University of Nevada, 1999.

[264] Y.A. Cengel, Y. Cerci, B. Wood, Second law analysis of separation processes of mixtures, ASME International Mechanical Engineering Congress and Exposition, Nashville, Tennessee, November 14e19, 1999.

[265] Y. Cerci, Exergy analysis of a reverse osmosis desalination plant in California, Desalination 142 (2002) 257e266.

[266] N. Kahraman, Y.A. Cengel, B. Wood, Y. Cerci, Exergy analysis of a combined RO, NF, and EDR desalination plant, Desalination 171 (2004) 217e232.

[267] N. Kahraman, Y.A. Cengel, Exergy analysis of a MSF distillation plant, Energy Conversion and Management 46 (2005) 2625e2636.

[268] F. Banat, N. Jwaied, Exergy analysis of desalination by solar-powered membrane distillation units, Desalination 230 (2008) 27e40.

[269] A.S. Nafeya, H.E. Fath, A.A. Mabrouka, Exergy and thermo-economic evaluation of MSF process using a new visual package, Desalination 201 (2006) 224e240.

[270] A.A. Mabrouka, A.S. Nafeya, H.E. Fath, Analysis of a new design of a multi-stage flash-mechanical vapor compression desalination process, Desalination 204 (2007) 482e500.

[271] A.S. Nafeya, H.E. Fath, A.A. Mabrouka, Thermo-economic design of a multi effect evaporation mechanical vapor compression (MEEeMVC) desalination process, Desalination 230 (2008) 1e15.

[272] R.K. Kamali, S. Mohebinia, Experience of design and optimization of multi-effects desalination systems in Iran, Desalination 222 (2008) 639–645.

[273] R.K. Kamali, A. Abbassi, S.A. Sadough Vanini, and M. Saffar Avval, Thermodynamic design and parametric study of MED-TVC, Desalination 222 (2008) 596–604.

[274] Mohammad Ameri, Saeed Seif Mohammadi, Mehdi Hosseini, and Maryam Seifi, Effect of design parameters on multi-effect desalination system specifications, Desalination 245 (2009) 266–283

[275] Yongqing Wang and Noam Lior, Performance analysis of combined humidified gas turbine power generation and multi-effect thermal vapor compression desalination systems-Part 1: The desalination unit and its combination with a steam-injected gas turbine power system, Desalination 196 (2006) 84–104.

[276] R. Chacartegui, D. Sánchez, N. di Gregorio, F.J. Jiménez-Espadafor, A. Muñoz and T. Sánchez, Feasibility analysis of a MED desalination plant in a combined cycle based cogeneration facility, Applied Thermal Engineering 29 (2009) 412–417

[277] M.A. Darwish, S. Al Otaibi and Khawla Al Shayji, Suggested modifications of power-desalting plants in Kuwait, Desalination 216 (2007) 222–231

[278] M.A. Darwish, S. Alotaibi and S. Alfahad, On the reduction of desalting energy and its cost in Kuwait, Desalination 220 (2008) 483–495.

[279] Runya Deng, Lixin Xie, Hu Lin, Jie Liu and Wei Han, Integration of thermal energy and seawater desalination, Energy 35 (2010) 4368–4374.

[280] Patricia Palenzuela, Guillermo Zaragoza , Diego Alarcón and Julián Blanco, Simulation and evaluation of the coupling of desalination units to parabolic-trough solar power plants in the Mediterranean region, Desalination 281 (2011) 379–387

[281] Chapter 2; Global Desalination Situation, Sabine Lattemann, Maria D. Kennedy, Jan C. Schippers and Gary Amy

[282] Global water intelligence (GWI) http://www.globalwaterintel.com/archive/13/10/general/technology-choice-still-open-yanbu-3.html

[283] IPCC Guidelines for National Greenhouse Gas Inventories, 2006, volume 2, Energy.

[284] UNFCCC/CCNUCC, "Tool to calculate the emission factor for an electricity system Information on emission factor"

[285] Information on Emission factors, Singapore National Environmental Agency, (2009).

Appendix A1: MED steam generator design detail

Design Steps			Comments
MED Steam Generator Parameters			
Steam generator temperature	50°C		Design Capacity
Capacity	10	KW	
hg at 50°C	2581	kJ/kg	
Vapor production	**0.00387**	**Kg/sec**	
Hot Water Parameters			
Hot water inlet temperature	330.15	K	50°C
Del T	5		ΔT 3~5°C (from literature)
Outlet temperature	325.15	K	
Effect temperature	323.15	K	ΔT 2~3°C (from literature)
Mass flow rate of hot water	**0.57**	**kg/sec**	
	34.29	**LPM**	
Overall Heat Transfer Coefficient from Literature			
H (evaporation)	1500	W/m^2k	Literature 0~1500 W/m^2K
H (Inside tube)	2000	W/m^2k	Literature 1500~2500 w/m^2K
U	**823.31**	**W/m^2k**	
LMTD	3		LMTD 3~5 (from literature)
Area of Heat Transfer (AHT)			
Area of heat transfer	**4.05**	**m^2**	Q = U x AHT x (LMTD)
Tubes Parameters			
Tube diameter (outer)	16	mm	Design parameter (do)
Thickness	0.7	mm	Design parameter (t)
Inside diameter	14.6	mm	
X-sec area	0.000167	m^2	
Tube length (single)	1.3	m	Design parameter (l)
Required length of tubes	**80.55**	**m**	
Total number of tubes	62.0		
Number of tubes in one row	8		Design parameter (n1)
Total number of rows	7.74		
Total number of rows (actual)	**8**		n2
Total number of tubes in cluster (actual)	**64**		N
Tube/Tube Cluster Parameters			
Horizontal tube pitch	24	mm	pitch=1.5*dtube
Vertical tube pitch	24	mm	pitch=1.5*dtube
Width of tube matrix	177.88	mm	w=((n-1)*pitch)+dtube
Height of tube matrix	184	mm	
Spray Nozzles Specifications			
Spray nozzle angle	90°	full cone	from nozzle technical data
Distance of spray header	175	mm	from nozzle technical data
Flow through one nozzle	0.216	LPM	from nozzle technical data
Total number of nozzle required	9.69	≈10 nozzles	(n3)
Nozzle pitch	134.21	mm	Pitch
Shell Design			
Shell diameter	459	mm	ID=tube matrix height+
			spray header height+100
	500	**mm**	standard pipe size
Shell length	**1300**	**mm**	

Appendix A2: MED steam generator design verification

MED Steam generator design parameters calculated in first step are verified. Overall heat transfer coefficient is calculated and then area of heat transfer is calculated. This area of heat transfer is than compared with area of heat transfer calculated in first step.

X-Check for Heat Transfer Coefficients			
Verification Steps			**Comments**
1-Tube side heat transfer coefficient			
ρl of hot water at 50C	988	kg/m^3	From steam table
µl of hot water at 50C	0.000544	kJ/m-sec	From steam table
liquid velocity	0.42665454	m/sec	
Raynold number	11313.2		
Nusselt number	66.41		
Heat transfer coefficient ($h_{tube,side}$)	**2474.41**	**w/m^2k**	**Within range**
2-Shell side heat transfer coefficient			
By Ng & Wakil correlation			
Vapor space temperature	44°C		ΔT 1~2°C (from literature)
Spray water needed	0.0387	kg/s	$\dot{m}_{evaporation}$ x 10
Number of tubes in a row	8		
Length	1.3	m	
Etha (Γ)	0.00186	kg/m-sec	$\Gamma=\dot{m}_{feed}/(2 \times n \times L)$
µl @ effect temperature (44°C)	0.000594	kg/m-sec	From steam table
ρl @ effect temperature (44°C)	990.20	kg/m^3	From steam table
Kl @ effect temperature (44°C)	0.638	W/mk	From steam table
Re_Γ	12.54		$Re_\Gamma = (4 \times \Gamma)/ \mu l$
Pr	3.91		
vg @ effect temperature (44°C)	16.03	m^3/kg	From steam table
vref @ effect temperature (295K)	52.65	m^3/kg	
q (heat flux)	2469.92	W/m^2	
Heat transfer coefficient ($h_{evaporation}$)	**1327.41**	**W/m^2K**	**Within range**
X-Check for U & AHT			
over all heat transfer coefficient U	**835.95**	**W/m^2k**	**Within range**
Area of heat transfer	**3.99**		**Within range**
Design Summary			
Tube detail	**16 x 0.7 x 1300**		OD x t x L
Total number of tubes	**64**		
Tube matrix detail	**8 x 8 x 24 x 24**		n1 x n2 x N
Nozzles detail	**10 x 178**		n3 x pitch
Shell ID	**500**	**mm**	
Shell thickness	**5**	**mm**	
Shell length	**1300**	**mm**	
End cover diameter	**500**	**mm**	
End cover thickness	**10**	**mm**	
Project Detail			
Equipment name	**MED Steam generator**		
Capacity	**12.5KW (25% margin)**		
Exchanger type	**Shell & tube, horizontal, falling film type**		
Material (1-Shell, 2- tubes)	**1-SS 2-Cu-Ni (90/10)**		
Dated: 01/03/2012	**Revision-03**		**Designed by: Wakil**

Appendix B1: MED stage design detail

MED Stage Parameters			
Design Steps			**Comments**
Vapor flow rate	0.0039	kg/s	From steam generator
MED stage temperature	42	°C	ΔT 1~2°C (from literature)
	315.15	K	
h_g at 42 °C	2577.20	kJ/kg	
Capacity	**10.1**	**kW**	
Overall Heat Transfer Coefficient from Literature			
H (Evaporation)	1500	W/m^2K	h_{evap} 1000~1500 W/m^2K
H (Condenser)	4000	W/m^2K	h_{cond} 4000~6000 W/m^2K
U	**1073.83**	**W/m^2K**	
LMTD	3		LMTD 3~5 (from literature)
Area of Heat Transfer (AHT)			
A for the evaporator	**3.12**	**m^2**	
Tubes Parameters			
Tube diameter (outer)	25.4	mm	Design parameter (do)
Thickness	0.7	mm	Design parameter (t)
Inside diameter	24	mm	
X-sec area	0.000452	m^2	
Tube length (single)	1.3	m	Design parameter (l)
Required length of tubes	**39.10**	**m**	
Total number of tubes	30.08		
Number of tubes in one row	8		Design parameter (n1)
Total number of rows	3.76		
Total number of rows (actual)	**4**		n2
Total number of tubes in cluster (actual)	**32**		N
Tube/Tube Cluster Parameters			
Horizontal tube pitch	38.1	mm	pitch=1.5*dtube
Vertical tube pitch	38.1	mm	pitch=1.5*dtube
Width of tube matrix	130.54	mm	w=((n-1)*pitch)+dtube
Height of tube matrix	139.7	mm	
Spray Nozzles Specifications			
Spray nozzle angle	90°	full cone	from nozzle technical data
Distance of spray header	175	mm	from nozzle technical data
Flow through one nozzle	0.216	LPM	from nozzle technical data
Total number of nozzle required	9.75	≈10 nozzles	(n3)
Nozzle pitch	133.33	mm	Pitch
Shell Design			
Shell diameter	414.7	mm	ID=tube matrix height+
			spray header height+100
	500	**mm**	standard pipe size
Shell length	**1300**	**mm**	

Appendix B2: MED stage design verification

MED Stage design parameters calculated in first step are varified. Overall heat transfer coefficient is calculated and than area of heat transfer is calculated. This area of heat transfer is than compared with area of heat transfer calculated in first step.			
X-Check for heat transfer coefficients			
Condensation HTC by Nusselt condensation correlation			
Verification Steps			**Comments**
Condenser temperature	44°C		
ρl @ condenser temperature (44C)	990.2	kg/m^3	From steam table
ρg @ condenser temperature (44C)	0.062383	kg/m^3	From steam table
μl @ condenser temperature (44C)	0.000594	kg/m-sec	From steam table
kl @ condenser temperature (44C)	0.638	W/m-k	From steam table
hfg @ condenser temperature (44C)	2396.6	KJ/kg	From steam table
Heat transfer coefficient ($h_{condensation}$)	**3919.00**	**W/m^2k**	**Within range**
2-Shell side heat transfer coefficient (by Ng & Wakil correlation)			
Evaporation space temperature	315.15	K	ΔT 1~2°C (from literature)
Spray water needed	0.039	kg/s	$\dot{m}_{evaporation}$ x 10
Number of tubes in a row	8		
Length	1.3	m	
Etha (Γ)	0.001875	kg/m-sec	$\Gamma=\dot{m}_{feed}/(2 \times n \times L)$
μl @ effect temperature (42C)	0.000622	kg/m-sec	From steam table
ρl @ effect temperature (42C)	991.17	kg/m^3	From steam table
Kl @ effect temperature (42C)	0.635	W/mk	From steam table
Re_{Γ}	12.06		
Pr	4.11		
vg @ effect temperature (42C)	17.69	m^3/kg	From steam table
vref @ effect temperature (295K)	52.65	m^3/kg	
q (heat flux)	3221.48	W/m^2	
Heat transfer coefficient ($h_{evaporation}$)	**1583.10**	**W/m^2K**	**Within range**
X-Check for U & AHT			
Over all heat transfer coefficient U	**1108.99**	**W/m^2K**	almost same as assumed
Area of heat transfer	**3.02**	**m^2**	almost same as calculated
Design Summary			
Tube detail	**25.4 x 0.7 x 1300**		OD x t x L
Total number of tubes	**32**		
Tube matrix detail	**8 x 4 x 38.1 x 38.1**		n1 x n2 x N
Nozzles detail	**10 x 134**		n3 x pitch
Shell ID	**500**	**mm**	
Shell thickness	**5**	**mm**	
Shell length	**1300**	**mm**	
End cover diameter	**500**	**mm**	
End cover thickness	**10**	**mm**	
Project Detail			
Equipment name	**MED Stage/Effcet**		
Capacity	**12.5KW (25% margin)**		
Exchanger type	**Shell & tube, horizontal, falling film type**		
Material (1-Shell, 2- tubes)	**1-SS 2-Cu-Ni (90/10)**		
Dated: 01/04/2012	**Revision-03**		**Designed by: Wakil**

Appendix C1: Steam jet ejector detail design

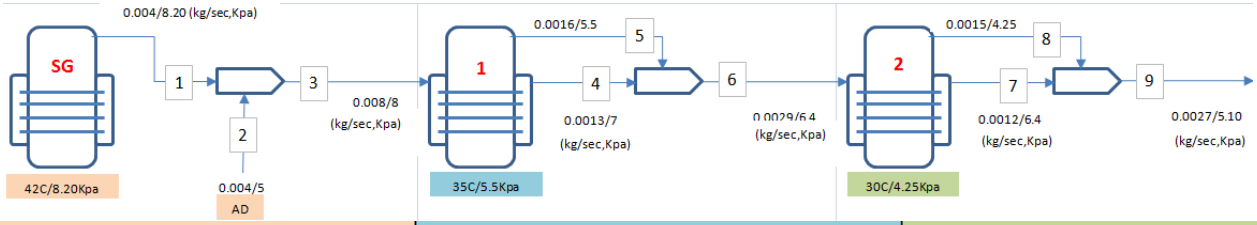

System Parameters (Steam Generator)			System Parameters (1st Stage)			System Parameters (2nd Stage)		
Tsat	42	C	Tsat	35	C	Tsat	30	C
Psat	8.2	Kpa	Psat	5.5	Kpa	Psat	4.25	Kpa
T_{AD}	40	C						
$m_{vap,AD}$	0.0040	kg/sec	$m_{3,vapor\ available}$	0.0029	kg/sec (5%losses)	$m_{6,vapor\ available}$	0.0027	kg/sec (5%losses)
			Spe.vol.	20.000	m^3/kg	Spe.vol.	21.0	m^3/kg
			V_{vapor}	0.057	m^3/sec	V_{vapor}	0.057	m^3/sec
Assumptions			**Assumptions**			**Assumptions**		
P1	8.2	Kpa	P4	7.5	Kpa	P7	6.325	Kpa
P2 (P_{AD})	5	Kpa	P5	5.5	Kpa	P8	4.25	Kpa
Cr* (P3/P2)	1.5		Cr* (P6/P5)	1.15		Cr* (P9/P8)	1.2	
n	1.135	for steam	n	1.13	for steam	n	1.135	for steam
Calculations			**Calculations**			**Calculations**		
Pt	4.7349293	Kpa	Pt	4.3384047	Kpa	Pt	3.6522473	Kpa
P3	7.5	Kpa	P6	6.325	Kpa	P9	5.10	Kpa
PCF	1.6026402		PCF	1.6032669		PCF	1.6043195	
TCF	0.980732		TCF	0.9837245		TCF	0.986718	
m_{motive}/m_{sec}	1.005065		$m_{4,motive}/m_{5,sec}$	0.7391445		$m_{7,motive}/m_{8,sec}$	0.747246	
$m_{motive,required}$	0.004	kg/sec						
$m_{vapor\ produced}$	0.004	kg/sec	$m_{4,non-condensed}$	0.0013	kg/sec (45%)	$m_{7,non-condensed}$	0.0012	kg/sec (45%)
			$m_{5,vapor,produced}$	0.0016	kg/sec	$m_{8,vapor,produced}$	0.0015	kg/sec
			$m_{motive,required}$	0.0012	kg/sec	$m_{motive,required}$	0.0011	kg/sec
Results			**Results**			**Results**		
$m_{vapor\ produced} \approx m_{motive,required}$			$m_{4,non-condensed} \approx m_{motive,required}$			$m_{7,non-condensed} \approx m_{motive,required}$		

Appendix C2: Steam jet ejector design example calculations

CASE-1

Discharge Pressure P_d= 7Kpa

$\rho_1 = \rho_{m\ @\ Tm=42C} = 0.05653\ Kg/m^3$, $h_{m\ @\ Tm=42C} = h_g = 2577.20\ KJ/Kg$

$\rho_2 = \rho_{e\ @\ Te=33C} = 0.03570\ Kg/m^3$, $h_{e\ @\ Te=33C} = h_g = 2562.0\ KJ/Kg$

$\rho_3 = \rho_{d\ @\ Pd=7Kpa} = 0.04857\ Kg/m^3$, $h_{d\ @\ Pd=7Kp} = h_g = 2572.0\ KJ/Kg$

Assumption:
d2=2*dt= 26mm
A_2= 5.30929 x 10^{-4} m^2

By ejector energy balance equation (4.33):

$$\rho_1 A_1 C_1 h_1 + \rho_2 A_2 C_2 h_2 = [\rho_1 A_1 C_1 + \rho_2 A_2 C_2] h_3$$

$$[0.05653x(1.46152x10^{-4})x392.69730x2577.20] + [0.03570x(5.30929x10^{-4})xC_2x2562.0] = \begin{bmatrix} 0.05653x(1.46152x10^{-4})x392.69730 + \\ 0.03570x(5.30929x10^{-4})xC_2 \end{bmatrix} 2572.0$$

$$[8.36161] + [0.04856C_2] = [3.24445x10^{-3} + 1.89542x10^{-5}C_2]2572.0$$

$$[8.36161] + [0.04856C_2] = [8.34473 + 0.04875C_2]$$

$$0.01688 = 1.9x10^{-4}C_2$$

$$C_2 = 88.84211 m/\sec$$

By ejector momentum balance equation (4.29):

$$\rho_1 A_1 C_1^{\ 2} + \rho_2 A_2 C_2^{\ 2} = C_3[\rho_1 A_1 C_1 + \rho_2 A_2 C_2]$$

$$[0.05653x(1.46152x10^{-4})x(392.69730)^2] + [0.03570x(5.30929x10^{-4})x(88.84211)^2] = C_3 \begin{bmatrix} 0.05653x(1.46152x10^{-4})x(392.69730) + \\ 0.03570x(5.30929x10^{-4})x(88.84211) \end{bmatrix}$$

$$[1.27409] + [0.14960] = C_3[3.24445x10^{-3} + 1.68393x10^{-3}]$$

$$C_3 = 288.87598 m/\sec$$

By ejector mass balance equation (4.27):

$$\frac{\rho_1}{\rho_3} A_1 C_1 + \frac{\rho_2}{\rho_3} A_2 C_2 = A_3 C_3$$

$$\left[\frac{0.05653}{0.04857} x\left(1.46152 x 10^{-4}\right) x 392.69730\right] +$$
$$\left[\frac{0.03570}{0.04857} x(5.30929 x 10^{-4}) x 88.84211\right]$$
$$= 288.87598 x A_3$$

$$[0.06680] + [0.03467] = 288.87598 A_3$$

$$A_3 = 3.51258 x 10^{-4} m^2$$

$$d_3 = 21.15 mm$$

Results

Pressures:

Pm = 8.20 kPa
Pt = 4.73 kPa
Pd = 7 kPa
Cr ≈ 1.5

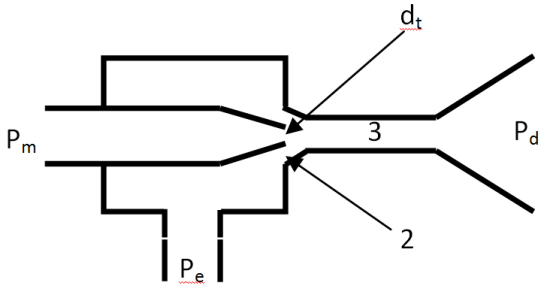

Velocities:

Ct = 392.69730 m/sec
C2 = 88.84711 m/sec
C3 = 288.87589 m/sec

Diameters:

dt = 13.64 mm
d2 = 26.0 mm
d3 = 21.15 mm

Appendix D: MED plant detailed P & ID

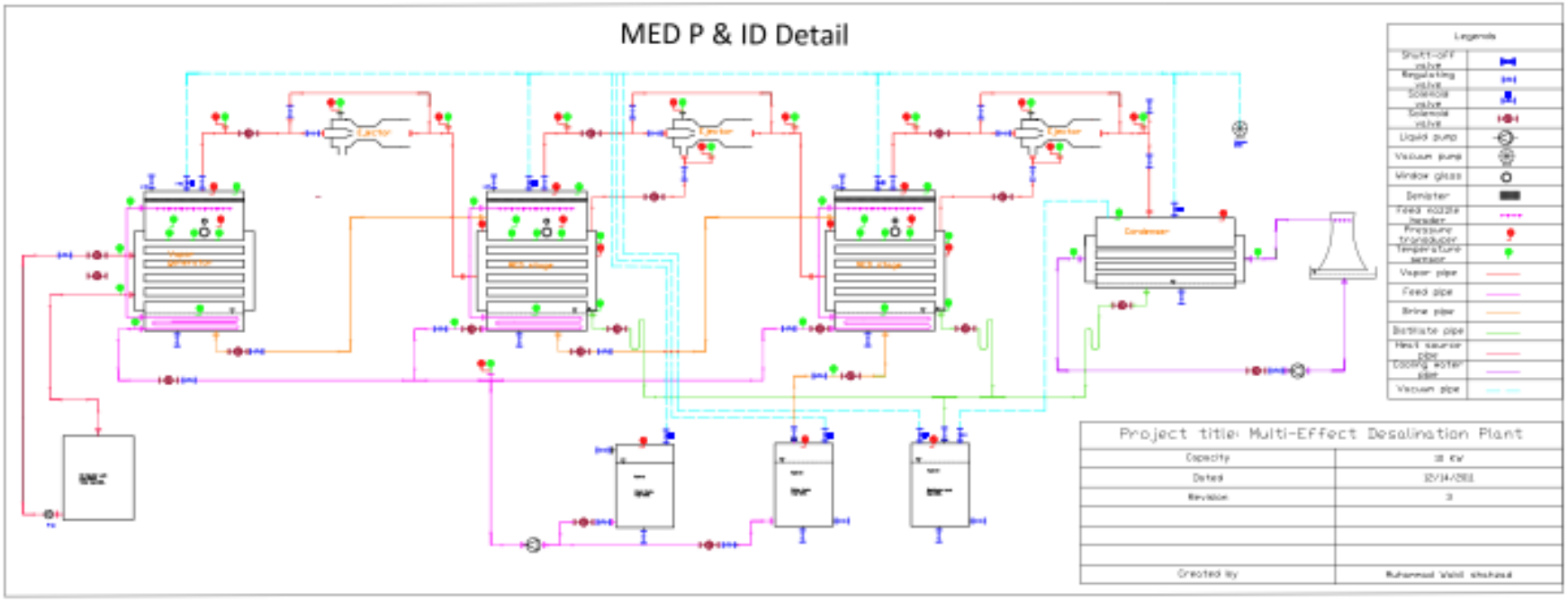

Appendix E1: MED steam generator instrumentation detail

Steam Generator Instrumentation					
Channel no.	**Sensor no.**	**Location/Purpose**	**Manufacturer**	**Accuracy**	**Comments**
Temperature Sensors					
101	108	Hot water inlte temperature	OMEGA	±0.1	1/8" Thermistor
102	109	Hot water outlet temperature	OMEGA	±0.1	1/8" Thermistor
103	106	Feed water inlet temperature	OMEGA	±0.1	1/8" Thermistor
104	101	SG vapor temperature	OMEGA	±0.1	1/8" Thermistor
105	107	SG vapor after demister	OMEGA	±0.1	1/8" Thermistor
106	110	SG brine temperature	OMEGA	±0.1	1/8" Thermistor
107	111	SG tube temperature	OMEGA	±0.2	1/4" RTD
108	13	SG tube-1	OMEGA	±0.1	Button thermistor installted on tubes
109	14	SG tube-2	OMEGA	±0.1	Button thermistor installted on tubes
110	15	SG tube-3	OMEGA	±0.1	Button thermistor installted on tubes
111	16	SG tube-4	OMEGA	±0.1	Button thermistor installted on tubes
112	17	SG tube-5	OMEGA	±0.1	Button thermistor installted on tubes
113	18	SG tube-6	OMEGA	±0.1	Button thermistor installted on tubes
114	19	SG tube-7	OMEGA	±0.1	Button thermistor installted on tubes
115	20	SG tube-8	OMEGA	±0.1	Button thermistor installted on tubes
Pressure transmitters					
116	P1	SG vapor	GE	±0.04%FS	Range 0-60 kPa(abs)
117	P2	S1 vapor box	GE	±0.04%FS	
118	P3	S1 distillate box	GE	±0.04%FS	
Steam/ vapor flow meters					
119	FM1	SG Vapor flow rate	SURE Instruments		Measurements in m3/hr
120	FM2	S1 Vapor flow rate	SURE Instruments		
121	FM3	S2 Vapor flow rate	SURE Instruments		
122	FM4	Aux. evap. Vapor flow rate	SURE Instruments		

Appendix E2: MED stage-2 instrumentation detail

Stage-2 Instrumentation					
Channel no.	**Sensor no.**	**Location/Purpose**	**Manufacturer**	**Accuracy**	**Comments**
Temperature Sensors					
201	201	S1 vapor temperature	OMEGA	±0.1	1/8" Thermistor
202	207	S1 vapor after demister	OMEGA	±0.1	1/8" Thermistor
203	208	S1 brine temperature	OMEGA	±0.1	1/8" Thermistor
204	206	S1 feed temperature	OMEGA	±0.1	1/8" Thermistor
205	211	S1 tube temperature	OMEGA	±0.2	1/8" Thermistor
206	10	S1 tube-1-1	OMEGA	±0.1	Button thermistor installted on tube-1
207	11	S1 tube-1-2	OMEGA	±0.1	Button thermistor installted on tube-1
208	12	S1 tube-1-3	OMEGA	±0.1	Button thermistor installted on tube-1
209	7	S1 tube-2-1	OMEGA	±0.1	Button thermistor installted on tube-2
210	8	S1 tube-2-2	OMEGA	±0.1	Button thermistor installted on tube-2
211	9	S1 tube-2-3	OMEGA	±0.1	Button thermistor installted on tube-2
212	407	Tcw,out	OMEGA	±0.1	Condenser cooling water outlet temperature
213	406	Tcw,in	OMEGA	±0.1	Condenser cooling water inlet temperature
Pressure transmitters					
214	P4	S1 vapor	GE	±0.04%FS	Range 0-60 kPa(abs)
215	P5	S2 vapor box	GE	±0.04%FS	
217	P6	S2 distillate box	GE	±0.04%FS	
Feed flow meters/ CW & HW water flow meter					
218	OMEGA-1	SG feed flow rate	OMEGA	±1 AF	Measurements in LPM
219	OMEGA-2	S1 feed flow rate	OMEGA	±1 AF	
220	OMEGA-3	S2 feed flow rate	OMEGA	±1 AF	
221	HW	Hot water flowrate	LAKE MONITORS	±2 FS	
222	CW	Cooling water flow rate	LAKE MONITORS	±2 FS	

Appendix E3: MED stage-3 instrumentation detail

Stage-2 Instrumentation					
Channel no.	**Sensor no.**	**Location/Purpose**	**Manufacturer**	**Accuracy**	**Comments**
Temperature Sensors					
301	302	S2 vapor temperature	OMEGA	±0.1	1/8" Thermistor
302	307	S2 vapor after demister	OMEGA	±0.1	1/8" Thermistor
303	306	S2 brine temperature	OMEGA	±0.1	1/8" Thermistor
304	305	S2 feed temperature	OMEGA	±0.1	1/8" Thermistor
305	311	S2 tube temperature	OMEGA	±0.2	1/8" Thermistor
306	4	S2 tube-1-1	OMEGA	±0.1	Button thermistor installted on tube-1
307	5	S2 tube-1-2	OMEGA	±0.1	Button thermistor installted on tube-1
308	6	S2 tube-1-3	OMEGA	±0.1	Button thermistor installted on tube-1
309	1	S2 tube-2-1	OMEGA	±0.1	Button thermistor installted on tube-2
310	2	S2 tube-2-2	OMEGA	±0.1	Button thermistor installted on tube-2
311	3	S2 tube-2-3	OMEGA	±0.1	Button thermistor installted on tube-2
312	402	Tcond	OMEGA	±0.1	1/8" Thermistor
313	408	Tfeed	OMEGA	±0.1	1/8" Thermistor
314	403	Tevap, aux.	OMEGA	±0.1	1/8" Thermistor
Pressure transmitters					
315	P12	Aux. evaporator pressure	GE	±0.04%FS	Range 0-60 kPa(abs)
316	P7	S2 vapor pressure	GE	±0.04%FS	
317	P8	Condenser pressure	GE	±0.04%FS	
318	P9	Brine tank pressure	GE	±0.04%FS	
319	P10	Distillate tank pressure	GE	±0.04%FS	
320	P11	Feed tank pressure	GE	±0.04%FS	
321					
322		Distillate flow meter	Aichi Tokei		

Appendix D1: Instrumentation intermediate control box-1

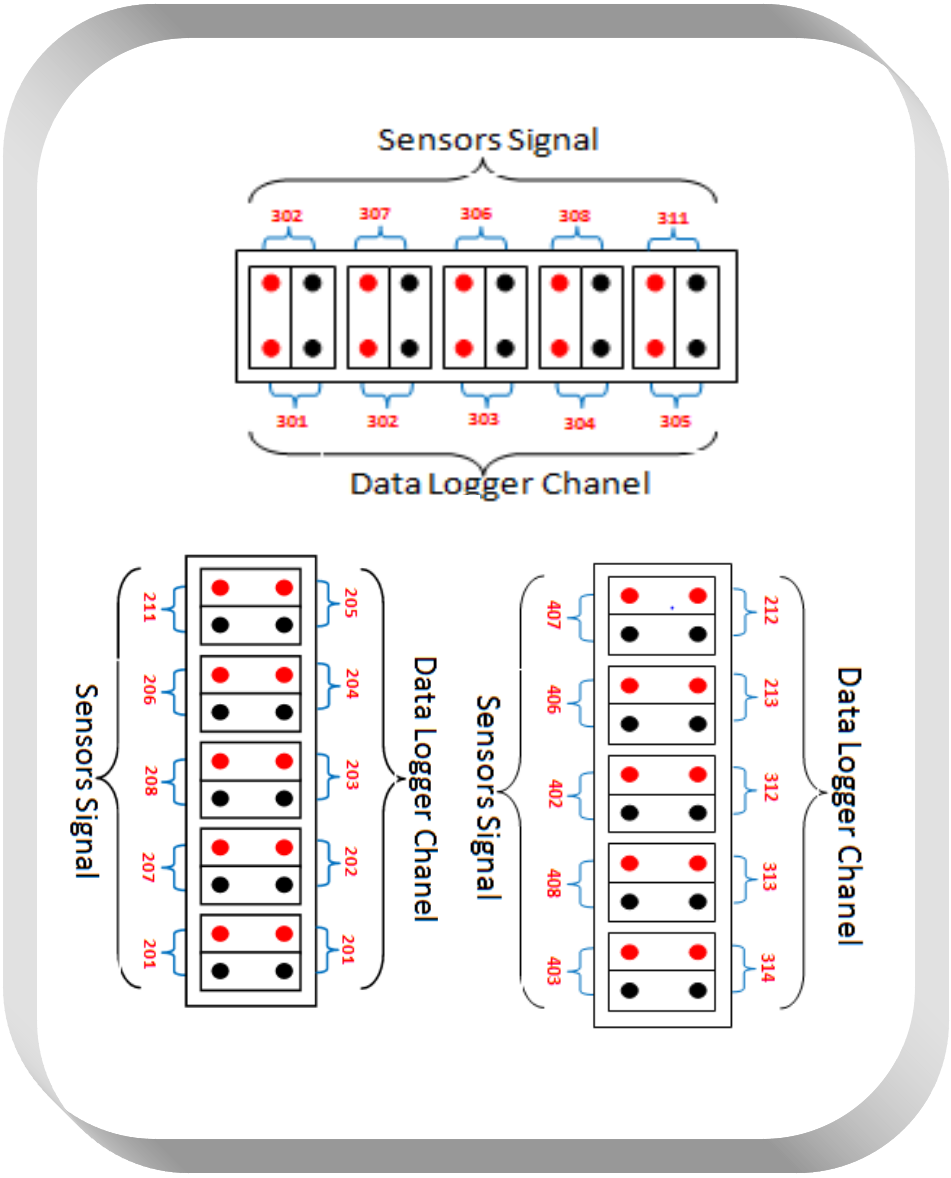

Appendix D2: Instrumentation intermediate control box-2

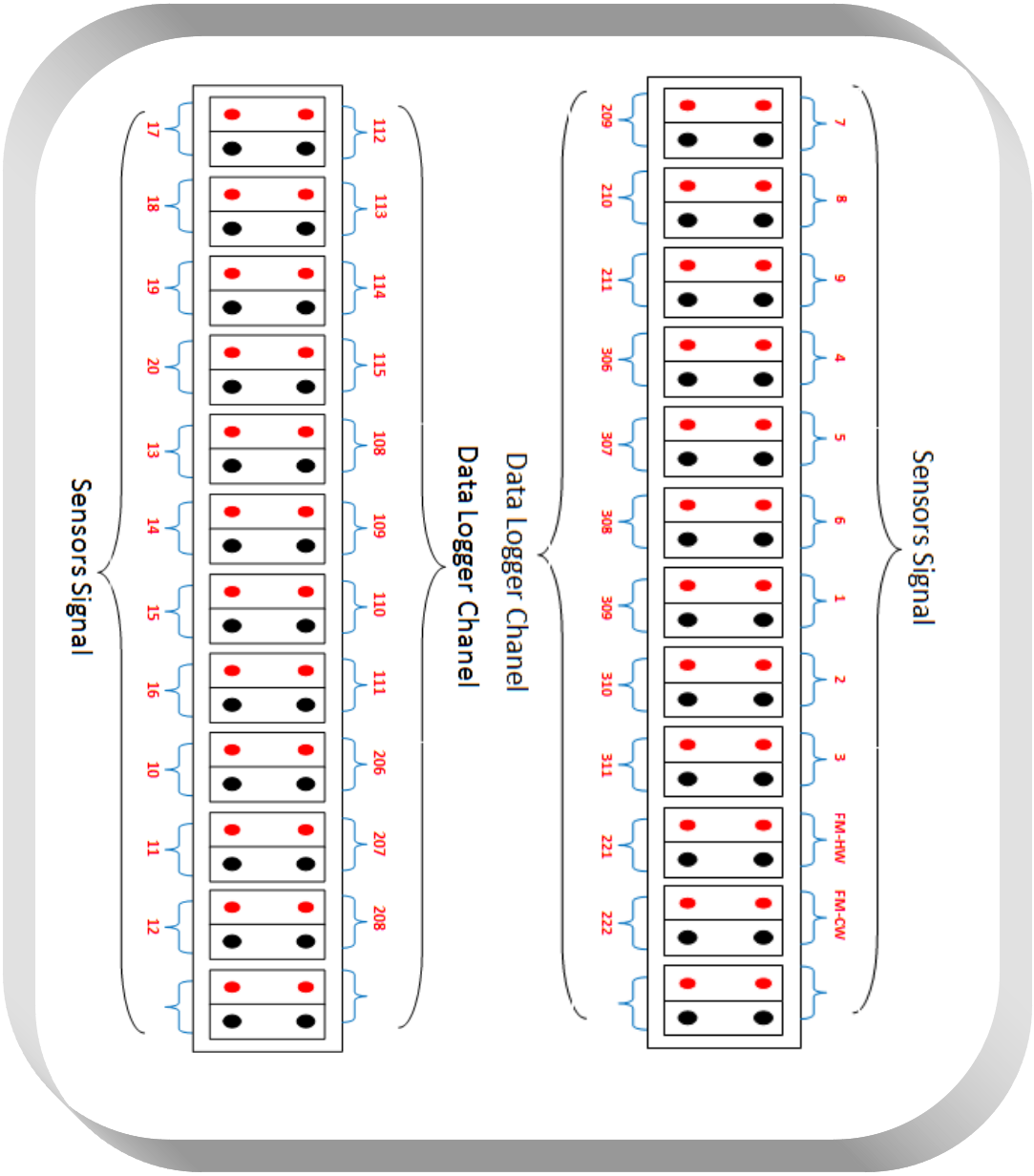

Appendix D3: Instrumentation intermediate control box-3